

Laboratory of Biochemistry, Department of Biological Applications and Technology,
University of Ioannina
Biomedical Research Institute – Foundation for Research and Technology-Hellas
(BRI-FORTH)
Ioannina, Greece

Inter-institutional Interdepartmental Program of Postgraduate Studies
Molecular and Cellular Biology and Biotechnology

Master's Thesis:

Understanding the Anxious Female Brain: How Early Handling Shapes Adult Behavior Through Mitochondria

Afroditi Divane

Chemist

Supervisor:

Michaela Filiou, Associate Professor

Department of Biological Applications and Technology,

University of Ioannina

Ioannina, September 2024

ACKNOWLEDGMENTS

This thesis was conducted at the Biochemistry Laboratory of the Department of Biological Applications and Technology at the University of Ioannina, and the Biomedical Research Institute, Foundation of Research and Technology-Hellas (BRI-FORTH) during the academic year 2023-2024 under the supervision of Dr. Filiou Michaela, Associate Professor.

Before anything else, I would like to thank my supervisor Dr. Filiou Michaela, for her guidance and help throughout this academic year. The knowledge I have gained under her mentorship has been invaluable, and her feedback and insight at every step of this project has shaped this thesis into the scientific work that it is now and improved my skill set as a scientist. I would also like to thank the other members of my thesis committee, Prof. Frilingos Efstathios, Assistant Prof. Liakopoulos Dimitris, Assistant Prof. Leontaritis George, and Assistant Prof. Lamprakakis Charalambos for evaluating my work.

Extending my heartfelt thanks to Dr. Samiotaki Martina, Senior Research Scientist at B.S.R.C. “Alexander Fleming” for performing the label-free mass spectrometry (MS)-based quantitative proteomics analysis and offering us her insight whenever it was necessary.

Additionally, I would like to thank all members of the Biochemistry Laboratory, past and present. Firstly, many thanks to Laboratory Teaching Staff Dr. Konidaris Constantinos for his help and advice around the lab, and Research Technician Nussbaumer Markus for providing his knowledge about animal work. I would like to thank former diploma thesis student Grammenou Elena and former master’s student Thomou Christina for all their help on passing the torch of the early handling project and for always being available when I had questions. I am also thankful to former Postdoctoral Researcher Dr. Komini Chrysa for training me during my early days in the lab. Last but not least, I could not but thank PhD students Papageorgiou Maria and Anousi Elissavet, for their guidance and advice to all of my inquiries, no matter how silly, as well as diploma thesis students Panteli Eirini and Mitka Anastasia for the company they kept me and the knowledge we exchanged. My days in the lab were as joyful as they were educational, the laughs that we shared and the memories we made during the hours we spent together will stay with me for a long time.

I must also thank the members of the Cellular and Developmental Biology laboratory, led by Associate Prof. Marangos Petros, namely Postdoctoral Researcher Dr. Niaka Konstantina, PhD student Zorzompokou Chrysoula and diploma thesis student Fotara Maria for their collaboration and help throughout the year.

Finally, a note of gratitude towards my family, my friends and my partner, for their endless love and support in all my endeavors, this master’s included. Thank you for believing in me even when I doubted myself, and for always encouraging me to keep going!

TABLE OF CONTENTS

ACKNOWLEDGMENTS.....	2
ABSTRACT.....	6
ΠΕΡΙΛΗΨΗ.....	7
ABBREVIATION LIST.....	8
1. INTRODUCTION	11
1.1. Early handling (EH)	11
1.1.1. Early life experiences modulate adult behavior – the example of EH.....	11
1.1.2. EH impacts the behavior of male rats and mice.....	11
1.1.3. Molecular underpinnings of EH on male rats and mice.....	12
1.2. Anxiety	13
1.2.1. Definition and categories of anxiety	13
1.2.2. Anxiety neurocircuits: the hypothalamus and the prefrontal cortex (PFC).....	13
1.2.3. The high anxiety-related behavior (HAB) mouse model.....	14
1.3. Mitochondria.....	16
1.3.1. “The powerhouse of the cell”	16
1.3.2. Mitochondrial dynamics: Biogenesis, Fusion, Fission, and Mitophagy.....	18
1.3.3. Mitochondria in anxiety research.....	21
1.4. The gender dimension	22
1.4.1. Females in psychiatric research	22
1.4.2. The sexually dimorphic brain: Truth or a myth?	23
1.4.3. Females in EH research	23
1.5. Proteomics.....	24
1.5.1. What is proteomics?	25
1.5.2. Proteomics in psychiatric research	25
1.5.3. Proteomics in anxiety research.....	26
2. AIM OF THE STUDY	28
3. MATERIALS AND METHODS	29
3.1. Animals - EH paradigm	29
3.2. Protein extraction.....	30
3.3. Bradford Assay.....	30
3.4. Western Blot.....	31
3.5. Total Antioxidant Capacity (TAC) Assay	35
3.6. DNA and RNA extraction.....	36
3.7. DNA Electrophoresis.....	36
3.8. Quantitative PCR (qPCR) – Mitochondrial DNA copy number (MtDNAcn)	37

3.9. Quantitative, Reverse Transcriptase PCR (qRT-PCR)	38
3.10. Mass spectrometry (MS)-based Proteomics.....	41
3.11. Proteomics: In Silico Analysis.....	41
3.12. Statistical Analysis.....	43
4. RESULTS.....	44
4.1. EH exerted anxiolytic effects on adult HAB female mice	44
4.2. HYPOTHALAMUS: Label-free, MS-based proteomics analysis.....	45
4.2.1. Overlook of our proteomics results – Top ten upregulated protein hits	45
4.2.2. Manual categorization revealed the abundance of oxidative phosphorylation (OXPHOS) proteins in the differentially expressed dataset.....	48
4.2.3. In silico analysis with STRING showcased two main groups in the full and the upregulated dataset: OXPHOS proteins and ribosomal proteins.....	49
4.2.4. Correlation matrices for the OXPHOS and ribosome protein expression levels for HAB EH female mice with behavior	52
4.2.5. Gene Ontology overrepresentation analysis validated mRNA splicing, ribosomes and OXPHOS as main EH mediators	56
4.3. HYPOTHALAMUS: Molecular assays.....	63
4.3.1. EH altered mitochondrial biogenesis and fission mRNA levels in the hypothalamus of HAB EH female mice.....	63
4.3.2. EH decreased the mtDNAcn in the hypothalamus of HAB EH female mice	67
4.4. PREFRONTAL CORTEX (PFC).....	69
4.4.1. EH reduced PKLR protein expression levels in the PFC of HAB female mice	70
4.4.2. EH did not affect OXPHOS protein expression in the PFC of HAB female mice	72
4.4.3. EH did not affect mitochondrial dynamics markers in the PFC of HAB female mice	72
4.4.4. EH decreased the protein expression levels of PRDX3 in the PFC of HAB female mice	75
4.4.5. EH did not alter the expression levels of selected mitochondrial transport/import proteins in the PFC of HAB female mice.....	76
4.5. PLASMA.....	77
4.5.1. EH did not alter TAC levels in the plasma of HAB female mice	78
4.5.2. EH induced a trend for decreased protein expression levels of CYTC in the plasma of HAB EH female mice	78
4.5.3. EH did not alter the expression levels of antioxidant proteins in the plasma of HAB female mice.....	80

5. DISCUSSION 82
 5.1. Hypothalamus: the mediator of EH-driven molecular responses 83
 5.2. PFC: EH-instigated molecular alterations are brain region-specific..... 90
 5.3. Plasma: Brain alterations are not reflected in the peripheral material 93
 5.4. Summary of the results..... 94
 5.5. EH research between HAB males and females: What is the difference? 96
 5.6. Limitations and future outlook 98
6. REFERENCES 100
7. APPENDIX 125

ABSTRACT

Interventions during the neonatal window are pivotal for the modulation of adult behavior. Early Handling (EH) is the brief and repeated separation of pups from their dam during their first postnatal days, which has been shown to reduce emotionality during adulthood. Previous work from our lab investigated the EH-driven alterations in high anxiety-related behavior (HAB) male mice, demonstrating that EH induced an anxiolytic effect along with EH-driven alterations of mitochondrial pathways. However, the impact of EH on HAB female mice is poorly understood.

The aim of this thesis was to investigate the effects of EH in the hypothalamus and prefrontal cortex, regions that modulate anxiety responses, as well as in the plasma of HAB female mice. Similar to their HAB male counterparts, EH also exerted anxiolytic effects in HAB female mice. To unravel the hypothalamic profile of these animals, we used mass spectrometry (MS)-based proteomics. In silico proteomics analysis revealed alterations in processes related to gene transcription, protein synthesis and energy production in HAB EH compared to HAB non-handled (NH) female mice. Using qRT-PCRs in the hypothalamus, we also discovered differential mRNA expression for genes involved in mitochondrial dynamics, namely mitochondrial biogenesis and fission, as well as changes to the mitochondrial DNA copy number (mtDNAcn) in HAB EH vs. HAB NH female mice. To assess whether these findings are region-specific, we conducted western blots in the prefrontal cortex and observed alterations in the expression level of metabolic and antioxidant proteins of HAB EH vs. HAB NH female mice. Lastly, in plasma, we used total antioxidant capacity (TAC) and western blots to understand whether these metabolic and antioxidant changes are brain-specific and found altered levels for proteins involved in energy production in HAB EH vs. HAB NH female mice. Correlation of our molecular results on HAB EH female mice with behavior showcased a link between alterations in brain metabolism, mitochondrial dynamics and antioxidant defense and anxiety-like behavior.

Taken together, our data pin the mitochondrion at the epicenter of complex EH-driven alterations that are brain region- and sex-specific. Understanding the molecular background of neonatal interventions like EH can elucidate the long-lasting impacts of early life events and pave the way for the treatment of anxiety disorders.

ΠΕΡΙΛΗΨΗ

Οι παρεμβάσεις κατά τη διάρκεια της νεογνικής ζωής είναι ύψιστης σημασίας για την διαμόρφωση της ενήλικης συμπεριφοράς. Ο πρώιμος χειρισμός (early handling/EH) αφορά στον σύντομο και επαναλαμβανόμενο αποχωρισμό των νεογνών από τη μητέρα τους κατά τις πρώτες ημέρες ζωής, και έχει αποδειχθεί ότι έχει ευεργετικές συνέπειες στη διαχείριση των συναισθημάτων κατά την ενήλικη ζωή. Προηγούμενη δουλειά του εργαστηρίου μας διερεύνησε τις αλλαγές που προκαλεί το EH σε αρσενικά ποντίκια με υψηλό άγχος (high anxiety-related behavior/HAB). Το EH είχε αγχολυτικά αποτελέσματα και οι επακόλουθες μοριακές αναλύσεις κατέδειξαν εμπλοκή μιτοχονδριακών μονοπατιών. Ωστόσο, η επίδραση του EH σε HAB θηλυκά ποντίκια δεν έχει ακόμα κατανοηθεί.

Ο στόχος αυτής της διατριβής ήταν να ερευνηθούν οι επιπτώσεις του EH στον υποθάλαμο και τον προμετωπιαίο φλοιό, περιοχές που ρυθμίζουν αποκρίσεις στο άγχος, και στο πλάσμα των HAB θηλυκών ποντικίων. Όπως και στα αρσενικά HAB ποντίκια, το EH είχε αγχολυτικές επιπτώσεις στα HAB θηλυκά. Χρησιμοποιήσαμε πρωτεομική με φασματομετρία μάζας για να μελετήσουμε το υποθαλαμικό προφίλ αυτών των ζώων. In silico ανάλυση των αποτελεσμάτων της πρωτεομικής έδειξε αλλαγές σε μονοπάτια γονιδιακής μεταγραφής, πρωτεϊνσύνθεσης και παραγωγής ενέργειας. Χρησιμοποιώντας qRT-PCR στον υποθάλαμο, ανακαλύψαμε επίσης διαφορετική έκφραση mRNA για γονίδια που εμπλέκονται με τη μιτοχονδριακή δυναμική, συγκεκριμένα με τη μιτοχονδριακή βιογένεση και σχάση, και αλλαγές στον αριθμό αντιγράφων μιτοχονδριακού DNA (mtDNAcn) στα HAB EH θηλυκά ζώα σε σύγκριση με τα HAB ζώα μάρτυρες. Για να ελέγξουμε αν αυτά τα ευρήματα είναι ειδικά για τον υποθάλαμο, πραγματοποιήσαμε western blot στον προμετωπιαίο φλοιό και παρατηρήσαμε μεταβολές στα επίπεδα έκφρασης μεταβολικών και αντιοξειδωτικών πρωτεϊνών στα HAB EH σε σύγκριση με τα HAB θηλυκά ζώα μάρτυρες. Τέλος, στο πλάσμα, πραγματοποιήσαμε δοκιμασία ολικής αντιοξειδωτικής ικανότητας (total antioxidant capacity/TAC) και western blot για να διαπιστώσουμε αν αυτές οι μεταβολικές και αντιοξειδωτικές αλλαγές παρατηρούνται μόνο στον εγκέφαλο, και βρήκαμε διαφορετικά επίπεδα για πρωτεΐνες που εμπλέκονται στην παραγωγή ενέργειας στα HAB EH σε σύγκριση με τα HAB θηλυκά ζώα μάρτυρες. Συσχέτιση των αποτελεσμάτων μας στα HAB EH θηλυκά ζώα αποκάλυψαν μια σύνδεση του εγκεφαλικού μεταβολισμού, μιτοχονδριακής δυναμικής και αντιοξειδωτικής άμυνας με την αγχώδη συμπεριφορά.

Συνοψίζοντας, τα δεδομένα μας τοποθετούν τα μιτοχόνδρια στο επίκεντρο των πολύπλοκων μεταβολών που προκαλεί το EH, οι οποίες εξαρτώνται από την εγκεφαλική περιοχή και το φύλο. Η κατανόηση του μοριακού προφίλ νεογνικών παρεμβάσεων όπως το EH μπορεί να βοηθήσει στην διαλεύκανση των μακροχρόνιων επιπτώσεων που έχουν οι πρώιμες εμπειρίες και να συμβάλλει στην εύρεση νέων θεραπειών για αγχώδεις διαταραχές.

ABBREVIATION LIST

5-HT - 5-Hydroxytryptamine (Serotonin)
ABS - Absorbance
ACTH - Adrenocorticotropic Hormone
ADP - Adenosine Diphosphate
AMPA - α -Amino-3-Hydroxy-5-Methyl-4-Isoxazolepropionic acid
ATP - Adenosine Triphosphate
ATP4A - Potassium-transporting ATPase Alpha chain 1
ATP5B - ATP Synthase subunit beta, mitochondrial
ATP5D - ATP Synthase subunit delta, mitochondrial
BSA - Bovine Serum Albumin
BDNF - Brain-Derived Neurotrophic Factor
BP - Biological Process
CC - Cellular Component
CKM - Creatine Kinase M-type
CNS - Central Nervous System
CORT - Corticosterone
CRF - Corticotropin-Releasing Factor
CS - Citrate Synthase
CYTC - Cytochrome C
DaLi - Dark-light box
DCIP - Dichlorophenolindophenol
dH₂O - Distilled water
DNM2 - Dynamin 2
DRP1 - Dynamin-related Protein 1
EH - Early Handling
ELS - Early Life Stress
EPM - Elevated Plus Maze
ETC - Electron Transport Chain
FADH₂ - Flavin Adenine Dinucleotide
FIS1 - Mitochondrial Fission 1 Protein
FST - Forced-Swim Test
GABA - Gamma-Aminobutyric Acid
GAPDH - Glyceraldehyde-3-Phosphate Dehydrogenase
GDAP1 - Ganglioside Induced Differentiation Associated Protein 1
GLO1 – Glyoxalase 1
GO – Gene Ontology

GR - Glucocorticoid Receptor
GSH - Glutathione
GSK3B - Glycogen Synthase Kinase 3-beta
GSR - Glutathione Reductase
H₂O₂ - Hydrogen Peroxide
HAB - High Anxiety-Related Behavior
HK2 - Hexokinase 2
HPA - Hypothalamic-Pituitary-Adrenal
HYP - Hypothalamus
IDH1 - Isocitrate Dehydrogenase 1
IMM - Inner Mitochondrial Membrane
IMMT - MICOS complex subunit Mic60 (Mitofilin)
IMS - Intermembrane Space
LAB - Low Anxiety-Related Behavior
LC-MS/MS – Liquid Chromatography, Tandem Mass Spectrometry
LDHB - Lactate Dehydrogenase B
MF – Molecular Function
MFF - Mitochondrial Fission Factor
MFN1 - Mitofusin 1
MFN2 - Mitofusin 2
MID49 - Mitochondrial dynamics protein 49 kDa
MID51 - Mitochondrial dynamics protein 51 kDa
MS - Mass Spectrometry
mtDNA - Mitochondrial DNA
mtDNAcn - Mitochondrial DNA Copy Number
mt-ND1 - Mitochondrially Encoded NADH Ubiquinone Oxidoreductase Core Subunit 1
MSTO1 - Misato Mitochondrial Distribution And Morphology Regulator 1
NAB - Normal Anxiety-related Behavior
NADH - Nicotinamide-Adenine Dinucleotide
NDUFB11 - NADH Dehydrogenase (Ubiquinone) 1 Beta subcomplex subunit 11, mitochondrial
NDUFS1 - NADH-Ubiquinone Oxidoreductase 75 kDa subunit 1, mitochondrial
NH - Non-Handling
NMDA - N-Methyl-D-Aspartic acid
NRF-1 - Nuclear Respiratory Factor 1
NRF-2 - Nuclear Respiratory Factor 2
OFT - Open Field Test
OMM - Outer Mitochondrial Membrane
OPA1 - Dynamin-like 120 kDa protein, mitochondrial

OXPHOS - Oxidative Phosphorylation
pCREB - Cyclic-AMP Response Element Binding protein, phosphorylated
PFC - Prefrontal Cortex
PFKFB1 - 6-Phosphofructo-2-Kinase/Fructose-2.6-Biphosphatase 1
PGC1A - Peroxisome Proliferator-Activated Receptor Gamma Coactivator-1 alpha
PINK1 - PTEN Induced Kinase 1
PKLR - Pyruvate Kinase, Liver
PND - Postnatal Day
PNPT1 - Polynucleotide Phosphorylase 1
PRDX3 - Peroxiredoxin 3
PRKN - E3 ubiquitin-protein Ligase Parkin
PRX - Peroxiredoxin
qPCR – Quantitative Polymerase Chain Reaction
qRT-PCR - Quantitative Reverse Transcriptase Polymerase Chain Reaction
ROS - Reactive Oxygen Species
RPSA - Small Ribosomal Subunit Protein uS2
SDHA - Succinate Dehydrogenase a
SFXN1 - Sideroflexin 1
SLC25A46 - Solute Carrier Family 25 Member 46
snRNP - Small Nuclear Ribonucleoprotein
SOD1 - Superoxide Dismutase 1
SOD2 - Superoxide Dismutase 2
SPAT - Social Preference-Avoidance Test
SRP14 - Signal Recognition Particle 14
TAC - Total Antioxidant Capacity
TAE - Tris base, Acetic acid, EDTA
TBS - Tris-Buffered Saline
TBS-T - Tris-Buffered Saline, Tween 20
TCA - Tricarboxylic Acid
TFAM - Transcription Factor A, mitochondrial
TIM23 - Mitochondrial Import Inner Membrane Translocase Subunit TIM23
TIM - Translocase of the Inner Mitochondrial Membrane
TOM - Translocase of the Outer Mitochondrial Membrane
TST - Tail Suspension Test
YME1L - ATP-Dependent Zinc Metalloprotease

1. INTRODUCTION

1.1. Early handling (EH)

1.1.1. Early life experiences modulate adult behavior – the example of EH

Environmental factors and external stimuli play a significant role in infant development, especially during the perinatal window. Within this window lies the postnatal period, in which brain plasticity and neuronal development are highly active (Ismail et al., 2017). For this reason, early life experiences modulate behavior during adulthood, steering the neonatal brain away from or toward neuropathology (Bock et al., 2014). This is commonly mentioned in the literature as developmental programming (Gluckman & Hanson, 2004), and it is why early life environment manipulation paradigms are studied.

Early handling (EH), otherwise known as neonatal or postnatal handling, is a brief and repeated separation of newborn rodent pups from their dam during their first days of life. The parameters of the EH protocol vary between laboratories, lasting between 1 (Levine, 1956; Levine et al., 1956) to 15 min (Meaney et al., 1985; Pryce et al., 2001), for about 10 (Padoin et al., 2001) to 21 days of the early postnatal life (Levine, 1956; Pryce et al., 2001). Earlier iterations of EH referred to individual handling of the pups (Meaney et al., 1985) but lately, it is more common to handle each litter as a group, removing it from the home cage and transferring it to a different cage or holding box for the duration of the intervention (Luchetti et al., 2015). However, despite the differences among the EH protocols, EH has been shown to induce changes both at behavioral and molecular levels (Flanigan & Cook, 2011; Meaney et al., 1985; Rainekei et al., 2014).

1.1.2. EH impacts the behavior of male rats and mice

Male rodents subjected to the EH protocol during neonatal life display reduced emotionality and anxiety-like behaviors. More specifically, EH resulted in increased avoidance learning (Levine, 1956; Levine et al., 1956), reduced stress response (Sieck & Ramaley, 1975) and increased exploratory behavior in the open field test (OFT), perceived as lowered anxiety (Vallée et al., 1997) in Sprague-Dawley rats. In albino rats, EH reduced ultrasonic vocalizations and their resistance to being picked up, which is interpreted as increased adaptation to external stimulus (Ader, 1965). In Long-Evans hooded rats, EH enhanced contextual fear conditioning (Beane et al., 2002) and decreased fearful and startle responses when exposed to novelty conditions (Caldji, 2000). In Wistar rats, EH reduced anxiety-like behavior (Meerlo et al., 1999) as well as innate and learned fear responses (Madruga et al., 2006). EH also decreased behavioral inhibition in a novel and potentially harmful environment, signifying lowered fearfulness (Padoin et al., 2001). Interestingly, EH also seemed to reverse the anxiogenic behavior of Wistar rats that were prenatally stressed, improving stress responses and emotionality as it was assessed in the OFT (Castelli et al., 2020).

Similar findings in male mice are more limited. In Swiss-Webster mice, EH decreased stress-related behaviors and responsiveness (Sternberg & Ridgway, 2003). In C57BL/6J mice, a trend for

reduced anxiety-like behavior in the elevated zero maze, a test measuring anxiety-like behavior and emotionality (Flanigan & Cook, 2011), as well as improved spatial learning on the Morris water maze (Akatsu et al., 2015) were reported. Lastly, NMRI mice showed reduced emotionality in the elevated plus maze (EPM), a widely used test for the assessment of anxiety-like behavior (Luchetti et al., 2015).

1.1.3. Molecular underpinnings of EH on male rats and mice

The molecular background of these EH-induced behavioral alterations have mostly been investigated on a neurobiological level. For instance, handled Long-Evans hooded rats had increased GABA_A receptor levels in the brainstem, increased central benzodiazepine receptor levels in the amygdala, the frontal cortex and the brainstem, and also increased mRNA levels of a GABA_A receptor complex subunit $\gamma 2$ in the amygdala and the brainstem (Bodnoff et al., 1989; Caldji, 2000). Also, in the hippocampus and the frontal cortex of Long-Evans hooded rats, glucocorticoid receptor (GR) concentrations were increased in the EH group compared to the control group (Meaney et al., 1985; Meaney et al., 1989). Since the effect of serotonin (5-HT) on GR expression is mediated by cAMP formation, cAMP levels were studied in relation with EH, and they were increased in the hippocampus of handled Long-Evans hooded rats, along with the activity of protein kinase A, and the protein expression of selected cAMP-inducible transcription factors (Meaney et al., 2000). In Wistar rats, c-Fos expression was used as an index of neuronal activity in the hippocampus and the cortex, and following EH, c-Fos levels were increased, hinting at altered stress responses in the brain (Garoflos et al., 2008). The same research group also investigated the effect of EH on hippocampal pCREB, brain-derived neurotrophic factor (BDNF), and neurotrophin-3 expression, which were all increased in handled rats compared to controls (Garoflos et al., 2005; Garoflos et al., 2007), as well as the mRNA levels of selected NMDA receptor subunits in limbic brain areas, which were increased too (Stamatakis et al., 2009). EH also resulted in altered monoamine turnover in the hypothalamus, the hippocampus, and the striatum of Wistar rats (Papaioannou et al., 2002), as well as increased mRNA expression levels of 5-HT receptors in the cerebral cortex and the hippocampus of C57BL/6NCr mice (Akatsu et al., 2015).

The neuroendocrine profile of rodents subjected to the EH protocol has also been studied. Plasma corticosterone levels of handled male Sprague-Dawley rats were decreased after subjecting the animals to high shock intensity (Weinberg & Levine, 1977), showcasing increased resilience upon a stressful situation. Lowered corticosterone levels were also observed in other studies, with two using Long Evans hooded rats (Beane et al., 2002; Vallée et al., 1997), and another one using NMRI mice (Luchetti et al., 2015). In Wistar rats, handled animals had lower blood levels of stress hormones like adrenaline, prolactin, and corticosterone, in accordance with the EH-induced anxiolytic effect (Meerlo et al., 1999). Lastly, handled Long-Evans hooded rats also showed reduced corticosterone levels following restraint stress, and they secreted less adrenocorticotrophic hormone (ACTH) (Meaney et al., 1989).

1.2. Anxiety

1.2.1. Definition and categories of anxiety

Anxiety is a state of unease over the anticipation of a potential threat, and is associated with enhanced vigilance, worry, and distress (Bishop, 2007). In moderation, anxiety is considered a protective adaptive mechanism, shielding against danger (Scott, 2013). However, excess anxiety can become pathological on both an emotional, and a physiological level, interfering with one's ability to cope with challenges (Steimer, 2002). There are two distinct ways in which anxiety is manifested: state and trait anxiety (Saviola et al., 2020). State anxiety is a temporary, immediate reaction to adversity that is not accompanied by specific pathological conditions. Trait anxiety is considered a stable personality feature, defined as the constant tendency of an individual to respond with concern or worry to various, not necessarily threatening situations. Whether state and trait anxiety are behaviorally correlated or should be considered to be separate, multidimensional constructs is still under dispute (Endler & Kocovski, 2001; Vagg et al., 1980), however, both anxiety entities can be measured using the Spielberger State-Trait Anxiety Inventory (Spielberger et al., 1983).

Once anxiety becomes pathological, it gives rise to anxiety disorders. Anxiety disorders include disorders that have symptoms of excessive and enduring fear, anxiety and avoidance of a perceived threat. They commence early in life (Kessler et al., 2007) and have a chronic course (Antony & Stein, 2009). The Diagnostic and Statistical Manual of Mental Disorders (DSM-V) (American Psychiatric Association, 2013) lists about 12 different conditions, including: generalized anxiety disorder, social anxiety disorder, panic disorder, agoraphobia, and others. Anxiety disorders are the most prevalent mental health conditions, with statistics showing that 7.3% of people worldwide suffer from some type of anxiety disorder (Baxter et al., 2013). If untreated, anxiety disorders become debilitating due to functional and somatic impairments (Craske et al., 2017) and are often comorbid with other conditions, such as depression (Beesdo et al., 2010). Thus, neuroscience research has been focusing on the elucidation of the molecular underpinnings of anxiety, as well as the underlying neurocircuits and pertinent biological pathways.

1.2.2. Anxiety neurocircuits: the hypothalamus and the prefrontal cortex (PFC)

The fact that all anxiety disorders share similar symptomatology hints at common pathophysiological mechanism (Sylvester et al., 2012). To understand these mechanisms, one must turn to the brain. Regions that regulate cognitive and emotional processing, such as the prefrontal cortex (PFC) and the hypothalamus, the control panel of the central nervous system (CNS), have come at the forefront of this research (Fischer, 2021; McEwen et al., 2016).

The hypothalamus is located in the diencephalon, above the pituitary gland. Structurally and based on developmental data, the hypothalamus can be divided into three subregions, namely the alar and basal hypothalamus and the hypothalamic floor plate (Schröder et al., 2020). The hypothalamus plays a central role in the homeostatic regulation of the neuroendocrine system, controlling various physiological tasks, including temperature and circadian rhythm regulation,

reproduction, endocrine system function, and food intake (Shimogori et al., 2010). This region has also been implicated in behavioral and stress response regulation, which is achieved through activation of the hypothalamic-pituitary-adrenal (HPA) axis. The HPA axis is characterized by a cascade of endocrine pathways which respond to negative feedback loops (Sheng et al., 2021). Under stress, corticotropin-releasing factor (CRF) is produced in the hypothalamus, stimulating the production of ACTH from the anterior pituitary which in turn stimulates corticosterone and cortisol release from the adrenal glands (Kageyama et al., 2021). The release of these two glucocorticoids into the bloodstream is what creates the negative feedback needed to suppress the HPA axis, causing the physiological recovery from stress (Kageyama et al., 2021). Hyperactivity of the HPA axis leads to increased synthesis and release of CRF, with CRF-containing neurons interacting with serotonergic and noradrenergic systems, which appear to be involved in the pathophysiology of mood and anxiety disorders (Nemeroff, 2004). Other hypothalamic systems that partake in the regulation of anxiety-related responses are oxytocin, which modulates social cognition and the expression of positive emotions, deficits of which are characteristic for social anxiety (Leppanen et al., 2017) and thyrotropin-releasing hormone, which activates the release of thyroid-stimulating hormone in the pituitary, which in turn stimulates the release of thyroid hormones (Fischer, 2021). Given that anxiety symptoms such as nervousness, palpitations and perspiration are also prevalent in hyperthyroidism, a link between the thyroid gland and anxiety disorders has been proposed (Fischer & Ehlert, 2018).

The PFC is located at the very front of the brain, at the frontal lobe. It is not as much of a region as it is a collection of structurally and functionally different subdomains, which include in mice the dorsomedial PFC, ventromedial PFC, and ventrolateral PFC (Le Merre et al., 2021). The main roles of the PFC include the regulation of working memory, executive function, self-regulatory and goal-oriented behavior, as well as stress responses (McEwen & Morrison, 2013). For this reason, the PFC contributes to the organization and regulation of emotion (Dixon et al., 2017), which is why its dysfunction is implicated in the etiology of mood disorders such as depression (Drevets et al., 2008) and anxiety (Bishop et al., 2004). Additionally, the PFC mediates anxiety disorders through its connections with limbic cortical regions such as the amygdala and the brainstem. These regions underlie emotional and psychological regulation and convey information about environmental threats, dysfunction of which leads to anxiety-related symptoms (Kenwood et al., 2022).

1.2.3. The high anxiety-related behavior (HAB) mouse model

The molecular etiology of mood disorders can be elucidated using animal models which intend to replicate the general physiological and behavioral phenotypes of said disorders in humans (Campos et al., 2013). In rodents, behavior, which constitutes the basis for anxiety phenotypes, can be assessed using a battery of tests (EPM, dark-light box (DaLi), or OFT) (Steimer, 2011). Tests assessing depression-like behavior (forced swim test (FST)) or sociability (social preference-avoidance test (SPAT)) can also be included, due to the high comorbidity with depression in humans

who suffer from anxiety disorders (Kalin, 2020) and the anxiety-driven impact on social behavior (Wu et al., 2013).

Creating a rodent model for the study of anxiety can take place in various ways. One method is to use animal models of trait anxiety, where selective breeding guarantees the inheritance and enhancement of this trait and improves the chances of uncovering the neurobiological basis of anxiety (Singewald, 2007; Steimer, 2011). Other methods include the use of genetic tools, such as transgenic or knockout rodents where anxiety candidate genes have been manipulated, or rodents transfected with viruses or short interfering RNA silencing (siRNA), to study specific gene products. Quantitative trait loci studies, where chromosomal regions associated with target traits are measured as continuous variables, or DNA microarrays for the identification of genes that are all expressed at the same time in the same tissue type, have also been applied (Jacobson & Cryan, 2010).

Krömer et al. first described a high (HAB), normal (NAB) and low (LAB) anxiety-related behavior mouse model (Krömer et al., 2005). CD1 mice were selectively and bidirectionally bred for anxiety after being behaviorally tested on the EPM at 7 weeks of age. Mice that preferred to spend more time in the closed arms of the EPM were mated, to establish the HAB mouse line and, accordingly, mice that preferred to spend more time in the open arms of the EPM were mated to establish the LAB mouse line. CD1 mice that exhibited intermediate behavior on the EPM were used, to establish the NAB mouse line. Details about each line's performance on the EPM are shown in Figure 1.

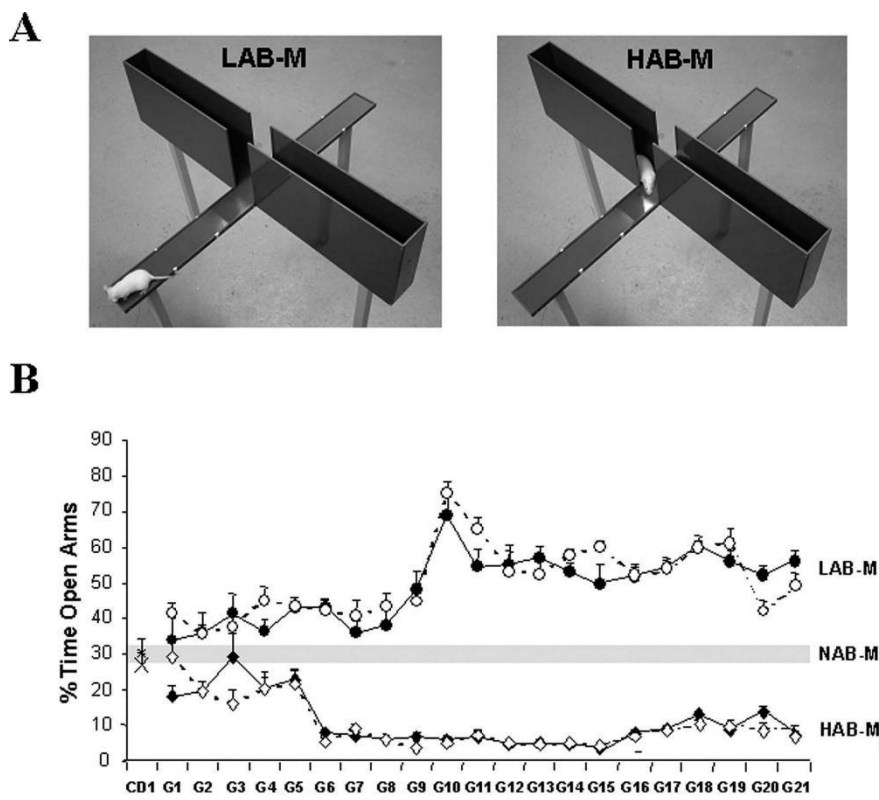


Figure 1. (A) HAB mice prefer to spend more time in the closed arms of the EPM, whereas LAB mice prefer to explore the open arms. (B) HAB and LAB mice show a difference in the percentage of time spent in the open

arms of the EPM, emphasizing the difference in anxiety-like behavior. HAB and LAB female animals are displayed in the graph as white circles or diamonds, respectively, and HAB and LAB male animals are highlighted as solid black circles or diamonds. HAB: high anxiety-related behavior, LAB: low anxiety-like behavior, NAB: normal anxiety like behavior, EPM: elevated plus maze; G: generation (Ditzen et al., 2006).

Aside from the differences on the EPM, HAB and LAB mice also exhibited behavioral extremes in other tests assessing anxiety- and depression-like behavior, namely on the DaLi test, with HAB mice spending less time in the lit compartment of the box than NAB or LAB mice, on the open arm exposure test, with HAB mice dipping their heads less than NAB or LAB mice, on the ultrasound vocalization test, with HAB mice emitting more ultrasound vocalizations than the NAB or LAB mice, and on the tail suspension test (TST) and FST, where HAB mice spent more time being immobile than the NAB or LAB mice, which is indicative of depression-like behavior (Krömer et al., 2005). The molecular underpinnings of these behavioral alterations are observed on both a proteomic and a metabolic level. Proteomics and metabolomics analyses showcased differences in multiple metabolic pathways, such as the inositol pathway, the tricarboxylic acid (TCA) cycle, amino acid and pyruvate metabolism as well as processes related to oxidative stress and detoxification, apoptosis, and neurotransmission (Ditzen et al., 2006; Filiou et al., 2011a; Filiou et al., 2014; Krömer et al., 2005; Zhang et al., 2011).

1.3. Mitochondria

1.3.1. “The powerhouse of the cell”

The mitochondrion, best known as the energy capital of the cell, is a product of the integration of an endosymbiotic α -proteobacterium into a host cell, ancestor of the modern eukaryote. This transition from endosymbiotic bacterium to organelle required numerous evolutionary changes, hundreds of new genes, creation of protein import systems, gene transfers, and the integration of metabolism and reproduction (Roger et al., 2017). However, the role of mitochondria extends far beyond just energy production through aerobic respiration, as they are also involved in ion and redox homeostasis, apoptosis and programmed cell death, signaling, immunity and inflammation as well as numerous metabolic processes (Dawson & Dawson, 2017; Filiou & Sandi, 2019).

Unlike other cellular organelles, mitochondria carry their own genome. Mitochondrial DNA (mtDNA) is small, similar to bacterial plasmid DNA, with a structure and gene organization that is highly conserved among mammals (Taanman, 1999). MtDNA is a closed-circular, double stranded DNA molecule that is about 16.6 kb long. The two strands can be differentiated into the heavy (H-strand) and the light (L-strand) strand depending on their G+T base composition. MtDNA is polycistronic, which means that both the H- and the L-strand encode genes, which are 37 in total: 13 protein components of oxidative phosphorylation (OXPHOS) complexes, 22 tRNAs, and 2 large and small rRNA subunits (Garcia et al., 2017). The mitochondrion conducts its DNA replication, transcription and translation independently than the nucleus, using enzymes and factors that are

predominantly nuclear-encoded, as are most of its mitochondrially located proteins, which is why the mitochondria are dubbed “semi-autonomous” organelles (Taanman, 1999).

The mitochondrial proteome is made up of over 1,000 proteins, with the exact number varying across species (Garcia et al., 2017). Of these, the most known ones are involved in carbohydrate metabolic machinery. Carbohydrate metabolism starts at the cytoplasm with glycolysis; however, glycolysis is highly connected with mitochondria, since the glycolytic pathway is responsible for oxidizing glucose into pyruvate, which under aerobic conditions gets transported into the mitochondrial matrix either to be further oxidized and react with Coenzyme A to produce acetyl-CoA, or to be carboxylated and form oxaloacetate (Vakifahmetoglu-Norberg et al., 2017). Glycolytic enzymes include, among others, hexokinase 2 (HK2), phosphorylating glucose into glucose-6-phosphate, glyceraldehyde-3-phosphate dehydrogenase (GAPDH), which catalyzes the reversible oxidative phosphorylation of glyceraldehyde-3-phosphate, a-enolase (ENO1), which converts 2-phosphoglycerate to phosphoenolpyruvate, and pyruvate kinase liver type (PKLR), which produces pyruvate from phosphoenolpyruvate (Berg et al., 2015). Under anaerobic conditions, pyruvate gets converted into lactate by lactate dehydrogenase (LDHB). Metabolites enter the TCA cycle via distinct pathways, where substrates are interconverted, producing reducing power in the form of NADH and FADH₂ and energy in the form of ATP (Ferne et al., 2004). TCA cycle enzymes include citrate synthase (CS), which converts oxaloacetate to citrate, isocitrate dehydrogenase 1 (IDH1), which produces α -ketoglutarate and CO₂ from isocitrate, and succinate dehydrogenase A (SDHA), which oxidizes succinate to produce fumarate (Berg et al., 2015). NADH and FADH₂, the reducing equivalents produced from the TCA cycle are used by the mitochondrial electron transport chain (ETC) to power the ATP synthase complex of OXPHOS and produce energy for the cell (Reichert & Neupert, 2004).

OXPHOS consists of the four ETC multi-subunit respiratory complexes (complexes I-IV), with an ATP synthase making up the fifth complex (complex V). Complexes I-IV create an electrochemical proton gradient across the inner mitochondrial membrane (IMM) which complex V then uses to produce ATP, the energy currency of the cell (Chaban et al., 2014). Individually, each complex takes on a different role; complex I, or NADH dehydrogenase, is responsible for binding the NADH substrate and transferring two electrons to the bound ubiquinone. Complex II, or succinate dehydrogenase, also transfers electrons to ubiquinone, but this time through the oxidation of succinate. Complex III, or cytochrome c oxidoreductase, exists in the membrane as a dimer, and oxidizes ubiquinone to pump protons to the intermembrane space. Complex IV, or cytochrome c oxidase, accepts electrons from cytochrome c (CYTC) to deliver them to an oxygen molecule, converting it to two H₂O and pumping four protons to the intermembrane space. Finally, complex V or ATP synthase, uses the energy stored as a proton gradient to convert ADP into ATP, coupling the oxidative phosphorylation process of complexes I-IV with energy production (Berg et al., 2015; Chaban et al., 2014).

Electron leaks from the ETC as well as after the impact of stressors like hypoxia, nutrient unavailability, cytokine stimulation or membrane potential alterations lead to the production of reactive

oxygen species (ROS) (Spinelli & Haigis, 2018). ROS refers to molecules that derive from molecular O₂, such as hydrogen peroxide (H₂O₂), the superoxide anion (O₂⁻) or the hydroxyl radical (·OH), that in moderate cellular concentrations contribute to redox and metabolic regulation through protein-protein signaling (Sies & Jones, 2020). However, increased ROS concentrations lead to oxidative stress, harming lipids, proteins, DNA, and RNA molecules and contributing to cellular death (Filiou & Sandi, 2019). To counteract oxidative stress, cells employ antioxidant enzymes, whose role is to scavenge ROS and interconvert them, to protect against ROS-produced molecular damage. These enzymes include catalase (CAT), which prevents the accumulation of H₂O₂ by turning it to O₂ and H₂O, glutathione reductase (GSR), which reduces oxidized glutathione (GSH), superoxide dismutase 1 and 2 (SOD1 and 2, respectively, with SOD1 being a cytoplasmic isoform and SOD2 a mitochondrial isoform), which convert superoxide into O₂ and H₂O₂, and peroxiredoxins (PRX), a family of six peroxidases that neutralize reactive oxygen and nitrogen species (Lee & Park, 2021).

Mitochondria could not function without mitochondrial membrane transport/import systems, which ensure correct import translocation and sorting of all nuclear-encoded mitochondrial proteins (Baker et al., 2007). The gateway of all proteins into the mitochondrion is the translocase (TOM) of the outer mitochondrial membrane (OMM), a multi-protein complex which mediates import into the intermembrane space (Bauer et al., 2000). Import into the mitochondrial matrix requires coordination with the translocase of the IMM (TIM), consisting of two multi-protein sub-complexes: TIM23, the main component of TIM, and TIM22, with each one differing in their specificity for pre-cursor protein substrates (Bauer et al., 2000; Pfanner & Geissler, 2001). Another important component in this machinery is the mitochondrial carrier family (solute carrier family 25, or else SLC25), responsible for the transportation of solute molecules like amino acids, nucleotides, ions, or fatty acids across the IMM (Ruprecht & Kunji, 2020). One of the amino acid carriers, SLC25A12 or ARALAR, is responsible for carrying aspartate/glutamate across the IMM, contributing to the function of the malate-aspartate shuttle, gluconeogenesis and myelin synthesis (Palmieri et al., 2001; Ruprecht & Kunji, 2020). Another SLC family is the SLC56 family, or the sideroflexin (SFXN) family of mitochondrial transporters. Their exact role is elusive, but they are thought to be metabolite transporters which are implicated in iron homeostasis and utilization inside the mitochondrion (Tifoun et al., 2021). A notable SFXN member is SFXN1, an IMM protein implicated in serine transportation across the membrane with roles in coenzyme Q, α-ketoglutarate and one-carbon metabolism (Acoba et al., 2021).

1.3.2. Mitochondrial dynamics: Biogenesis, Fusion, Fission, and Mitophagy

The way mitochondria function and respond to stimuli depends on their complex and dynamic structure. Their morphology is defined by two membrane systems, the IMM and the OMM, which are separated by the intermembrane space (IMS). The two membranes meet at specific contact sites and fold inward, creating the cristae. Depending on cellular needs, the two membrane systems undergo changes, altering the number and structure of the mitochondria in events that are collectively called mitochondria dynamics. The term describes reshaping, rebuilding and recycling processes that affect

mitochondrial stability, abundance, distribution and quality, allowing for compensatory changes to occur when cells face a challenge (Eisner et al., 2018). The four dynamics processes, which are biogenesis, fusion, fission and mitophagy, are explained below and schematically shown in Figure 2.

Mitochondrial Biogenesis

Mitochondria cannot be created *de novo*, therefore when there is increased energy demand in the cells, the biogenesis process is jumpstarted (Popov, 2020). It is a tightly regulated process which requires the coordination of both mitochondrial and nuclear factors for the transcription and translation of every mitochondrial proteome component. The key players in this process are two nuclear-encoded proteins: peroxisome proliferator-activated receptor-gamma coordinator 1 alpha (PGC1A) and mitochondrial transcription factor A (TFAM). PGC1A is the master regulator of biogenesis, whose activation by growth signals or energy deprivation triggers the activation of a series of nuclear transcription factors like nuclear respiratory factor 1 and 2 (NRF1 and NRF2, respectively), which in turn increase TFAM expression (Popov, 2020; Zhang & Xu, 2016). TFAM is the final effector of mtDNA replication and transcription, responsible for initiating mitochondrial transcription and compacting the mitochondrial genome (Kang et al., 2018). Both PGC1A and TFAM are biogenesis markers, with TFAM also regulating mtDNA copy number (mtDNA_{cn}), a marker for the measurement of mitochondrial content and health in the cells (Filograna et al., 2021).

Mitochondrial Fusion

The term mitochondrial fusion refers to the process of merging two or more mitochondria to create a larger organelle. Fusion is a GTPase-driven process, with three proteins playing the leading role: mitofusin 1 and 2 (MFN1 and MFN2, respectively), and optic atrophy 1 (OPA1). MFNs tethered on the surface of both fusing organelles are required for the event to take place, forming homo- or hetero-oligomers and depending on GTP hydrolysis for the effective fusion of the OMM (Gao & Hu, 2021). Once it is complete, OPA1 on one IMM bind in *trans* with cardiolipin on the other IMM and facilitated by heterotypic interactions of long and short OPA1 isoforms and GTP hydrolysis, the two IMMs are fused together (Quintana-Cabrera & Scorrano, 2023). OPA1 is also responsible for shaping the cristae and helping tie the mtDNA to the IMM (Yapa et al., 2021), while MFN2 splice variants also mediate mitochondrial interactions with the endoplasmic reticulum (Naon et al., 2023). Due to the brain's high energy demand, dysfunction in the fusion machinery primarily affects the neurons, with mutations in *OPA1* causing autosomal dominant optic atrophy, a form of inherited childhood blindness, and mutations in *MFN2* causing Charcot-Marie-Tooth disease type 2a, characterized by progressive distal sensory and motor neuron impairments (Westermann, 2010). MFN2 has also been implicated in behavior, with differential levels of the gene or protein being noted with relation to anxiety- or depression-like behavior as well as social behavior (Gebara et al., 2021; Ghosal et al., 2023).

Mitochondrial Fission

Mitochondrial fusion and fission are two antagonistic events in the cell, but while fusion seeks to join two mitochondria, fission seeks to divide one mitochondrion into two. Fission removes damaged or dysfunctional mitochondria via mitophagy and contributes to metabolic regulation,

increasing the cell's mitochondrial content when there are increased energy demands (Tilokani et al., 2018; Yu et al., 2023). There are two types of fission, depending on cellular needs: midzone fission leads to the proliferation of the mitochondria, whereas peripheral fission enables damaged material to be degraded through mitophagy (Kleele et al., 2021). Both fissions are mediated by key fission proteins dynamin-related protein 1 (DRP1) and dynamin 2 (DNM2), responsible for constriction and scission of the mitochondrion. If the fission site is at the midzone, mitochondrial fission factor (MFF) along with mitochondrial dynamics protein 49 and 51 (MID49 and MID51, respectively) recruit DRP1 to the surface for fission to occur in a GTP-dependent manner (Samangouei et al., 2018; Yu et al., 2023). If the fission site is at the periphery, then DRP1 is recruited by mitochondrial fission 1 protein (FIS1), and the mitochondrial product is then degraded in a lysosomal manner (Ihenacho et al., 2021; Quintana-Cabrera & Scorrano, 2023). SLC25A46, an SLC25 family member is located in the OMM (Perivolidi et al., 2022), and it plays a role in fission, because deletion in its expression promotes mitochondrial hyperfusion and abnormal architecture (Duchesne et al., 2017; Steffen et al., 2017; Terzenidou et al., 2017). Fission is crucial for proper metabolic function, with dysregulation in its machinery implicated in metabolic diseases such as diabetes (Yoon et al., 2011) as well as neurodegenerative conditions such as Parkinson's disease (Youle & Van Der Bliek, 2012).

Mitochondrial Mitophagy

Mitophagy is a form of autophagy that involves selectively targeting and engulfing mitochondria for degradation by the lysosomes (Killackey et al., 2020). It gets activated by either dysfunctional mitochondria, which cannot be salvaged with other quality control methods, or superfluous mitochondria (Palikaras et al., 2018). There are multiple mitophagy regulators, with each one responding to different intracellular or environmental stimuli, and they all work in perfect harmony to coordinate a fine-tuned mitochondrial quality control (Borboldis & Palikaras, 2022). However, the most extensively studied mitophagy is the phosphatase and tensin homologue (PTEN)-induced putative kinase protein 1 (PINK1) and E3 ubiquitin ligase Parkin (PRKN). The dissipation of the membrane potential from damaged mitochondria triggers the accumulation of PINK1 on their surface. There, it activates PRKN, and ubiquitin molecules attach to OMM proteins and are recognized and degraded by the proteasome, leading to mitochondrial degradation (Borboldis & Palikaras, 2022). Dysfunction in the mitophagy machinery has been linked with major neurodegenerative diseases, such as early onset Parkinson's disease (Yapa et al., 2021) or Alzheimer's disease (Fang et al., 2019).

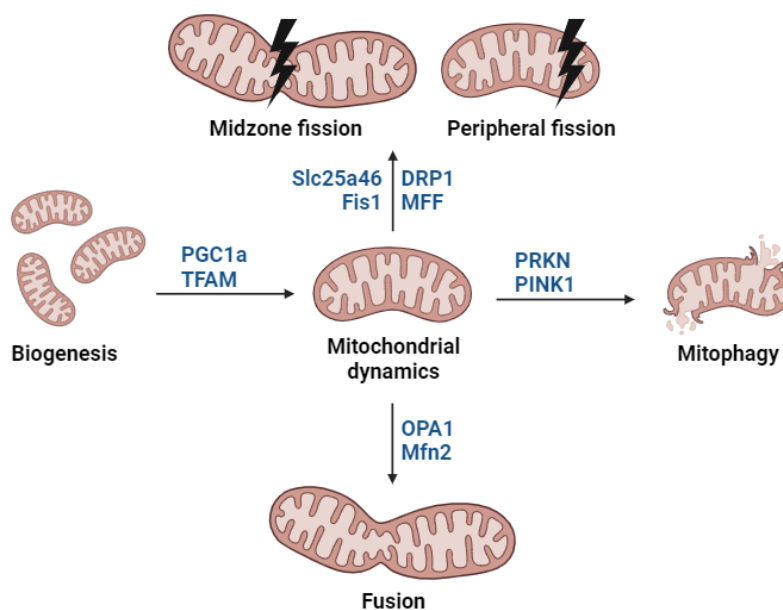


Figure 2. Schematic representation of the events encompassed by the term mitochondrial dynamics. The four processes are: mitochondrial biogenesis, fusion, fission and mitophagy. Main protein players for each process are displayed on each arrow. The figure was created with BioRender.com.

1.3.3. Mitochondria in anxiety research

The brain only takes up about 2 to 3% of the human body’s mass, and yet, it needs the highest amount of energy, consuming 20% of our oxygen and 25% of our glucose (Pei & Wallace, 2018). Given how the mitochondria are at the epicenter of energy metabolism, it is to be expected that most of the weight of the brain’s high energy demand falls on them (Filiou & Sandi, 2019). Additionally, the stress response, jump started by the HPA axis, is aimed at reinstating homeostasis after the trigger of a stressor. This whole-body process that engages numerous systems is collectively called allostasis (De Kloet et al., 2005). If this stress response is prolonged or excessive, it becomes pathological, and therefore it can be dubbed as allostatic load, a somewhat paradoxical concept which explains that the same mediators responsible for helping the body and the brain adapt to stress can also be pathological when dysregulated (Picard & McEwen, 2018). Given that any homeostatic disruption (and therefore, any allostatic state) requires energy for the equilibrium to be reinstated, neuropsychiatric disorders such as anxiety, which are exacerbated by chronic stress, are also energetically taxing for the body (Filiou & Sandi, 2019). All these have led to the establishment of a mitochondria-centric theory on anxiety. Further insight into the bidirectional relationship between mental disorders and mitochondria will help elucidate the physiological underpinnings of anxiety disorders (Daniels et al., 2020).

Since mitochondria play a key role in the etiology of psychiatric disorders, researchers have been looking into mitochondria-driven alterations in behavior and biology during early life environmental interventions. Numerous studies have investigated the impact negative early life interventions have on the mitochondria, with the findings indicating that this organelle is sensitive to the early life stress (ELS)-driven programming of the brain (Hoffmann & Spengler, 2018). Early life

stress causes alterations of the mitochondrial content as indicated by mtDNAcn (Picard & McEwen, 2018), the cellular metabolic and respiratory machinery (McCoy et al., 2016), and the redox equilibrium (Marković et al., 2017). Previously in our lab, to understand how positive early life interventions impact adult behavior and possibly mitochondrial processes, we applied an EH protocol on HAB male mice. After observing that EH exerts an anxiolytic effect on these mice, we found a notable mitochondrial involvement in the EH-driven molecular alterations, with multiple metabolic and mitochondrial dynamics-related genes and proteins having differential levels on multiple brain regions of HAB EH male mice (Thomou et al., 2024). This indicates that mitochondria mediate the molecular effects of early life interventions.

1.4. The gender dimension

Our lab's earlier findings concerning the mitochondrial background of EH have contributed to the elucidation of how the behavioral profile of handled animals correlates with their biology. However, so far this study has only focused on HAB male mice, and little is yet known about how EH affects HAB females.

1.4.1. Females in psychiatric research

Historically, psychiatric research has sidelined women, and it was not until 1992 that a mandate was established by the NIH to ensure their inclusion (Mastroianni et al., 1994). The reason for that exclusion pertained to the belief that women are more difficult to study than men, due to the hormonal variations of their menstrual cycle, and worries that the incorporation of women of reproductive age would have lasting effects on their future offspring (Hodes & Epperson, 2019; Mastroianni et al., 1994). Despite the imposed mandate, however, preclinical studies, which predominantly use animal models, continued to exclude females, as no such mandate was in place for animals. Even after the dawn of the 21st century, data showed that a male bias was prominent in 8 out of the 10 biological fields that were investigated in literature published on 2009 (Beery & Zucker, 2011). Interestingly, the highest bias was found in neuroscience research, with single-sex male studies outnumbering those of females 5.5 to 1 (Beery & Zucker, 2011). These numbers had slightly decreased by 2017, with 52% of the literature examined using both males and females (Mamlouk et al., 2020).

These statistics appear paradoxical considering women are twice as likely to be diagnosed with anxiety disorders and depression (Bekker & van Mens-Verhulst, 2007; Palanza, 2001). Aside from the statistical discrepancy, there is also a gender gap regarding the presentation, course of illness and treatment response to both medication and therapy (Palanza, 2001; Pavlidi et al., 2022). Additionally, anxiolytic drugs, developed mostly on male animal models are not always effective for women. In fact, in the field of pharmacology, adverse reactions to medical treatment are higher in women than they are in men, which can be attributed to gender differences in pharmacokinetics and pharmacodynamics that are not accounted for at the time of drug development (Franconi et al., 2007;

Soldin & Mattison, 2009). For this reason, it is essential for more inclusive steps to be made in neuroscientific research, so the gender gap in science can truly be bridged.

1.4.2. The sexually dimorphic brain: Truth or a myth?

As much as it is interesting to understand gender-driven discrepancies in behavior and mood disorder research, it is also worth looking into how they are translated on a brain level. Contrary to popular belief, the brain is not fully “male”, or “female” (Joel, 2011). A 2015 study analyzing the MRIs of more than 1,400 human brains showed that there is extensive overlap in the gray matter, white matter and measures of connectivity distributions for men and women, meaning that the sexually dimorphic brain hypothesis, which would be based on little overlap of these features, is not accurate (Joel et al., 2015). It would be more accurate to refer to a mosaic brain, that is, a brain with one component with a form that is typical for females and another component whose form is typical for males (Joel & Fausto-Sterling, 2016).

Even though early in development the brain depends on gonadal hormones to be shaped into a “male-typical” or “female-typical” phenotype, to simplify brain development like this and underestimate the impact of other factors would be limiting (McCarthy, 2016). The effect environmental factors have on brain structure and function, either through epigenetics or more complex, behavior-driven mechanisms, has been shown in rodent models to reverse, abolish, create, or exaggerate sex differences in specific brain characteristics (Joel, 2011). Acute stress exposure affected spine density of the hippocampus in opposite directions for male and female rats while simultaneously having no effect on the somatosensory cortex (Shors et al., 2001). Additionally, maternal stress led to sex-driven effects for males and females; males were more prone to experience early onset schizophrenia or other neurodegenerative diseases such as Alzheimer’s disease, while the same adversity’s effect for females showed up later in life as an increase in schizophrenia and depression-related diagnoses (Bale & Epperson, 2017). That is not to say that males and females do not exhibit differences in their stress response. Female rodents prefer more passive coping strategies in response to stress, such as increased immobility time in the TST or the FST (Mueller & Bale, 2008), which in humans translates to resorting more often to dysfunctional ways of coping, such as self-blame, venting anger, and presenting more depressive symptoms (Hanninen & Aro, 1996). Behavior is gender-specific, and so are selected brain characteristics and molecular signatures. However, deducing the brain of men and women as inherently male or female would be reductive, so instead, it would be more precise to study sex as a biological variable in context, with methods that consider the heterogeneity of the brain as a whole.

1.4.3. Females in EH research

In the context of EH, studies that do include both male and female rodents often find no sex-dependent alterations, pooling results from both sexes together (Beane et al., 2002; Garoflos et al., 2005; Garoflos et al., 2007; Meaney et al., 1985). However, discrepancies have been observed, with

most studies referring to rats. Considering behavior, the investigation of latent inhibition after the EH paradigm application on both male and female Wistar rats showed that even though both sexes developed latent inhibition, only males showcased it (Weiner et al., 1985). Also, handled female Wistar rats exhibited different exploration patterns than handled males on the hole-board apparatus, a test assessing anxiety-like behavior, with females head-dipping more than males (Weinberg et al., 1978). In a study done only on female Sprague-Dawley rats, handled animals exhibited decreased emotionality on the EPM and also had blunted reactions to a two-way active avoidance test compared to the control group, which confirmed that EH reduces emotionality and reactivity during adulthood (Nunez et al., 1995). Lastly, EH had a protective effect on female Wistar rats subjected to prenatal stress, reversing the anxiogenic behavior that was observed on the EPM (Bogoch et al., 2007).

On a neurobiological level, EH lowered CREB and BDNF levels in the olfactory bulb of handled female Wistar rats, proteins that are responsible for the transcription of factors involved in memory formation (Reis et al., 2014). This alteration was not observed on handled males, which instead had an increase of BDNF in their olfactory bulb (Reis et al., 2014). In the hippocampus of handled female Wistar rats, decreased GSH peroxidase activity and total thiol content, a marker of oxidative imbalance, were noted, alterations that were not observed in males (Noschang et al., 2020). Additionally, mRNA expression levels of AMPA receptors were sexually dimorphic in different brain regions of male and female Wistar rats. In the hippocampus, *glua1* mRNA levels were increased in handled male rats but decreased in females, *glua4* mRNA density was also higher in males but lower in females following the EH paradigm (Katsouli et al., 2014). In the amygdala, *glua2* mRNA levels were decreased in females but had no differences in males (Katsouli et al., 2014). A different study assessing the mRNA levels of NMDA receptors showed that the *nr2b* subunit only was increased in handled Wistar females but not in males, suggesting sex-specific, EH-driven mediation of brain plasticity (Stamatakis et al., 2009). Finally, the impact of EH on sexual maturation and the neuroendocrinological phenotype was investigated, and it was found that EH delayed puberty and attenuated blood corticosterone levels in response to ether stress for female Sprague-Dawley rats (Sieck & Ramaley, 1975). Lower corticosterone levels were also observed in handled female rats subjected to active avoidance learning, but after comparing corticosterone levels to those of handled males, females had a decreased corticosterone response altogether, indicating higher resilience for females (Weinberg & Levine, 1977). Additionally, for handled female Wistar rats, EH reduced plasma progesterone concentration (Gomes et al., 2006) and other estrus-related hormone concentrations such as estradiol, luteinizing hormone, luteinizing-hormone-releasing hormone, follicle-stimulating hormone, as well as prolactin, effects which may explain the reduced sexual receptiveness that was also noted (Gomes et al., 2005). Further elucidation of the sex-driven discrepancies between the impact of EH on male and female rodents will help unravel how the two sexes differ in anxiety-related behavior.

1.5. Proteomics

1.5.1. What is proteomics?

The concept of a “proteome” was first proposed by Marc R. Wilkins in 1995 to describe the full protein content that is expressed by a specific genome, a cell, or a tissue type (Wilkins et al., 1996). The study of the proteome, or else proteomics, was initiated to examine large-scale gene expression and provide a better understanding of an organism as a whole. Proteomics can provide information about the interactions, functions, compositions, roles, and structures of proteins in order to help elucidate the complex pathways and networks that control cell function and provide therapeutic solutions to pathological conditions (Al-Amrani et al., 2021; Wilkins et al., 1996).

The methodology to generate such results has evolved over the 30 years since its introduction, as has experimental technology. Conventional proteomics analysis methods include immunohistochemistry staining, chromatography-based techniques, two-dimensional gel electrophoresis (2-DE) or two-dimensional differential gel electrophoresis (2D-DIGE), or enzyme-linked immunosorbent assays (Cui et al., 2022). To decrease analysis time and increase accuracy and depth of proteome coverage, high-throughput methods were introduced, such as tissue microarray, protein pathway array and mass spectrometry (MS) (Aslam et al., 2017; Cui et al., 2022). Of these, MS is the tool most often used, and it is usually combined with other separation methods to simplify the complex biological samples prior to analysis and increase yields (Yates et al., 2009). The most common techniques here are 2-DE as a gel-based separation method, or shotgun proteomics/liquid chromatography–tandem MS (LC-MS/MS) as a gel-free method with increased accuracy and sensitivity (Martins-de-Souza et al., 2010).

The quantification of each protein’s concentration in a given proteome would generate useful information for the overall state of the proteome and allow for comparisons to be made between groups. This is where quantitative proteomics methods step in, with the most common approaches being either label-free proteomics methods or labeling-based methods (Yates et al., 2009). Label-based methods normally insert stable isotopes (^2H , ^{13}C , ^{15}N , ^{18}O) into peptides or proteins and compare them with unlabeled ones, whereas with label-free methods assumes that the chromatographic peak area of any peptide corresponds to its concentration (Filiou et al., 2011b).

1.5.2. Proteomics in psychiatric research

Psychiatric disorders display a complex symptomatology which is attributed to complex etiology. Therefore, the identification of candidate biomarkers and subsequently, novel therapeutics, is not as straightforward as one would think. The discovery of a single differentially expressed protein, which could have potential as a candidate biomarker, is not possible in psychiatric research due to complex etiology that underlies each psychiatric disorder (Filiou et al., 2011b). Therefore, the discovery of a set of differentially expressed proteins, whose existence in the same dataset could more represent a behavioral or pathological phenotype, could be of use (Filiou et al., 2011b). Additionally, since the symptoms each psychiatric condition displays are not always heterogeneous, there is a certain degree of overlap and comorbidity between mental disorders, which hinders

biological research (Comes et al., 2018). It must also be noted that animal models only recapitulate aspects of specific disorders, such as schizophrenia or bipolar disorder, because their behavioral phenotype is complex enough that animal models cannot properly represent human conditions (Martins-de-Souza et al., 2010). A proteomics approach could help expand the scope of psychiatric research, since the identification and quantification of multiple proteins offers insight into specific biological processes or protein interactions which by extent could explain the pathological underpinnings of common disorders (Martins-de-Souza et al., 2009). The subsequent validation of proteomics-identified candidate biomarkers using other techniques, such as protein arrays or biochemical assays would help pave the way for the application of novel therapeutics for the treatment of mental disorders (Martins-de-Souza et al., 2011).

1.5.3. Proteomics in anxiety research

MS-based proteomics approaches have been utilized to study anxiety disorders, mainly through the utilization of rodent models. NMRI mice crossbred with MG15 mice were bred for many generations to have anxiety-like behavior based on their anticipatory anxiety behavior when handled; mice that approached the experimenter's hand were bred for normal-to-low anxiety-like behavior, while mice that never volunteered to be handled were bred for anxiety-like behavior (Szego et al., 2010). 2D-DIGE proteomics in total brain samples showed that proteins involved in processes like synaptic transmission, signal transduction, protein biosynthesis, carbohydrate, nucleotide, as well as lipid metabolism were differentially expressed (Szego et al., 2010). In the HAB-LAB mouse model of anxiety developed by Kromer et al., 2D SDS PAGE proteomics found that the detoxification enzyme glyoxalase 1 (GLO1) was decreased in multiple brain regions of HAB compared to LAB mice, namely the hypothalamus, the amygdala and motor cortex, as was enolase phosphatase, an enzyme associated with energy production (Ditzen et al., 2006; Krömer et al., 2005). In the cingulate cortex of this same mouse anxiety model, a labeling-based MS proteomics analysis revealed a molecular network of anxiety-related alterations between HAB and LAB mice, at the center of which laid mitochondrial processes, implicating a mitochondria-driven hypothesis for anxiety-like behavior (Filiou et al., 2011a). Further analysis showed that the inositol pathway was also implicated in the anxiety phenotype, as were oxidative stress-related pathways and carbohydrate-metabolism processes such as the TCA cycle (Zhang et al., 2011). 2-DE electrophoresis followed by LC-MS/MS evaluation in the hippocampus of rats exposed to prenatal stress and displaying an anxiety-like phenotype in adulthood caused differential expression of proteins involved in signal transduction, synaptic vesicles, protein synthesis, and energy metabolism, results that are in line with previously mentioned findings (Mairesse et al., 2012). Lastly, in a chronic mild stress rat model, an intervention that induces anxiety- and depression-related behaviors in rodents in order to mirror the effects of chronic stress on humans, label-based MS proteomics showed that neurological processes, such as signaling-, secretion- and synapse-related functions, as well as mitochondrial and metabolic processes were differentially

expressed in the hippocampus of these animals (Tang et al., 2019), findings that were mirrored in the PFC too (Liao et al., 2021).

These findings indicate that proteomics-based approaches are beneficial for the elucidation of the molecular mechanisms of anxiety disorders. However, to date, no such proteomics application for the investigation of the EH-driven impact. A system-based approach will allow for a better understanding of the alterations that EH induces on a molecular level, helping to unravel and contribute to the decades-old research for probable anxiety biomarkers.

2. AIM OF THE STUDY

Previous research in our lab has highlighted the effects of EH on HAB male mice at both behavioral and molecular levels (Thomou et al., 2024). As seen on the DaLi test, EH exerts an anxiolytic effect in these animals. Biology-wise, in the hypothalamus, altered expression levels for proteins involved in carbohydrate metabolism and mitochondrial dynamics were observed, while on the PFC, the mRNA expression levels of mitochondrial dynamics players were altered, indicating that the mitochondria are heavily implicated in the molecular underpinnings of EH.

In this thesis, we asked how does EH impact HAB female mice. To answer this question:

- We reported the behavioral impact of EH on HAB female mice.
- We investigated the molecular underpinnings of the EH-driven impact on behavior, and, encouraged by our previous results on HAB EH male mice, investigated the extent to which the mitochondria are involved in these underpinnings.
- We analyzed non-targeted LC-MS/MS proteomics data to understand on a systemic level the correlation between EH, behavior and neurobiology.

To achieve our aim, we conducted the following analyses:

- In the hypothalamus of HAB EH vs. HAB NH female mice:
 - An LC-MS/MS proteomics analysis at the Biomedical Sciences Research Center (B.S.R.C.) “Alexander Fleming” was conducted by Dr. Samiotaki Martina and analyzed by us to look for the overrepresentation of pathways relevant to the mitochondria.
 - We searched for alterations in the mRNA expression levels of genes involved in mitochondrial dynamics.
 - We assessed the mtDNAcn, to derive results about the content and quality of mitochondria.
- In the PFC of HAB EH vs HAB NH female mice:
 - We searched for alterations in the expression levels of proteins involved in carbohydrate metabolism, OXPHOS, mitochondrial dynamics, antioxidant defense, and mitochondrial transport/import.
- In the plasma of HAB EH vs HAB NH female mice:
 - We looked for alterations in oxidative stress.
 - We assessed the expression levels of proteins involved in carbohydrate metabolism and antioxidant defense.

3. Materials and Methods

3.1. Animals - EH paradigm

Breeder mice for HAB and NAB lines were tested at 8 weeks on the Elevated Plus Maze test (EPM) to ensure that they maintain their line-specific and anxiety-related behaviors. Mice from both groups were then mated, and as soon as pregnancy was observed, the males were removed from the breeding cages. The pregnant females were left undisturbed until birth (PND 0 for the pups). All animals were kept in type 3 macrolone cages under normal conditions (12 h light/12 h dark cycle with lights on at 6:30 am, temperature 21-25 °C, humidity at 60%, food and tap water ad libitum). All mouse work was done in the animal facility of the University of Ioannina, having been accepted by the local authorities and conducted according to the European Communities Council Directives 2010/63/EU.

On PND 0, HAB and NAB litters were randomly assigned into two groups, the early handling (EH) group and the non-handling (NH) group which was the control. For the EH group, pups were separated from their dam for 15 min per day and kept in a smaller box in a different room for the duration of the intervention. The protocol lasted from PND 1 to PND 14. NH mice only received standard animal facility rearing care change during this time, from PND 8 on and once a week for cage change. This weekly cage change was also performed for the EH group. After weaning, on PND 31, the social preference-avoidance test (SPAT) was performed, and when animals reached adulthood, the other behavioral tests (DaLi, OFT and FST) were conducted to assess anxiety- and depression-like behavior between the two experimental groups.

On PND 70, all mice were weighed, anesthetized using isoflurane and decapitated for the subsequent collection of brain and blood samples. The three brain regions of interest namely the prefrontal cortex (PFC), the hypothalamus and the hippocampus were dissected according to the mouse brain atlas (Paxinos & Franklin, 2019), snap-frozen in liquid nitrogen, weighed, and stored in -80 °C until further analysis. Trunk blood was collected in EDTA coated tubes, from which plasma was then isolated by centrifugation at 1300 g for 10 min at 4 °C by PhD student Papageorgiou Maria. Responsible for animal work, namely mice breeding, the EH protocol, behavioral testing and analysis was research technician Nussbaumer Markus and former diploma thesis student Grammenou Elena. Previous work in our lab focuses on the comparison between HAB EH and HAB NH male mice, where an anxiolytic effect was observed (Thomou et al., 2024). In this thesis, we focus on the comparison between HAB EH and HAB NH female mice. We do not discuss behavioral or molecular alterations between NAB EH and NAB NH mice or lineage-related (HAB versus NAB mice) alterations. The brain regions studied in this thesis are the hypothalamus and the PFC only, as work on the hippocampus was conducted by diploma student Panteli Eirini. The assays used on each of the two brain regions as well as the plasma are shown in Table 1.



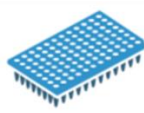
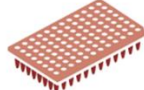

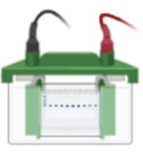

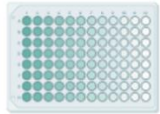
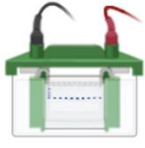
Brain region/ Sample type	Assay
	   <p>Label-free, LC-MS/MS proteomics IN SILICO ANALYSIS</p> <p>qRT-PCR</p> <p>qPCR (mtDNAcn)</p>
	 <p>Western Blot</p>
 <p>PLASMA</p>	  <p>TAC Assay</p> <p>Western Blot</p>

Table 1. Schematic representation of the assays used on each brain region as well as plasma samples. HYP: hypothalamus, PFC: prefrontal cortex, LC-MS/MS: liquid chromatography, tandem mass spectrometry, qRT-PCR: quantitative, reverse transcriptase PCR, TAC: total antioxidant capacity. Table was created with BioRender.com.

3.2. Protein Extraction

PFC tissue samples of HAB EH (n = 12) and HAB NH (n = 11) female mice were used for protein extraction. 0.1% w/v of RIPA lysis buffer (150 mM, 1% NP-40, 0.5% Sodium Deoxycholate, 0.1% SDS, 50 mM Tris-HCl pH = 8) containing 0.01% v/v protease/phosphoprotease inhibitor cocktail (Sigma-Aldrich, Darmstadt, Germany) was added to each sample followed by homogenization using green pestles. Homogenates were left in ice for 10 min and then were sonicated in a Branson Digital Sonifier (Marshall Scientific, Hampton, USA) at 35% for 10 sec. Samples were then centrifuged at 10,000 g for 10 min at 4 °C, the supernatants were collected in pre-labelled tubes and finally they were stored at -80 °C until analysis.

3.3. Bradford Assay

The protein concentration of each PFC sample was assessed by the Bradford Assay. For the standard protein curve, Bovine Serum Albumin (BSA) (Biosera, Cholet, France) was used, diluted to a concentration of 1 mg/mL in PBS. Different concentrations of BSA were diluted with dH₂O and measurements of their absorbance at $\lambda = 595$ nm were conducted in a Spectro UV-11 (MRC Ltd, Holon, Israel) under dim light conditions. Concentrations of BSA making up the standard curve are shown in Table 2. Once the R² of the curve was > 0.98, sample measurements were conducted. Two

μL of brain lysate were diluted with 48 μL of dH_2O and measured quickly after adding 950 μL of Bradford Solution (100 mg Coomassie, 50 mL Ethanol 100%, 100 mL Orthophosphoric Acid 85%) due to the photosensitivity of the solution. All standard curve BSA dilutions and PFC protein samples were measured in duplicates and the concentration of each sample was estimated using the average of its measured absorbance and the equation formed by the standard curve.

BSA (μL)	dH_2O (μL)	Bradford (μL)
5	45	950
10	40	950
15	35	950
20	30	950
25	25	950
30	20	950

Table 2. BSA (1 $\mu\text{g}/\text{mL}$) dilutions used for the construction of the standard curve in the Bradford Assay.

3.4. Western Blot

To determine the levels of expression for proteins of interest on the PFC and the plasma, western blot was used. First, Sodium Dodecyl Sulphate-Polyacrylamide Gel Electrophoresis (SDS-PAGE) was conducted to separate the protein content of each sample based on their molecular weight. The polyacrylamide gel for the electrophoresis consisted of two parts of different acrylamide concentration: the first part was the stacking gel, responsible for lining up the proteins of all samples, and the second part was the separating gel, responsible for separating the proteins. Each gel's concentration and ingredients are shown in Table 3. Stacking and separating gels concentrations were selected based on the molecular weight range of our proteins of interest. For proteins between 17-100 kDa, a 5% stacking gel and a 12% separating gel were used.

Reagents	Stacking gel 5%
dH_2O	1.7 mL
30% acrylamide	415 μL
Tris-HCl 0.5 M pH = 6.8	315 μL
10% SDS	25 μL
10% APS	25 μL
TEMED	2.5 μL

Reagents	Separating gel 12%
----------	--------------------

dH ₂ O	1.6 mL
30% acrylamide	2 mL
Tris-HCl 1.5 M pH = 8.8	1.3 mL
10% SDS	50 µL
10% APS	50 µL
TEMED	2 µL

Table 3. *Ingredients of the stacking 5% and separating 12% gel used for SDS-PAGE electrophoresis of proteins for the PFC and plasma of HAB EH and HAB NH animals. Information about the concentrations and volumes used for each gel are displayed above. The final volume of each gel was adjusted according to the size of electrophoresis chamber used and subsequently, the number of samples for each analysis.*

For the brain samples, PFC protein lysates of HAB EH (n = 12) and HAB NH (n = 11) were diluted with RIPA lysis buffer containing a 0.01% v/v protease/phosphoprotease inhibitor cocktail (Sigma-Aldrich) and 25% v/v SDS loading buffer (3/4 Tris base 0.5 M pH = 6.8, 20% w/v SDS, 20% v/v Glycerol) so as each sample would contain 15 µg of protein. Samples were denatured in a heatblock (Thermomixer Comfort, Eppendorf, Hamburg, Germany) for 5 min at 95 °C before being loaded onto the stacking gel. If the Mitoprofile antibody cocktail was used, which is responsible for the immunodetection of protein subunits of OXPHOS complexes, heat denaturation was not performed, because the manufacturers' instructions advise against it. Electrophoresis was run in a 26-well Criterion™ Cell Chamber (Bio-Rad, Hercules, CA, USA) with 1x Running Buffer pH = 8.3 (Tris base 25 mM, glycine 250 mM, SDS 0.1%) at 90 V for 30 min and 150 V for 2.5 h (EV 233, Consort, Turnhout, Belgium). After electrophoresis was completed, the stacking gel was discarded and the separating gel was incubated with a nitrocellulose membrane (Macherey-Nagel, Düren, Germany) in 1x Transfer Buffer pH = 8.3 (Tris base 25 mM, Glycine 192 mM, 20% Methanol). Protein electrotransfer was performed with wet transfer in a Criterion™ Blotter (Bio-Rad) at 100 V/250 mA for 1.5 h in ice, with the setup of the gel/membrane sandwich being: fiber pad, three Whatman filter paper sheets (Whatman, Maidstone, United Kingdom), gel, membrane, three Whatman filter paper sheets and another fiber pad. After electrotransfer, the gel was stained with Coomassie staining buffer (0.125% Coomassie, 50% Methanol, 10% Acetic Acid), while the nitrocellulose membrane was stained with Ponceau staining solution (Ponceau S, Biotium, San Francisco, CA, USA), to ensure equal protein loading and successful protein transfer. Afterwards, the membrane was washed with Tris-Buffered Saline (TBS) buffer containing 0.1% Tween 20 (TBS-T), then it was blocked with 5% non-fat dry milk diluted in TBS-T for 1.5 h and lastly, it was incubated overnight at room temperature with the primary antibodies. The following day, the membrane was washed three times for 5 min each with the TBS-T buffer under gentle rocking, and then incubated for 2 h with the secondary antibody in room temperature. After the incubation, three more washes with TBS-T buffer followed and antibody

signal was detected using 1 mL of ECL Millipore chemiluminescence Forte (Millipore, Burlington, MA, USA) for 5 min in the dark. Signal intensity was visualized in a ChemiDoc™ XRS and quantified with the ImageLab Software (version 5.0.0.27863, Bio-Rad). One HAB EH and two HAB NH PFC samples were not used in all western blots due to low protein lysate volume.

For plasma samples, 0.75 µL of plasma of HAB EH (n = 7) and HAB NH (n = 7) female mice were diluted with dH₂O and 25% v/v SDS loading buffer. Samples were denatured as described above and loaded onto the stacking gel. Electrophoresis ran in a 15-well Mini Trans-Blot™ Cell Chamber (Bio-Rad) with 1x Running Buffer at 90 V for 30 min and 150 V for 2.5 h. Proteins from the separating gel were electrotransferred with wet transfer onto a nitrocellulose membrane using a Mini Trans-Blot™ Cell Chamber (Bio-Rad) at 100 V/250 mA for 1.5 h in ice. The gel and membrane were stained with Coomassie and Ponceau stain as described above, the membrane was blocked for 1.5 h with 5% non-fat dry milk in TBS-T buffer and incubated with the primary antibody overnight at room temperature. Prior to the secondary antibody incubation the next morning, the membrane was washed 3x with TBS-T buffer, and immunodetection proceeded using 0.5 mL of Millipore chemiluminescence Forte (Millipore) and antibody signal was detected with the Chemidoc™ XRS system. Quantification of the signal was conducted on the ImageLab software (version 5.0.0.27863, Bio-Rad).

All antibodies used for the western blots are shown on Table 4.

Function	Name	Full protein name	Manufacturer	Dilution	Secondary antibody
OXPHOS	Mitoprofile	CI complex: NDUFB8 CII complex: SDHB CIII complex: UQCRC2 CIV complex: MTCO1 CV complex: ATP5A	MS604 (Abcam)	1:1000	Anti-mouse (#170-6516, Bio-Rad)
	CYTC	Cytochrome c	sc-13156 (Santa Cruz Biotechnology)	1:800	Anti-mouse (#170-6516, Bio-Rad)
Antioxidant defense	GSR	Glutathione Reductase	sc-133245 (Santa Cruz Biotechnology)	1:500	Anti-mouse (#170-6516, Bio-Rad)
	PRX	Peroxioredoxin	sc-137222 (Santa Cruz Biotechnology)	1:200	Anti-mouse (#170-6516, Bio-Rad)
	CAT	Catalase	sc-271803 (Santa Cruz Biotechnology)	1:500	Anti-mouse (#170-6516, Bio-Rad)

	PRDX3	Peroxiredoxin 3	ab16751 (Abcam)	1:2000	Anti-mouse (#170-6516, Bio-Rad)
	SOD2	Superoxide Dismutase 2	sc-137254 (Santa Cruz Biotechnology)	1:200	Anti-mouse (#170-6516, Bio-Rad)
Glycolysis	ENO1	Alpha-enolase	sc-100812 (Santa Cruz Biotechnology)	1:200	Anti-mouse (#170-6516, Bio-Rad)
	GAPDH	Glyceraldehyde-3- Phosphate Dehydrogenase	sc-32233 (Santa Cruz Biotechnology)	1:500	Anti-mouse (#170-6516, Bio-Rad)
	HK2	Hexokinase 2	22029-1-AP (Proteintech)	1:15000	Anti-rabbit (20402-1, BIOTIUM)
	PKLR	Pyruvate Kinase, Liver	sc-166228 (Santa Cruz Biotechnology)	1:800	Anti-mouse (#170-6516, Bio-Rad)
Glycogen metabolism	GSK3B	Glycogen synthase kinase-3 beta	9315 (Cell Signaling Technology)	1:500	Anti-rabbit (20402-1, BIOTIUM)
Lactate metabolism	LDHB	Lactate dehydrogenase B	NB110-57160 (NOVUSBIO)	1:2000	Anti-rabbit (20402-1, BIOTIUM)
TCA cycle	CS	Citrate synthase, mitochondrial	GTX110624 (GeneTex)	1:1000	Anti-rabbit (20402-1, BIOTIUM)
	IDH1	Isocitrate dehydrogenase	12332-1-AP (Proteintech)	1:1000	Anti-rabbit (20402-1, BIOTIUM)
	SDHA	Succinate dehydrogenase	sc-98253 (Santa Cruz Biotechnology)	1:500	Anti-rabbit (20402-1, BIOTIUM)
Fission	DRP1	Dynamin-1-like protein	sc-271583 (Santa Cruz Biotechnology)	1:500	Anti-mouse (#170-6516, Bio-Rad)
	SLC25A46	Mitochondrial outer membrane solute carrier protein	12277-1-AP (Proteintech)	1:500	Anti-rabbit (20402-1, BIOTIUM)

	MFF	Mitochondrial Fission Factor	17090-1-AP (Proteintech)	1:500	Anti-rabbit (20402-1, BIOTIUM)
Biogenesis	PGC1a	Peroxisome proliferator-activated receptor Gamma Coactivator-1 alpha	66369-1-Ig (Proteintech)	1:2000	Anti-mouse (#170-6516, Bio-Rad)
Fusion	MFN2	Mitofusin 2	12186-1-AP (Proteintech)	1:2000	Anti-rabbit (20402-1, BIOTIUM)
	IMMT	Mitofilin	10179-1-AP (Proteintech)	1:10000	Anti-rabbit (20402-1, BIOTIUM)
	OPA1	Optic atrophy 1	66583-1-Ig (Proteintech)	1:500	Anti-mouse (#170-6516, Bio-Rad)
Transport/Import	SFXN1	Sideroflexin 1	12296-1-AP (Proteintech)	1:1000	Anti-rabbit (20402-1, BIOTIUM)
	TIM23	Mitochondrial import inner membrane translocase 23	611222 (BD Biosciences)	1:500	Anti-mouse (#170-6516, Bio-Rad)
	ARALAR	Solute carrier family 25 number 12	sc-271056 (Santa Cruz Biotechnology)	1:1500	Anti-mouse (#170-6516, Bio-Rad)
	PNPT1	Polynucleotide Phosphorylase 1	14487-1-AP (Proteintech)	1:1000	Anti-rabbit (20402-1, BIOTIUM)

Table 4. Primary antibodies used for all western blots of this thesis. Information about the protein name, the manufacturer, the dilution used and the secondary antibody required for each one are depicted above.

3.5. Total Antioxidant Capacity (TAC) Assay

TAC was measured in plasma samples from all HAB EH (n = 22) and HAB NH (n = 21) female animals as previously described (Ciuti & Liguri, 2017). 50 µL of each plasma sample were used for the assay. A chromogenic reagent was used for the determination of TAC. Details for the reagent's ingredients are shown in Table 5. Plasma samples and GSH (0.1 mM), which was used as a calibrator, were mixed with the pre-heated at 37 °C reagent in a microplate and absorbance (ABS) was determined at 630 nm in a microplate reader (UT 2100C, MRC Ltd, Holon, Israel). Measurements

were conducted after the reagent was dispersed in two different time points, first at 20 sec (T1) and then at 120 sec (T2). TAC for plasma was calculated according to the following equation:

$$GSH_{eq} \left[\frac{mmol}{L} \right] = \left\{ \frac{[ABS(T2) - ABS(T1) \text{ sample}]}{[ABS(T2) - ABS(T1) \text{ GSH}]} \right\} \times GSH \text{ concentration} \left[\frac{mmol}{L} \right]$$

Reagent ingredients	V(final) = 10 mL
0.1 M phosphate buffer pH = 8.3	7.5 mL
EtOH 100%	1.77 mL
100 mM EDTA	500 µL
H ₂ O for injection	176.5 µL
Thesit (0.5 g/5 mL)	30 µL
DCIP (5 mg/500 µL)	23.5 µL

Table 5. TAC chromogenic reagent ingredients with information about their concentration and volumes for a demonstrative final volume of 10 mL. The final volume of the reagent is determined according to the number of samples meant for the TAC assay.

3.6. DNA and RNA extraction

DNA and RNA extraction from the hypothalamus of HAB EH (n = 9) and HAB NH (n = 8) female mice was conducted using the NucleoSpin® RNA/DNA Buffer set (Macherey-Nagel, Düren, Germany) combined with the NucleoSpin® RNA kit (Macherey-Nagel). Extraction steps were followed according to the manufacturer's instructions. Briefly, hypothalamus samples that were previously stored in -80 °C were homogenized with lysis buffer (buffer RA1 and b-Mercaptoethanol) and filtered through NucleoSpin® Filters by centrifugation to increase clarity. Ethanol 70% was added to adjust the nucleic acid's binding conditions, the lysates were loaded to NucleoSpin® RNA columns and centrifuged. The nucleic acids that were collected were used for DNA isolation, which was conducted by washing the samples twice with the DNA wash solution and centrifuging them to get rid of impurities. The NucleoSpin® RNA columns were dried for 3 min and the kit's DNA elution buffer was applied to collect the DNA samples, which were then stored in -20 °C. For the RNA isolation, the NucleoSpin® RNA columns used previously for the DNA extraction were incubated with the rDNase reaction mixture for 15 min and then washed once with the RAW2 buffer and twice with the RA3 buffer followed by centrifugation to purify the ribonucleotides. RNA was collected by elution with RNase-free H₂O and centrifugation twice to increase the RNA yield. RNA samples were stored in -80 °C. Concentration of all DNA and RNA samples was determined by quantification through Nanodrop (Thermo Fisher Scientific, Waltham, MA, USA). Three HAB NH DNA samples were not used for further analysis due to low DNA concentration.

3.7. DNA Electrophoresis

To assess the quality of the DNA extracted from the hypothalamus samples of HAB EH (n = 9) and HAB NH (n = 5) female mice as mentioned above, agarose gel electrophoresis was used. For the electrophoresis, 0.8% Agarose was added to 1x Tris base, Acetic Acid and EDTA (TAE) buffer and left to melt at 170 °C under constant stirring. When the gel solution was homogenous, it was left to cool in a water bath until the agarose temperature was approximately 65 °C. 12% Ethidium Bromide was subsequently added, for the staining and the visualization of DNA. The agarose gel was poured onto the casting apparatus and a 20-well comb was placed for the creation of the wells. The gel was left to set for 30 min at room temperature. 200 ng of DNA of each hypothalamus sample were diluted with H₂O and 20% v/v loading buffer and loaded onto the agarose gel along with the DNA ladder, prepared according to the manufacturer's instructions. In brief, 1 µL of Lambda DNA/Hind III Marker (Thermo Fisher Scientific) was diluted with 4 µL dH₂O and heated for 5 min at 65 °C for the better separation of the bands. The ladder was cooled in ice for 3 min and 20% v/v loading buffer was added before loading the ladder to the gel. DNA electrophoresis was run for 60 min at 90 V. Detection of assessment of the bands was conducted through UV imaging.

3.8. Quantitative PCR (qPCR) – Mitochondrial DNA copy number (mtDNAcn)

Hypothalamic DNA samples from HAB EH (n = 9) and HAB NH (n = 5) female mice were used for the determination of mtDNAcn through qPCR. DNA samples, primers and reagents for the qPCR were placed in ice. All preparatory steps for the assay were conducted in a PCR UV cabinet which was sterilized with UV light and cleaned with Ethanol 70% and chlorine before and after every use. DNA samples were diluted with PCR-grade H₂O so that each reaction would contain 20 ng of DNA. Master mixes for the polymerization reaction were then prepared, using the appropriate primers and the KAPA SYBR fast qPCR Universal kit (Kapa Biosystems, Potters Bar, UK) according to the manufacturers' instructions. Master mix and diluted DNA sample volumes were loaded on a FrameStar® Break-A-Way PCR plate (4titude, Wotton, UK) which was placed on an ice rack to maintain a cool temperature and avoid activation of the master mix enzymes. Each reaction contained 6 µL of master mix (5 µL KAPA SYBR buffer and 0.5 µL of each primer, forward and reverse) and 4 µL of DNA. The plate was sealed with a Q-stick™ qPCR Seal (4titude) and centrifuged at 1200 rpm for 2 min at 4 °C. Polymerization reactions were performed in a CFX Connect™ Optics Module thermocycler (Bio-Rad) and the appropriate thermal protocol was applied according to the PCR kit instructions and the primer melting temperature. The thermal protocol applied can be seen in Table 6. Each sample had two technical replicates, and a mitochondrial (*Nd1*, mtDNA) gene and a nuclear (*Mapk*, nDNA) gene were simultaneously quantified for the determination of the relative expression of mitochondrial DNA. MtDNAcn was calculated using the 2^{-ΔCt} method (Rosenberg et al., 2023) and comparing the 2^{-ΔCt} values of HAB EH samples with the values of HAB NH samples. The primer sequences used for this qPCR are displayed in Table 8.

Step	Temperature	Time
Initial denaturation and polymerase activation	95 °C	10 min
Denaturation	95 °C	45 cycles/15 sec each
Annealing	59 °C	45 cycles/1 min each
Elongation (melting curve analysis)	65 °C	5 sec
Denaturation	95 °C	50 sec
Cooling	4 °C	10 min/forever

Table 6. Thermal protocol applied for the determination of the mtDNAcn for hypothalamus samples of HAB EH and HAB NH female mice. Cycling conditions (temperature and time) are displayed above.

3.9. Quantitative, Reverse Transcriptase PCR (qRT-PCR)

Hypothalamic RNA samples from HAB EH (n = 9) and HAB NH (n = 8) female mice were used for the determination of mRNA levels of genes of interest. RNA samples, reagents and primers were placed in ice. All preparatory steps for the assay were conducted in a PCR UV cabinet which was sterilized with UV light and cleaned with Ethanol 70% and chlorine before and after every use. RNA samples were diluted with PCR-grade H₂O so that each reaction would contain 20 ng of RNA. Master mixes for the polymerization reaction were then prepared according to the manufacturer's instructions using the KAPA SYBR fast one-step qRT-PCR Universal kit (Kapa Biosystems) containing the reaction buffer and the reverse transcriptase (RT) mixture, and the appropriate primers. Master mix and RNA samples were loaded on a FrameStar® Break-A-Way PCR plate (4titude) which was placed on an ice rack to maintain a cool temperature and avoid activation of the master mix enzymes. Each reaction contained 6.2 µL of master mix (5 µL KAPA SYBR buffer, 0.5 µL of each primer, forward and reverse, and 0.2 µL RT) and 3.8 µL of RNA. The plate was sealed with an optically clear windowed qPCR Seal (Azenta Life Sciences, Burlington, MA, USA) and centrifuged at 1200 rpm for 2 min at 4 °C. Polymerization reactions were performed in a CFX Connect™ Optics Module thermocycler (Bio-Rad) and the appropriate thermal protocol was applied according to the PCR kit instructions and the primer melting temperatures. The thermal protocol applied can be seen on Table 7. Each sample had two technical replicates and relative expression of genes was calculated using the 2^{-ΔCt} method by comparing the 2^{-ΔCt} values of HAB EH samples with the values of HAB NH samples. The primer sequences used for this qPCR are displayed in Table 8. Signal Recognition Particle 14 (*srp14*) was used as the reference gene for all qRT-PCR reactions.

Step	Temperature	Time
RT reaction and cDNA synthesis	42 °C	5 min
Initial denaturation and polymerase activation	95 °C	4 min

Denaturation	95 °C	35 cycles/2 sec each
Annealing	X °C	35 cycles/20 sec each
Elongation (melting curve analysis)	65 °C	5 sec
Denaturation	95 °C	50 sec
Cooling	4 °C	10 min/forever

Table 7. Thermal protocol applied for qRT-PCRs conducted on hypothalamus samples of HAB EH and HAB NH female mice. Cycling conditions (temperature and time) are displayed above. Annealing temperature (shown as X) is determined according to the melting temperature of each set of primers.

Function	Primer	Full gene name	Forward (F') primer sequence	Reverse (R') primer sequence	Product length (bp)	Melting temperature (Tm)
MtDNAcn	<i>nd1</i>	Mitochondrially Encoded NADH Ubiquinone Oxidoreductase Core Subunit 1	(F') CCCAGCTACTA CCATCATTCAA GT	(R') GATGGTTTGG GAGATTGGTT GATGT	117	59 °C
	<i>mapk1</i>	Mitogen-Activated Protein Kinase 1	(F') GCTTATGATAA TCTCAACAAAG TTCG	(R') GATGTTCTCAT GTCTGAAGCG	126	59 °C
Reference gene	<i>srp14</i>	Signal Recognition Particle 14	(F') CAGCGTGTTT ATCACCTCAA	(R') GGCTCTCAAC AGACACTTGTT TT	109	60 °C
Biogenesis	<i>tfam</i>	Mitochondrial transcription factor A	(F') TCCACAGAAC AGCTACCCAA	(R') CCACAGGGCT GCAATTTTCC	89	61 °C
	<i>pgc1a</i>	Peroxisome proliferator-activated receptor gamma coactivator 1-alpha	(F') GTAAATCTGCG GGATGATGG	(R') ATTGCTTCCGT CCACAAAA	145	60 °C

Fission	<i>fis1</i>	Mitochondrial Fission Factor	(F') CAAAGAGGAA CAGCGGGACT	(F') CAAAGAGGAA CAGCGGGACT	95	61 °C
	<i>mff</i>	Mitochondrial Fission 1 protein	(F') TCGGGTCTGT CCTCCCCATA	(F') TCGGGTCTGT CCTCCCCATA	145	60 °C
	<i>dnm2</i>	Dynamin 2	(F') CAGGTGGAGA CCATCCGTAAC	(R') GGTAAGCCAG CAGCTCATGG	142	60 °C
	<i>mid51</i>	Mitochondrial Dynamic Protein Of 51 Kda	(F') GGAAGCCTCA GGTGAGCAAT	(F') GGAAGCCTCA GGTGAGCAAT	134	60 °C
	<i>gdap1</i>	Ganglioside Induced Differentiation Associated Protein 1	(F') CACCCAGGTT AATGCCCGAT	(R') GCATAAGCGG GGATCATGGA	151	59 °C
	<i>drp1</i>	Dynamin-related protein 1	(F') TGACCAAAGTA CCTGTAGGCG	(R') GCATCAGTACC CGCATCCAT	229	59 °C
Fusion	<i>mfn2</i>	Mitofusin 2	(F') CTGTGCCAGC AAGTTGACAT	(R') TTCCTGAGCA GTTTGGCTCT	113	60 °C
	<i>msto1</i>	Misato Mitochondrial Distribution And Morphology Regulator 1	(F') CATTATGATGC CACTCTGCC	(R') TGCTTCTGCTG TCACCACCT	159	60 °C
Mitophagy	<i>pink1</i>	PTEN induced kinase 1	(F') GTGGACCATC TGGTTCAGCA	(R') TGAGTCCCAC TCCACAAGGA	75	60°C
	<i>prkn</i>	E3 ubiquitin-protein ligase parkin	(F') AAGAAGACCA CCAAGCCTTG TC	(R') CAAACCAGTG ATCTCCCATGC	157	60°C
OXPHOS	<i>mt-nd1</i>	Mitochondrially Encoded NADH Ubiquinone	(F') GGATGAGCCT CAAACCTCAA	(R') GGTCAGGCTG GCAGAAGTAA		60 °C

		Oxidoreductase Core Subunit 1				
--	--	-------------------------------	--	--	--	--

Table 8. Primers used for all quantitative PCRs mentioned in this thesis. Gene names, the primer sequence, the length of each PCR product along with the melting temperature (T_m) of each set (forward, F' , and reverse, R') are shown.

3.10. Label-free, LC-MS/MS Proteomics

Label-free proteomics measurements were conducted for the hypothalamus tissue of HAB EH (n = 5) and HAB NH (n = 5) female mice at the Proteomics facility of the Biomedical Sciences Research Center (BSRC) “Alexander Fleming”, by Dr. Samiotaki Martina, senior researcher and operations specialist, by liquid chromatography-tandem mass spectrometry-based (LC-MS/MS), using a Thermo Q Exactive HF-X Orbitrap Mass Spectrometer (Thermo Scientific, Waltham, MA, USA).

Raw data was analyzed by Samiotaki Martina using the Perseus software (version 1.6.13.0). 1 HAB NH sample was excluded from in silico analysis due to the detection of low protein content during the LC-MS/MS proteomics.

Of all 5503 proteins that were quantified in the hypothalamus of the HAB EH and HAB NH samples with the label-free proteomics approach, 839 of them were found differentially expressed, with 429 of them being upregulated and the rest downregulated in HAB EH vs. HAB NH female mice. This thesis presents results only for the full protein dataset, that is, analysis for the full set of 839 proteins found differentially expressed, and for the upregulated dataset, meaning the 429 proteins found to be upregulated in the HAB EH female mice when compared with the HAB NH mice. Results for the downregulated dataset are the subject of the diploma thesis of Panteli Eirini and are only discussed in her work. All samples had three technical replicates, and subsequent analysis was conducted using the average protein abundance values of each sample for each protein.

3.11. Proteomics: In Silico Analysis

Before the use of in silico programs for the analysis of the proteomics data, upregulated proteins were manually categorized and grouped depending on the processes and pathways they are a part of using protein and gene databases, such as UniProt (uniprot.org) (Bateman et al., 2023), GeneCards (genecards.org) (Stelzer et al., 2016), Mouse MitoCarta 3.0 and Mouse MitoPathways 3.0 (broadinstitute.org/mitocarta) (Rath et al., 2021), as well as KEGG Pathway (genome.jp/kegg) (Kanehisa, 2000).

For an understanding of the molecular functions, biological processes and cellular components that the differentially expressed proteins showcased, two main tools were used, namely STRING (Search Tool for the Retrieval of Interacting Genes/Proteins, string-db.org) (Szklarczyk et al., 2023) and Gene Ontology (geneontology.org) (Aleksander et al., 2023; Ashburner et al., 2000).

Regarding STRING analysis, STRING is a tool responsible for the visualization of protein-protein interactions and the establishment of protein networks within a given dataset. On the database, each protein-protein association stored in STRING is given a confidence score scaled between 0 and 1. The confidence score indicates the estimated likelihood that a given interaction between two proteins has a biological meaning. Degrees of confidence vary, however for our analysis of the datasets we set the minimum interaction score as that of the highest confidence (0.900). The network type chosen was the full STRING network, with the edges indicating both functional and physical protein interactions, and the meaning of network edges was confidence-based, with the line thickness indicating the strength of data support. The active interaction sources selected were experiments and co-expression. Of the STRING image generated, disconnected nodes were excluded from the network to simplify the image and highlight the most prominent clusters showing up. These prominent clusters, indicating key pathways from our proteomics analysis were color-coded and also clustered individually with a separate color-coding system, to shed light on the proteins making up these pathways. The settings used for the generation of the protein-protein interaction networks are shown in Figure 3.

The screenshot shows the STRING database settings interface, divided into two main sections: Basic Settings and Advanced Settings.

Basic Settings:

- Network type:**
 - full STRING network (the edges indicate both functional and physical protein associations)
 - physical subnetwork (the edges indicate that the proteins are part of a physical complex)
- meaning of network edges:**
 - evidence (line color indicates the type of interaction evidence)
 - confidence (line thickness indicates the strength of data support)
- active interaction sources:**
 - Textmining
 - Experiments
 - Databases
 - Co-expression
 - Neighborhood
 - Gene Fusion
 - Co-occurrence
- minimum required interaction score:**
 - highest confidence (0.900)
- max number of interactors to show:**
 - 1st shell: - none / query proteins only -
 - 2nd shell: - none -

Advanced Settings:

- network display mode:**
 - static png (network is a simple bitmap image; not interactive)
 - interactive svg (network is a scalable vector graphic [SVG]; interactive)
- network display options:**
 - Enable node coloring mode
 - enable 3D bubble design
 - disable structure previews inside network bubbles
 - center protein names on nodes
 - show your query protein names
 - hide disconnected nodes in the network
 - hide protein names
 - 12 protein name font size

Figure 3. Settings used for the generation of protein-protein interaction networks in STRING.

After STRING, Gene Ontology was used, to functionally interpret the differentially expressed protein dataset and connect them with Gene Ontology terms. The three functional terms used to associate genes are: Biological Process (BP), Cellular Component (CC), and Molecular Function (MF). First, a PANTHER Overrepresentation test (released 2024-01-17) (Thomas et al., 2022) was conducted, using as the analyzed list the full differentially expressed dataset or only the upregulated dataset, and as a reference list our quantified proteome, that is, the 5503 proteins that were quantified with our proteomics analysis. The reference organism chosen from the list was *Mus musculus*. The two analyzed proteome lists mentioned above were then also analyzed without using a reference list, for a more generalized understanding of our datasets. Bar charts were subsequently generated based

on the relevant results of this analysis, using the $-\log(\text{FDR})$ values taken from the overrepresentation test and plotting them from largest to smallest to highlight the strongest components of each term. Figure 4 depicts the settings used for all GO analyses.

Analysis Type: PANTHER Overrepresentation Test (Released 20240226)

Annotation Version and Release Date: GO Ontology database DOI: 10.5281/zenodo.12173881 (Released 2024-01-17)

Test Type: Fisher's Exact Binomial

Correction: Calculate False Discovery Rate Use the Bonferroni correction for multiple testing No correction

Figure 4. Settings used in PANTHER Overrepresentation Test for the GO analysis of the full differentially expressed dataset and the upregulated dataset.

3.12. Statistical Analysis

Two group comparisons for all molecular data were analyzed on Graphpad Prism 8.0.1 (GraphPad Software, San Diego, CA, USA). Normality was checked by the Shapiro-Wilk test. If data were normally distributed, an unpaired two-tailed t test with Welch's correction was conducted assuming non equal standard deviations. If data were not normally distributed, a non-parametric two-tailed Mann-Whitney test was performed instead.

Correlation analyses were performed for all molecular data with all behavioral parameters, namely: for the DaLi test (time in the light compartment, number of entries to the light compartment and latency to the light compartment), for the OFT (time in the center, number of entries to the center, latency to the center and line crossings), for the FST (time floating, time swimming, time struggling and latency floating) and for the SPAT (total time of interaction and SPA index). Prior to correlation, a normality check was conducted using the Shapiro-Wilk test. If data were normally distributed, Pearson correlation was used, and for non-normally distributed data, the non-parametric Spearman correlation was used instead.

Correlations were also performed for the ten proteins with the highest numerical fold change found on the upregulated dataset of our proteomics results with all behavioral data as mentioned above. Depending on the results of the Shapiro-Wilk normality check either the Pearson or the Spearman correlation was used. The r values from these correlations were then plotted onto correlation matrices on Microsoft 365 Excel, with the X axis showcasing the behavioral tests and the Y axis the proteins. Gradient color-coding was used based on the r value for each correlation, and significant correlations were marked on the matrices with stars on the corresponding box.

Significant results are determined by p value < 0.05 . A trend (T) refers to $0.05 \leq p$ value ≤ 0.1 . All graphs are displayed as mean with \pm SEM unless otherwise specified.

4. RESULTS

4.1. EH exerted anxiolytic effects on adult HAB EH female mice

The EH protocol applied for this thesis is described in Figure 5A (for more details, see section 3.1 of Materials and Methods). Our lab's earlier work on EH had shown that EH exerts an anxiolytic effect for HAB EH vs. HAB NH male mice in the DaLi box, while it has no effect for NAB EH vs. NAB NH male mice (Thomou et al., 2024). Similarly for our female mice, it was observed that EH also has an anxiolytic effect for HAB EH vs. HAB NH female mice, as seen on the time in the light compartment parameter of the DaLi box (Figure 5B). The NAB EH vs. NAB NH comparison for female mice showed no effect in behavior, and for this reason our molecular assays concerned only HAB EH vs. HAB NH female mice. Behavioral characterization and data analysis were done by research technician Nussbaumer Markus, diploma thesis student Grammenou Elena and master's student Thomou Christina. Molecular analysis was conducted in three brain regions in total, the hypothalamus, the PFC, and the hippocampus, as well as in plasma extracted from whole blood. Since the hippocampus is the subject of diploma thesis student Panteli Eirini's work, in this thesis we analyze the results concerning the hypothalamus and the PFC. Details about the assays conducted in each region are displayed in Table 1 of Materials and Methods.

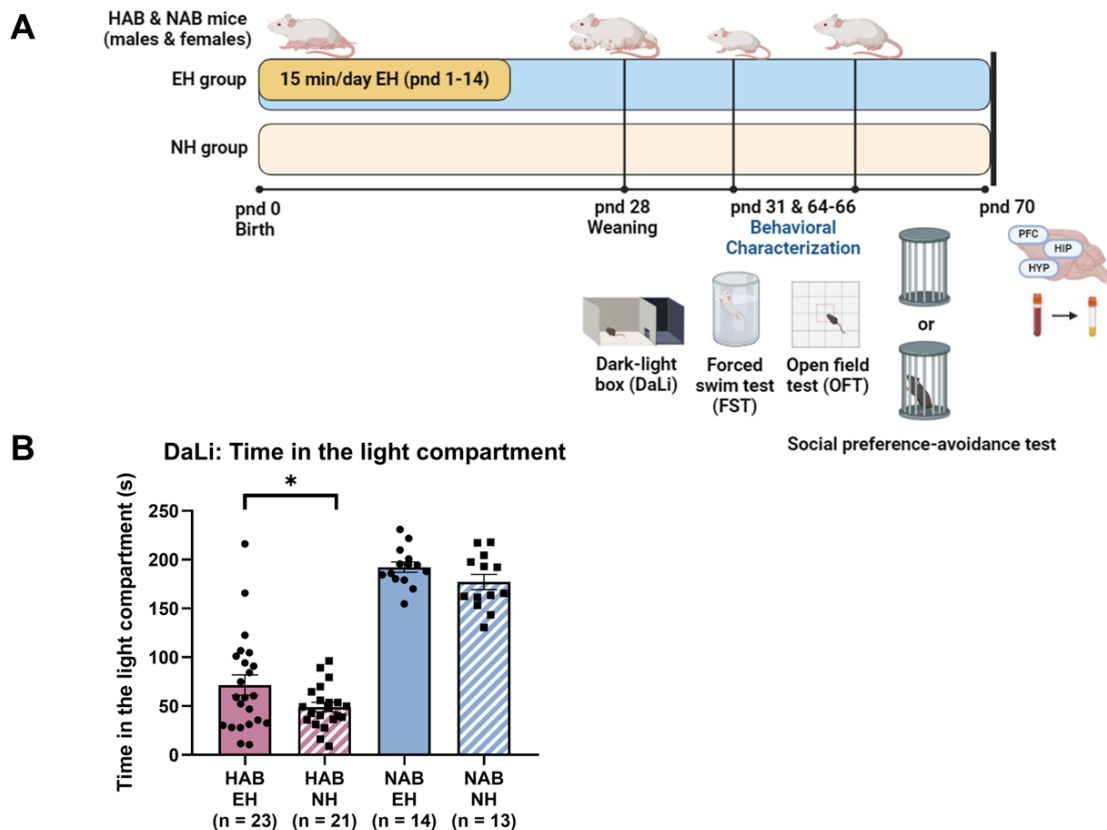


Figure 5. (A) Schematic representation of the early handling (EH) protocol. The 4 animal groups used were: HAB EH (HAB early handling), HAB NH (HAB non handling), NAB EH (NAB early handling), NAB NH (NAB non-handling). The EH paradigm was applied from PND 1 to PND 14. Handling was performed for 15 min per

day by removing the litter from the dam's cage and keeping it in a small box in a separate room for the duration of the protocol. Pups from the NH group were not subjected to the handling procedure. After weaning, on PND 31, SPAT was performed, while DaLi, OFT and FST were performed on PND 64-66. Sampling on PND 70 was performed for the hypothalamus (HYP), the prefrontal cortex (PFC), and the hippocampus (HIP), and plasma was extracted from whole blood samples. The figure was created with BioRender.com. (B) EH induced an anxiolytic effect on HAB EH vs. HAB NH female mice, as seen in the DaLi parameter of time in the light compartment ($*p=0.0328$). Animal work and behavioral characterization was conducted by Nussbaumer Markus and Grammenou Elena.

4.2. HYPOTHALAMUS: Label-free, MS-based proteomics analysis

4.2.1. Overview of our proteomics results – Top ten upregulated protein hits

Our application of the EH protocol on male mice showed that the brain region predominantly affected by the early life intervention was the hypothalamus (Thomou et al., 2024). Therefore, we analyzed the hypothalamus of HAB EH and HAB NH female mice using proteomics. Label-free, LC-MS/MS proteomics analysis was conducted on the hypothalamus of 5 HAB EH and 4 HAB NH female mice at the Proteomics Facility of the Biomedical Sciences Research Center (B.S.R.C.) “Alexander Fleming” by Dr. Samiotaki Martina, senior researcher and operations specialist. Raw data were analyzed by Dr Samiotaki Martina using the Perseus software (version 1.6.13.0), and the list of differentially expressed proteins obtained was used for manual categorization and in silico analysis using online tools (for more details, see section 3.12 of the Materials and Methods).

Of the 5503 proteins quantified in the hypothalamus of 5 HAB EH and 4 HAB NH samples, 839 of them were differentially expressed in HAB EH female mice. Of these proteins, 429 were upregulated and the other 410 were downregulated in HAB EH compared to HAB NH female mice ($FDR<0.05$, $S0>0.1$). The proteins are visualized in the volcano plot of Figure 6A, with blue representing the downregulated proteins and red the upregulated proteins. A list of all the differentially expressed proteins, both upregulated and downregulated, are depicted in Appendix 1.

The differentially expressed proteins were sorted from largest to smallest fold change value, and this way, the top ten upregulated protein hits were pinpointed (Figure 6B). The proteins were: potassium-transporting ATPase alpha chain 1 (ATP4A), adhesion G protein-coupled receptor E1 (ADGRE1), aquaporin-2 (AQP2), mitochondrial acyl-CoA synthetase short-chain family member 3 (ACSS3), creatine kinase M-type (CKM), retinoblastoma-like protein 2 (RBL2), acidic leucine-rich nuclear phosphoprotein 32 family member B (ANP32B), transcobalamin-2 (TCN2), and 6-phosphofructo-2-kinase/fructose-2.6-biphosphatase 1 (PFKFB1).

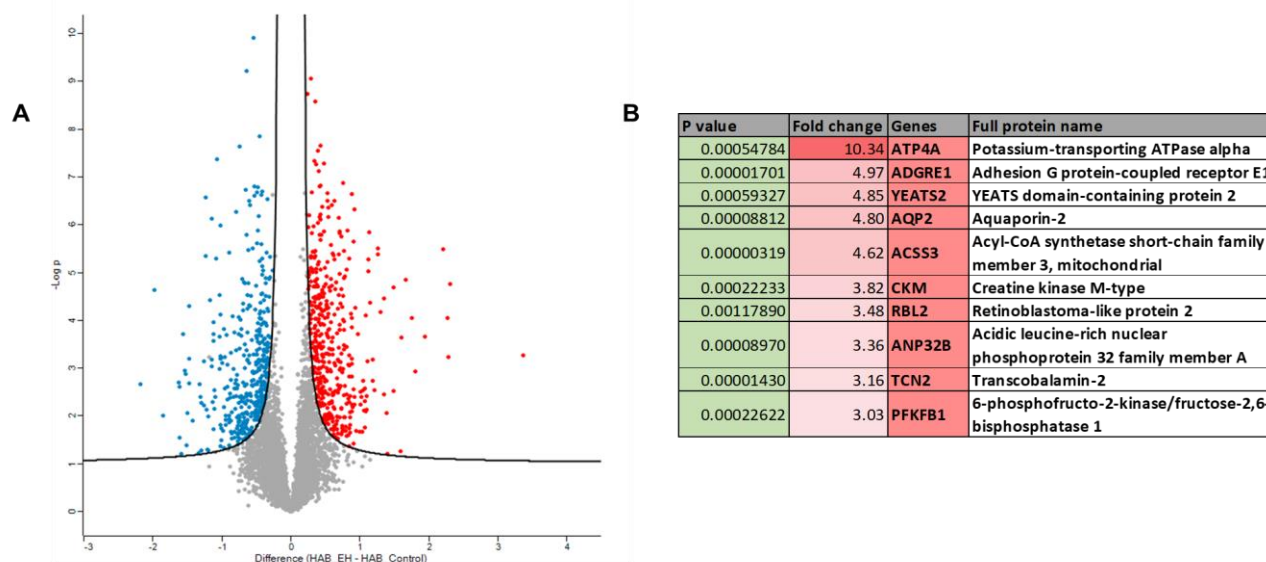
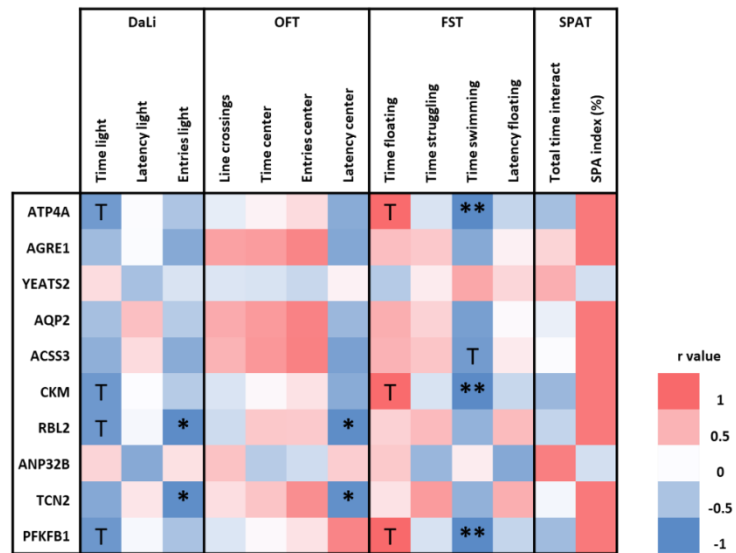


Figure 6. (A) Volcano plot depicting the 5503 proteins quantified with label-free LC-MS/MS proteomics. The Y axis represents the $-\log(P \text{ value})$, and the X axis represents the difference ($\log_2(\text{fold change})$). 839 of the quantified proteins were differentially expressed, 429 were upregulated (depicted with red) and 410 were downregulated (depicted with blue) in HAB EH compared to HAB NH female mice. Non-significant proteins are depicted with grey. $FDR < 0.05$, $S_0 > 0.1$. (B) Table depicting the top ten upregulated protein hits, which were determined by sorting the differentially expressed proteins according to the fold change value (from largest to smallest).

The average intensity of each top hit protein for the HAB EH group was correlated with all behavioral parameters for the battery of tests used to assess behavior following the EH protocol (DaLi, OFT, FST and SPAT), and heat maps were generated to present the results (Figure 7A). R values depicted range from blue ($r = -1.0$) to red ($r = 1.0$) depending on the directionality of the correlation (negative or positive, respectively), significant correlations are depicted with stars and trends with T. The 3 proteins the expression levels of which highly correlated with anxiety-related and depression-like parameters were: ATP4A, CKM and PFKFB1, which positively correlated with increased anxiety- and depression-like behavior (Figure 7B).

A



B

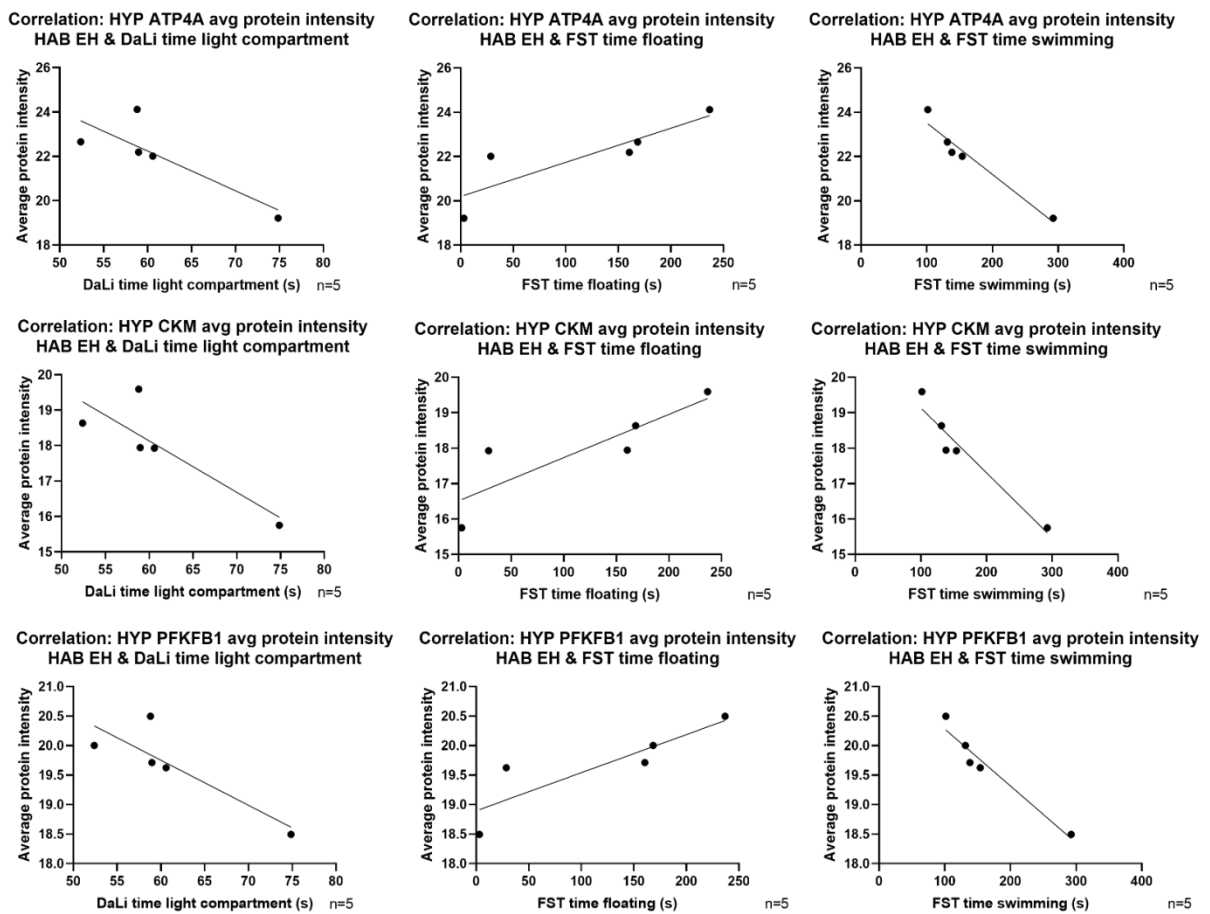


Figure 7. Correlation of the ten top upregulated proteins from our hypothalamic proteomics analysis with behavior. (A) Matrices plotting the Pearson or Spearman r values of each correlation. The behavioral parameters for all tests (DaLi, OFT, FST, SPAT) are listed horizontally, while the ten proteins are vertically. The color coding represents the directionality of the correlation, red for positive, and blue for negative. Significant correlations are depicted with stars, while trends with T. (B) ATP4A protein expression had a trend for negative correlation with the time in the light compartment of DaLi (Pearson $r=-0.8335$, $p=0.0795$ (T)), a trend for positive correlation with the time floating of the FST (Pearson $r=0.8619$, $p=0.0603$ (T)), and correlated negatively with the time swimming

of the FST (Pearson $r=-0.9717$, $**p=0.0067$). CKM protein expression had a trend for negative correlation with the time in the light compartment of DaLi (Pearson $r=-0.8513$, $p=0.0672$ (T)), a trend for positive correlation with the time floating of the FST (Pearson $r=0.8593$, $p=0.0620$ (T)), and correlated negatively with the time swimming of the FST (Pearson $r=-0.9648$, $**p=0.0079$). PFKFB1 protein expression had a trend for negative correlation with the time in the light compartment of DaLi (Pearson $r=-0.8587$, $p=0.0624$ (T)), a trend for positive correlation with the time floating of the FST (Pearson $r=0.8706$, $p=0.0548$ (T)), and correlated negatively with the time swimming of the FST (Pearson $r=-0.9728$, $**p=0.0054$).

4.2.2. Manual categorization revealed the abundance of oxidative phosphorylation (OXPHOS) proteins in the differentially expressed dataset

The 839 differentially expressed proteins were manually categorized into groups of interest using mitochondrial proteome databases. The results are presented in the tables of Figure 8, with red font indicating upregulation and blue font downregulation.

A

OXPHOS				
Complex	Protein	Gene name	Fold change	P value
Complex I	NADH dehydrogenase [ubiquinone] iron-sulfur protein 6, mitochondrial	NDUFS6	1.63	0.0000015
Complex I	NADH dehydrogenase [ubiquinone] 1 beta subcomplex subunit 7	NDUFB7	0.66	0.0000477
Complex I	NADH dehydrogenase [ubiquinone] flavoprotein 2, mitochondrial	NDUFV2	1.45	0.0001554
Complex I	NADH dehydrogenase [ubiquinone] 1 beta subcomplex subunit 11	NDUFB11	1.85	0.0006288
Complex I	NADH-ubiquinone oxidoreductase 75 kDa subunit, mitochondrial	NDUFS1	1.3	0.0016524
Complex I	NADH dehydrogenase [ubiquinone] 1 beta subcomplex subunit 8	NDUFB8	1.57	0.0029563
Complex I	NADH dehydrogenase [ubiquinone] 1 beta subcomplex subunit 3	NDUFB3	1.74	0.0167617
Complex III	Cytochrome c1, heme protein, mitochondrial	CYC1	0.69	0.0000000
Complex III	Cytochrome b-c1 complex subunit 9	UQCR10	0.72	0.0001997
Complex III	Cytochrome b-c1 complex subunit 1, mitochondrial	UQCRC1	1.46	0.0002322
Complex III	Cytochrome b-c1 complex subunit 2, mitochondrial	UQCRB	0.77	0.0004098
Complex IV	Cytochrome c oxidase subunit 7A-related protein, mitochondrial	COX7A2L	1.26	0.0000335
Complex IV	Cytochrome c oxidase subunit 7B, mitochondrial	COX7B	0.28	0.0096515
Complex IV	Cytochrome c oxidase subunit 5A, mitochondrial	COX5A	1.82	0.0105318
Complex IV	Cytochrome c oxidase subunit 2	MTCO2	1.61	0.0297516
Complex V	ATP synthase subunit O, mitochondrial	ATP5O	1.38	0.0000324
Complex V	ATP synthase F(0) complex subunit C1, mitochondrial	ATP5MC1	1.32	0.0000927
Complex V	ATP synthase subunit epsilon, mitochondrial	ATP5E	1.23	0.0003053
Complex V	ATP synthase subunit beta, mitochondrial	ATP5B	1.54	0.0007663
Complex V	ATP synthase subunit alpha, mitochondrial	ATP5A	1.38	0.0015065
Complex V	ATP synthase subunit delta, mitochondrial	ATP5D	1.8	0.0015191

B

Mitochondrial dynamics				
Pathway	Protein	Gene name	Fold change	P value
Fusion	ATP-dependent zinc metalloprotease YME1L1	YME1L1	1.58	0.0000163
Fusion	ADP-ribosylation factor-like protein 2	ARL2	0.74	0.0002071
Fusion	Protein misato homolog 1	MSTO1	1.30	0.0051120
Fusion	Mitofusin 2	MFN2	1.33	0.0059547
Fission	Mitochondrial fission factor	MFF	0.79	0.0000561
Fission	Mitochondrial fission 1 protein	FIS1	0.71	0.0011523
Mitophagy	Serine/threonine-protein phosphatase PGAM5, mitochondrial	PGAM5	1.44	0.0000003
Mitophagy	Bcl-2-like protein 13	BCL2L13	0.63	0.0086013

C

TCA cycle				
Krebs cycle step	Enzyme	Gene name	Fold change	P value
Succinyl-CoA -> Succinate	succinate-CoA ligase, GDP-forming, alpha subunit	SUCLG1	1.29	0.0000001
OAA -> Citrate	Citrate synthase	CS	1.35	0.0000016
PEP -> OAA	Phosphoenolpyruvate carboxykinase 2, mitochondrial	PCK2	1.21	0.0000095

D

Detoxification				
Category	Protein	Gene name	Fold change	P value
ROS & Glutathione metabolism	Peroxiredoxin-6	PRDX6	0.66	0.0000004
ROS & Glutathione metabolism	Peroxiredoxin-2	PRDX2	1.33	0.0000502
ROS & Glutathione metabolism	Oxidation resistance protein 1	OXR1	0.79	0.0007633
ROS & Glutathione metabolism	Superoxide dismutase [Mn], mitochondrial	SOD2	0.76	0.0019256

Figure 8. Manual categorization of proteins that were differentially expressed in our hypothalamic proteomics analysis of HAB EH vs. HAB NH female mice. Categories involve pathways of interest, such as: (A) OXPHOS, (B) mitochondrial dynamics, (C) mitochondrial metabolism (TCA cycle), (D) detoxification proteins. Upregulated proteins of each group are indicated with red font, whereas downregulated proteins with blue font. Information derived from Mouse MitoPathways 3.0 and KEGG Pathways.

A number of proteins comprising the full dataset from our analysis were involved in ETC and OXPHOS machinery. Twenty one proteins were OXPHOS subunits, 7 of them for complex I (NDUFB11, NDUFB3, NDUFB7, NDUFB8, NDUFS1, NDUFS6, NDUFV2), 4 for complex III (CYC1, UQCR10, UQCRB, UQCRC1), 4 for complex IV (COX5A, COX7A2L, COX7B, MTCO2), and the remaining 6 for complex V (ATP5A, ATP5B, ATP5D, ATP5E, ATP5MC1, ATP5O) (Figure 8A). No complex II subunits were differentially expressed between the two groups. Regarding the directionality of the altered expression, for complex I, only one protein, NDUFB7, was downregulated in the hypothalamus of HAB EH female mice. In complex III, only one protein, UQCRC1, was upregulated in the hypothalamus of HAB EH female mice. In complex IV, only one of the 4 protein subunits, COX7B, was downregulated in the hypothalamus of HAB EH female mice. And lastly, all of the complex V proteins that were differentially expressed were upregulated in the hypothalamus of HAB EH female mice.

Moving on to mitochondrial dynamics-related processes, few proteins had altered expression levels. Four proteins were related to the mitochondrial fusion machinery (ARL2, MFN2, MSTO1, YME1L1), with 3 of them being upregulated in the hypothalamus of HAB EH female mice. Two fission proteins were differentially expressed (MFF, FIS1), and both were downregulated in the hypothalamus of HAB EH female mice. Two proteins involved in mitophagy were also differentially expressed, with BCL2L13 being downregulated and PGAM5 upregulated in the hypothalamus of HAB EH female mice (Figure 8C). No proteins involved in mitochondrial biogenesis were differentially expressed between HAB EH and HAB NH female mice.

Even though glycolytic enzymes were not differentially expressed in the hypothalamus of HAB EH female mice there was a pattern for the expression of TCA cycle proteins. All 3 enzymes of the TCA cycle that were differentially expressed in our proteomics analysis (SUCLG1, CS, PCK2) were upregulated in the hypothalamus of HAB EH female mice (Figure 8D).

Lastly, a number of proteins involved in cellular detoxification, and more specifically ROS and glutathione metabolism were also differentially expressed between HAB EH and HAB NH female mice. OXR1, PRDX6, SOD2 were all downregulated, while PRDX2 was upregulated in the hypothalamus of HAB EH female mice (Figure 8E).

4.2.3. In silico analysis with STRING showcased two main groups in the full and the upregulated dataset: OXPHOS proteins and ribosomal proteins

After manual categorization, we analyzed our two datasets, the differentially expressed one and the upregulated one, in silico using the STRING database.

Protein network results for the full differentially expressed dataset are shown in Figure 9. The network was created using the highest confidence provided by the database (0.9), by using experiments and co-expression as the active interaction sources. The complete image, color coded to showcase different protein groups, revealed the existence of two main clusters, an OXPHOS cluster (color coded with red in the network), and a ribosome cluster (color coded with blue). Other prominent groups included proteins responsible for mitochondrial organization (color coded with yellow), and proteins responsible for mRNA splicing (color coded with pink). All mitochondrial proteins, since mitochondrial functions are of interest for us, were color coded with green (Figure 9A). The two main clusters were also visualized separately, with individual color coding, to gain a better understanding of the proteins comprising it. The OXPHOS cluster showcased 11 complex I proteins (color coded with red), 4 complex III proteins (color coded with blue), 4 complex IV proteins (color coded with green), and 5 complex V protein proteins (color coded with yellow) (Figure 9B). The number of proteins for complex I and complex V is different here than it was for the manual categorization, which may be due to the settings chosen for the network analysis and how recent the information of each database is. Similarly for the ribosomal cluster, there are 14 proteins of cytosolic ribosomes (color coded with red), and 5 proteins of mitochondrial ribosomes (color coded with blue). Proteins of the large ribosomal subunit or the small ribosomal subunit are color coded with green and yellow, respectively (Figure 9C).

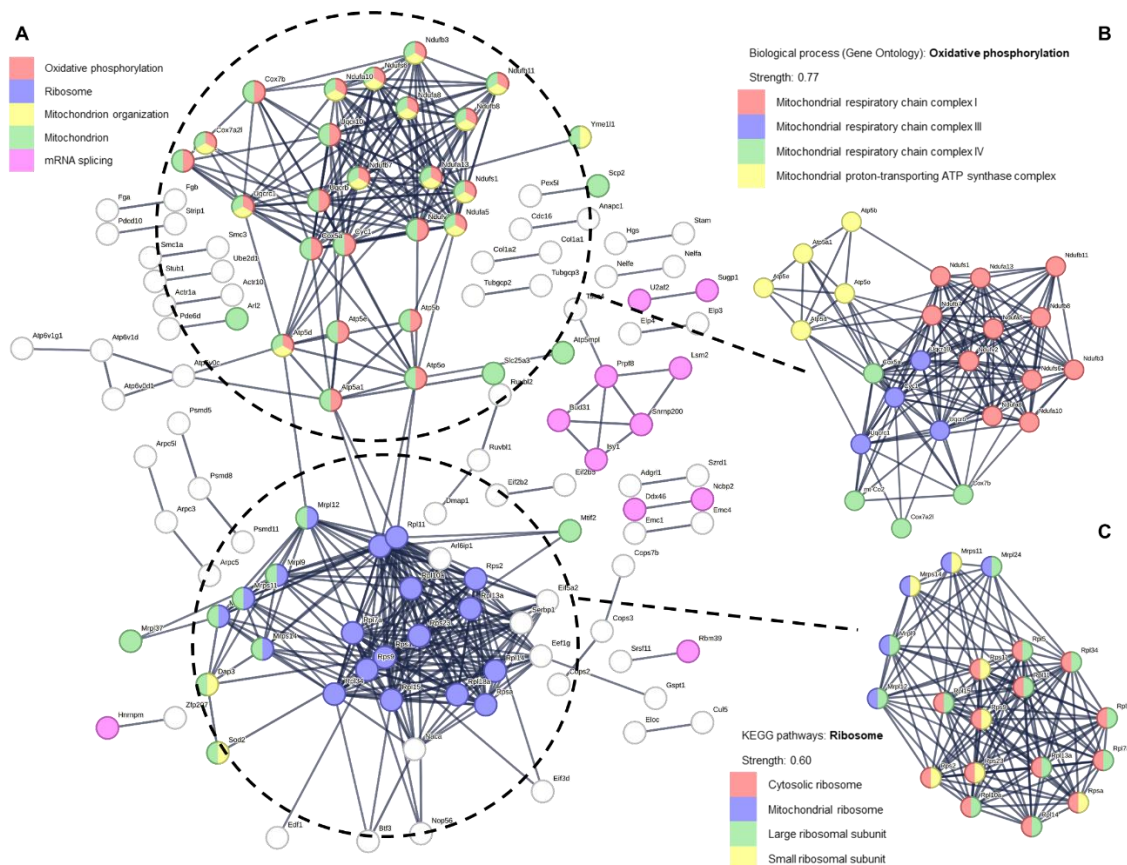


Figure 9. STRING-generated protein network for the full differentially expressed dataset. Network type: full STRING network, meaning of network edges: confidence, active interaction sources: experiments, co-expression, minimum required interaction score: highest confidence (0.9), network display options: disable structure previews inside network bubbles, hide disconnected nodes in the network. (A) The full protein network. Pathways: Oxidative phosphorylation (GO:0006119, strength 0.77, FDR 3.44E-09, red), ribosome (mmu03010, strength 0.60, FDR 6.86E-05, blue), mitochondrion organization (GO:0007005, strength 0.48, FDR 5.25E-09, yellow), mitochondrion (KW-0496, strength 0.42, FDR 5.93E-18, green), mRNA splicing (KW-0508, strength 0.39, FDR 0.0026, green). (B) OXPHOS cluster. Protein complexes: mitochondrial respiratory chain complex I (GO:0005747, strength 2.25, FDR 5.27E-20, red), mitochondrial respiratory chain complex III (GO:0005750, strength 2.43, FDR 2.27E-07, blue), mitochondrial respiratory chain complex IV (GO:0005751, strength 2.11, FDR 2.66E-06, green), mitochondrial proton transporting ATP synthase complex (GO:0005753, strength 2.31, FDR 7.98E-09, yellow). (C) Ribosome cluster. Protein groups: cytosolic ribosome (GO:0022626, strength 2.16, FDR 7.50E-28, red), mitochondrial ribosome (GO:0005761, strength 1.79, FDR 2.78E-06, blue), large ribosomal subunit (GO:0015934, strength 2.03, FDR 5.85E-20, green), small ribosomal subunit (GO:0015935, strength 1.98, FDR 2.04E-10, yellow).

Similar work was conducted for the upregulated dataset as well (Figure 10). The highest confidence (0.9) was chosen for the network, and experiments and co-expression were used as the active interaction sources. The upregulated network that was generated, similar to the full dataset, showcased two main protein clusters, an OXPHOS cluster (color coded with red), and a ribosome cluster (color coded with blue). Other protein groups included proteins involved in mitochondrial organization (color coded with light green), proteins part of an ER protein-containing complex (color coded with pink), and proteins involved in RNA splicing (color coded with dark green). All mitochondrial proteins were color coded with yellow (Figure 10A). The OXPHOS group was also clustered individually to gain a better understanding of its components, and it was observed that 7 proteins were a part of complex I (color coded with red), 1 protein was a part of complex III (color coded with blue), 3 proteins were a part of complex IV (color coded with green), and as they also were for the full dataset, 5 proteins were a part of complex V (color coded with yellow) (Figure 10B). The ribosomal cluster contains the 14 cytosolic ribosome proteins (color coded with red) that were noted in the ribosome cluster of the full dataset, and 4 mitochondrial ribosome proteins (color coded with blue). Large ribosomal subunit and small ribosomal subunit proteins were color coded with green and yellow, respectively (Figure 10C).

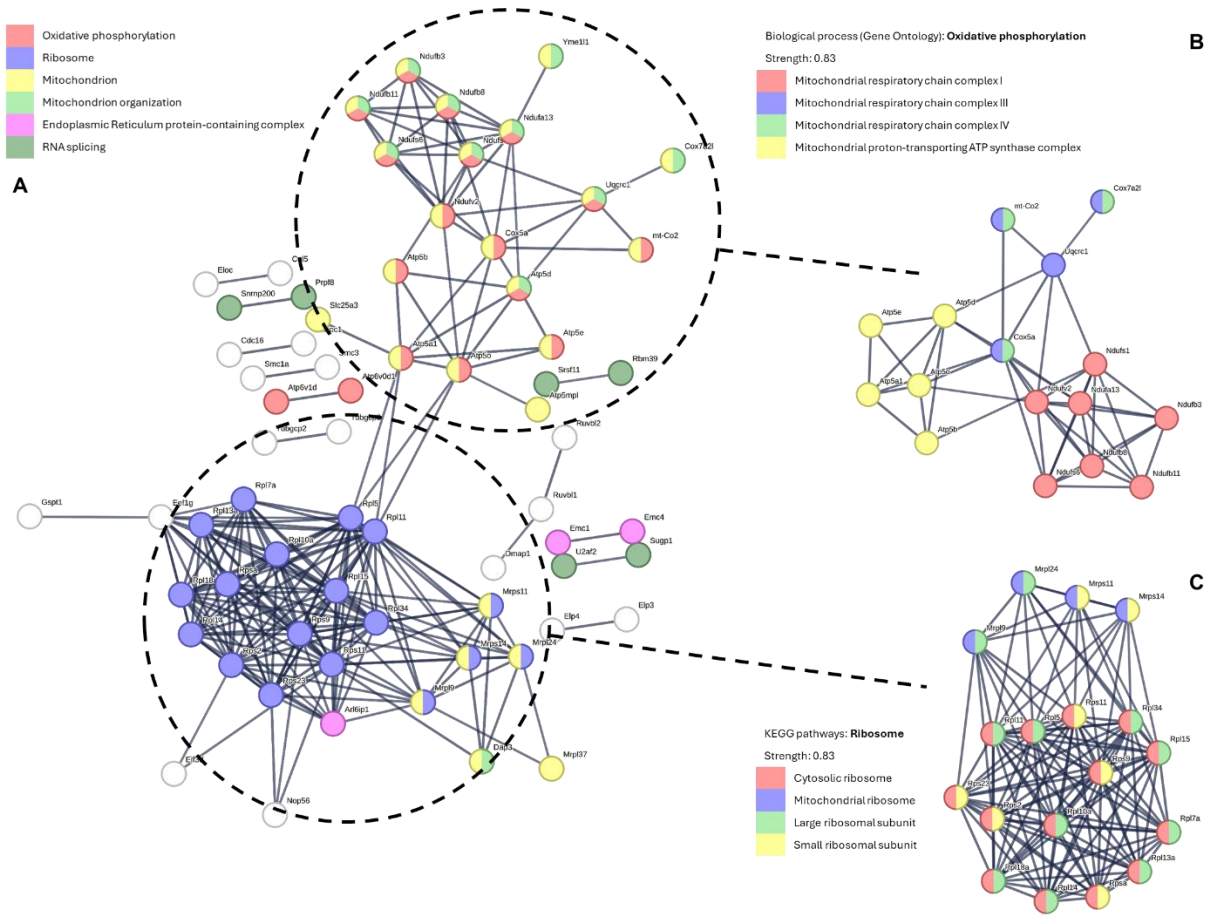


Figure 10. STRING-generated protein network for the upregulated dataset. Network type: full STRING network, meaning of network edges: confidence, active interaction sources: experiments, co-expression, minimum required interaction score: highest confidence (0.9), network display options: disable structure previews inside network bubbles, hide disconnected nodes in the network. (A) The upregulated protein network. Pathways: Oxidative phosphorylation (GO:0006119, strength 0.83, FDR 2.94E-06, red), ribosome (mmu03010, strength 0.86, FDR 5.93E-08, blue), mitochondrion (KW-0496, strength 0.51, FDR 1.04E-15, yellow), mitochondrion organization (GO:0007005, strength 0.52, FDR 6.74E-06, green), ER protein-containing complex (GO:0140534, strength 0.73, FDR 5.96E-05, pink), RNA splicing (GO:0008380, strength 0.43, FDR 0.0213, dark green). (B) OXPHOS cluster. Protein complexes: mitochondrial respiratory chain complex I (GO:0005747, strength 2.28, FDR 9.21E-13, red), cytochrome c complex (GO:0070069, strength 2.14, FDR 1.80E-06, blue), mitochondrial respiratory chain complex IV (GO:0005751, strength 2.21, FDR 7.12E-05, green), mitochondrial proton transporting ATP synthase complex (GO:0005753, strength 2.53, FDR 1.59E-28, yellow). (C) Ribosome cluster. Protein groups: cytosolic ribosome (GO:0022626, strength 2.18, FDR 1.59E-28, red), mitochondrial ribosome (GO:0005761, strength 1.71, FDR 0.00014, blue), large ribosomal subunit (GO:0015934, strength 2.02, FDR 1.73E-33, green), small ribosomal subunit (GO:0015935, strength 2.00, FDR 1.66E-10, yellow).

4.2.4. Correlation matrices for the OXPHOS and ribosome protein expression levels for HAB EH female mice with behavior

The proteins comprising the two groups that arose from our STRING analysis for the full differentially expressed dataset, OXPHOS and ribosomes, were correlated for the HAB EH female

mice with all behavioral parameters for all tests used in the EH protocol. In the matrices, directionality of the correlation is indicated with red, if it was positive, and blue, if it was negative. Significant correlations are shown with stars, and trends with T. Of all the proteins in each group, the ones that were downregulated are marked with blue. As diploma thesis student Panteli Eirini was responsible for the analysis of the downregulated group, only relevant correlations from the upregulated proteins will be discussed here.

Figure 11A depicts the OXPHOS matrix, based on the differentially expressed proteins of the OXPHOS cluster that was noted for HAB EH female mice (Figure 11B). A variety of significant correlations are observed, especially for complex I, III and V. However, the proteins that stand out are NADH dehydrogenase 1 beta subcomplex subunit 11, mitochondrial (NDUFB11), NADH-ubiquinone oxidoreductase 75 kDa subunit, mitochondrial (NDUFS1), two complex I subunits, ATP synthase subunit delta, mitochondrial (ATP5D) and ATP synthase subunit beta, mitochondrial (ATP5B), two complex V subunits. For complex I, NDUFB11 protein expression correlated negatively with the time spent in the light compartment and had a trend for negative correlation with the number of entries to the light compartment of the DaLi box, so the higher NDUFB11 protein expression, the higher the anxiety-like behavior. NDUFB11 also correlated negatively with the latency to the center of the OFT, so for this test, higher NDUFB11 protein expression correlates with a lower anxiety-like behavior. Similarly, for NDUFS1, its protein expression correlated negatively with the time and the number of entries to the light compartment of the DaLi box, so the higher NDUFS1 protein expression, the higher the anxiety-like behavior. NDUFS1 also correlated negatively with the latency to the center of the OFT, so for this test, higher NDUFB11 protein expression correlates with lower anxiety-like behavior (Figure 11C). For complex V, ATP5D protein expression correlated negatively with the latency to the light compartment of DaLi, meaning that the higher the ATP5D protein expression correlates with lower anxiety-like behavior. Additionally, ATP5D showed a trend for negative correlation in the time struggling and a negative correlation with the latency to float on the FST, meaning that the higher the ATP5D protein expression, the higher the depression-like behavior. ATP5B protein expression correlated negatively with the time spent and number of entries to the light compartment of the DaLi box, therefore higher ATP5B protein expression correlates with higher anxiety-like behavior (Figure 11D).

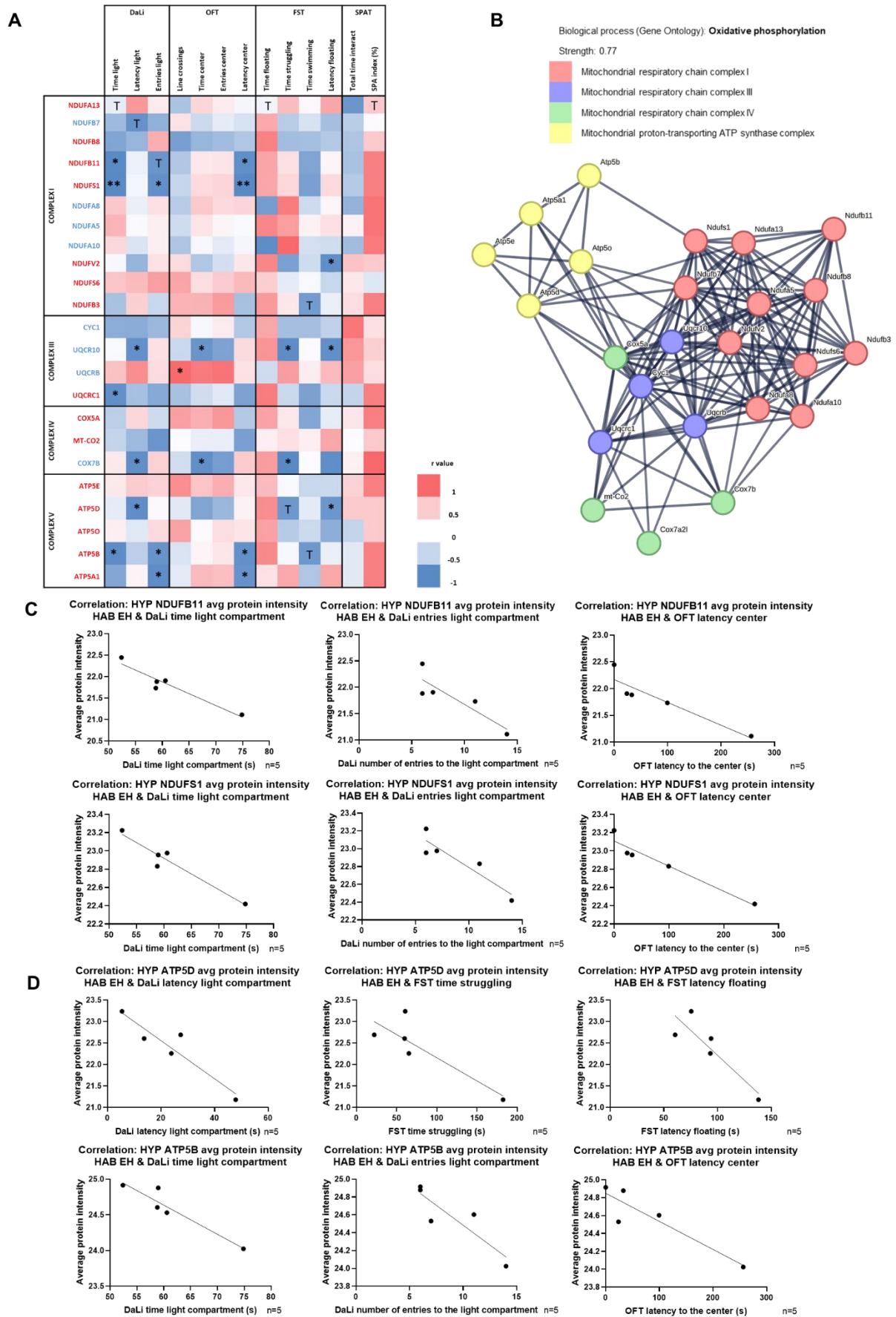


Figure 11. Correlations for proteins comprising the OXPPOS cluster from our STRING analysis with behavior. (A) Heat map matrix plotting the Pearson or Spearman r values of each correlation. The behavioral parameters

for all tests (DaLi, OFT, FST, SPAT) are listed horizontally, while the ten proteins are listed vertically. Upregulated proteins are indicated with red font, while downregulated proteins with blue font. The color coding represents the directionality of the correlation, red for positive, and blue for negative. Significant correlations are depicted with stars, while trends with T. (B) The OXPHOS cluster generated with STRING, on which the correlation matrix was based. (C) Complex I correlations for NDUFB11 and NDUFS1. NDUFB11 correlated negatively with the time in the light compartment (Pearson $r=-0.9572$, $*p=0.0105$) and had a trend for negative correlation with the number of entries to the light compartment of DaLi (Pearson $r=-0.8751$, $p=0.0520$ (T)), and it also correlated negatively with the latency to the center of the OFT (Pearson $r=-0.9284$, $*p=0.0227$). NDUFS1 correlated negatively with the time (Pearson $r=-0.9641$, $**p=0.0081$) and the number of entries to the light compartment of DaLi (Pearson $r=-0.9160$, $*p=0.0289$), and with the latency to the center of the OFT (Pearson $r=-0.9679$, $**p=0.0069$). (D) Complex V correlations for ATP5D and ATP5B. ATP5D correlated negatively with the latency to the light compartment of DaLi (Spearman $r=-0.9338$, $*p=0.0203$) and had a trend for negative correlation with the time struggling (Pearson $r=-0.8601$, $p=0.0615$ (T)) and a negative correlation with the latency to float in the FST (Pearson $r=-0.8866$, $*p=0.0460$). ATP5B protein expression correlated negatively with the time in the light compartment (Pearson $r=-0.9456$, $*p=0.0151$) and the number of entries to the light compartment of DaLi (Pearson $r=-0.8859$, $*p=0.0454$), and it also correlated negatively with the latency to the center of the OFT (Pearson $r=-0.9120$, $*p=0.0309$).

The ribosome matrix, based on the differentially expressed proteins of the ribosome cluster that was noted for HAB EH female mice (Figure 12B), does not include as many significant correlations (Figure 12A). The protein that stands out here is small ribosomal subunit protein uS2 (RPSA), a cytosolic ribosome protein part of the small subunit. RPSA protein expression showed a trend for negative correlation with the time in the light compartment of DaLi, which means that the higher the RPSA protein expression, the higher the anxiety-like behavior. Also, it correlated positively with the time floating and negatively with the time swimming of the FST, indicating that RPSA protein expression positively correlates with depression-like behavior (Figure 12C).

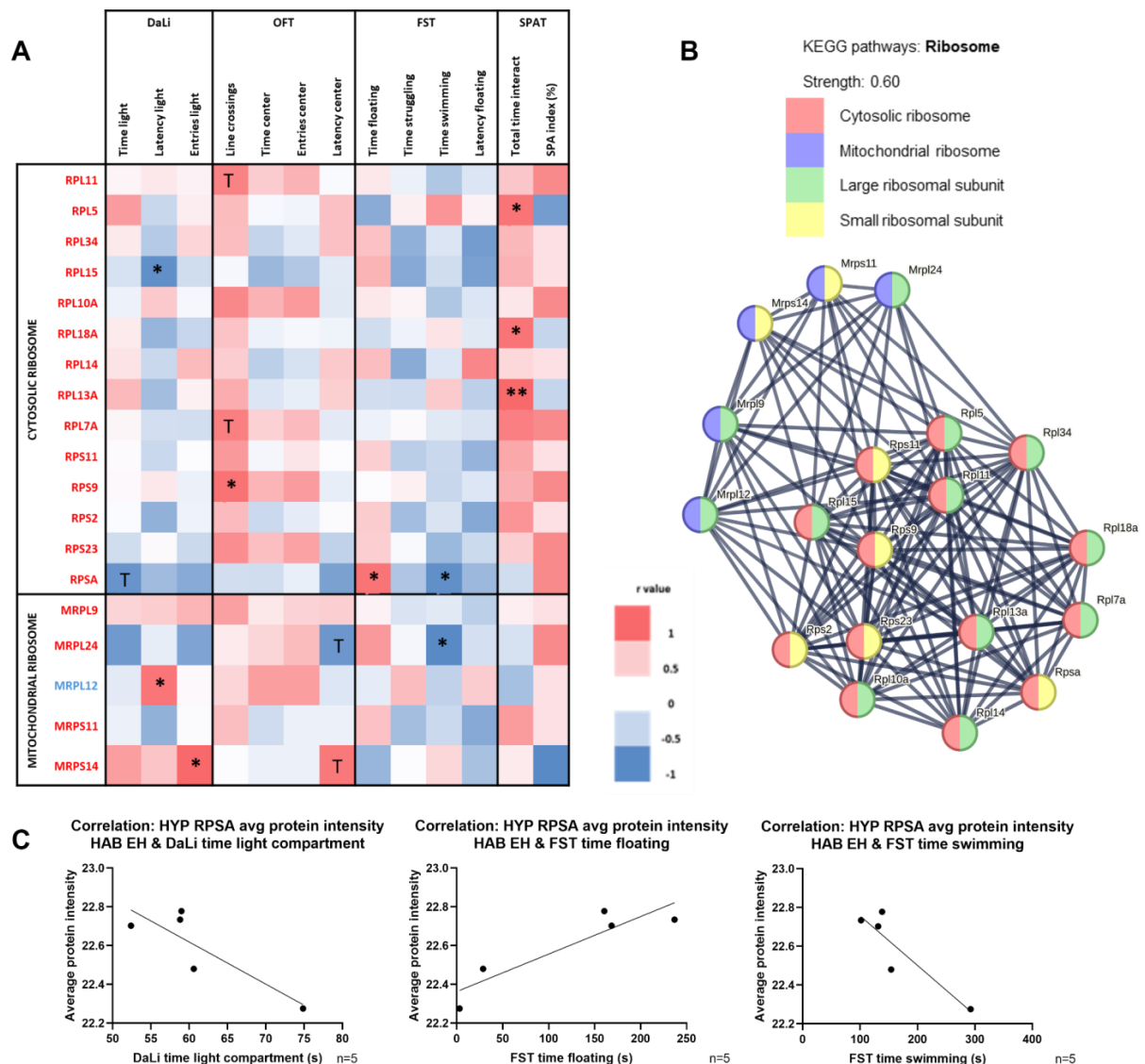


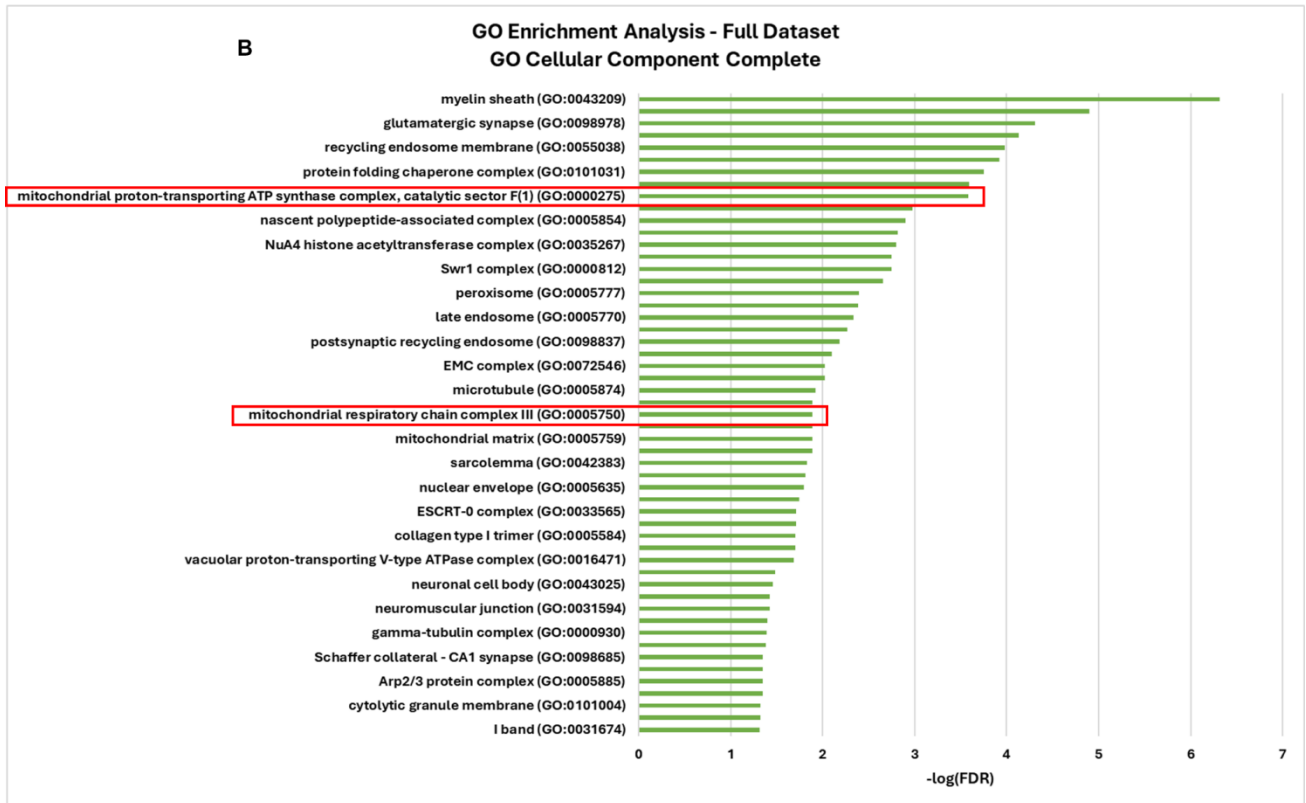
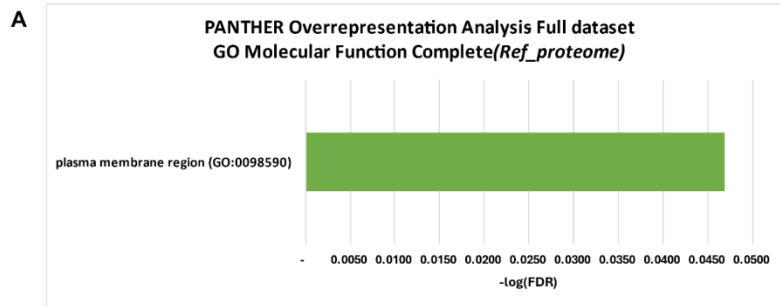
Figure 12. Correlations for proteins comprising the ribosome cluster from our STRING analysis with behavior. (A) Heat map matrix plotting the Pearson or Spearman r values of each correlation. The behavioral parameters for all tests (DaLi, OFT, FST, SPAT) are listed horizontally, while the ten proteins are listed vertically. Upregulated proteins are indicated with red font, while downregulated proteins are indicated with blue font. The color coding represents the directionality of the correlation, red for positive, and blue for negative. Significant correlations are depicted with stars, while trends with T. (B) The ribosome cluster generated with STRING, on which the correlation matrix was based. (C) Correlations for RPSA, a cytosolic ribosome, small ribosomal subunit protein. RPSA protein expression had a trend for negative correlation with the time in the light compartment of DaLi (Pearson $r=-0.8509$, $p=0.0675$ (T)), correlated positively with the time floating of the FST (Pearson $r=0.9089$, $*p=0.0326$), and negatively with the time swimming of the FST (Pearson $r=-0.8987$, $*p=0.0381$).

4.2.5. Gene Ontology overrepresentation analysis validated mRNA splicing, ribosomes and OXPHOS as main EH mediators

To corroborate our findings from the protein-protein interaction network analysis of STRING, Gene Ontology enrichment analysis was used. The full differentially expressed dataset and the

upregulated dataset were both analyzed conducting a PANTHER Overrepresentation test (released 2024-01-17), for all three of the functional terms used for the classification of proteins: Biological Process (BP), Cellular Component (CC) and Molecular Function (MF). As a reference genome, the *Mus musculus* genome was selected, but the analysis was also conducted using our quantified proteome from the proteomics analysis as a reference, that is, the list of 5503 proteins that were quantified in the HYP. Based on the results from each analysis, bar charts were generated, using the $-\log(\text{FDR})$ values from the overrepresentation tests and sorting them from largest to smallest, to highlight the strongest components of each term.

For the full dataset using as a reference our quantified proteome, PANTHER overrepresentation analysis for the GO BP and the GO CC term gave no significant results, however, PANTHER overrepresentation analysis for GO MF showed that proteins in the plasma membrane region are significantly overrepresented in the hypothalamus of HAB EH compared to HAB NH female mice (Figure 13A). GO enrichment analysis using the mouse genome as a reference for the GO CC term highlighted that two OXPHOS complexes, complex III and complex V, are significantly enriched (Figure 13B). GO enrichment analysis for the GO BP term highlighted multiple OXPHOS-related processes, such as proton motive force-driven mitochondrial ATP synthesis, complex I assembly, mitochondrial electron transport from NADH to ubiquinone, as well as gene transcription and protein translation-related processes like cytoplasmic translation, translation at the pre-synapse, mRNA splicing, RNA splicing regulation, and translation regulation. Lastly, one process related to mitochondrial dynamics came up, and that was regulation of mitochondrial fission (Figure 13C). GO enrichment analysis for the GO MF term highlighted the enrichment of proteins which are structural constituents of ribosomes (Figure 13D).



C

GO Enrichment Analysis - Full Dataset
GO Biological Process Complete

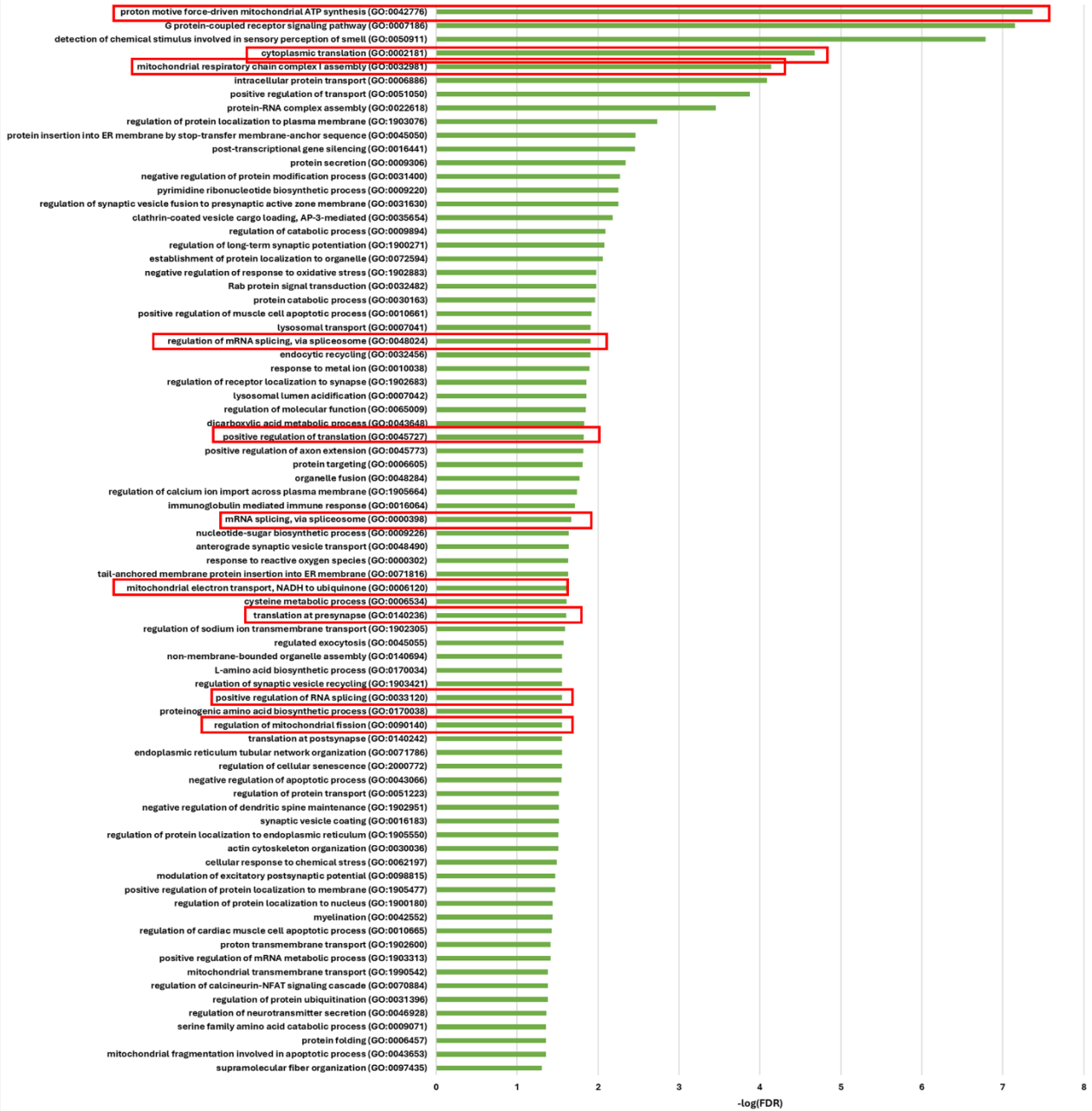
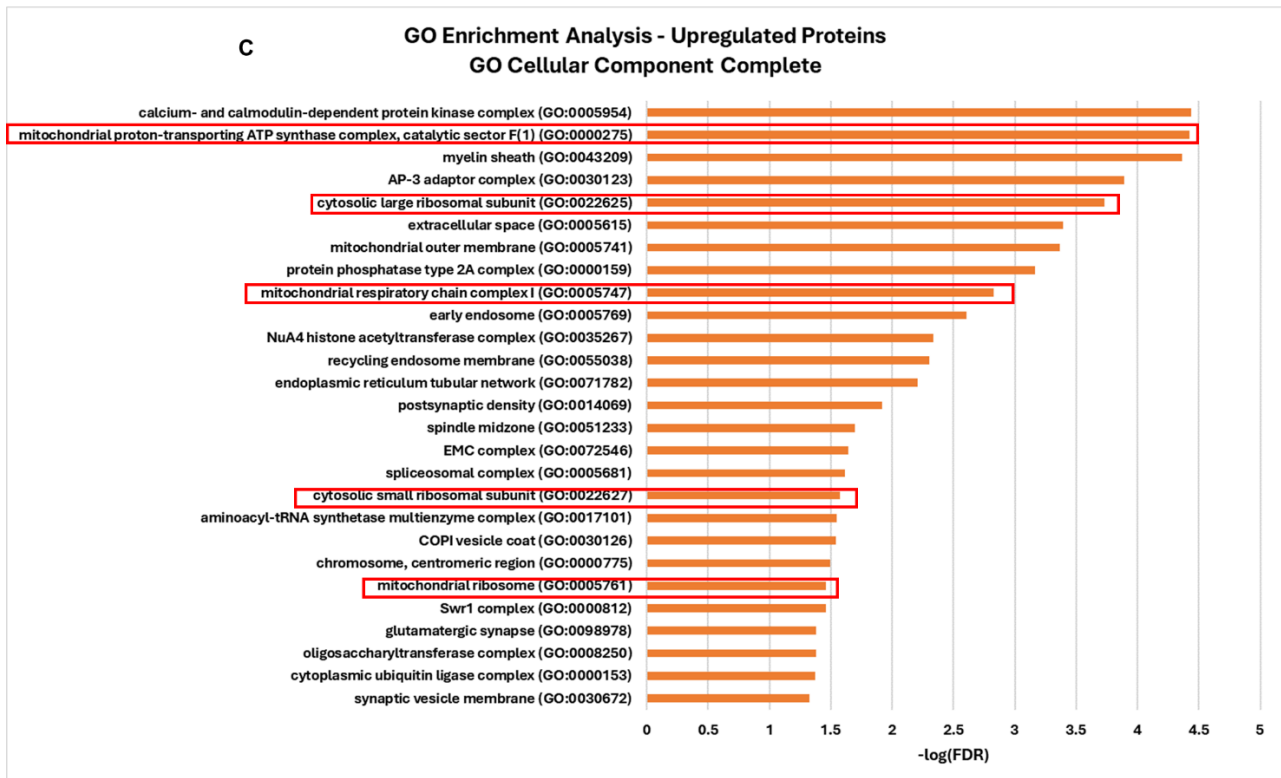
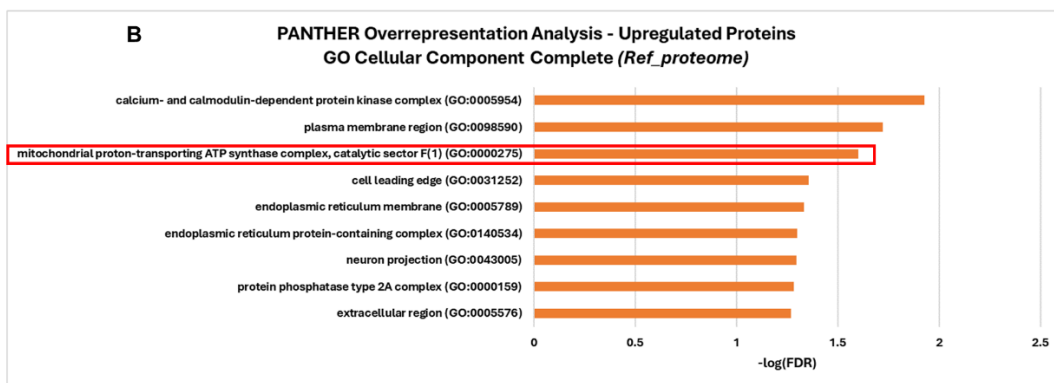
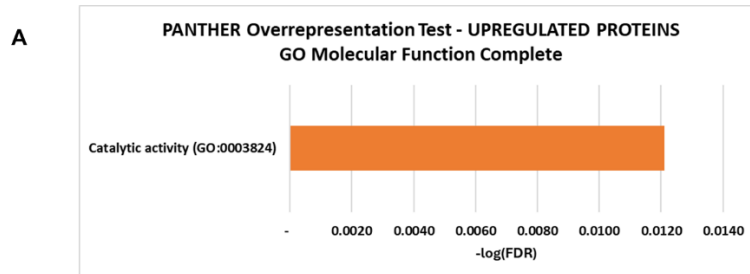




Figure 13. Gene Ontology bar charts for the full differentially expressed dataset. $-\log(\text{FDR})$ values retrieved from the analysis were sorted from largest to smallest to highlight the most enriched terms. (A) PANTHER overrepresentation test for the GO term Molecular Function (MF). As a reference, our full quantified proteome was used. (B) GO enrichment analysis for the GO term Cellular Component (CC). As a reference, the mouse genome was used. Terms related to OXPHOS are highlighted with red. (C) GO enrichment analysis for the GO term Biological Process (BP). As a reference, the mouse genome was used. Terms related to gene transcription, translation, OXPHOS and mitochondrial dynamics are highlighted with red. (D) GO enrichment analysis for the GO term Molecular Function (MF). As a reference, the mouse genome was used. Terms related to gene translation are highlighted with red.

Similar analyses were conducted for the upregulated dataset. Using our quantified proteome as a reference PANTHER overrepresentation analysis for the GO BP term gave no statistically significant results. However, overrepresentation analysis for the GO MF term showed that proteins with a catalytic activity are significantly overrepresented in the hypothalamus of HAB EH compared to HAB NH female mice (Figure 14A), and analysis for the GO CC term highlighted the overrepresentation of the OXPHOS complex V, specifically the catalytic sector F(1) (Figure 14B). GO enrichment analysis for the GO CC term using as a reference the mouse genome highlighted terms that also showed up in the protein network analysis using STRING. Specifically, OXPHOS complexes I and V were both significantly enriched, and so was the cytosolic large and small ribosomal unit, the

mitochondrial ribosome, and the spliceosome (Figure 14C). GO enrichment analysis for the GO BP term highlighted the enrichment of OXPHOS-related processes such as complex I assembly, mitochondrial ATP synthesis-coupled electron transport, as well as protein translation-related processes like cytoplasmic translation, translation at pre- and post-synapse, and mRNA splicing (Figure 14D). Lastly, GO enrichment analysis for the GO MF term highlighted the enrichment of proteins which are structural constituents of the ribosomes (Figure 14E).



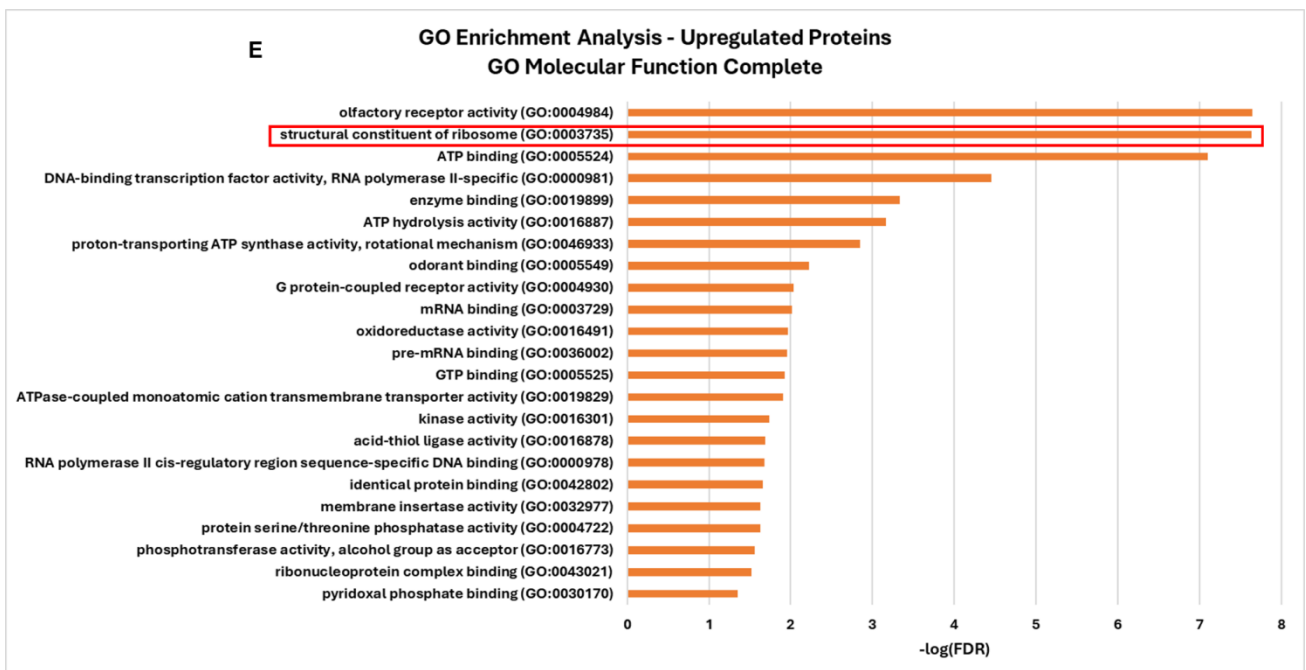
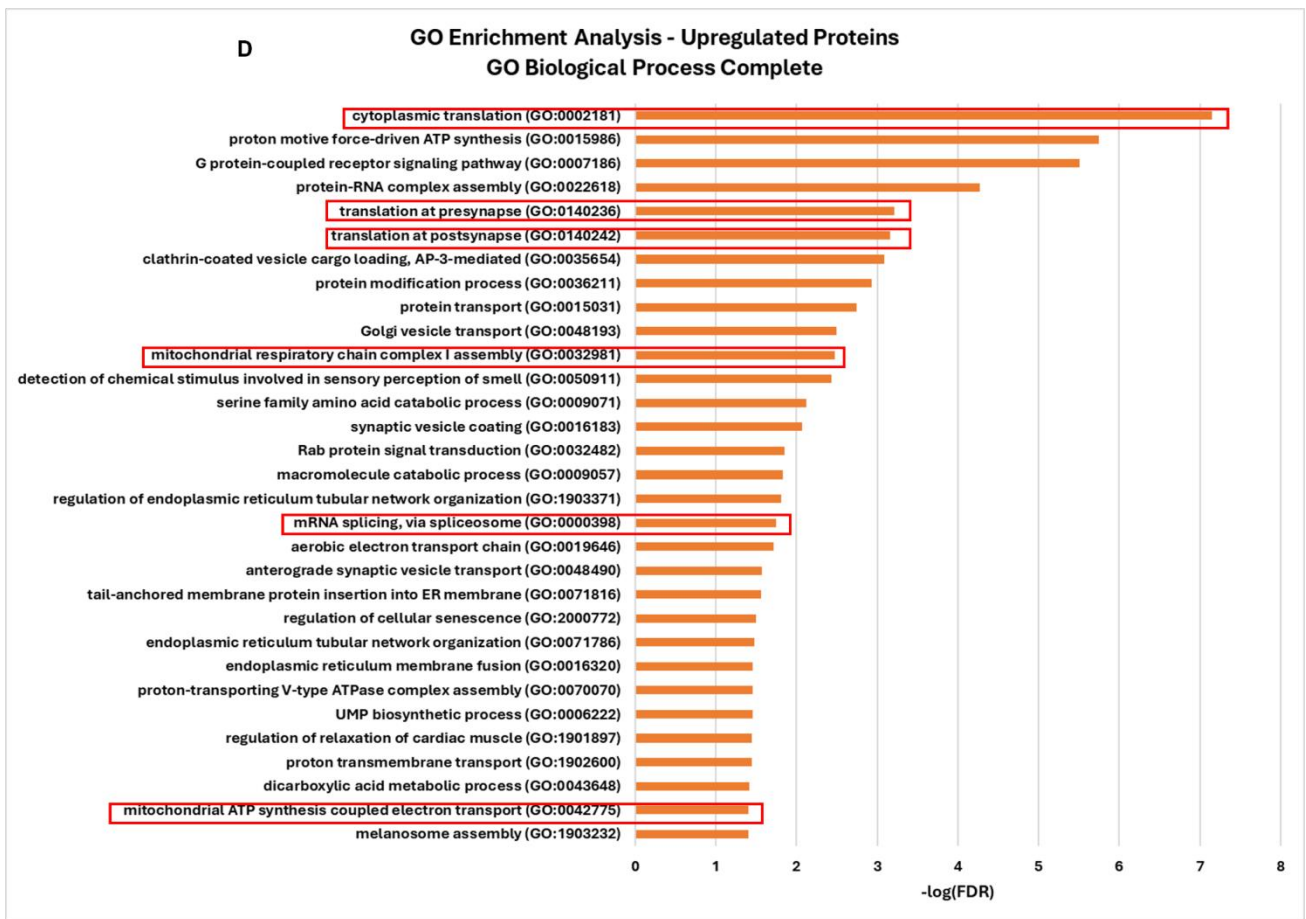


Figure 14. Gene Ontology bar charts for the upregulated dataset. $-\log(\text{FDR})$ values retrieved from the analysis were sorted from largest to smallest to highlight the most enriched terms. (A) PANTHER overrepresentation test for the GO MF term. As a reference, our full quantified proteome was used. (B) PANTHER overrepresentation test for the GO CC term. As a reference, our full quantified proteome was used. Terms related to OXPHOS are highlighted with red. (C) GO enrichment analysis for the GO term Cellular Component (CC). As a reference, the

mouse genome was used. Terms related to gene translation and OXPHOS are highlighted with red. (D) GO enrichment analysis for the GO term Biological Process (BP). As a reference, the mouse genome was used. Terms related to gene transcription, translation, and OXPHOS are highlighted with red. (E) GO enrichment analysis for the GO term Molecular Function (MF). As a reference, the mouse genome was used. Terms related to gene translation are highlighted with red.

In conclusion for the proteomics analysis of the hypothalamus, multiple types of analyses that were conducted both through manual research and in silico work point to gene transcription (RNA splicing), gene translation (ribosomes) and OXPHOS as the main molecular pathways involved in EH-driven effects. The protein-protein interaction network generated with STRING for both the full differentially expressed, and the upregulated hypothalamic dataset of HAB EH compared to HAB NH female mice showed a distinct cluster made up of ribosomal proteins, as well as proteins with a regulatory role in mRNA splicing. The protein-protein interaction network also showcased a cluster consisting of OXPHOS components, namely for complexes I, III, IV and V. Gene Ontology analyses confirmed the overrepresentation of ribosomal machinery and OXPHOS complexes I and V for HAB EH female mice, as well as the overrepresentation of proteins involved in mRNA splicing for HAB EH female mice. Lastly, ribosomal and OXPHOS components correlated with behavior, as observed from the correlation matrices that were generated for all proteins of each cluster.

4.3. HYPOTHALAMUS: Molecular assays

4.3.1. EH altered mitochondrial biogenesis and fission mRNA levels in the hypothalamus of HAB EH female mice

Our hypothalamic proteomics analysis helped us gain a better understanding of the EH-induced alterations in the HAB EH female proteome. With our manual work, it was revealed that selected proteins involved in mitochondrial dynamics pathways had differentially expressed protein levels in the hypothalamus of HAB EH vs. HAB NH female mice (see Figure 8B). The fission process was also significantly enriched for HAB EH female mice, as revealed with GO enrichment analysis of the full differentially expressed dataset for GO BP (see Figure 13C). Therefore, we wanted to assess the mRNA expression levels of gene mediators for mitochondrial dynamics processes. Biogenesis (*tfam*, *pgc1a*), fusion (*mfn2*, *msto1*), fission (*fis1*, *mff*, *dnm2*, *drp1*, *gdap1*, *mid51*), and mitophagy (*pink1*, *prkn*) mediators were assessed using qRT-PCRs.

Mitochondrial Biogenesis

EH resulted in a trend for reduced *tfam* mRNA levels in the hypothalamus of HAB EH compared to HAB NH female mice. *Pgc1a* on the other hand, was not affected and its mRNA expression did not differ between HAB EH and HAB NH female mice (Figure 15A). In HAB EH female mice, correlation of *tfam* and *pgc1a* levels with behavior showed that *tfam* mRNA expression levels negatively correlated with the time and the number of entries to the center, as well as with the number of line crossings in the OFT, indicating that the higher the *tfam* mRNA expression, the higher the

anxiety-like behavior. Additionally, *tfam* mRNA expression had a trend for positive correlation with the SPA index of the SPAT, meaning that the higher the *tfam* mRNA expression, the lower the sociability tends to be. *Pgc1a* mRNA expression levels correlated positively with the total time of interaction on the SPAT, meaning that the higher the *pgc1a* mRNA expression, the lower the sociability (Figure 16A).

Mitochondrial Fusion

For fusion mediators *msto1* and *mfn2*, no mRNA alterations were found between HAB EH and HAB NH female mice (Figure 15B). In HAB EH female mice, correlation of *msto1* and *mfn2* mRNA expression levels with behavior showed that *msto1* mRNA expression levels correlated positively with the time and the number of entries to the center of the OFT, which means that the higher the *msto1* mRNA expression levels, the higher the anxiety-like behavior. *Msto1* mRNA expression levels also correlated negatively with the time struggling of the FST. *Mfn2* mRNA expression levels showed a trend for negative correlation with the time struggling of the FST (Figure 16B).

Mitochondrial Fission

EH increased the mRNA expression levels of *fis1* in the hypothalamus of HAB EH female mice (Figure 15C). mRNA expression levels for *mff*, *dnm2*, *drp1*, *gdap1* and *mid51* were not altered by EH. For the HAB EH female mice, correlation of fission genes' mRNA levels showed that *fis1* mRNA expression levels negatively correlated with the latency to the light compartment of the DaLi test, which means that the higher the *fis1* mRNA expression, the lower the anxiety-like behavior. Notably, FIS1 protein expression levels, which were observed with LC-MS/MS proteomics to be downregulated for HAB EH female mice (see Table B of Figure 8) correlated positively with the latency to the light compartment of DaLi, which indicates that the *fis1* gene's mRNA and protein expression levels correlate with anxiety-like behavior in a contradictory way (Figure 16C). *Mff* mRNA expression levels showed a trend for negative correlation with the latency to the center of the OFT, meaning that the higher the *mff* mRNA expression levels, the lower the anxiety-like behavior. *Dnm2* mRNA expression levels correlated negatively with the latency to the center of the OFT, meaning that the higher the *dnm2* mRNA expression, the lower the anxiety-like behavior. *Gdap1* mRNA expression levels correlated negatively with the latency to the light compartment of DaLi, meaning that the higher the *gdap1* mRNA expression, the lower the anxiety-like behavior. Lastly, *mid51* mRNA expression levels correlated positively with the time floating and negatively with the time swimming and the latency to float in the FST, meaning that the higher the *mid51* mRNA expression, the higher the depression-like behavior (Figure 16D).

Mitophagy

EH did not impact the mRNA expression levels of *pink1* and *prkn* between HAB EH and HAB NH female mice (Figure 15D). *Pink1* mRNA expression levels for the HAB EH female mice, however, showed a trend for negative correlation with the time struggling on the FST (Figure 16E).

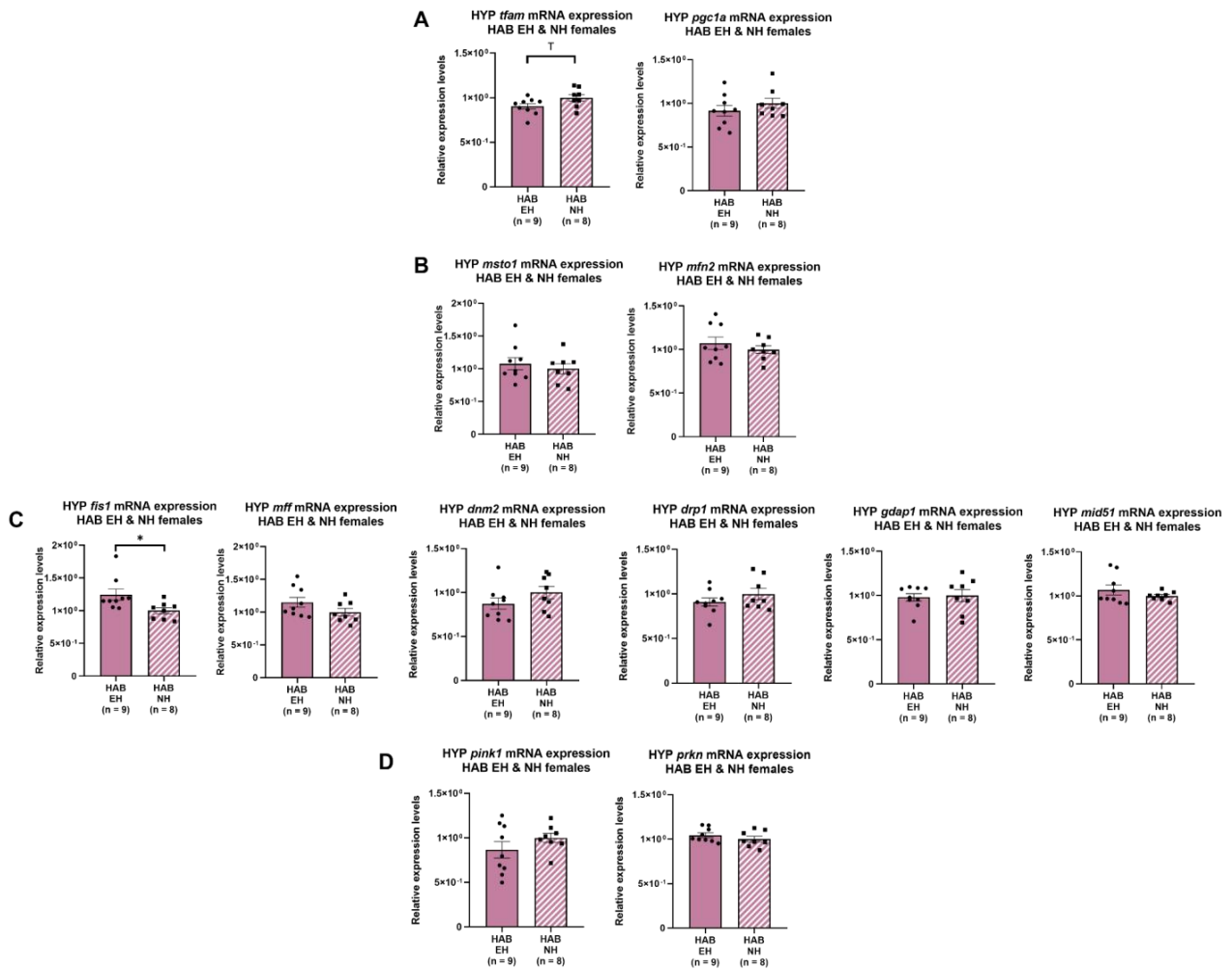


Figure 15. Hypothalamus qRT-PCR results for the mRNA expression levels of genes involved in mitochondrial dynamics. (A) EH produced a trend for reduced *tfam* mRNA expression in the HYP of HAB EH female mice (Welch's *t* test, $p=0.0795$ (T)). *Pgc1a* expression levels were not altered between HAB EH and HAB NH female mice. (B) EH increased the *fis1* mRNA levels in the HYP of HAB EH female mice (Mann-Whitney, $*p=0.0202$). EH did not alter the mRNA expression levels of *msto1* and *mfn2* in the HYP of HAB EH female mice. (C) *Mff*, *dnm2*, *drp1*, *gdap1* and *mid51* mRNA expression levels were not altered by EH. (D) EH did not impact the mRNA expression levels of *pink1* and *prkn*.

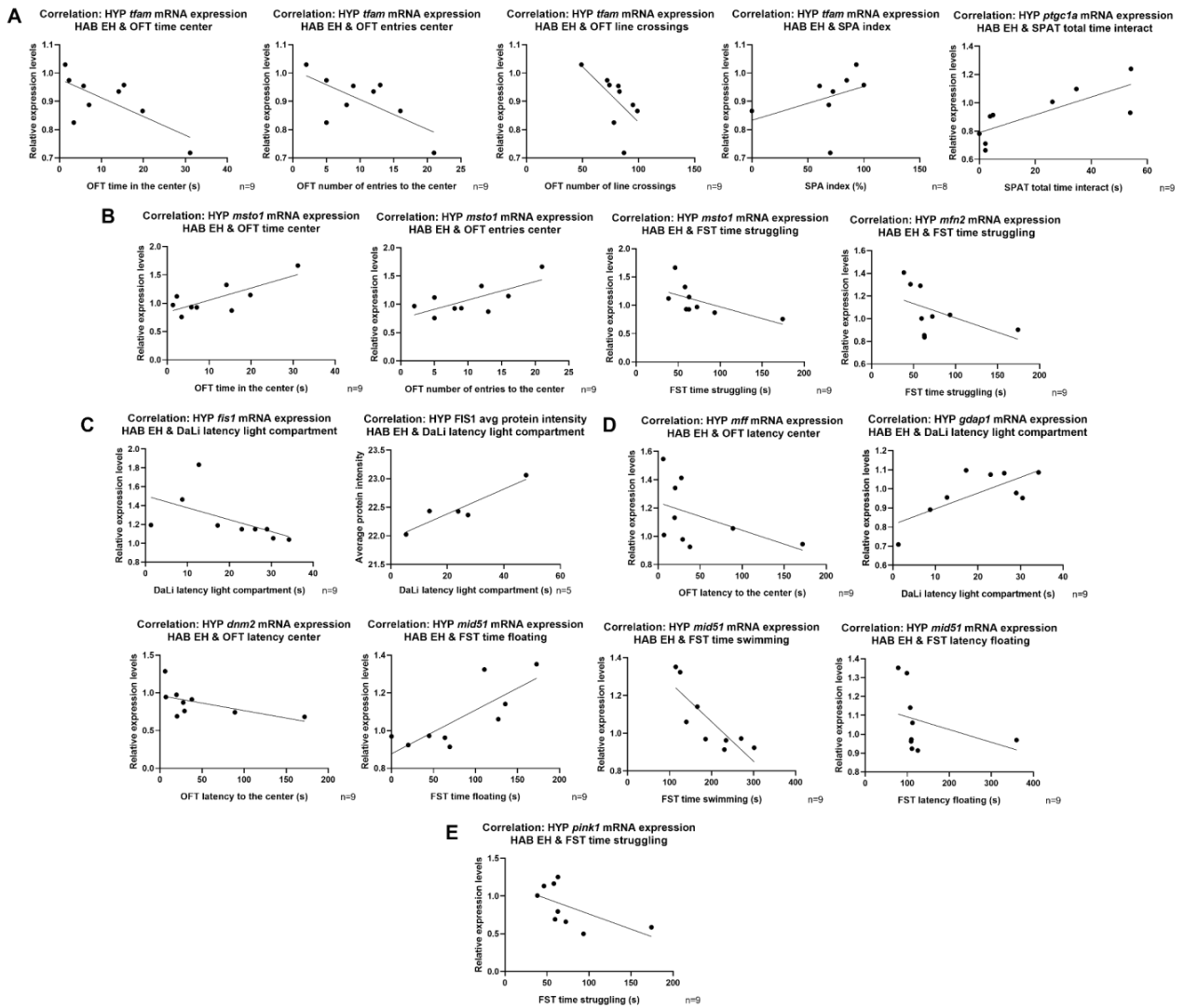


Figure 16. Correlation of hypothalamic mRNA expression levels for genes involved in mitochondrial dynamics processes with behavior. (A) *Tfam* correlates negatively with the time in the center (Pearson $r=-0.7015$, $*p=0.0352$), and had a trend for negative correlation with the number of entries to the center (Pearson $r=-0.6760$, $*p=0.0458$) and the number of line crossings of the OFT (Pearson $r=-0.6143$, $p=0.0784$ (T)). *Tfam* mRNA expression levels also had a trend for positive correlation with the SPA index of the SPAT (Spearman $r=0.6905$, $p=0.0694$ (T)). *Pgc1a* mRNA expression correlated positively with the total time of interaction in the SPAT (Spearman $r=0.8954$, $**p=0.0022$). (B) *Msto1* correlated positively with the time in the center (Pearson $r=0.7648$, $*p=0.0164$) and the number of entries to the center of the OFT ($r=0.7083$, $*p=0.0327$), and it also correlated negatively with the time struggling of the FST (Spearman $r=-0.7333$, $*p=0.0311$). *Mfn2* had a trend for negative correlation with the time struggling of the FST ($r=-0.6167$, $p=0.0857$ (T)). (C) *Fis1* mRNA expression levels correlated negatively with the latency to the light compartment of DaLi (Spearman $r=-0.9154$, $**p=0.0012$), while *FIS1* protein expression levels correlated positively (Pearson $r=0.9154$, $*p=0.0215$). (D) *Mff* had a trend for negative correlation with the latency to the center of the OFT (spearman $r=-0.6500$, $p=0.0666$ (T)). *Dnm2* mRNA expression correlated negatively with the latency to the center of the OFT (Spearman $r=-0.7667$, $*p=0.0214$). *gdap1* mRNA expression correlated positively with the latency to the light compartment of DaLi (Pearson $r=0.7210$, $*p=0.0284$). *Mid51* mRNA expression correlated positively with the time floating (Spearman $r=0.7000$, $*p=0.0433$) and negatively with the time swimming (Spearman $r=-0.8167$, $*p=0.0108$) and the latency to float in

the FST (Spearman $r=0.7333$, $*p=0.0311$). (E) *Pink1* mRNA expression levels had a trend for negative correlation with the time struggling in the FST (Spearman $r=-0.6500$, $p=0.0666$ (T)).

4.3.2. EH decreased the mtDNAcn in the hypothalamus of HAB EH female mice

As part of our investigation of the hypothalamic profile of HAB EH female mice, we used mtDNAcn. MtDNAcn is an indirect biomarker of mitochondrial function that carries information about cellular energy reserves, oxidative stress, and mitochondrial membrane potential imbalances (Castellani et al., 2020). To assess it, we used qPCR on hypothalamic DNA extracts and combined it with DNA electrophoresis to verify the quality of the extracted DNA.

We found that EH significantly decreased the mtDNAcn in the hypothalamus of HAB EH compared to HAB NH female mice (Figure 17A). This result was also verified by DNA electrophoresis, which showed that the DNA used for the mtDNAcn was not degraded, so the decrease in copy number reflected a genuine mitochondrial alteration (Figure 17B). Correlation of the mtDNAcn for HAB EH female mice with behavioral parameters showed that mtDNA has a trend for negative correlation with the time spent in the light compartment of DaLi as well as with the number of entries to the light compartment, meaning that the higher the relative mtDNA expression levels, the higher the anxiety-like behavior. Additionally, the relative mtDNA expression had a trend for negative correlation with the number of line crossings and correlated negatively with the latency to the center of the OFT, indicating that the higher the relative mtDNA expression levels, the lower the locomotion of the animal and the higher the anxiety-like behavior (Figure 17C).

Keeping in mind this result, we wanted to investigate whether this alteration in the mtDNAcn affects mitochondrial transcription. For this purpose, we assessed the mRNA levels of *mt-nd1*, a mitochondrial-encoded gene. We found that EH did not impact the *mt-nd1* mRNA expression levels between HAB EH and HAB NH female mice (Figure 17D).

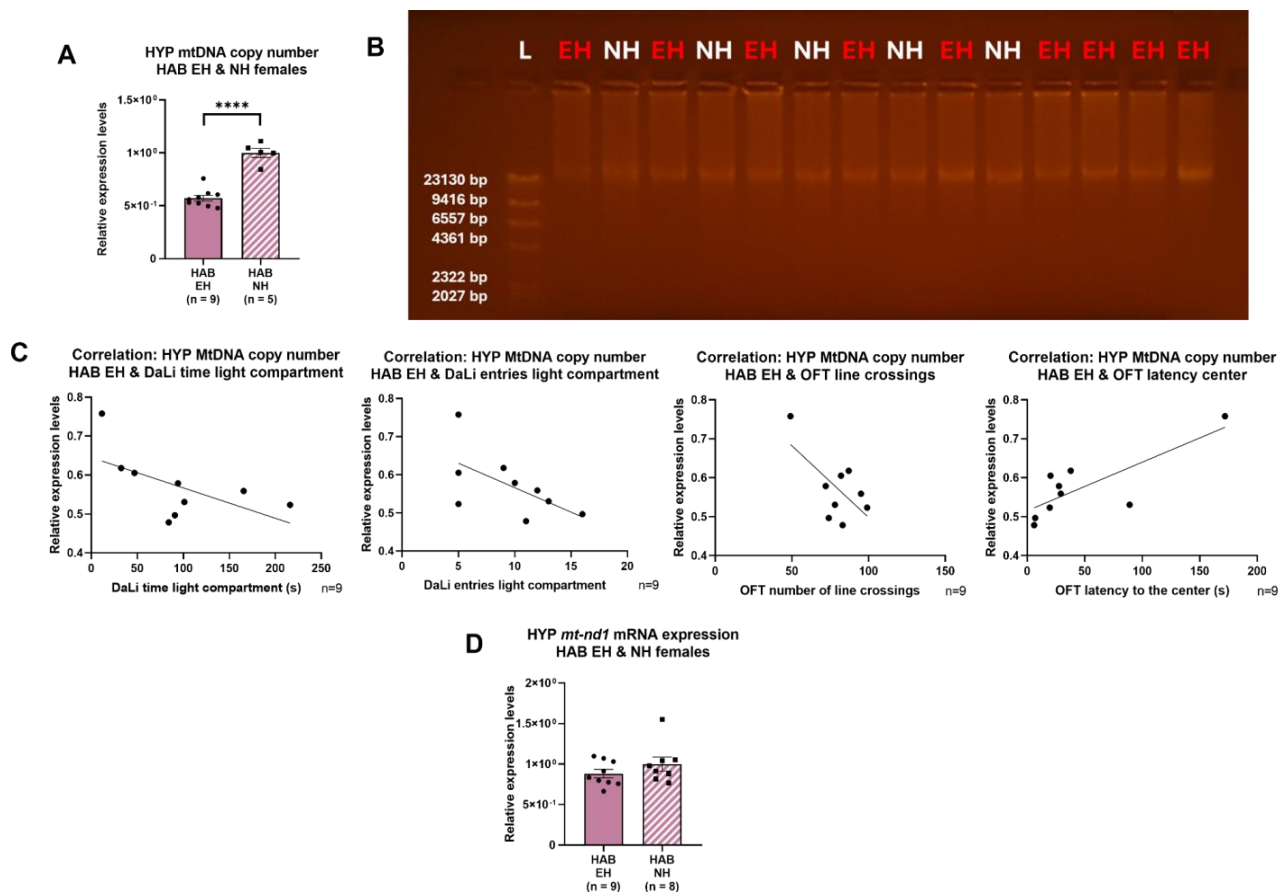


Figure 17. Hypothalamic mtDNAcn results. (A) EH decreased the relative expression levels of mtDNA for HAB EH female mice (Welch's *t* test, **** $p < 0.0001$). (B) DNA electrophoresis results for the HAB EH and HAB NH HYP DNA extracts used for the mtDNAcn assessment. The main band detected was at 23130 bp, which is where the genomic DNA appears. The band was clear and there was no smearing below the 23130 bp, which indicated that the DNA was of good quality. L: DNA ladder, EH: early handling, NH: non-handling. (C) Correlations of mtDNAcn with behavior. Relative mtDNA expression levels had a trend for negative correlation with the time spent in the light compartment (Pearson $r = -0.5957$, $p = 0.0905$ (T)) and with the number of entries to the light compartment of DaLi (Pearson $r = -0.6014$, $p = 0.0867$ (T)). Relative mtDNA expression levels also had a trend for negative correlation with the number of line crossings (Spearman $r = -0.6401$, $p = 0.0633$ (T)) and positively correlated with the latency to the center of the OFT (Spearman $r = 0.7667$, $*p = 0.0214$). (D) EH did not affect the mRNA expression levels of *mt-nd1*, a mitochondrial-encoded gene.

In conclusion for the molecular results in the hypothalamus, EH induced a trend for lower *tfam* mRNA expression levels in the hypothalamus of HAB EH female mice, while also correlating positively with anxiety-like behavior. Additionally, even though FIS1 protein expression was downregulated in the hypothalamus (see Table B of Figure 8), *fis1* mRNA expression levels were increased in the HYP of HAB EH female mice. No other gene related to mitochondrial fusion, fission and mitophagy machinery was altered, however *msto1* correlated with anxiety-like behavior and *mid51* showed a clear link with depression-like behavior, as observed by its correlations with the FST behavioral parameters. Finally, EH induced a decrease in the mtDNAcn for HAB EH female mice, with mtDNAcn

showing a trend for increased anxiety-like behavior when correlated with behavioral parameters. The mRNA levels for mitochondrial-encoded gene *mt-nd1* were not affected by this result.

4.4. PREFRONTAL CORTEX

Our proteomics analysis in the hypothalamus highlighted several mitochondrial pathways of interest. Therefore, our next step was to deduce whether these alterations were hypothalamus-specific, or whether they applied to other brain regions as well, such as the PFC. Table 9 showcases some of the proteins the expression levels of which were altered in the hypothalamus, and as a result were chosen to be quantified on the PFC too. All protein expression levels were assessed using western blots. All blot images used for the quantification of protein expression levels are shown in Appendix 2.

PROTEINS FOR WESTERN BLOT			
Full protein name	Name	Fold change	P value
Citrate synthase	CS	1.35	0.0000016036
Glycogen synthase kinase-3 beta	GSK-3B	1.33	0.0000297574
NADH dehydrogenase [ubiquinone] 1 beta subcomplex subunit 8	NDUFB8	1.57	0.0029562920
ATP synthase subunit alpha, mitochondrial	ATP5A	1.38	0.0015064963
Mitofusin 2	MFN2	1.33	0.0059547254
Mitochondrial fission factor	MFF	0.79	0.0000560526
Superoxide dismutase [Mn], mitochondrial	SOD2	0.76	0.0019255533
Electrogenic aspartate/glutamate antiporter SLC25A12, mitochondrial	SLC25A12 (Aralar)	1.50	0.0185564213
Sideroflexin-1	SFXN1	1.58	0.0145318679
Polyribonucleotide nucleotidyltransferase 1, mitochondrial	PNPT1	1.39	0.0015862988

Table 9. A list of proteins that were differentially expressed on the hypothalamus and whose levels were also assessed on the PFC using western blots. Fold change and P values refer to the alteration of expression on the hypothalamus of HAB EH female mice as shown by LC-MS/MS proteomics. Directionality of the differential expression for each protein is shown with red font if upregulated, and blue font if downregulated.

4.4.1. EH reduced PKLR protein expression levels in the PFC of HAB EH female mice

Our proteomics analysis in the hypothalamus showed that EH altered the protein expression levels of enzymes involved in carbohydrate metabolic processes, namely the TCA cycle and glycogen synthesis. Consequently, we assessed the protein expression levels of glycolytic (HK2, GAPDH, ENO1, PKLR), TCA cycle (CS, IDH1, SDHA) and glycogen synthesis enzymes (GSK3B) in the PFC.

Our findings indicated that, even though the TCA cycle and glycogen metabolism processes were not altered by EH (Figure 18B,C), glycolysis was affected, because for HAB EH female mice, EH induced a decrease in PKLR protein expression (Figure 18A). This is a PFC region-specific result, since PKLR was not differentially expressed in the hypothalamus of HAB EH female mice.

Correlation of these four glycolytic enzyme expression levels (HK2, GAPDH, ENO1, PKLR) with behavior showed that HK2 significantly correlated with a number of behavioral parameters (Figure 18D). HK2 had a trend for negative correlation with the number of line crossings and entries to the center of the OFT, meaning that the higher the HK2 protein expression, the lower the locomotion of the animal and the higher the anxiety-like behavior. Additionally, HK2 correlated negatively with the time floating and positively with the time swimming in the FST, which signifies that the higher the HK2 protein expression, the lower the depression-like behavior. At the same time, correlation with the TCA cycle protein expression levels (CS, IDH1, SDHA) with behavior showed that there is a trend for negative correlation of CS protein expression with the latency center of the OFT, so the higher the CS protein expression, the lower the anxiety-like behavior, and a trend for negative correlation of SDHA with the time floating of the FST, meaning that the higher the SDHA protein expression, the lower the depression-like behavior. IDH1 protein expression correlated positively with the time spent in the light compartment of DaLi, meaning the higher the IDH1 protein expression, the lower the anxiety-like behavior (Figure 18E). Lastly, GSK3B protein expression correlated positively with the number of entries to the light compartment of DaLi, which means that the higher the GSK3B protein expression, the lower the anxiety-like behavior (Figure 18F).

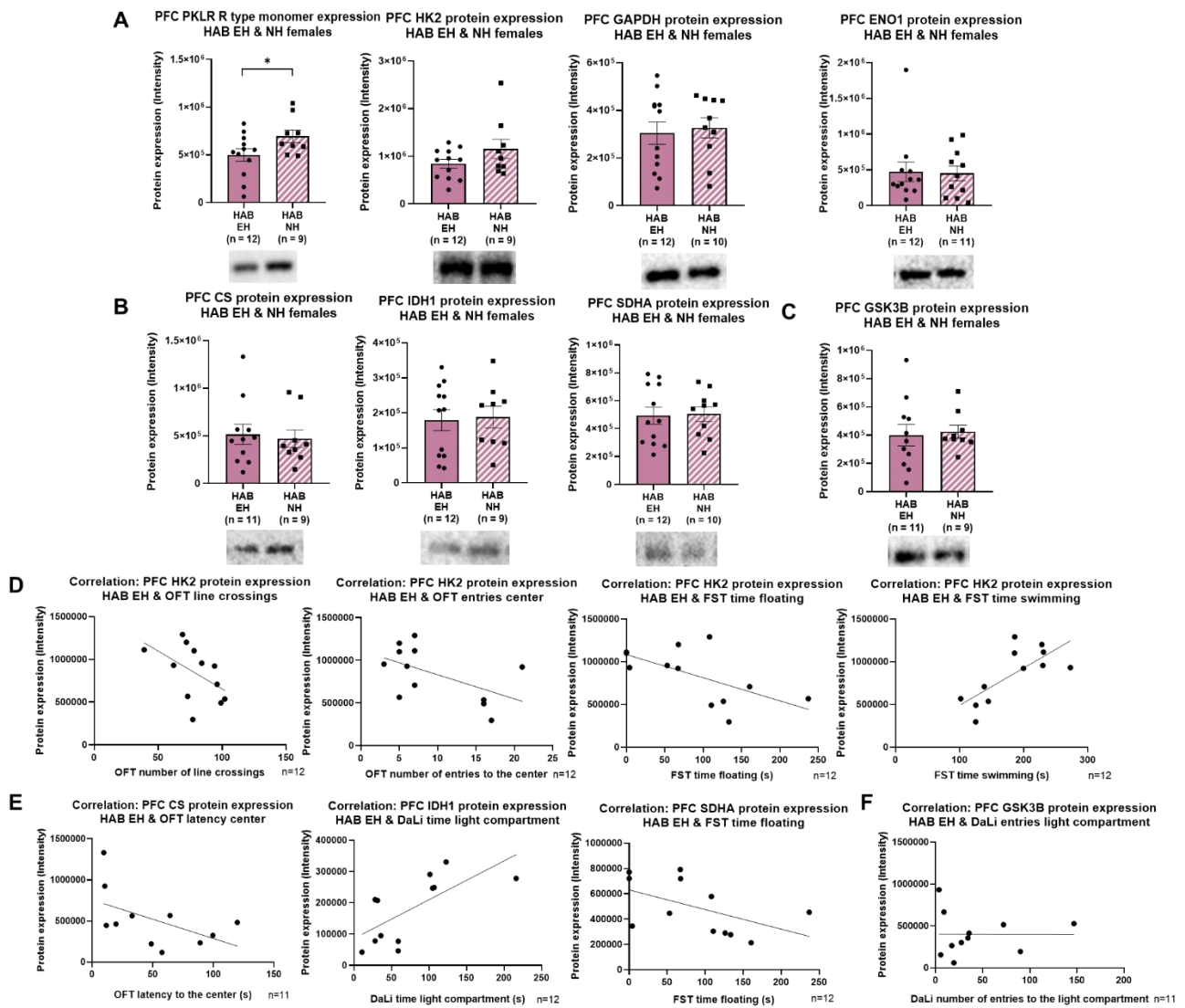


Figure 18. PFC western blot results for glycolysis, TCA cycle and glycogen synthesis enzymes. Blot images are below each bar graph. (A) PKLR protein expression was reduced in the PFC of HAB EH female mice (Welch's *t* test, $*p=0.0465$), while for other enzymes, namely HK2, GAPDH, and ENO1, protein expression levels were not altered. (B) For TCA cycle enzymes (CS, IDH1 and SDHA), protein expression levels in the PFC were not significantly altered between HAB EH and HAB NH female mice. (C) EH did not induce alterations in the protein expression levels of GSK3B in the PFC of HAB EH female mice. (D) HK2 protein expression for HAB EH female mice showed a trend for negative correlation with the number of line crossings (Pearson $r=-0.5012$, $p=0.0969$ (T)), and the number of entries to the center of the OFT (Spearman $r=-0.5152$, $p=0.0892$ (T)), while correlating negatively with the time floating (Pearson $r=-0.6122$, $*p=0.0344$) and positively with the time swimming of the FST (Pearson $r=0.7366$, $**p=0.0063$). (E) CS protein expression had a trend for negative correlation with the latency to the center of the OFT (Pearson $r=-0.5231$, $p=0.0987$ (T)). IDH1 protein expression correlated positively with the time in the light compartment of DaLi (Pearson $r=0.6903$, $*p=0.0130$). SDHA protein expression had a trend for negative correlation with the time floating of the FST (Pearson $r=-0.5176$, $p=0.0848$ (T)). (F) GSK3B protein expression correlated positively with the number of entries to the light compartment of DaLi (Pearson $r=0.6196$, $*p=0.0421$).

4.4.2. EH did not affect OXPHOS protein expression in the PFC of HAB EH female mice

OXPHOS was a significantly overrepresented pathway in the proteomics analysis conducted in the hypothalamus of HAB EH female mice, so we investigated whether there were any OXPHOS protein expression alterations in the PFC as well. For this purpose, we used the Mitoprofile antibody cocktail, which assesses the protein expression levels of five OXPHOS proteins, one for each complex.

EH did not induce any changes in the protein levels of any of the five OXPHOS complexes (Figure 19A). However, when correlating each protein's expression levels in the HAB EH group with behavior, it was observed that complex I protein expression had a trend for negative correlation with the number of entries to the center of the OFT, meaning that the higher the complex I protein expression, the higher the anxiety-like behavior. Complex II protein expression had a trend for positive correlation with the total time of interaction on the SPAT, which means that the higher the complex II protein expression, the higher the sociability of the HAB EH animals. Lastly, complex III protein expression had a trend for positive correlation with the time spent in the center of the OFT, meaning the higher the complex III protein expression, the lower the anxiety-like behavior (Figure 19B).

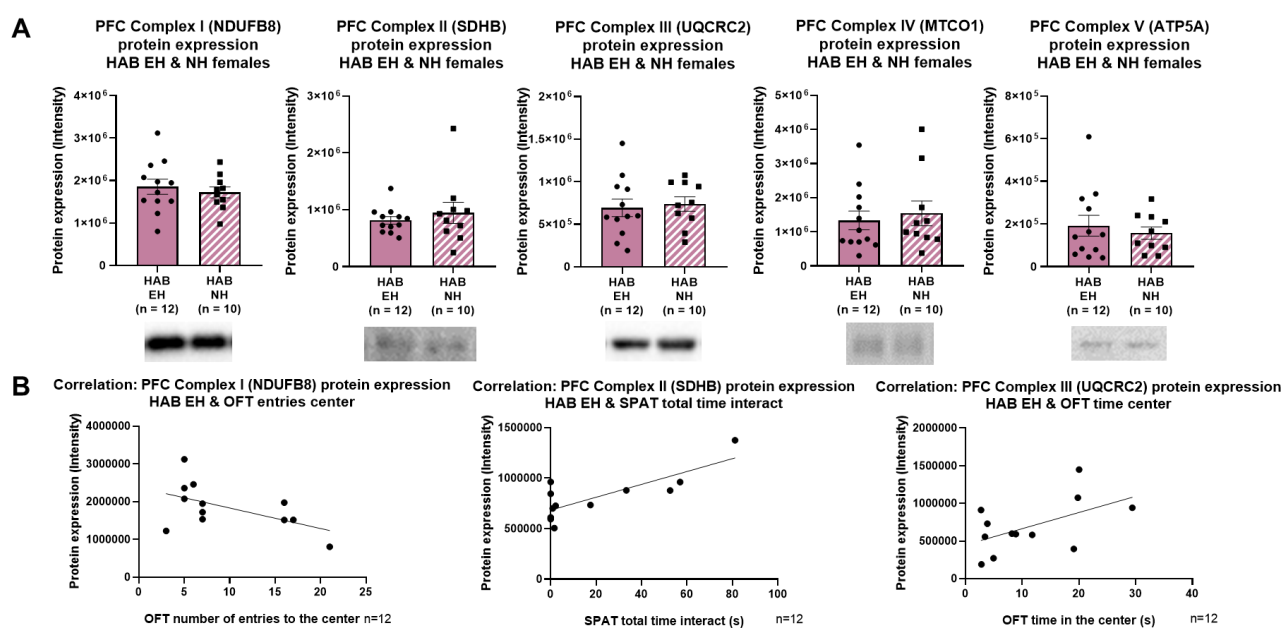


Figure 19. PFC western blot results for OXPHOS proteins. Blot images are below each bar graph. (A) EH did not induce expression level alterations for complex I (NDUFB8), II (SDHB), III (UQCRC2), IV (MTCO1) and V (ATP5A) in the PFC of HAB EH female mice. (B) Complex I (NDUFB8) protein expression had a trend for negative correlation with the number of entries to the center of the OFT (Spearman $r = -0.5010$, $p = 0.0995$ (T)), complex II (SDHB) protein expression had a trend for positive correlation with the total time of interaction of the SPAT (Spearman $r = 0.5303$, $p = 0.0790$ (T)), and complex III (UQCRC2) protein expression had a trend for positive correlation with the time in the center of the OFT (Pearson $r = 0.5312$, $p = 0.0755$ (T)).

4.4.3. EH did not affect mitochondrial dynamics markers in the PFC of HAB EH female mice

A number of mitochondrial dynamics key players for the processes of fusion and fission were differentially expressed in the hypothalamus of HAB EH female mice (see Table B of Figure 8). The next step was to investigate possible mitochondrial dynamics alterations in the PFC.

Mitochondrial Biogenesis

EH did not alter the protein expression levels of either PGC1A splice variant (100 kDa and 60 kDa) (Figure 20A), however in HAB EH female mice, the 100 kDa variant showed a trend for negative correlation of its protein expression with the time swimming in the FST. Additionally, the 60 kDa variant's protein expression correlated positively with the latency to float on the FST, meaning that the higher the PGC1A (60 kDa) protein expression, the lower the depression-like behavior (Figure 20D).

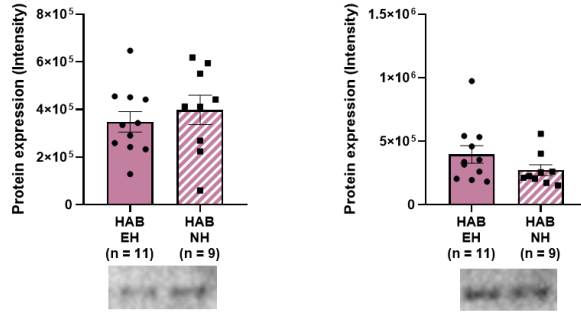
Mitochondrial Fusion

There was no EH-induced alteration in the protein levels of mitochondrial fusion players like MFN2, mitofilin (IMMT) and OPA1 between HAB EH and HAB NH female mice (Figure 20B). Correlation of fusion protein levels for HAB EH female mice with behavior only indicated a trend for positive correlation of MFN2 protein expression with the total time of interaction in the SPAT, meaning that the higher the MFN2 protein expression, the higher the sociability (Figure 20E).

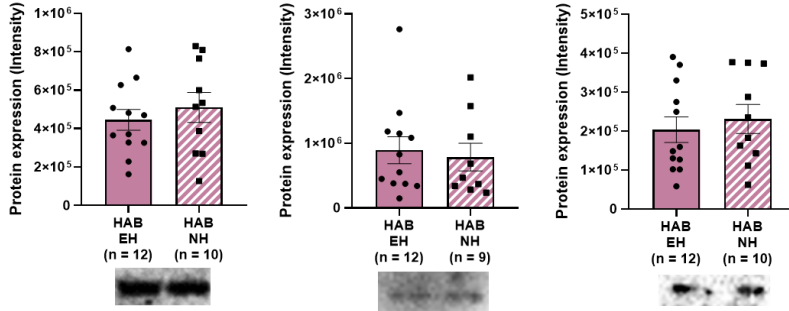
Mitochondrial Fission

There were no EH-induced alterations found in the PFC of HAB EH female mice for the protein expression of fission regulators DRP1, MFF, and SLC25A46 (Figure 20C). DRP1 protein expression for HAB EH female mice had a trend for positive correlation with the total time of interaction on the SPAT, which means that the higher the DRP1 protein expression, the higher the sociability. Additionally, MFF protein levels positively correlated with the time spent in the light compartment of DaLi, which means that the higher the MFF protein expression, the lower the anxiety-like behavior. SLC25A46 protein expression levels showed a trend for negative correlation with the SPA index ($\text{SPA index}(\%) = \frac{\text{time of social interaction}}{\text{time of non-social interaction} + \text{time of social interaction}} \times 100$) of the SPAT, meaning that the higher the SLC25A46 protein expression, the lower the sociability. Additionally, there was a positive correlation with the time spent in the light compartment and a negative correlation with the latency to the light compartment in the DaLi box, indicating that the higher the SLC25A46 levels, the lower the anxiety-like behavior (Figure 20F).

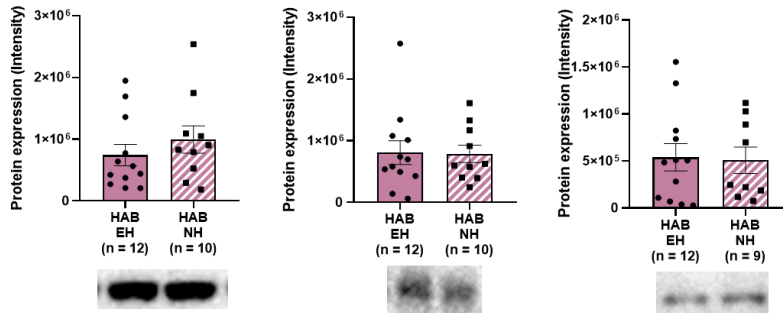
A PFC PGC1A (100kDa) protein expression HAB EH & NH females PFC PGC1A (60kDa) protein expression HAB EH & NH females



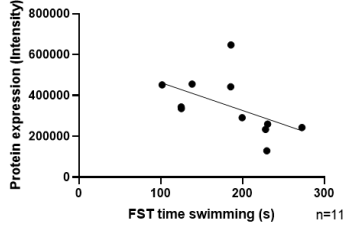
B PFC MFN2 protein expression HAB EH & NH females PFC IMMT protein expression HAB EH & NH females PFC OPA1 protein expression HAB EH & NH females



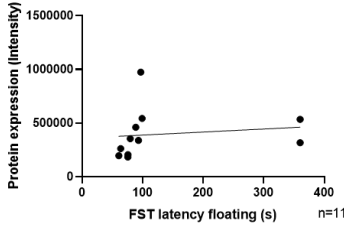
C PFC DRP1 protein expression HAB EH & NH females PFC MFF protein expression HAB EH & NH females PFC SLC25A46 protein expression HAB EH & NH females



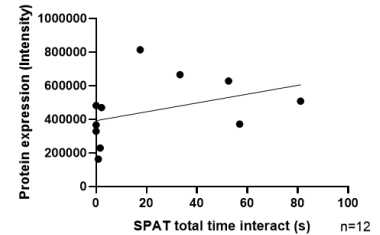
D Correlation: PFC PGC1A (100kDa) protein expression HAB EH & FST time swimming



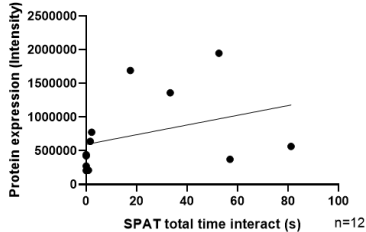
Correlation: PFC PGC1A (60kDa) protein expression HAB EH & FST latency floating



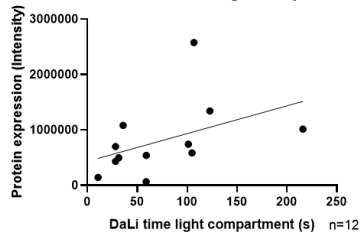
E Correlation: PFC MFN2 protein expression HAB EH & SPAT total time interact



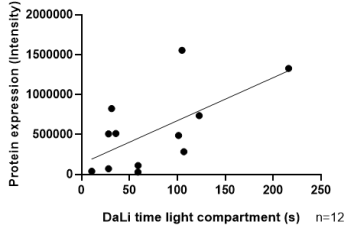
F Correlation: PFC DRP1 protein expression HAB EH & SPAT total time interact



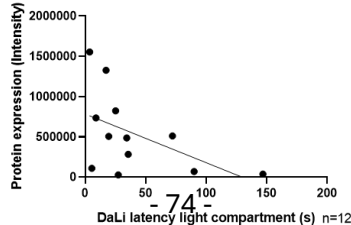
Correlation: PFC MFF protein expression HAB EH & DaLi time light compartment



Correlation: PFC SLC25A46 protein expression HAB EH & DaLi time light compartment



Correlation: PFC SLC25A46 protein expression HAB EH & DaLi latency light compartment



Correlation: PFC SLC25A46 protein expression HAB EH & SPA index

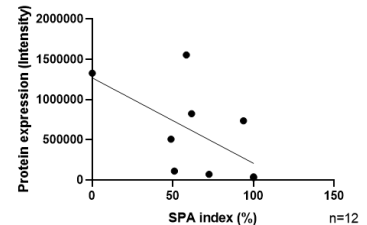


Figure 20. PFC western blot results for the expression levels of proteins involved in mitochondrial biogenesis, fusion and fission. Blot images are below each bar graph. (A) EH did not alter the expression levels of the two splice variants of PGC1A (100 kDa and 60 kDa). (B) There were no statistical differences in the protein expression of MFN2, IMMT and OPA1 between HAB EH and HAB NH female mice. (C) EH did not induce changes in protein expression of DRP1, MFF and SLC25A46. (D) In HAB EH female mice, PGC1A (100 kDa) protein expression had a trend for negative correlation with the time swimming on the FST (Pearson $r=-0.5254$, $p=0.0969$ (T)), while PGC1A (60 kDa) positively correlated with the latency to float on the FST (Spearman $r=0.7198$, $*p=0.0155$). (E) In HAB EH female mice, MFN2 protein expression levels had a trend for positive correlation with the total time of interaction on the SPAT (Spearman $r=0.5552$, $p=0.0645$ (T)). (F) DRP1 protein expression had a trend for positive correlation with the total time of interaction on the SPAT (Spearman $r=0.5517$, $p=0.0663$ (T)). MFF protein expression correlated positively with the time in the light compartment of DaLi (Spearman $r=0.6434$, $*p=0.0278$). SLC25A46 protein expression had a trend for negative correlation with the SPA index of SPAT (Pearson $r=-0.5834$, $p=0.0992$ (T)), a positive correlation with the time in the light compartment of DaLi (Pearson $r=0.6265$, $*p=0.0293$) and a negative correlation with the latency to the light compartment of DaLi (Spearman $r=-0.5874$, $*p=0.0489$).

4.4.4. EH reduced the protein expression levels of PRDX3 in the PFC of HAB EH female mice

Antioxidant proteins, as observed in the hypothalamic proteomics analysis, were differentially expressed for HAB EH female mice (see Table D of Figure 8). In the PFC of HAB EH and HAB NH female mice, western blots showed that EH induced a reduction in the protein expression levels of PRDX3 (Figure 21A). CAT and SOD2 protein levels were not affected by the EH intervention.

PRDX3 protein expression for HAB EH female mice also showed a trend for positive correlation with the time spent in the light compartment of the DaLi test, meaning that the higher the PRDX3 protein expression, the lower the anxiety-like behavior. Additionally, there was a trend for negative correlation with the time floating on the FST, meaning that the higher the PRDX3 expression, the lower the depression-like behavior. CAT protein expression had a trend for negative correlation with the time in the light compartment of DaLi, meaning that the higher the CAT protein expression, the higher the anxiety-like behavior. Lastly, SOD2 protein expression correlated negatively with the number of line crossings, and positively with the latency to the center of the OFT and had a trend for negative correlation with the number of entries to the center of the OFT, meaning that the higher the SOD2 protein expression, the lower the locomotion of the animal and the higher the anxiety-like behavior. SOD2 protein expression also had a trend for positive correlation with the time swimming in the FST, and a trend for negative correlation with the total time of interaction on the SPAT, meaning that the higher the SOD2 protein expression, the higher the sociability (Figure 21B).

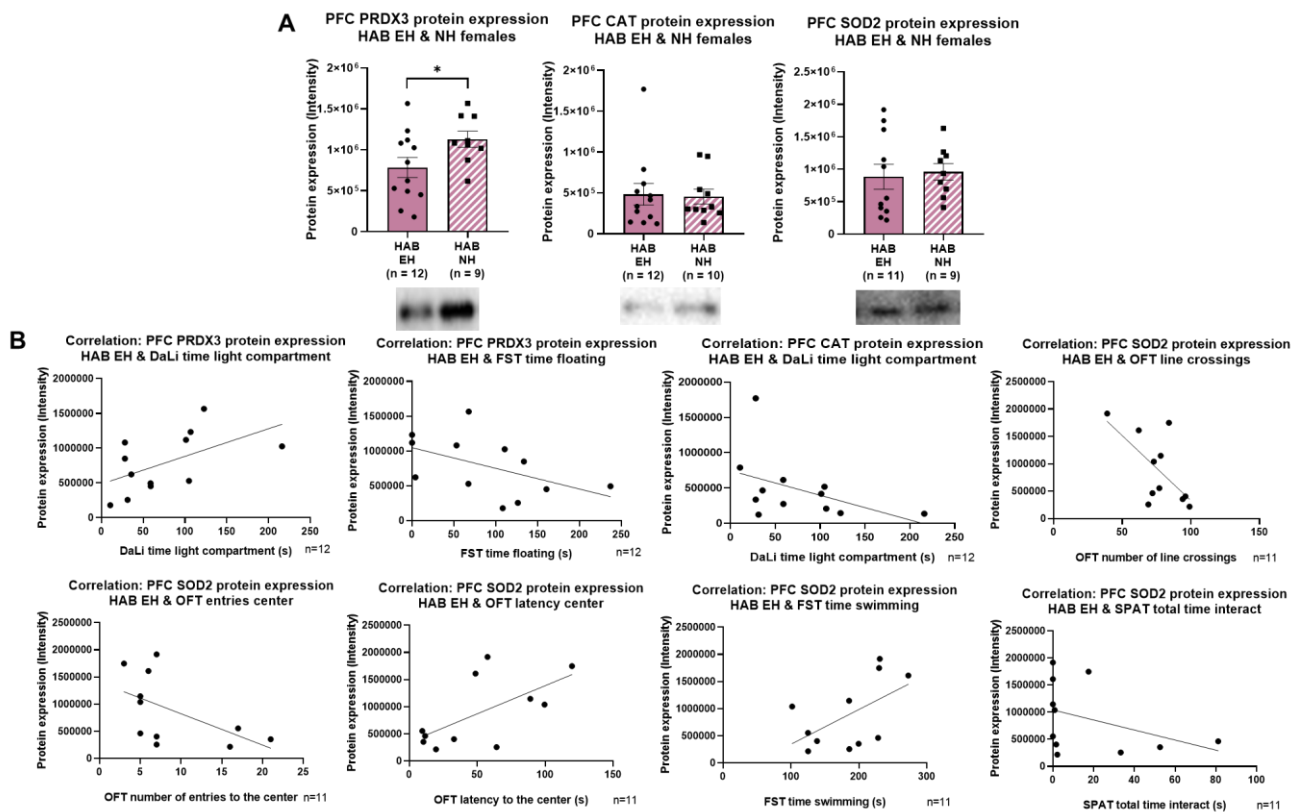


Figure 21. PFC western blot results for the expression levels of antioxidant proteins. Blot images are below each bar graph. (A) PRDX3 was decreased in the PFC of HAB EH female mice, while CAT and SOD2 had no significant alterations. (B) Correlations with behavior. PRDX3 protein expression had a trend for positive correlation with the time in the light compartment of DaLi (Pearson $r=0.5422$, $p=0.0686$ (T)), and a trend for negative correlation with the time floating in the FST (Pearson $r=-0.4983$, $p=0.0992$ (T)). CAT protein expression had a trend for negative correlation with the time in the light compartment of DaLi (Spearman $r=-0.5664$, $p=0.0591$ (T)). SOD2 protein expression had a negative correlation with the number of line crossings (Pearson $r=-0.6393$, $*p=0.0342$), a trend for negative correlation with the number of entries to the center (Spearman $r=-0.5557$, $p=0.0807$ (T)), and a positive correlation with the latency to the center of the OFT (Pearson $r=0.6280$, $*p=0.0386$). It also had a trend for positive correlation with the time swimming on the FST (Pearson $r=0.5496$, $p=0.0799$ (T)) and for negative correlation with the total time of interaction on the SPAT (Spearman $r=-0.5769$, $p=0.0676$ (T)).

4.4.5. EH did not alter the expression levels of selected mitochondrial transport/import proteins in the PFC of HAB EH female mice

Proteins involved in the transport or import of compounds into the mitochondrial matrix, such as ARALAR, TIM23, SFXN1, as well as PNPT1, were identified in the hypothalamic proteomics dataset. Polyribonucleotide nucleotidyltransferase 1 (PNPT1) is a protein located in the mitochondrial intermembrane space responsible for importing RNA molecules into the matrix (Falchi et al., 2022). Western blot assays in PFC lysates aimed to identify differential protein expressions of these carriers in HAB EH female mice.

EH did not alter the protein expression levels of ARALAR, TIM23, SFXN1 and PNPT1 (Figure 22A). However, correlations with behavioral parameters showed that ARALAR protein levels positively correlated with the time in the center of the OFT, meaning that the higher the ARALAR protein expression, the lower the anxiety-like behavior of the animal. Additionally, SFXN1 protein expression showed a trend for negative correlation with the time spent in the light compartment of DaLi, signifying that the higher the SFXN1 protein expression, the higher the anxiety-like behavior (Figure 22B).

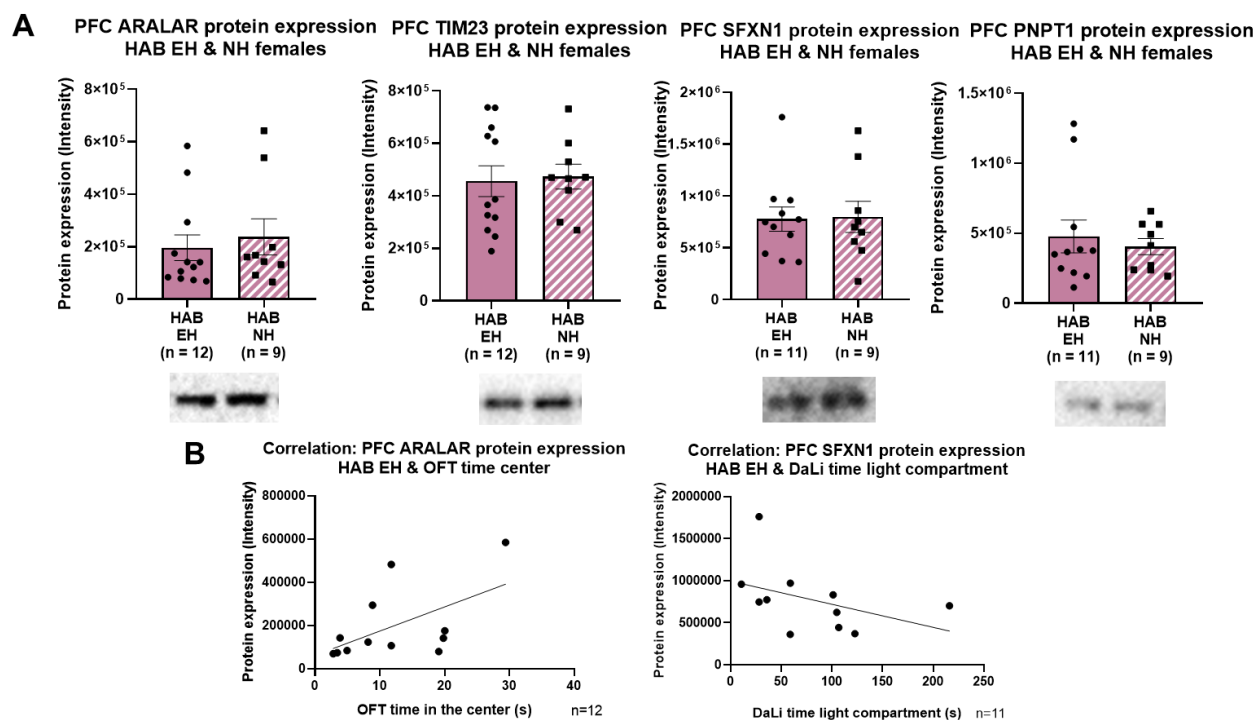


Figure 22. PFC western blot results for the expression levels of proteins involved in mitochondrial transport/import. Blot images are below each bar graph. (A) EH did not alter the expression levels of ARALAR, TIM23, SFXN1 and PNPT1. (B) ARALAR protein expression significantly correlated positively with the time in the center of the OFT (Spearman $r=0.6165$, $*p=0.0361$). SFXN1 had a trend for negative correlation with the time in the light compartment in the DaLi box (Spearman $r=-0.5818$, $p=0.0656$ (T)).

To summarize our PFC results, EH induced a reduction of PKLR, a key regulator of glycolysis, and PRDX3, an antioxidant protein, in the PFC of HAB EH female mice. These alterations are PFC-specific, since neither protein was differentially expressed in the hypothalamus of HAB EH female mice, as deduced by our proteomics analysis. No alterations were observed for mitochondrial dynamics-related proteins, or proteins participating in mitochondrial transport/import and mitochondrial energy production. Correlations of the expression levels of all proteins assessed in the PFC showed that for HAB EH female mice, HK2, another glycolytic enzyme, fission proteins MFF, DRP1 and SLC25A46, as well as SOD2, an antioxidant enzyme correlated with anxiety- and depression-like behavior.

4.5. PLASMA

In the hypothalamus and PFC of HAB EH female mice, altered antioxidant protein levels were noted, hinting at an EH-induced differential expression of redox markers. Additionally, in the PFC of HAB EH female mice, glycolysis was altered, with PKLR being reduced for HAB EH female mice. To follow up on these findings, we assessed the redox status as well as the protein levels for enzymes involved in carbohydrate metabolism and energy production in the plasma of HAB EH vs. HAB NH female mice. All blot images used for the quantification of protein expression levels are shown in Appendix 3.

4.5.1. EH did not alter TAC levels in the plasma of HAB EH female mice

To investigate whether EH impacts the redox balance and the antioxidant capacity in the HAB female mice, we measured TAC levels in plasma. Comparison between HAB EH and HAB NH female mice showed no significant differences in the TAC levels for the two groups (Figure 23A). Correlation of the TAC values with the behavioral parameters for all four tests (DaLi, OFT, FST, SPAT) showed that plasma TAC for HAB EH mice had a trend towards a negative correlation with the number of line crossings on the OFT, which means that the higher the TAC levels, the lower the locomotion in the OFT (Figure 23B).

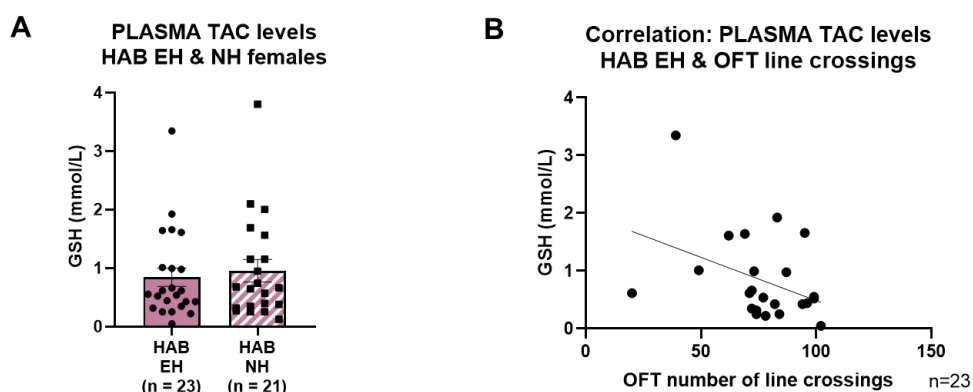


Figure 23. Results for the TAC assay in plasma. (A) TAC levels for HAB EH vs. HAB NH female mice do not exhibit significant differences. (B) Plasma TAC levels for HAB EH female mice showcase a trend for reduced correlation with the number of line crossings on the OFT (Spearman $r=-0.4065$, $p=0.0543$ (T)).

4.5.2. EH induced a trend for decreased protein expression levels of CYTC in the plasma of HAB EH female mice

Following up our investigation of the carbohydrate metabolism machinery protein levels in the PFC, we studied the protein expression of glycolytic and energy production enzymes in plasma, namely GAPDH, ENO1, LDHB, an enzyme partaking in lactate metabolism, and CYTC. CYTC is a small heme protein the main role of which is to participate in the ETC of OXPHOS as an electron carrier (Hüttemann et al., 2011).

We found no difference for the protein expression levels of glycolytic enzymes GAPDH and ENO1, as well as for the expression levels of LDHB (Figure 24A). TCA cycle enzymes as well as

protein subunits of the OXPHOS complexes are at the center of cellular metabolism and mitochondrial function. The EH intervention led to a trend for decreased protein expression of CYTC in the plasma of HAB EH female mice (Figure 24B).

Correlation of plasma protein expression levels of HAB EH female mice with behavioral parameters for all four tests showed that plasma GAPDH protein expression levels positively correlated with the latency to the light compartment of the DaLi box, as well as with the SPA index (%), which means that the higher the GAPDH protein expression, the higher the anxiety-like behavior and the sociability. GAPDH protein expression levels also correlated negatively with the time floating on the FST, meaning that the higher the GAPDH protein expression, the lower the depression-like behavior. Plasma LDHB protein expression levels correlated positively with the time floating on the FST, meaning that the higher the LDHB protein expression, the higher the depression-like behavior (Figure 24C). Lastly, CYTC protein expression levels correlated positively with the time struggling on the FST and negatively with the total time of interaction on the SPAT, meaning that the higher the CYTC protein expression levels, the lower the sociability (Figure 24D).

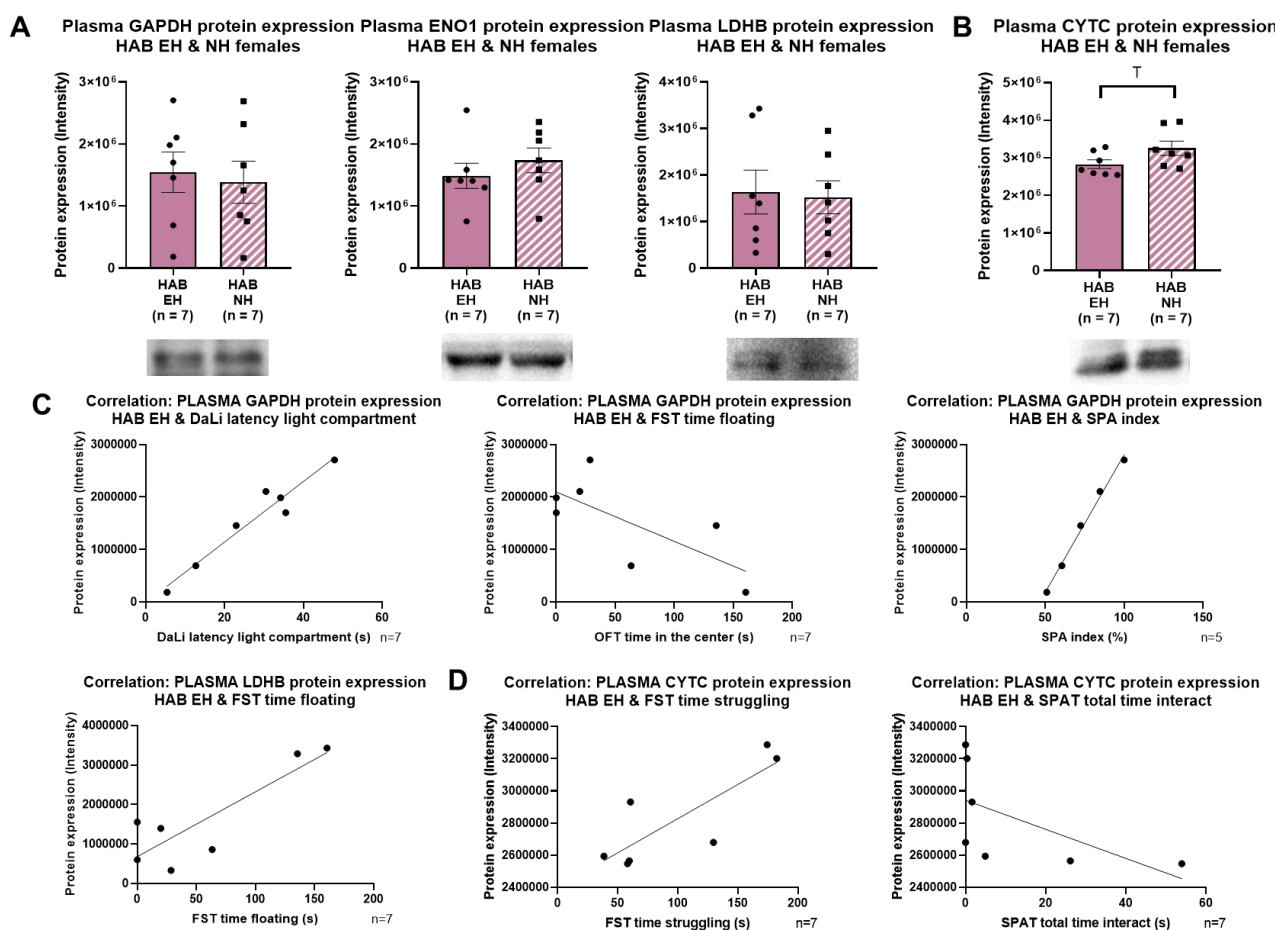


Figure 24. Plasma western blot results for proteins involved in carbohydrate metabolism and energy production. Blot images are below each bar graph. (A) GAPDH, ENO1, LDHB expression levels had no significant alterations for HAB EH vs. HAB NH female mice. (B) CYTC showcased a trend for reduced protein expression in the plasma of HAB EH female mice (Welch's *t* test, $p=0.0858$ (T)). (C) Correlations of protein expression

levels for HAB EH female mice with behavior. GAPDH protein levels correlated positively with the latency to the light compartment of DaLi (Pearson $r=0.9682$, $***p=0.0003$) and the SPA index (%) (Pearson $r=0.9960$, $***p=0.0003$), and had a trend for negative correlation with FST's time floating (Pearson $r=-0.7125$, $p=0.0724$ (T)). LDHB correlated positively with the time floating on the FST (Pearson $r=0.8570$, $*p=0.0137$). CYTC correlated positively with the time struggling on the FST (Pearson $r=0.8225$, $*p=0.0231$) and negatively with the total time of interaction on the SPAT (Spearman $r=-0.8469$, $*p=0.0254$).

4.5.3. EH did not alter the expression levels of antioxidant proteins in the plasma of HAB EH female mice

To further investigate the EH-driven effect on the redox status, we conducted western blots to study the protein expression levels of antioxidant proteins such as SOD2, PRDX3, PRX and GSR in plasma. Antioxidant protein expression levels in the plasma showed no differences for HAB EH vs. HAB NH female mice (Figure 25A).

The plasma protein expression for these four proteins, SOD2, PRDX3, PRX and GSR, was correlated with all behavioral parameters as well as with the TAC levels for these animals. We found that PRDX3 correlated negatively with TAC levels in plasma of HAB EH female mice. Additionally, PRX protein expression levels correlated negatively with two parameters of the OFT, namely time in the center and entries to the center, meaning that the higher the PRX expression, the higher the anxiety-related behavior (Figure 25B).

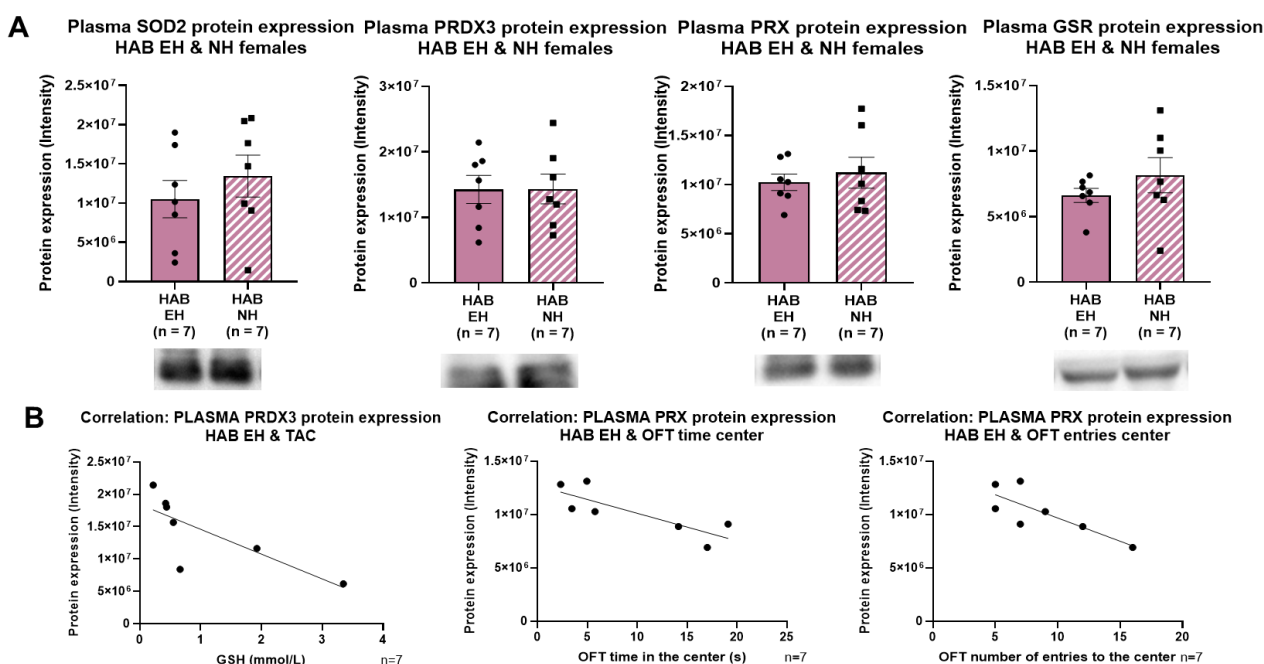


Figure 25. Plasma western blot results for antioxidant proteins. Blot images are below each bar graph. (A) SOD2, PRDX3, PRX and GSR protein expression levels showed no significant alterations for HAB EH vs. HAB NH female mice. (B) Correlations of plasma protein expression levels for HAB EH female mice with TAC values and behavior. PRDX3 protein expression levels correlated negatively with TAC for HAB EH female mice (Spearman $r=-0.9643$, $**p=0.0028$). PRX protein expression levels correlated negatively for time in the center

*(Pearson $r=-0.8185$, $*p=0.0244$) and entries to the center (Pearson $r=-0.7944$, $*p=0.0328$) of the OFT for HAB EH female mice.*

To summarize our plasma results, EH did not induce differences in the TAC or the expression levels of proteins with antioxidant role and proteins involved in carbohydrate metabolism. Alterations noted in the PFC for PKLR and PRDX3, proteins involved in glycolysis and antioxidant defense respectively, appear to be brain-specific and do not reflect peripheral material alterations. Additionally, EH led to a trend for reduced expression for CYTC, a protein that is part of the ETC of the OXPHOS machinery, hinting at energy production alterations in the periphery as well as the brain. Correlations of these protein expression levels for HAB EH female mice with TAC levels and behavior showed that GAPDH, a glycolytic enzyme, and antioxidant proteins correlated significantly with anxiety-like behavior.

5. DISCUSSION

A gap in the literature surrounding early life interventions and particularly EH deals with the impact of such interventions in a high anxiety background, and the potential involvement of mitochondria in their molecular underpinnings. Applying an EH protocol in our lab has helped elucidate these mechanisms. Male and female pups from both HAB and NAB lines were handled from PND 1 to PND 15 for 15 min each day. SPAT was conducted on PND 31 to assess the adolescent pups' sociability, and during adulthood, DaLi, OFT and FST took place, to investigate EH-driven alterations in anxiety- and depression-like behavior. Our previous study, focusing on male mice only, showed that EH exerts an anxiolytic effect on HAB mice. On a molecular level, this anxiolysis was accompanied in the HYP by protein expression alterations for glycolytic enzymes PKLR and ENO1 as well as mitochondrial dynamics mediators DRP1, PGC1a and OPA1, and an mRNA expression reduction for biogenesis instigator gene *tfam*. In the PFC, there were no alterations to protein expression, however the mRNA levels of mitochondrial biogenesis (*pgc1a*, *tfam*), fusion (*opa1*), fission (*fis1*) and mitophagy (*prkn*) genes were significantly altered, implicating mitochondrial pathways as the biological basis of EH (Thomou et al., 2024)

In this thesis, we investigated whether similar findings are reflected in HAB female mice. To achieve that, after observing the behavior of HAB EH female mice following the EH intervention, we used MS-based proteomics to assess the EH-driven effect on the hypothalamic proteome. Following this analysis in the hypothalamus, we assessed the mRNA levels of genes involved in mitochondrial dynamics using qRT-PCRs, and measured the mtDNA_{cn}, a proxy marker for mitochondrial numbers, using qPCR. To study whether the EH-driven molecular impact on the proteome is limited to the hypothalamus, we used western blots to check the protein levels of enzymes involved in carbohydrate and mitochondrial metabolism, OXPHOS, mitochondrial dynamics, mitochondrial import/transport, as well as antioxidant proteins. Antioxidant activity was also assessed in plasma using the TAC assay and additionally, western blots were conducted to examine the protein expression levels of redox enzymes as well as enzymes participating in carbohydrate metabolism and OXPHOS.

Assessment of the behavioral phenotype of HAB female mice exposed to the EH intervention showed that they, similar to HAB male mice, also exhibit decreased anxiety-related behavior in the DaLi box, a test assessing anxiety-like behavior, compared to HAB NH female mice. Molecularly, our proteomics data primarily revealed alterations in three main protein groups, mRNA splicing regulators, ribosomal components and OXPHOS components. Alterations in mitochondrial dynamics mediators were also observed at the mRNA level in the hypothalamus of HAB EH female mice. In our results, there was both region specificity, because in the PFC we observed alterations in carbohydrate metabolism enzymes and antioxidant proteins, and brain specificity, since only OXPHOS protein expression alterations were observed in plasma. Correlations of these readouts with behavior on both the mRNA and the protein levels indicate a link between EH-driven molecular alterations and anxiety-like behavior.

5.1. Hypothalamus: the mediator of EH-driven molecular responses

The hypothalamus is known for being the control panel of the brain; it brings together a variety of sensory inputs and based on them, activates autonomic, behavioral and endocrine responses to maintain the body's homeostasis and control basic life functions (Saper & Lowell, 2014). Homeostatic equilibrium is majorly maintained through the actions of the HPA axis, the role of which is to release glucocorticoids that activate short-term physiological responses to stress (Sheng et al., 2021). Short-term stress is necessary for development; however, prolonged stress leads to HPA axis dysregulation and pathology, which has been associated with mood and anxiety disorders (Dunlavy, 2018; Fischer, 2021). For this reason, we have placed the hypothalamus at the center of the EH research featured in this work.

Our investigation of the molecular underpinnings of EH was guided by the results granted by our proteomics analysis, which we conducted on the hypothalamus to gain a systemic understanding of the EH-driven alterations in this region. Of the 5503 proteins that were quantified, 839 were differentially expressed, and 429 were upregulated. Sorting these upregulated proteins based on descending fold change value, ten hits were highlighted, and these proteins were then correlated with the behavioral parameters of all the tests we conducted for the EH protocol, to evaluate whether their levels correlate with anxiety- or depression-like behavior. Three proteins were highlighted that way: ATP4A, CKM and PFKFB1.

ATP4A is an ATP-dependent proton pump responsible for the exchange of H⁺ cations with K⁺ cations across the cell membranes. ATP4A protein expression is mainly enriched in the stomach tissue, where it is associated with gastric acid secretion. *ATP4A* mutations cause gastric epithelium abnormalities as well as achlorhydria and hypergastrinemia, conditions associated with insufficient gastric acid production (Spicer et al., 2000). In our findings, we reported that increased ATP4A protein expression levels in the hypothalamus correlated with increased depression- and anxiety-like behavior. To our knowledge, this is the first instance of this protein being associated with behavior, however, ATP4A has been associated with proper mitochondrial function, because *ATP4A* mutations impede mitochondrial biogenesis and cause mitochondrial malfunction, which in turn activates ROS signaling to trigger cellular apoptosis (Benítez et al., 2020).

CKM is a transferase responsible for the transfer of phosphate between ATP and various phosphogens, such as creatine phosphate. The exchange between creatine and creatine phosphate in the cells is considered essential for energy transport and regulation of ATP levels. For this reason, CKM cytosolic and mitochondrial isoenzymes are located in ATP generation and consumption sites, working to maintain the energetic homeostasis of the cells by mediating metabolic reactions outside and inside of the mitochondria, like glycolysis and OXPHOS (Font et al., 1987; Schlattner et al., 2018; Schlattner et al., 2006). Consequently, the role of CKM in behavioral alterations could be related to its link with energy production, processes for which the mitochondria play a central role.

PFKFB1 catalyzes the synthesis and degradation of fructose 2,6-biphosphate, a substrate responsible for the simultaneous activation of glycolysis and the inhibition of gluconeogenesis. PFKFB1 contributes to glucose homeostasis and metabolic control within the cell, which is highly important in organs with high energy demands such as the brain and the liver. Specifically in the brain, dysregulated PFKFB1 expression has been associated with autism spectrum disorder as well as mood disorders, including bipolar disorder and schizophrenia (Guan et al., 2019), with one study specifically indicating that rats exhibiting depression-like behavior had elevated *pfkfb1* mRNA expression levels in both the cerebellum and the PFC (Yamamoto et al., 2015). Our data, which had increased PFKFB1 protein expression levels correlating with increased depression-like behavior agree with this study, hinting at a link between glycolytic regulation and mood disorders.

Our main findings in the hypothalamus highlighted the overrepresentation of two pathways for HAB EH female mice, one of them having to do with RNA processing and protein synthesis. Regarding RNA processing, a number of components that were differentially expressed were proteins associated with the spliceosome, a large RNA-protein complex that is responsible for nuclear pre-mRNA processing. The spliceosome catalyzes both the splicing of introns from the pre-mRNA substrate and the ligation of exons, and it is comprised of two components, five RNA-protein subunits (snRNPs), U1, U2, U4, U5, U6 and other non-snRNP protein splicing factors (Lamond, 1993). Differential expression was noted for both snRNP components, like SNRNP200, part of the U5-snRNP complex, and other protein splicing factors, such as U2AF2, an auxiliary U2-snRNP factor and PRPF8, a U2-, U5, and U6-snRNP assembly factor. Spliceosome dysregulation causes neurological deficits that are specifically associated with neurodevelopmental and neurodegenerative disorders like autism spectrum disorder and Alzheimer's disease, respectively (Hsieh et al., 2019; Li et al., 2024). Our findings, which hint at a link between RNA splicing and behavior, may imply a novel field for anxiety and early life experiences research.

Ribosomal components of the protein synthesis machinery were also differentially expressed in the hypothalamus, and interestingly, they were all upregulated in HAB EH compared to HAB NH female mice. Ribosomes, like the spliceosome, are RNP complexes consisting of two subunits with distinct roles in protein synthesis: the large ribosomal subunit, responsible for the catalytic formation of peptide bonds between amino acids, and the small ribosomal subunit, responsible for binding the mRNA and reading genetic information. Ribosomes are localized to the cytosol, but organelles such as mitochondria, that carry their own DNA, also have ribosomes, which are often referred to as mitoribosomes. Mitoribosomes are structurally different from cytosolic ribosomes; their sedimentation coefficient is 55S as opposed to 80S for cytosolic ribosomes, and they consist of a 39S large subunit and a 28S small subunit as opposed to cytosolic ribosomes, which consist of a 60S large and a 40S small subunit, respectively. Additionally, mitoribosomes are poorer in rRNA, since they contain 25-30% rRNA compared to cytosolic ribosomes, which contain 50-60% (Spremulli, 2016). The assembly of mitoribosomal subunits requires the coordination of both nuclear and mitochondrial gene expression, since mitoribosomal proteins are nuclear-encoded, and mitoribosomal RNAs are

mitochondrial-encoded. If an imbalance is created between the two processes, mitoribosomes are not assembled correctly, which leads to mitochondrial dysfunction, and an arrest in cell proliferation, generating pro-apoptotic signaling pathways (Raimundo, 2014). For this reason, it can be assumed that anything that affects the ribosomal machinery, either inside or outside the mitochondrion, does also affect proper mitochondrial function.

A potential link between ribosomes and behavior has been investigated in the literature. In male mice subjected to chronic social defeat stress, upregulated ribosomal and mitoribosomal gene expression was observed in the hypothalamus due to the development of anxiety- and depression-like behaviors (Smagin et al., 2016). The same group has also reported upregulated ribosomal and mitoribosomal gene expression in the hypothalamus of male mice with long and repeated experience of aggression and wins in fights (Smagin et al., 2018). In a study comparing the PFC ribosomal gene expression of postmortem major depressive disorder patients and mice with chronic variable stress, which is an intervention simulating major depressive disorder features, it was found that in both conditions, the expression levels of ribosomal genes were decreased (Zhang et al., 2023). Consequently, a ribosome hypothesis for mood disorders has been proposed, due to the fact that ribosomal gene dysregulation can alter the number and composition of ribosomes, leading to impaired protein synthesis and therefore, neuronal dysregulation (Sharma et al., 2024). In our research, readouts for all cytosolic and most mitochondrial ribosome protein levels were upregulated in the hypothalamus of HAB EH compared to HAB NH female mice, which, considering the fact that EH ameliorated high anxiety-like behavior, contradicts previously mentioned findings. Whether this ribosomal upregulation is involved in a feedback mechanism following hypothalamic activation caused by the EH intervention, or whether it indicates ribosomal and mitochondrial dysfunction following the EH-induced resilience, remains to be elucidated through further investigation.

Recent evidence suggests that mitochondrial and cytosolic translations are not as isolated events as previously thought. Ribosomes are often localized in proximity to organelles with increased protein synthesis needs, which is frequently the case for mitochondria. This localized translation mediates mitochondrial quality control, by responding to mitochondrial damage with the synthesis of proteins involved in mitophagy, such as PINK1, but more importantly, it plays a role in mitochondrial regulation, catering translation of mitochondrial proteins according to cellular and energetic needs (Cohen et al., 2024). A series of studies investigating the localization of mRNAs encoding mitochondrial proteins showed that mRNAs localized near the mitochondria predominantly concerned OXPHOS components, highlighting the high degree of coordination needed for the translation of both nuclear- and mitochondrial-encoded OXPHOS subunits and their subsequent assembly (Fazal et al., 2019; Marc et al., 2002; Matsumoto et al., 2012). Interestingly, in our data, aside from the noted upregulation in ribosomal protein expression, a number of OXPHOS components were also differentially expressed in the hypothalamus of HAB EH female mice.

OXPHOS is a cellular respiratory process which takes place in the mitochondria. Its first four complexes, complex I (NADH dehydrogenase), II (succinate dehydrogenase), III (cytochrome c

oxidoreductase), and IV (cytochrome c oxidase), comprise the ETC and are responsible for the production of reductive power which is then used by the last complex, complex V (ATP synthase), to generate ATP. Due to the increased energy demands of the brain, and the additional energetic toll of high anxiety states (Filiou & Sandi, 2019), the impact of anxiety-like behaviors on OXPHOS efficiency has been extensively investigated, however its results have been conflicting. In cortical synaptosomes from HAB mice, subunits from all five complexes had upregulated expression compared to synaptosomes from LAB mice, which led to reduced efficiency of the ETC and increased ROS production (Filiou et al., 2011a). However, in the nucleus accumbens of highly anxious Wistar rats, there was decreased complex I and II protein expression levels, respiratory capacity and ATP levels, as well as decreased complex I activity and maximal mitochondrial respiration when compared to low anxious animals (Gebara et al., 2021; Hollis et al., 2015). In the hypothalamus of Sprague-Dawley male rats subjected to a chronic mild stress paradigm used for the assessment of depression- and anxiety-like behavior, there was differential expression of selected complex I and V protein subunits, indicating HPA axis energy imbalances (Gong et al., 2021). These findings imply a brain region- and rodent model-specific relationship between anxiety and OXPHOS. In our results, hypothalamic expression levels for complex I-IV subunits varied, however protein expression for complex V was increased for HAB EH female mice. This increase indicates that there is a noted imbalance in energy production through OXPHOS following the EH paradigm. So, the EH intervention, through its induced anxiolysis, may ameliorate the high anxiety phenotype by adapting hypothalamic energy production. Further research concerning the metabolic efficiency and the respiratory capacity in HAB EH animals could provide valuable insight into the mechanisms of this alteration.

Fluctuating metabolic and energetic demands in the cell are met by adjusting the morphology, number and content of mitochondria through mitochondrial biogenesis, fusion, fission and mitophagy events, collectively called mitochondrial dynamics. Biogenesis involves the transcription and translation of mtDNA, as well as the synthesis, import and assembly of mitochondrial proteins encoded by nuclear DNA, so new mitochondria can be created from already existing ones (Popov, 2020). In fusion, two mitochondria are joined at the OMM and IMM to increase their mitochondrial membrane potential and their energy production through OXPHOS (Yao et al., 2019). Antagonistic to fusion is fission, where a mitochondrion is either divided into two daughter mitochondria via midzone scission, or degraded via peripheral scission, which activates signals for mitophagy (Adebayo et al., 2021). Mitophagy is a mitochondrial quality control mechanism which removes and recycles dysfunctional mitochondria to prevent cell death (Picca et al., 2023).

Even though the field of mitochondrial dynamics is a recent addition to mitochondrial biology, emerging data suggests that mitochondrial dynamics perturbations are implicated in psychopathologic phenotypes. The mitophagy PINK1/PRKN pathway has been shown to mediate anxiety- and depressive-like responses, while reduced mitochondrial biogenesis is involved in the mediation of depression (Jiang et al., 2024; Papageorgiou & Filiou, 2024). With correlation of our mRNA expression data for genes involved in mitochondrial dynamics with anxiety- and depression-

like behavior, some behavioral patterns were observed. mRNA expression levels for biogenesis mediators *tfam* and *pgc1a* correlated with anxiety-like behavior and sociability, with higher mRNA levels indicating higher anxiety and sociability in the OFT and the SPAT, respectively. For fusion genes, specifically *msto1* and *mfn2*, their mRNA expression correlated positively with anxiety-like behavior, meaning that the higher the mRNA levels, the higher the anxiety-like behavior as it was observed in the OFT. Fission mediators showed a complex relationship with behavioral parameters, with mRNA levels for *mid51* correlating positively with depression-like behavior in the FST, meaning that the higher the mRNA expression, the higher the depression-like behavior. *Gdap1* mRNA levels correlated positively with anxiety-like behavior in the DaLi box, meaning that the higher the mRNA expression, the higher the anxiety-like behavior, however for other genes, namely *fis1*, *mff* and *dnm2*, the mRNA levels correlated negatively with anxiety-like behavior in DaLi and the OFT, meaning that the higher their mRNA levels, the lower the anxiety-like behavior. These findings hint at the complex yet increasingly acknowledged relationship between behavior and mitochondrial dynamics.

At a molecular level, in our findings, a number of proteins involved in mitochondrial fusion, fission and mitophagy had differential expression in the hypothalamus of HAB EH female mice (see Table B of Figure 8). Due to these protein readouts, the mRNA expression levels of mitochondrial dynamics genes for all four processes were assessed in the hypothalamus of HAB EH female mice. *Fis1* mRNA levels were reduced for HAB EH female mice, whereas *tfam* mRNA levels has a decreasing trend.

FIS1 is an integral membrane protein anchored to the OMM and consists of a transmembrane and a cytosolic domain. The transmembrane domain is made up of the C-terminal of the protein, which is anchored to the OMM. The cytosolic domain contains six alpha helices, with four of them containing two tandem tetratricopeptide repeat-like motifs, which fold together to produce a single domain that creates a concave surface (Lees et al., 2012). The N-terminal, often dubbed the FIS1 arm, does not belong in the tetratricopeptide repeat fold and is inherently dynamic. It exists in an equilibrium between open and closed states, modulating FIS1 function and interaction with other proteins, mediating fission events (Egner et al., 2022; Lees et al., 2012). In fission, FIS1 acts as a mitochondrial receptor for DRP1, which assembles at the mitochondrial fission sites and oligomerizes, constricting the OMM in a GTP-dependent manner (Otera et al., 2013). It has also been found that FIS1 is an important component of apoptotic and mitophagic pathways, not only by signaling the initiation of mitophagy after the peripheral scission of a damaged mitochondrion, but also by downstream interaction with mitophagy mediators (Ihenacho et al., 2021).

In our data, we observed that, even though hypothalamic FIS1 protein expression was reduced for HAB EH female mice, hypothalamic *fis1* mRNA expression was increased. In HAB EH male mice, an increase in *fis1* mRNA expression levels was also observed, but in the PFC instead of the hypothalamus (Thomou et al., 2024). The bidirectional effect for the HAB EH female mice was also made apparent when correlating *fis1* mRNA and FIS1 protein expression with anxiety-like behavior, with *fis1* mRNA expression correlating negatively with the latency to the light compartment

of DaLi, indicating low anxiety-like behavior, but FIS1 protein expression correlating positively with that same parameter, indicating high anxiety-like behavior (see Figure 16C). In an effort to understand this bidirectional effect of EH on *Fis1* gene expression, we analyzed the amino acid sequence of FIS1 and observed the exon distribution and the localization of both the FIS1 peptide fragments identified with our LC-MS/MS proteomics analysis, and the localization of the primers used for the assessment of the mRNA expression levels of *fis1*. The results are shown in Figure 26.

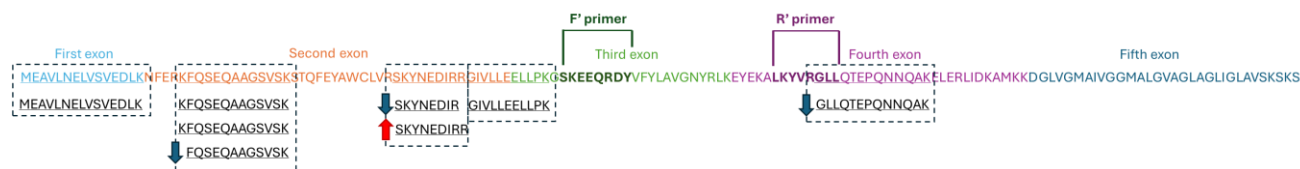


Figure 26. Schematic representation of the amino acid sequence for FIS1. The amino acids encoded by each of the five exons comprising the *fis1* mRNA sequence are color coded. First exon: light blue, second exon: orange, third exon: green, fourth exon: purple, fifth exon: dark blue. F' and R' primers used for the determination of the mRNA expression levels of *fis1* with qRT-PCR are indicated with brackets above the sequence and bold letters onto the sequence. The eight different FIS1 peptide fragments quantified with LC-MS/MS proteomics are shown below the sequence, aligned according to their localization and highlighted with boxes for easier observation. Of these eight peptides, only four were differentially expressed, with three of them being downregulated and the fourth being upregulated. Directionality of the expression is indicated next to each peptide using red (for upregulation) or blue (for downregulation) arrows.

The FIS1 peptides quantified in our proteomics analysis, as observed in Figure 26, are distributed across the amino acid sequence, with most of them being localized near the N-terminal. The *fis1* primers encoding the qRT-PCR product are localized within the tetratricopeptide repeat motifs, on the cytosolic domain, almost overlapping with one of the FIS1 peptides that was downregulated for HAB EH female mice. This information may suggest that the differential expression between the mRNA and protein of the *Fis1* gene is not due to structural differentiation between the PCR product and the proteomics peptides, and instead may be caused by discrepancies in the mRNA and protein concentrations within the cell. The production and maintenance of a protein includes mRNA- (transcription, processing, and degradation of the mRNA molecule), and protein-related processes (translation, localization, modification and programmed degradation of the protein) (Vogel & Marcotte, 2012). These events all function according to the maintenance of a complex cellular equilibrium, and consequently, mRNA abundance cannot always accurately reflect protein abundance within the cell (Prahabar et al., 2024). Protein level variations can account for mRNA level variations ~30 to ~85% of the time, with the remaining ~15 to ~70% being explained by post-transcriptional and post-translational regulations (de Sousa Abreu et al., 2009). Post-transcriptional events include alternative splicing, mRNA molecule cleavages, chemical modifications, or conformational changes (Machnicka et al., 2013), while post-translational events refer to biochemical modifications of specific amino acids (Zhong et al., 2023). FIS1 is subjected to a variety of post-translational modifications,

including phosphorylation (which promotes fission events), ubiquitination (for PRKN-mediated degradation), SUMOylation (which enhances mitochondrial localization) and acetylation (Qin & Xi, 2022).

Taking everything into consideration, the discrepancy between the *fis1* mRNA expression and the FIS1 protein expression described above may be the product of a series of complex alterations occurring between transcription and translation of the *Fis1* gene. These could lead to bidirectional expression levels for a gene product, without implying experimental error. Additional insight into EH-induced alterations to the hypothalamic transcriptome as well as the investigations of post-translational modifications for FIS1 could grant valuable knowledge about the underpinnings of this discrepancy while also elucidating anxiety and EH-induced alterations on *Fis1* expression.

TFAM is a DNA binding, nuclear-encoded protein that plays an active role in the expression, maintenance and organization of mtDNA. It binds upstream of the light- and heavy-strand promoters of mtDNA, promoting its transcription and subsequently its replication through the production of RNA transcripts used as primers, which are encoded by the light-strand promoter (Larsson et al., 1998). Additionally, TFAM also mediates mtDNA packaging; even though it is a sequence-specific transcription factor, it also has high affinity for non-specific DNA, and it therefore can organize the mtDNA into compact DNA-protein nucleoids within the mitochondrial matrix (Ngo et al., 2011). Concerning mitochondrial biogenesis, PGC1A activation leads to the activation of a series of transcription factors which mediate an increase in TFAM protein expression and subsequently the replication of mtDNA (Picca et al., 2023; Popov, 2020).

In our work, we observed a trend for reduced mRNA expression of *tfam* in the hypothalamus of HAB EH female mice. A similar alteration was not observed on a protein expression level; however, it indicates an EH-induced impairment in mitochondrial biogenesis. For HAB EH female mice, *tfam* mRNA levels were decreased both on the hypothalamus, as is the case here, and on the PFC (Thomou et al., 2024). Interestingly, *Tfam* expression highly correlates with mtDNA levels, which can be measured indirectly using the mtDNAcn measurement (Ekstrand et al., 2004). Indeed, in our results, aside from the decrease in *tfam* levels, we also report a significant reduction in hypothalamic mtDNAcn for HAB EH compared to HAB NH female mice.

MtDNAcn represents the number of copies of the mitochondrial genome per nucleated cell (Picard, 2021), and it can be measured using qPCR-based methods for the simultaneous assessment of the levels of a mitochondrial-encoded gene and a nuclear-encoded gene (Filograna et al., 2021). Alterations to the abundance of mtDNA can cause mitochondrial dysregulation and impair essential functions like respiration and energy production (El-Hattab et al., 2017). For this reason, mtDNAcn has been identified as a marker of pathology, with variations being reported in various health conditions, such as cardiovascular disease, chronic kidney disease, diabetes, and cancer (Castellani et al., 2020; Maassen et al., 2004), including neurodegenerative diseases like Alzheimer's and Parkinson's disease (Campbell et al., 2012; Coskun et al., 2012).

Regarding behavior, a multitude of studies investigating mtDNAcn with association to depressive disorders are conflicting, with some reporting an increase to mtDNAcn in brain (Torrell et al., 2013) and blood samples (Chung et al., 2019; Ochi et al., 2023; Ryan et al., 2023), while others have found a decrease for mtDNAcn in leukocytes (Chang et al., 2015; Kim et al., 2011) and plasma (Kageyama et al., 2018). An increase in mtDNAcn has been noted in blood (Wang et al., 2017) and leukocyte samples (Tyrka et al., 2016) of patients exhibiting anxiety symptoms. These findings are in contrast with our results, however, the noted reduction combined with our observed correlations of mtDNAcn with anxiety-like behavior on the DaLi test and the OFT, which indicated higher anxiety levels the higher the mtDNAcn, hint at the established, yet intriguing connection between mtDNA levels and anxiety. The decrease in mtDNAcn may be justified here by the significant association of TFAM with the mitochondrial genome, since manipulation of the copy number levels directly affect TFAM levels, and vice versa (Filograna et al., 2019). It must also be noted that, even though in our data, *tfam* mRNA expression levels directly reflected an alteration in mtDNAcn, mRNA levels for mitochondrial-encoded genes were not affected, as the mRNA levels of *mt-nd1* were not altered between HAB EH and HAB NH female mice. These alterations are part of complex regulatory structures within the mitochondrion, and also considering how in both anxiety studies mentioned earlier, mtDNAcn levels were measured in peripheral material and not the brain, further analysis and assessment of mtDNAcn in blood samples from HAB EH and HAB NH female mice could help elucidate this hypothalamic alteration and highlight potential mitochondrial dysfunction in EH.

5.2. PFC: EH-instigated molecular alterations are brain region-specific

Our investigation in the hypothalamus highlighted a series of molecular changes induced by the application of the EH paradigm. These changes involved genomic transcription and translation machinery, namely proteins participating in mRNA splicing and cytosolic as well as mitochondrial ribosomal protein subunits, OXPHOS subunits, and mitochondrial dynamics mediators. As a result, it is understood that the image that is being painted about the molecular underpinnings of EH on HAB female mice, has the mitochondrion at its epicenter. However, merely exploring the theoretical implications of such findings for the hypothalamus is not sufficient, so the next step of our research was to study whether these molecular alterations are brain-region specific.

EH research has so far underscored the differential effect of early life interventions on different brain areas. For instance, Papaioannou et al. investigated the effects of EH on the dopaminergic system and the dopamine metabolite turnover on the pre- and post-pubertal brain and observed a hypothalamus-specific increase on 3,4-dihydroxyphenylacetic acid/dopamine turnover of pre-pubertal EH female Wistar rats, which was reversed post-puberty (Papaioannou et al., 2002). Additionally, homovanillic acid/dopamine turnover, although increased in both the hypothalamus and the striatum for both male and female rats pre-puberty, post-puberty it was only increased in the hypothalamus (Papaioannou et al., 2002). In a different study, the mRNA expression levels of different AMPA receptors exhibited brain specific alterations in the hippocampus and the amygdala of Wistar rats;

glua1 mRNA expression as well as *glua4* mRNA density were altered in the hippocampus of EH rats, however in the amygdala, *glua2* mRNA expression was altered instead (Katsouli et al., 2014). In C57BL/6J mice that were either prenatally stressed or handled, there was differential effects for each environmental factor, for each brain region (the hippocampus, the cerebral cortex, or the frontal cortex), or each development stage, on the mRNA expression of 5-HT serotonin receptors (Akatsu et al., 2015). Taking these observations into account, the inclusion of other brain areas in our EH research could highlight potential region-specific alterations and give rise to novel neurobiological circuits involved in EH.

The second region we focused on was the PFC. The PFC is a multi-unit area of the brain with a critical role in the creation and modulation of emotion. It is mostly known for its regulation of executive functions, like goal-oriented behavior, working memory, planning, or problem solving, but it also participates in other essential functions, like language or intelligence regulation (Siddiqui et al., 2008). The various anxiety states are associated with the anticipation, response, and adaptation to potential threats. For an individual to be able to engage with these threats, predictions need to be made based on contexts, cues, and emotions for a specific outcome, which will be then followed by regulatory and adaptive responses to overcome them (Kenwood et al., 2022). In short, at the sight of a threat, one needs to interact with external stimuli, process them, and eventually overcome the threat. These are all processes to which the various functions of the PFC actively contribute, placing this region at the center of anxiety research, and therefore, urged us to include the PFC in our investigation of early life interventions as well.

Based on these, and guided by our results on the hypothalamus, we assessed the expression levels of proteins involved in a variety of mitochondria-related processes in the PFC of HAB EH and HAB NH female mice. We investigated the carbohydrate metabolism, such as glycolysis, TCA cycle, glycogen synthesis, and energy production through OXPHOS, mitochondrial dynamics perturbations, antioxidant enzyme levels and lastly, alterations in mitochondrial transport/import machinery.

Our results showed that on the PFC of HAB EH female mice, PKLR is decreased compared to HAB NH mice. Pyruvate kinase is the key rate-limiting enzyme of glycolysis, and it has four tissue isoforms, the PKLR isoform, which refers to the variants enriched in hepatocytes and red blood cells, the PKM1 variant, enriched in myocytes and neurons, and the PKM2 variant, which is ubiquitous in all cell types (Baig et al., 2019; Mazurek et al., 2005). Despite the PKLR variant being enriched in the liver and blood, it is also expressed in the brain, as seen on the Human Protein Atlas (proteinalas.org) (Sjostedt et al., 2020), so the detection of PKLR in the brain was substantive. Of the liver (L-) and red blood cell (R-) isoforms detected with PKLR, we found the R-type isoform to be decreased. Deficiency and depletion of PKLR protein levels directly affect energy metabolism in the cell, reducing the glycolytic flux and leading to decreased ATP production and ion pump dysfunctions (Nieborak et al., 2023; Wang et al., 2024). However, the exact role PKLR has in anxiety has not yet been elucidated. Glycolysis seems to mediate anxiety responses, as glycolytic enzymes, but not PKLR, had decreased protein expression levels in the synaptosomes of HAB mice (Filiou et al., 2011a). In HAB EH male

mice, PKLR (R-type) protein expression was increased in the hypothalamus but there were no results for the PFC (Thomou et al., 2024). Further investigation into the EH- and high anxiety-driven impact on glycolysis could contribute to our understanding of the role PKLR plays on it.

No other alterations to protein levels were found for either glycolytic, TCA cycle, or glycogen synthesis enzymes, even though relevant proteins were differentially expressed in the hypothalamus (see Table 9). However, correlation of their expression levels with behavior indicated anxiety- and depression-like behavioral patterns for glycolysis and the TCA cycle. For glycolysis, HK2 protein expression correlated negatively with depression-like behavior in the FST, which means that higher the HK2 protein levels, the lower the depression-like behaviors. For the TCA cycle, CS, IDH1 and SDHA protein expressions correlated negatively both with anxiety-like behavior in the DaLi box and the OFT, and with depression-like behavior in the FST, meaning that the higher the TCA cycle enzyme expression, the lower the anxiety- and depression-like behaviors. Similar findings for HAB EH male mice showed that CS protein expression correlated positively with anxiety-like behavior in DaLi, while IDH1 protein expression correlated negatively (Thomou et al., 2024). Collectively, these results highlight the important role of carbohydrate metabolism and specifically the TCA cycle plays in the mediation of anxiety.

Despite the profuse results on the hypothalamus linking the OXPHOS machinery to EH and anxiety, no such alterations were noted on the PFC. The same can be said about mitochondrial dynamics, with key players being differentially expressed on both mRNA and protein levels, but exhibiting no alterations on the PFC. This hints at a hypothalamus-specific response to the EH intervention and reinforces our hypothesis about the hypothalamus being a central node at the EH-induced molecular phenotype. However, correlation of OXPHOS and mitochondrial dynamics protein expression levels on the PFC with behavior did show that for mitochondrial fission, DRP1, MFF, and SLC25A46 protein expressions correlated negatively with anxiety-like behavior in the DaLi box, meaning that the higher the fission protein expression, the lower the anxiety-like behavior. Fission protein expression also correlated with sociability in the SPAT, which was increased the higher the DRP1 protein expression levels were, but decreased the higher the SLC25A46 levels were. So, despite the absence of significant alterations for the PFC levels of mitochondrial dynamics proteins, there is still a link with anxiety-related behaviors.

Investigation of the protein levels for antioxidant enzymes in the PFC showed that there was reduced protein expression of PRDX3 in the PFC of HAB EH female mice. PRDX3 belongs in the family of peroxiredoxins (PRXs), a ubiquitous family of peroxidases, which are essential peroxide scavenging enzymes (Perkins et al., 2015). They reduce about 90% of cytosolic and mitochondrial H₂O₂, along with other substrates like lipid hydroperoxides and peroxynitrites (Meng et al., 2017). Mammals have six different isoforms of PRXs, with each one localizing in different subcellular compartments; PRDX1, PRDX2 and PRDX6 are cytosolic, PRDX3 is mitochondrial, PRDX4 is present in the ER, and PRDX5 exists in the cytosol, the mitochondria as well as the peroxisomes (Fujii & Ikeda, 2002). Even though PRDX3 was not differentially expressed in the hypothalamus, PRDX2 and

PRDX6 were, with PRDX2 being upregulated and PRDX6 downregulated for HAB EH female mice (see Table D of Figure 8). Many members of the PRX family have been implicated in anxiety and other mental disorders. In a study utilizing MitoQ, an antioxidant which selectively targets the mitochondria, PRDX3 protein expression was increased in the cortex of HAB mice, which led to a decrease in anxiety-like behavior (Nussbaumer et al., 2016). This is in contrast with our data, where PRDX3 protein expression was reduced in HAB EH female mice, hinting at impaired antioxidant systems after the EH intervention. However, increased PRDX3 protein expression correlated negatively with anxiety-like behavior on the DaLi test, indicating decreased anxiety levels for the HAB EH mice. Another PRX member, PRDX1, was upregulated in the hippocampus of animals subjected to chronic unpredictable mild stress, which resulted in anhedonic and therefore depressive-like behavior in rats (Scotton et al., 2020). Lastly, PRDX6 has the most extensive involvement with neuropsychiatry, with reduced PRDX6 levels being observed in association with increased anxiety-like behavior after acute immobilization stress (Phasuk et al., 2021), enhanced fear memory (Phasuk et al., 2021), major depressive disorder (Martins-de-Souza et al., 2009), and schizophrenia (Martins-de-Souza et al., 2012). These findings, along with the observed alterations in anxiety, depression and sociability readouts when antioxidant protein expression levels (PRDX3, CAT and SOD2) were correlated with behavior, indicate the significance of antioxidant balance in the mediation of anxiety responses.

5.3. Plasma: Brain alterations are not reflected in the peripheral material

The encouraging results observed in the brain led us to inquire whether the EH-induced molecular alterations are also apparent in the peripheral material. We responded to this question by examining possible plasma readouts. Plasma is the blood compound with the largest concentration, and it contains water, coagulants, electrolytes, organic compounds, hormones and secreted proteins (Benjamin & McLaughlin, 2012). The roles of plasma proteins are diverse, and include processes such as cell-cell communication, differentiation, proliferation, survival and immune defense (Ranganathan & Garg, 2009). However, not all of these proteins are actively secreted, as some are a product of leakage, a marker of pathology (Uhlen et al., 2019). Consequently, insights on the plasma secretome can potentially offer valuable information for the phenotypical profile of an organism (Uhlen et al., 2019).

For our EH research, we referred to the Human Protein Atlas (proteatlas.org) to see which proteins of the ones found altered in the hypothalamus and the PFC could be detectable in plasma. Due to the low sensitivity of the western blot assay, which we used for these analyses, the only proteins with detectable plasma concentrations were antioxidants and metabolic enzymes of glycolysis, lactate production as well as OXPHOS components.

Antioxidant proteins, despite their differential expression in the hypothalamus and PFC, had unaltered levels in the plasma of HAB EH vs. HAB NH female mice. This was also reflected in the results of the TAC assay, which showed that the antioxidant capacity of HAB female mice is not affected by EH. However, correlations of antioxidant protein levels with behavioral readouts showed

that for PRX, a western blot antibody used to detect members PRDX1, PRDX2 and PRDX4 of the PRX family (antibody: Santa Cruz Biotechnology, sc-137222), expression levels correlated positively with anxiety-like behavior on the OFT, meaning that the higher the PRX protein levels, the higher the anxiety-like behavior. This is in line with extensive literature findings analyzed above (see section 5.2 of Discussion) that highlight the significance of PRX proteins in behavioral research due to their necessary regulation of oxidative stress, a molecular readout appearing often in anxiety phenotypes (Nussbaumer et al., 2016; Scotton et al., 2020).

In the plasma of HAB female mice, metabolic enzymes were not altered by EH, however there was a correlation of GAPDH protein expression levels with behavior, where the higher the GAPDH protein levels, the higher the anxiety-like behavior and sociability of HAB EH mice and the lower the depression-like behavior. Interestingly, there was also a trend for reduced CYTC protein expression.

CYTC is a small, nuclear-encoded mitochondrial heme protein mostly known for its participation in OXPHOS, where it acts as a single electron carrier from OXPHOS complex III to complex IV. However, its role extends far beyond energy production, as it has also been shown to act as a ROS producer and scavenger, contributing to redox balance (Pereverzev et al., 2003), as well as a regulator of apoptosis (Hüttemann et al., 2011). A key step in the apoptotic cascade is the release of CYTC into the cytosol, where it binds with apoptotic proteases and catalyzes the apoptosome formation, which activates Caspase-9 and Caspase-3 for apoptosis to begin (Wang, 2001). The interface between CYTC energy production and apoptosis is tightly regulated, contributing to the fate of the cell (Yu et al., 2009). Additional data shows that in response to apoptosis induction, CYTC not only gets translocated into the cytosol, but it can also get detected in extracellular space (Renz et al., 2001). Elevated CYTC levels in blood and plasma are a biomarker of mitochondrial and cellular dysfunction (Radhakrishnan et al., 2017), however no data exists correlating CYTC plasma protein levels with anxiety. This trend for reduced CYTC levels that was noted for HAB EH animals may be indicative of reduced apoptotic signaling as a result of EH, due to the fact that chronic stress, associated with anxiety and depressive behaviors, induces neuronal apoptosis (Bachis et al., 2008; Gao et al., 2014; Parul et al., 2021).

5.4. Summary of the results

Our previous results on the EH study conducted on HAB male mice heavily implicated the mitochondria as part of the molecular machinery underlining the EH-driven brain alterations, with molecular dynamics players being key mediators (Thomou et al., 2024). In this thesis, our goal was to add to these results by characterizing the molecular phenotype of adult HAB female mice exposed to the EH paradigm during their first days of life. After observing an anxiolytic effect on the DaLi box, where HAB EH females spent more time in the lit compartment than HAB NH females, indicating increased resilience during adulthood, we sought to uncover the biological mechanisms underlying this anxiolytic effect on two anxiety-related brain regions, the hypothalamus and the PFC, as well as

in the plasma, with a heavy focus being placed on mitochondrial pathways. Our obtained results for HAB EH female mice are summarized in Table 10.


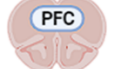

 <p>HYP</p>	<p>Non-targeted MS-based Proteomics:</p> <p>Gene transcription (mRNA splicing)</p> <p>Gene translation (ribosomes ↑)</p> <p>OXPPOS (Complex V ↑)</p>	<p>qRT-PCR: <i>fis1</i> ↑ <i>tfam</i> ↓ (T)</p> <p>Positive correlation of <i>fis1</i> & <i>tfam</i> with anxiety-like behavior</p> <p>Negative correlation of <i>mid51</i> with depression-like behavior</p> <p>qPCR: <i>mtDNAcn</i> ↓</p> <p>Positive correlation of <i>mtDNAcn</i> with anxiety-like behavior</p>
 <p>PFC</p>	<p>Western Blot:</p> <p>PKLR (R-type) ↓ PRDX3 ↓</p> <p>Negative correlation of <i>HK2</i> with depression-like behavior</p> <p>Negative correlation of <i>CS</i>, <i>IDH1</i> & <i>SDHA</i> with anxiety- & depression-like behavior</p> <p>Negative correlation of <i>DRP1</i>, <i>MFF</i> & <i>SLC25A46</i> with anxiety-like behavior</p> <p>Negative correlation of <i>PRDX3</i> with anxiety- & depression-like behavior</p>	
 <p>PLASMA</p>	<p>Western Blot:</p> <p>CYTC ↓ (T)</p> <p>Positive correlation of <i>GAPDH</i> with anxiety-like behavior and negative correlation with depression-like behavior</p> <p>Positive correlation of <i>PRX</i> with anxiety-like behavior</p>	

Table 10. Summary of our molecular results for each brain region and the plasma of HAB EH female mice. Red arrows: increased/higher, blue arrow: decreased/lower. HYP: hypothalamus, PFC: prefrontal cortex.

In the hypothalamus, which was the region we predominantly worked on, we used MS-based proteomics to discover differentially expressed proteins involved in gene transcription and translation. More specifically, mRNA splicing regulators and spliceosome components were both up and downregulated, indicating altered transcription signatures, and protein subunits of both cytosolic and mitochondrial ribosomes were upregulated, hinting at increased protein synthesis. EH also impacted energy production, with OXPPOS components from complexes I, III and IV being both up and downregulated, but components from complex V being upregulated for HAB EH female mice. This signifies an EH-induced increase of ATP production in the hypothalamus. With qRT-PCR, we assessed the mRNA expression levels of genes regulating mitochondrial dynamics processes, and observed that *fis1*, the mitochondrial fission and mitophagy regulator, was increased for HAB EH female mice, while *tfam*, a mitochondrial biogenesis instigator responsible for mtDNA organization, showed a trend for reduced mRNA expression. *Fis1* and *tfam* hypothalamic mRNA levels correlated positively with anxiety-like behavior, as observed in the DaLi box and the OFT, respectively, and *mid51* correlated negatively with depression-like behavior in the FST, indicating a strong connection between mitochondrial dynamics machinery and behavior. Lastly, measurements of the *mtDNAcn* in the hypothalamus showed that HAB EH female mice have decreased *mtDNAcn* compared to HAB NH female mice, an alteration which may be prompted by the drop in *tfam* mRNA expression for these animals.

In the PFC, driven by our observations in the hypothalamus, we assessed the expression levels of mitochondrial proteins, namely proteins involved in carbohydrate metabolism, energy production through OXPHOS, mitochondrial dynamics, antioxidant defense and mitochondrial transport/import. We found that PKLR, the rate limiting enzyme of glycolysis, was decreased for HAB EH compared to HAB NH female mice. No other metabolic enzymes were altered, however, expression levels for HK2, a glycolytic enzyme, correlated negatively with depression-like behavior on the FST, and three TCA cycle proteins (CS, IDH1 and SDHA) correlated negatively with anxiety-like behavior in the DaLi box and the OFT, as well as with depression-like behavior in the FST. Concerning mitochondrial dynamics, no significant readouts were found, however, fission protein (DRP1, MFF and SLC25A46) expression levels correlated negatively with anxiety-like behavior in the DaLi box. Lastly, PRDX3, an antioxidant protein, was reduced in the PFC of HAB EH female mice compared to HAB NH mice, with PRDX3 levels correlating negatively with anxiety-like behavior in the DaLi box and depression-like behavior in the FST.

In plasma, we assessed the antioxidant status of HAB EH vs. HAB NH female mice using the TAC assay, and also the expression levels of proteins participating in carbohydrate metabolism, energy production and antioxidant defense. No significant alterations were found, however CYTC, an OXPHOS electron carrier, had a trend for reduced expression levels in the plasma of HAB EH compared to HAB NH female mice. Expression levels of GAPDH, a glycolytic protein, correlated positively with anxiety-like behavior in the DaLi box and negatively with depression-like behavior in the FST. Finally, PRX expression levels, which is an antibody detecting three PRX family members, correlated positively with anxiety-like behavior in the OFT.

5.5. EH research between HAB males and females: What is the difference?

In our lab, following the findings on females that were included in this thesis, we have now applied the EH protocol on HAB mice of both sexes. Consequently, comparisons can be made between HAB males and HAB females on the results observed for each brain area. Examining the behavioral signatures, it can be said for both sexes that EH induced an anxiolytic effect on the DaLi test, however, the specific parameter that determined this anxiolysis in each sex was different. For HAB EH male mice, EH-driven effect on high anxiety was indicated by the higher number of entries as well as the lower latency of the first entry to the lit compartment of DaLi (Thomou et al., 2024), whereas for HAB EH female mice, the effect was based on the increased total time spent in the lit compartment (see Figure 5). To investigate sex variability on the molecular underpinnings of this anxiolysis, the results for the hypothalamus, the PFC and plasma for HAB EH male and HAB EH female mice are shown on Table 11. All HAB EH male results are from Thomou et al. (Thomou et al., 2024).

Before anything else, it must be taken into consideration that different assays were used between the two sexes for each tissue and sample type. In the hypothalamus, protein expression levels in HAB EH male mice were determined using western blots, but for females, due to the plethora

of protein signatures noted in the hypothalamus of male mice, we decided to investigate protein expression alterations on a systemic level using MS-based proteomics, which are high throughput, and their sensitivity range for the determination of protein expression alterations is much higher than the range of western blot. Therefore, the number of differentially expressed proteins identified for HAB EH females is much larger than those for HAB EH males. Despite this, the differentially expressed proteins on the hypothalamus of HAB EH male mice were not differentially expressed in the hypothalamus of HAB EH female mice. Glycolysis enzymes PKLR and ENO1 were increased for male mice, however in female mice, there were no differentially expressed glycolytic enzymes. Additionally, even though for female mice, proteomics showed differential expression for a number of mitochondrial dynamics mediators (see Table B of Figure 8), DRP1, OPA1 and PGC1A, proteins whose levels were increased for HAB EH male mice, were not among the mitochondrial dynamics protein readouts for HAB EH females. This indicates potential sex-specific findings and hints at a differential impact of EH on males and females. Additionally, CS, a TCA cycle enzyme, and ARALAR, a mitochondrial transporter protein, were both upregulated in the hypothalamus of females, but in males, their levels were not altered. CS and ARALAR in males only showcased a correlation with anxiety-like behavior. The only common readout in the hypothalamus has to do with *tfam*, whose mRNA levels were reduced on both males and females. Even though mtDNAcn, a marker impacted by *tfam* levels, was only measured in females, the reduced levels of *tfam* mRNA levels indicate that EH affects mitochondrial biogenesis and mtDNA organization and maintenance, functions for which *tfam* is essential, regardless of sex.

In the PFC of HAB EH male mice, western blots and qRT-PCRs were conducted, whereas in the PFC of HAB EH females, we only conducted western blots. Therefore, a comparison of the mRNA expression levels for mitochondrial dynamics players between the two sexes cannot be made. Regardless, it is discernible that the reductions on the protein levels of PKLR and PRDX3 in the PFC of HAB EH female mice are only specific to females, since male mice showed no EH-induced differences on any of the proteins examined. The correlations noted between the protein levels of carbohydrate metabolism enzymes, mitochondrial dynamics mediators, and PRDX3 and anxiety- or depression-like behavior were also specific to females, since no similar correlations were noted for males. With additional research concerning the mRNA profile of HAB EH female mice, more information could be derived about the extent of these sex-dependent protein alterations.

Lastly, in plasma of HAB EH male mice, only the TAC assay was conducted, which gave no significant results. Western blots assessing the expression levels of plasma-secreted proteins were only conducted for HAB EH female mice, therefore no conclusion can be reached about the plasma secretome and the discrepancies it exhibits between the sexes.

Taken together, the comparison indicates that even though EH was an anxiolytic intervention in both sexes, molecularly it induces sex-specific signatures in the brain of HAB EH male and HAB EH female mice. However, it must be said that comparing the molecular results of each sex in order to observe potential sex variabilities can only be done on a surface level since no internal control was

used at the time of the analysis. Therefore, statistical analysis to observe specific protein or mRNA level differences for HAB EH male vs. HAB EH female mice cannot be conducted. Nevertheless, these observations could be used as grounds for additional investigation in future EH work.







	HAB EH MALES 	HAB EH FEMALES 
	<p>Western Blot:</p> <p>PKLR (R-type) ↑ ENO1 ↑ (T)</p> <p>DRP1 ↑ OPA1 ↑ PGC1A ↑</p> <p>qRT-PCR: <i>tfam</i> ↓</p> <p>Positive correlation of CS with anxiety-like behavior</p> <p>Negative correlation of ARALAR with anxiety-like behavior</p>	<p>Non-targeted, MS-based Proteomics: CS ↑ ARALAR ↑</p> <p>qRT-PCR: <i>fis1</i> ↑ <i>tfam</i> ↓ (T)</p> <p>Positive correlation of <i>fis1</i> & <i>tfam</i> with anxiety-like behavior</p> <p>Negative correlation of <i>fis1</i> with depression-like behavior</p> <p>qPCR: <i>mtDNAcn</i> ↓</p> <p>Positive correlation of <i>mtDNAcn</i> with anxiety-like behavior</p>
	<p>Western Blot:</p> <p>no significant results</p> <p>qRT-PCR:</p> <p><i>fis1</i> ↑ <i>opa1</i> ↓ <i>pgc1a</i> ↑ <i>tfam</i> ↓ <i>prkn</i> ↑</p>	<p>Western Blot: PKLR (R-type) ↓ PRDX3 ↓</p> <p>Negative correlation of HK2 with depression-like behavior</p> <p>Negative correlation of CS, IDH1 & SDHA with anxiety- & depression-like behavior</p> <p>Negative correlation of DRP1, MFF & SLC25A46 with anxiety-like behavior</p> <p>Negative correlation of PRDX3 with anxiety- & depression-like behavior</p>
	<p>No significant results</p>	<p>Western Blot: CYTC ↓ (T)</p> <p>Positive correlation of GAPDH with anxiety-like behavior and negative correlation with depression-like behavior</p> <p>Positive correlation of PRX with anxiety-like behavior</p>

Table 11. Molecular results of the EH protocol on both HAB EH male and HAB EH female mice. Red arrows: increased/higher, blue arrow: decreased/lower. HYP: hypothalamus, PFC: prefrontal cortex.

5.6. Limitations and future outlook

Despite the importance of this work in identifying the molecular background of EH and elucidating anxiety mechanisms, its limitations must be acknowledged. One limitation has to do with the low sensitivity of the western blot assay, which makes it impossible to detect low fold protein expression alterations. Proteomics analyses are high throughput and therefore more sensitive in comparison to western blots, which hints at a possible discrepancy between the observed protein alterations in the PFC of HAB EH female mice and the actual proteomic profile that underlies the EH-driven effects in this brain region. Additionally, alterations at the mRNA level of expression do not always reflect alterations at the protein level of expression, as was observed here with the discrepancy between *fis1* and FIS1. The limited information these alterations have provided for us, albeit intriguing, cannot be fully explained without applying more techniques that assess potential transcriptional or translational control alterations.

With this in mind, for future work, insight into EH-induced alterations on transcriptional and translational regulation could be provided. Regulatory systems at all stages of gene transcription and translation influence mRNA and protein abundance in a complex manner, so considering the extent of which mRNA levels determine protein levels must always be done in the context of the gene being

discussed and the comparison being made (Liu et al., 2016). The use of appropriate tools to further examine the observed discrepancy between mRNA and protein alterations could aid our understanding of these alterations in the context of EH. These tools include techniques that examine post-transcriptional and post-translational modifications, mRNA and protein degradation, and protein localization, among others.

Additionally, further investigation into the altered pathways we observed with proteomics could be conducted, in order to be able to verify these findings. Considering the high overrepresentation of ribosomal proteins in our upregulated dataset, incorporating methods such as ribosome profiling to simultaneously examine both transcription and translation could offer significant insight into the specific underpinnings of this alteration. Regarding OXPHOS, the efficiency of the ETC could be assessed by conducting mitochondrial respirometry or ATP quantification in order to correlate OXPHOS subunit expression alterations with the efficiency of this pathway. Additionally, the effect of EH could be studied in other brain regions involved in the neurocircuitry of anxiety, namely the amygdala (Hu et al., 2022) or the cerebellum (Moreno-Rius, 2018), and more techniques could be introduced. Omics-based methods, such as metabolomics (Maehashi et al., 2024) or lipidomics (Kui et al., 2022) are just now starting to be added into the toolbox of anxiety research, so their incorporation into EH research could facilitate the elucidation of its molecular phenotype.

Lastly, given that in this thesis we hint at sex-dependent differences between HAB EH male and female mice, it would be valuable to further look into these differences by using external controls to conduct direct and detailed sex-based comparisons. Studies that examine sex differences demonstrate across many levels that males and females present significant differences across the life span (Bale & Epperson, 2017). This gender gap is especially apparent in psychiatric research, where men and women differ in both the statistical probability of developing specific disorders like autism (Davis & Pfaff, 2014), schizophrenia (Goldstein et al., 2002) or depression (Bale, 2006), and the symptom presentation and treatment efficacy (Bale et al., 2010; Bale & Epperson, 2017). For this reason, it is important to follow up on these comparisons between HAB EH males and females and treat sex as an effect that adds another layer of variability into our research.

The aim of this thesis was to further our knowledge on molecular underpinnings of EH by applying the protocol on HAB female mice. The anxiety background of an organism heavily influences its decision-making and molecular phenotype, and the application of innate anxiety models like the HAB/NAB mouse model in research helps us understand how specific environmental factors alter these pre-existing anxiety signatures. The study of early life interventions in specific is crucial for our understanding of anxiety mechanisms due to the high plasticity of the brain during the perinatal period, which defines behavior and biology well into adulthood. The observation of specific molecular readouts in various brain regions following the EH intervention may lead to the identification of the biological pathways shaping and shaped by the organism's behavioral phenotype, therefore leading to the discovery of novel biomarkers for the treatment of anxiety disorders.

6. REFERENCES

- Acoba, M. G., Alpergin, E. S. S., Renuse, S., Fernandez-Del-Rio, L., Lu, Y. W., Khalimonchuk, O., Clarke, C. F., Pandey, A., Wolfgang, M. J., & Claypool, S. M. (2021). The mitochondrial carrier SFXN1 is critical for complex III integrity and cellular metabolism. *Cell Rep*, *34*(11), 108869. <https://doi.org/10.1016/j.celrep.2021.108869>
- Adebayo, M., Singh, S., Singh, A. P., & Dasgupta, S. (2021). Mitochondrial fusion and fission: The fine-tune balance for cellular homeostasis. *FASEB J*, *35*(6), e21620. <https://doi.org/10.1096/fj.202100067R>
- Ader, R. (1965). Effects of early experience and differential housing on behavior susceptibility to gastric erosions in the rat. *J Comp Physiol Psychol*, *60*(2), 233-238. <https://doi.org/10.1037/h0022313>
- Akatsu, S., Ishikawa, C., Takemura, K., Ohtani, A., & Shiga, T. (2015). Effects of prenatal stress and neonatal handling on anxiety, spatial learning and serotonergic system of male offspring mice. *Neuroscience Research*, *101*, 15-23. <https://doi.org/j.neures.2015.07.002>
- Al-Amrani, S., Al-Jabri, Z., Al-Zaabi, A., Alshekaili, J., & Al-Khabori, M. (2021). Proteomics: Concepts and applications in human medicine. *World J Biol Chem*, *12*(5), 57-69. <https://doi.org/10.4331/wjbc.v12.i5.57>
- Aleksander, S. A., Balhoff, J., Carbon, S., Cherry, J. M., Drabkin, H. J., Ebert, D., Feuermann, M., Gaudet, P., Harris, N. L., Hill, D. P., Lee, R., Mi, H., Moxon, S., Mungall, C. J., Muruganugan, A., Mushayahama, T., Sternberg, P. W., Thomas, P. D., Van Auken, K., Ramsey, J., Siegele, D. A., Chisholm, R. L., Fey, P., Aspromonte, M. C., Nugnes, M. V., Quaglia, F., Tosatto, S., Giglio, M., Nadendla, S., Antonazzo, G., Attrill, H., Dos Santos, G., Marygold, S., Strelets, V., Tabone, C. J., Thurmond, J., Zhou, P., Ahmed, S. H., Asanitthong, P., Luna Buitrago, D., Erdol, M. N., Gage, M. C., Ali Kadhum, M., Li, K. Y. C., Long, M., Michalak, A., Pesala, A., Pritazahra, A., Saverimuttu, S. C. C., Su, R., Thurlow, K. E., Lovering, R. C., Logie, C., Oliferenko, S., Blake, J., Christie, K., Corbani, L., Dolan, M. E., Drabkin, H. J., Hill, D. P., Ni, L., Sitnikov, D., Smith, C., Cuzick, A., Seager, J., Cooper, L., Elser, J., Jaiswal, P., Gupta, P., Jaiswal, P., Naithani, S., Lera-Ramirez, M., Rutherford, K., Wood, V., De Pons, J. L., Dwinell, M. R., Hayman, G. T., Kaldunski, M. L., Kwitek, A. E., Laulederkind, S. J. F., Tutaj, M. A., Vedi, M., Wang, S.-J., D'Eustachio, P., Aimo, L., Axelsen, K., Bridge, A., Hyka-Nouspikel, N., Morgat, A., Aleksander, S. A., Cherry, J. M., Engel, S. R., Karra, K., Miyasato, S. R., Nash, R. S., Skrzypek, M. S., Weng, S., Wong, E. D., Bakker, E., Berardini, T. Z., Reiser, L., Auchincloss, A., Axelsen, K., Argoud-Puy, G., Blatter, M.-C., Boutet, E., Breuza, L., Bridge, A., Casals-Casas, C., Coudert, E., Estreicher, A., Livia Famiglietti, M., Feuermann, M., Gos, A., Gruaz-Gumowski, N., Hulo, C., Hyka-Nouspikel, N., Jungo, F., Le Mercier, P., Lieberherr, D., Masson, P., Morgat, A., Pedruzzi, I., Pourcel, L., Poux, S., Rivoire, C., Sundaram, S., Bateman, A.,

Bowler-Barnett, E., Bye-A-Jee, H., Denny, P., Ignatchenko, A., Ishtiaq, R., Lock, A., Lussi, Y., Magrane, M., Martin, M. J., Orchard, S., Raposo, P., Speretta, E., Tyagi, N., Warner, K., Zaru, R., Diehl, A. D., Lee, R., Chan, J., Diamantakis, S., Raciti, D., Zarowiecki, M., Fisher, M., James-Zorn, C., Ponferrada, V., Zorn, A., Ramachandran, S., Ruzicka, L., Westerfield, M., Aleksander, S. A., Balhoff, J., Carbon, S., Cherry, J. M., Drabkin, H. J., Ebert, D., Feuermann, M., Gaudet, P., Harris, N. L., Hill, D. P., Lee, R., Mi, H., Moxon, S., Mungall, C. J., Muruganugan, A., Mushayahama, T., Sternberg, P. W., Thomas, P. D., Van Auken, K., Ramsey, J., Siegele, D. A., Chisholm, R. L., Fey, P., Aspromonte, M. C., Nugnes, M. V., Quaglia, F., Tosatto, S., Giglio, M., Nadendla, S., Antonazzo, G., Attrill, H., Dos Santos, G., Marygold, S., Strelets, V., Tabone, C. J., Thurmond, J., Zhou, P., Ahmed, S. H., Asanitthong, P., Luna Buitrago, D., Erdol, M. N., Gage, M. C., Ali Kadhum, M., Li, K. Y. C., Long, M., Michalak, A., Pesala, A., Pritazahra, A., Saverimuttu, S. C. C., Su, R., Thurlow, K. E., Lovering, R. C., Logie, C., Oliferenko, S., Blake, J., Christie, K., Corbani, L., Dolan, M. E., Drabkin, H. J., Hill, D. P., Ni, L., Sitnikov, D., Smith, C., Cuzick, A., Seager, J., Cooper, L., Elser, J., Jaiswal, P., Gupta, P., Jaiswal, P., Naithani, S., Lera-Ramirez, M., Rutherford, K., Wood, V., De Pons, J. L., Dwinell, M. R., Hayman, G. T., Kaldunski, M. L., Kwitek, A. E., Laulederkind, S. J. F., Tutaj, M. A., VEDI, M., Wang, S.-J., D'Eustachio, P., Aimo, L., Axelsen, K., Bridge, A., Hyka-Nouspikel, N., Morgat, A., Aleksander, S. A., Cherry, J. M., Engel, S. R., Karra, K., Miyasato, S. R., Nash, R. S., Skrzypek, M. S., Weng, S., Wong, E. D., Bakker, E., Berardini, T. Z., Reiser, L., Auchincloss, A., Axelsen, K., Argoud-Puy, G., Blatter, M.-C., Boutet, E., Breuza, L., Bridge, A., Casals-Casas, C., Coudert, E., Estreicher, A., Livia Famiglietti, M., Feuermann, M., Gos, A., Gruaz-Gumowski, N., Hulo, C., Hyka-Nouspikel, N., Jungo, F., Le Mercier, P., Lieberherr, D., Masson, P., Morgat, A., Pedruzzi, I., Pourcel, L., Poux, S., Rivoire, C., Sundaram, S., Bateman, A., Bowler-Barnett, E., Bye-A-Jee, H., Denny, P., Ignatchenko, A., Ishtiaq, R., Lock, A., Lussi, Y., Magrane, M., Martin, M. J., Orchard, S., Raposo, P., Speretta, E., Tyagi, N., Warner, K., Zaru, R., Diehl, A. D., Lee, R., Chan, J., Diamantakis, S., Raciti, D., Zarowiecki, M., Fisher, M., James-Zorn, C., Ponferrada, V., Zorn, A., Ramachandran, S., Ruzicka, L., & Westerfield, M. (2023). The Gene Ontology knowledgebase in 2023. *GENETICS*, 224(1). <https://doi.org/10.1093/genetics/iyad031>

Antony, M. M., & Stein, M. B. (2009). *Oxford Handbook of Anxiety and Related Disorders*. Oxford University Press.

Ashburner, M., Ball, C. A., Blake, J. A., Botstein, D., Butler, H., Cherry, J. M., Davis, A. P., Dolinski, K., Dwight, S. S., Eppig, J. T., Harris, M. A., Hill, D. P., Issel-Tarver, L., Kasarskis, A., Lewis, S., Matese, J. C., Richardson, J. E., Ringwald, M., Rubin, G. M., & Sherlock, G. (2000). Gene Ontology: tool for the unification of biology. *Nature Genetics*, 25(1), 25-29. <https://doi.org/10.1038/75556>

- Aslam, B., Basit, M., Nisar, M. A., Khurshid, M., & Rasool, M. H. (2017). Proteomics: Technologies and Their Applications. *J Chromatogr Sci*, *55*(2), 182-196. <https://doi.org/10.1093/chromsci/bmw167>
- Association, A. P. (2013). *Diagnostic and Statistical Manual of Mental Disorders* (5 ed.). APA Publishing.
- Bachis, A., Cruz, M. I., Nosheny, R. L., & Mocchetti, I. (2008). Chronic unpredictable stress promotes neuronal apoptosis in the cerebral cortex. *Neurosci Lett*, *442*(2), 104-108. <https://doi.org/10.1016/j.neulet.2008.06.081>
- Baig, M. H., Adil, M., Khan, R., Dhadi, S., Ahmad, K., Rabbani, G., Bashir, T., Imran, M. A., Husain, F. M., Lee, E. J., Kamal, M. A., & Choi, I. (2019). Enzyme targeting strategies for prevention and treatment of cancer: Implications for cancer therapy. *Semin Cancer Biol*, *56*, 1-11. <https://doi.org/10.1016/j.semcancer.2017.12.003>
- Baker, M. J., Frazier, A. E., Gulbis, J. M., & Ryan, M. T. (2007). Mitochondrial protein-import machinery: correlating structure with function. *Trends Cell Biol*, *17*(9), 456-464. <https://doi.org/10.1016/j.tcb.2007.07.010>
- Bale, T. L. (2006). Stress sensitivity and the development of affective disorders. *Horm Behav*, *50*(4), 529-533. <https://doi.org/10.1016/j.yhbeh.2006.06.033>
- Bale, T. L., Baram, T. Z., Brown, A. S., Goldstein, J. M., Insel, T. R., McCarthy, M. M., Nemeroff, C. B., Reyes, T. M., Simerly, R. B., Susser, E. S., & Nestler, E. J. (2010). Early life programming and neurodevelopmental disorders. *Biol Psychiatry*, *68*(4), 314-319. <https://doi.org/10.1016/j.biopsych.2010.05.028>
- Bale, T. L., & Epperson, C. N. (2017). Sex as a Biological Variable: Who, What, When, Why, and How. *Neuropsychopharmacology*, *42*(2), 386-396. <https://doi.org/10.1038/npp.2016.215>
- Bateman, A., Martin, M.-J., Orchard, S., Magrane, M., Ahmad, S., Alpi, E., Bowler-Barnett, E. H., Britto, R., Bye-A-Jee, H., Cukura, A., Denny, P., Dogan, T., Ebenezer, T., Fan, J., Garmiri, P., Da Costa Gonzales, L. J., Hatton-Ellis, E., Hussein, A., Ignatchenko, A., Insana, G., Ishtiaq, R., Joshi, V., Jyothi, D., Kandasamy, S., Lock, A., Luciani, A., Lugaric, M., Luo, J., Lussi, Y., Macdougall, A., Madeira, F., Mahmoudy, M., Mishra, A., Moulang, K., Nightingale, A., Pundir, S., Qi, G., Raj, S., Raposo, P., Rice, D. L., Saidi, R., Santos, R., Speretta, E., Stephenson, J., Tootoo, P., Turner, E., Tyagi, N., Vasudev, P., Warner, K., Watkins, X., Zaru, R., Zellner, H., Bridge, A. J., Aimo, L., Argoud-Puy, G., Auchincloss, A. H., Axelsen, K. B., Bansal, P., Baratin, D., Batista Neto, T. M., Blatter, M.-C., Bolleman, J. T., Boutet, E., Breuza, L., Gil, B. C., Casals-Casas, C., Echioukh, K. C., Coudert, E., Cuche, B., De Castro, E., Estreicher, A., Famiglietti, M. L., Feuermann, M., Gasteiger, E., Gaudet, P., Gehant, S., Gerritsen, V., Gos, A., Gruaz, N., Hulo, C., Hyka-Nouspikel, N., Jungo, F., Kerhornou, A., Le Mercier, P., Lieberherr, D., Masson, P., Morgat, A., Muthukrishnan, V., Paesano, S., Pedruzzi, I., Pilbout, S., Pourcel, L., Poux, S., Pozzato, M., Pruess, M., Redaschi, N., Rivoire, C., Sigrist, C. J. A., Sonesson, K., Sundaram, S., Wu, C. H., Arighi, C. N., Arminski, L., Chen, C., Chen, Y., Huang, H., Laiho, K., McGarvey,

- P., Natale, D. A., Ross, K., Vinayaka, C. R., Wang, Q., Wang, Y., & Zhang, J. (2023). UniProt: the Universal Protein Knowledgebase in 2023. *Nucleic Acids Research*, *51*(D1), D523-D531. <https://doi.org/10.1093/nar/gkac1052>
- Bauer, M. F., Hofmann, S., Neupert, W., & Brunner, M. (2000). Protein translocation into mitochondria: the role of TIM complexes. *Trends Cell Biol*, *10*(1), 25-31. [https://doi.org/10.1016/s0962-8924\(99\)01684-0](https://doi.org/10.1016/s0962-8924(99)01684-0)
- Baxter, A. J., Scott, K. M., Vos, T., & Whiteford, H. A. (2013). Global prevalence of anxiety disorders: a systematic review and meta-regression. *Psychol Med*, *43*(5), 897-910. <https://doi.org/10.1017/S003329171200147X>
- Beane, M. L., Cole, M. A., Spencer, R. L., & Rudy, J. W. (2002). Neonatal handling enhances contextual fear conditioning and alters corticosterone stress responses in young rats. *Horm Behav*, *41*(1), 33-40. <https://doi.org/10.1006/hbeh.2001.1725>
- Beery, A. K., & Zucker, I. (2011). Sex bias in neuroscience and biomedical research. *Neurosci Biobehav Rev*, *35*(3), 565-572. <https://doi.org/10.1016/j.neubiorev.2010.07.002>
- Beesdo, K., Pine, D. S., Lieb, R., & Wittchen, H. U. (2010). Incidence and risk patterns of anxiety and depressive disorders and categorization of generalized anxiety disorder. *Arch Gen Psychiatry*, *67*(1), 47-57. <https://doi.org/10.1001/archgenpsychiatry.2009.177>
- Bekker, M. H., & van Mens-Verhulst, J. (2007). Anxiety disorders: sex differences in prevalence, degree, and background, but gender-neutral treatment. *Gend Med*, *4 Suppl B*, S178-193. [https://doi.org/10.1016/s1550-8579\(07\)80057-x](https://doi.org/10.1016/s1550-8579(07)80057-x)
- Benítez, J., Marra, R., Reyes, J., & Calvete, O. (2020). A genetic origin for acid–base imbalance triggers the mitochondrial damage that explains the autoimmune response and drives to gastric neuroendocrine tumours. *Gastric Cancer*, *23*(1), 52-63. <https://doi.org/10.1007/s10120-019-00982-4>
- Benjamin, R. J., & McLaughlin, L. S. (2012). Plasma components: properties, differences, and uses. *Transfusion*, *52*(s1), 9S-19S. <https://doi.org/10.1111/j.1537-2995.2012.03622.x>
- Berg, J. M., Tymoczko, J. L., Gatto Jr, G. J., & Stryer, L. (2015). *Biochemistry* (8 ed.). W. H. Freeman.
- Bishop, S., Duncan, J., Brett, M., & Lawrence, A. D. (2004). Prefrontal cortical function and anxiety: controlling attention to threat-related stimuli. *Nat Neurosci*, *7*(2), 184-188. <https://doi.org/10.1038/nn1173>
- Bishop, S. J. (2007). Neurocognitive mechanisms of anxiety: an integrative account. *Trends Cogn Sci*, *11*(7), 307-316. <https://doi.org/10.1016/j.tics.2007.05.008>
- Bock, J., Rether, K., Groger, N., Xie, L., & Braun, K. (2014). Perinatal programming of emotional brain circuits: an integrative view from systems to molecules. *Front Neurosci*, *8*, 11. <https://doi.org/10.3389/fnins.2014.00011>
- Bodnoff, S. R., Suranyi-Cadotte, B. E., Quirion, R., & Meaney, M. J. (1989). Role of the central benzodiazepine receptor system in behavioral habituation to novelty. *Behav Neurosci*, *103*(1), 209-212. <https://doi.org/10.1037//0735-7044.103.1.209>

- Bogoch, Y., Biala, Y. N., Linial, M., & Weinstock, M. (2007). Anxiety induced by prenatal stress is associated with suppression of hippocampal genes involved in synaptic function. *Journal of Neurochemistry*, *101*(4), 1018-1030. <https://doi.org/10.1111/j.1471-4159.2006.04402.x>
- Borboldis, F., & Palikaras, K. (2022). The compartmentalised nature of neuronal mitophagy: molecular insights and implications. *Expert Rev Mol Med*, *24*, e38. <https://doi.org/10.1017/erm.2022.31>
- Caldji, C. (2000). The Effects of Early Rearing Environment on the Development of GABAA and Central Benzodiazepine Receptor Levels and Novelty-Induced Fearfulness in the Rat. *Neuropsychopharmacology*, *22*(3), 219-229. [https://doi.org/10.1016/s0893-133x\(99\)00110-4](https://doi.org/10.1016/s0893-133x(99)00110-4)
- Campbell, C. T., Kolesar, J. E., & Kaufman, B. A. (2012). Mitochondrial transcription factor A regulates mitochondrial transcription initiation, DNA packaging, and genome copy number. *Biochim Biophys Acta*, *1819*(9-10), 921-929. <https://doi.org/10.1016/j.bbagr.2012.03.002>
- Campos, A. C., Fogaca, M. V., Aguiar, D. C., & Guimaraes, F. S. (2013). Animal models of anxiety disorders and stress. *Braz J Psychiatry*, *35 Suppl 2*, S101-111. <https://doi.org/10.1590/1516-4446-2013-1139>
- Castellani, C. A., Longchamps, R. J., Sun, J., Guallar, E., & Arking, D. E. (2020). Thinking outside the nucleus: Mitochondrial DNA copy number in health and disease. *Mitochondrion*, *53*, 214-223. <https://doi.org/10.1016/j.mito.2020.06.004>
- Castelli, V., Lavanco, G., Brancato, A., & Plescia, F. (2020). Targeting the Stress System During Gestation: Is Early Handling a Protective Strategy for the Offspring? *Frontiers in Behavioral Neuroscience*, *14*. <https://doi.org/10.3389/fnbeh.2020.00009>
- Chaban, Y., Boekema, E. J., & Dudkina, N. V. (2014). Structures of mitochondrial oxidative phosphorylation supercomplexes and mechanisms for their stabilisation. *Biochim Biophys Acta*, *1837*(4), 418-426. <https://doi.org/10.1016/j.bbabi.2013.10.004>
- Chang, C. C., Jou, S. H., Lin, T. T., Lai, T. J., & Liu, C. S. (2015). Mitochondria DNA change and oxidative damage in clinically stable patients with major depressive disorder. *PLoS One*, *10*(5), e0125855. <https://doi.org/10.1371/journal.pone.0125855>
- Chung, J. K., Lee, S. Y., Park, M., Joo, E. J., & Kim, S. A. (2019). Investigation of mitochondrial DNA copy number in patients with major depressive disorder. *Psychiatry Res*, *282*, 112616. <https://doi.org/10.1016/j.psychres.2019.112616>
- Ciuti, R., & Liguri, G. (2017). A Novel Assay for Measuring Total Antioxidant Capacity in Whole Blood and Other Biological Samples. *Journal of Biomedical Science and Engineering* *10*(2), 60-76. <https://doi.org/10.4236/jbise.2017.102007>
- Cohen, B., Golani-Armon, A., & Arava, Y. S. (2024). Emerging implications for ribosomes in proximity to mitochondria. *Semin Cell Dev Biol*, *154*(Pt B), 123-130. <https://doi.org/10.1016/j.semcdb.2023.01.003>
- Comes, A. L., Papiol, S., Mueller, T., Geyer, P. E., Mann, M., & Schulze, T. G. (2018). Proteomics for blood biomarker exploration of severe mental illness: pitfalls of the past and potential for the future. *Transl Psychiatry*, *8*(1), 160. <https://doi.org/10.1038/s41398-018-0219-2>

- Coskun, P., Wyrembak, J., Schriener, S. E., Chen, H. W., Marciniack, C., Laferla, F., & Wallace, D. C. (2012). A mitochondrial etiology of Alzheimer and Parkinson disease. *Biochim Biophys Acta*, *1820*(5), 553-564. <https://doi.org/10.1016/j.bbagen.2011.08.008>
- Craske, M. G., Stein, M. B., Eley, T. C., Milad, M. R., Holmes, A., Rapee, R. M., & Wittchen, H. U. (2017). Anxiety disorders. *Nat Rev Dis Primers*, *3*, 17024. <https://doi.org/10.1038/nrdp.2017.24>
- Cui, M., Cheng, C., & Zhang, L. (2022). High-throughput proteomics: a methodological mini-review. *Laboratory Investigation*, *102*(11), 1170-1181. <https://doi.org/10.1038/s41374-022-00830-7>
- Daniels, T. E., Olsen, E. M., & Tyrka, A. R. (2020). Stress and Psychiatric Disorders: The Role of Mitochondria. *Annual Review of Clinical Psychology*, *16*(1), 165-186. <https://doi.org/10.1146/annurev-clinpsy-082719-104030>
- Davis, E. P., & Pfaff, D. (2014). Sexually dimorphic responses to early adversity: implications for affective problems and autism spectrum disorder. *Psychoneuroendocrinology*, *49*, 11-25. <https://doi.org/10.1016/j.psyneuen.2014.06.014>
- Dawson, T. M., & Dawson, V. L. (2017). Mitochondrial Mechanisms of Neuronal Cell Death: Potential Therapeutics. *Annu Rev Pharmacol Toxicol*, *57*, 437-454. <https://doi.org/10.1146/annurev-pharmtox-010716-105001>
- De Kloet, E. R., Joëls, M., & Holsboer, F. (2005). Stress and the brain: from adaptation to disease. *Nature Reviews Neuroscience*, *6*(6), 463-475. <https://doi.org/10.1038/nrn1683>
- de Sousa Abreu, R., Penalva, L. O., Marcotte, E. M., & Vogel, C. (2009). Global signatures of protein and mRNA expression levels. *Mol Biosyst*, *5*(12), 1512-1526. <https://doi.org/10.1039/b908315d>
- Ditzen, C., Jastorff, A. M., Kessler, M. S., Bunck, M., Teplytska, L., Erhardt, A., Kromer, S. A., Varadarajulu, J., Targosz, B.-S., Sayan-Ayata, E. F., Holsboer, F., Landgraf, R., & Turck, C. W. (2006). Protein Biomarkers in a Mouse Model of Extremes in Trait Anxiety. *Molecular and Cellular Proteomics*, *5*(10), 1914-1920. <https://doi.org/10.1074/mcp.M600088-MCP200>
- Dixon, M. L., Thiruchselvam, R., Todd, R., & Christoff, K. (2017). Emotion and the prefrontal cortex: An integrative review. *Psychological Bulletin*, *143*(10), 1033-1081. <https://doi.org/10.1037/bul0000096>
- Drevets, W. C., Savitz, J., & Trimble, M. (2008). The Subgenual Anterior Cingulate Cortex in Mood Disorders. *CNS Spectrums*, *13*(8), 663-681. <https://doi.org/10.1017/s1092852900013754>
- Duchesne, A., Vaiman, A., Castille, J., Beauvallet, C., Gaignard, P., Floriot, S., Rodriguez, S., Vilotte, M., Boulanger, L., Passet, B., Albaric, O., Guillaume, F., Boukadiri, A., Richard, L., Bertaud, M., Timsit, E., Guatteo, R., Jaffrezic, F., Calvel, P., Helary, L., Mahla, R., Esquerre, D., Pechoux, C., Liuu, S., Vallat, J. M., Boichard, D., Slama, A., & Vilotte, J. L. (2017). Bovine and murine models highlight novel roles for SLC25A46 in mitochondrial dynamics and metabolism, with implications for human and animal health. *PLoS Genet*, *13*(4), e1006597. <https://doi.org/10.1371/journal.pgen.1006597>

- Dunlavey, C. J. (2018). Introduction to the Hypothalamic-Pituitary-Adrenal Axis: Healthy and Dysregulated Stress Responses, Developmental Stress and Neurodegeneration. *J Undergrad Neurosci Educ*, 16(2), R59-R60. <https://www.ncbi.nlm.nih.gov/pubmed/30057514>
- Egner, J. M., Nolden, K. A., Harwig, M. C., Bonate, R. P., De Anda, J., Tessmer, M. H., Noey, E. L., Ihenacho, U. K., Liu, Z., Peterson, F. C., Wong, G. C. L., Widlansky, M. E., & Hill, R. B. (2022). Structural studies of human fission protein FIS1 reveal a dynamic region important for GTPase DRP1 recruitment and mitochondrial fission. *J Biol Chem*, 298(12), 102620. <https://doi.org/10.1016/j.jbc.2022.102620>
- Eisner, V., Picard, M., & Hajnoczky, G. (2018). Mitochondrial dynamics in adaptive and maladaptive cellular stress responses. *Nat Cell Biol*, 20(7), 755-765. <https://doi.org/10.1038/s41556-018-0133-0>
- Ekstrand, M. I., Falkenberg, M., Rantanen, A., Park, C. B., Gaspari, M., Hultenby, K., Rustin, P., Gustafsson, C. M., & Larsson, N. G. (2004). Mitochondrial transcription factor A regulates mtDNA copy number in mammals. *Hum Mol Genet*, 13(9), 935-944. <https://doi.org/10.1093/hmg/ddh109>
- El-Hattab, A. W., Craigen, W. J., & Scaglia, F. (2017). Mitochondrial DNA maintenance defects. *Biochim Biophys Acta Mol Basis Dis*, 1863(6), 1539-1555. <https://doi.org/10.1016/j.bbadis.2017.02.017>
- Endler, N. S., & Kocovski, N. L. (2001). State and trait anxiety revisited. *J Anxiety Disord*, 15(3), 231-245. [https://doi.org/10.1016/s0887-6185\(01\)00060-3](https://doi.org/10.1016/s0887-6185(01)00060-3)
- Falchi, F. A., Pizzoccheri, R., & Briani, F. (2022). Activity and Function in Human Cells of the Evolutionary Conserved Exonuclease Polynucleotide Phosphorylase. *International Journal of Molecular Sciences*, 23(3), 1652. <https://doi.org/10.3390/ijms23031652>
- Fang, E. F., Hou, Y., Palikaras, K., Adriaanse, B. A., Kerr, J. S., Yang, B., Lautrup, S., Hasan-Olive, M. M., Caponio, D., Dan, X., Rocktäschel, P., Croteau, D. L., Akbari, M., Greig, N. H., Fladby, T., Nilsen, H., Cader, M. Z., Mattson, M. P., Tavernarakis, N., & Bohr, V. A. (2019). Mitophagy inhibits amyloid- β and tau pathology and reverses cognitive deficits in models of Alzheimer's disease. *Nature Neuroscience*, 22(3), 401-412. <https://doi.org/10.1038/s41593-018-0332-9>
- Fazal, F. M., Han, S., Parker, K. R., Kaewsapsak, P., Xu, J., Boettiger, A. N., Chang, H. Y., & Ting, A. Y. (2019). Atlas of Subcellular RNA Localization Revealed by APEX-Seq. *Cell*, 178(2), 473-490 e426. <https://doi.org/10.1016/j.cell.2019.05.027>
- Fernie, A. R., Carrari, F., & Sweetlove, L. J. (2004). Respiratory metabolism: glycolysis, the TCA cycle and mitochondrial electron transport. *Curr Opin Plant Biol*, 7(3), 254-261. <https://doi.org/10.1016/j.pbi.2004.03.007>
- Filiou, M. D., Asara, J. M., Nussbaumer, M., Teplytska, L., Landgraf, R., & Turck, C. W. (2014). Behavioral extremes of trait anxiety in mice are characterized by distinct metabolic profiles. *J Psychiatr Res*, 58, 115-122. <https://doi.org/10.1016/j.jpsychires.2014.07.019>

- Filiou, M. D., & Sandi, C. (2019). Anxiety and Brain Mitochondria: A Bidirectional Crosstalk. *Trends in Neurosciences*, 42(9), 573-588. <https://doi.org/10.1016/j.tins.2019.07.002>
- Filiou, M. D., Turck, C. W., & Martins-de-Souza, D. (2011)b. Quantitative proteomics for investigating psychiatric disorders. *Proteomics Clin Appl*, 5(1-2), 38-49. <https://doi.org/10.1002/prca.201000060>
- Filiou, M. D., Zhang, Y., Teplytska, L., Reckow, S., Gormanns, P., Maccarrone, G., Frank, E., Kessler, M. S., Hambsch, B., Nussbaumer, M., Bunck, M., Ludwig, T., Yassouridis, A., Holsboer, F., Landgraf, R., & Turck, C. W. (2011)a. Proteomics and metabolomics analysis of a trait anxiety mouse model reveals divergent mitochondrial pathways. *Biol Psychiatry*, 70(11), 1074-1082. <https://doi.org/10.1016/j.biopsych.2011.06.009>
- Filigrana, R., Koolmeister, C., Upadhyay, M., Pajak, A., Clemente, P., Wibom, R., Simard, M. L., Wredenberg, A., Freyer, C., Stewart, J. B., & Larsson, N. G. (2019). Modulation of mtDNA copy number ameliorates the pathological consequences of a heteroplasmic mtDNA mutation in the mouse. *Sci Adv*, 5(4), eaav9824. <https://doi.org/10.1126/sciadv.aav9824>
- Filigrana, R., Mennuni, M., Alsina, D., & Larsson, N. G. (2021). Mitochondrial DNA copy number in human disease: the more the better? *FEBS Lett*, 595(8), 976-1002. <https://doi.org/10.1002/1873-3468.14021>
- Fischer, S. (2021). The hypothalamus in anxiety disorders. In D. F. Swaab, F. Kreier, P. J. Lucassen, A. Salehi, & R. M. Buigis (Eds.), *Handbook of Clinical Neurology* (Vol. 180, pp. 149-160). Elsevier. <https://doi.org/10.1016/B978-0-12-820107-7.00009-4>
- Fischer, S., & Ehlert, U. (2018). Hypothalamic-pituitary-thyroid (HPT) axis functioning in anxiety disorders. A systematic review. *Depress Anxiety*, 35(1), 98-110. <https://doi.org/10.1002/da.22692>
- Flanigan, T. J., & Cook, M. N. (2011). Effects of an early handling-like procedure and individual housing on anxiety-like behavior in adult C57BL/6J and DBA/2J mice. *PLoS One*, 6(4), e19058. <https://doi.org/10.1371/journal.pone.0019058>
- Font, B., Eichenberger, D., Goldschmidt, D., & Vial, C. (1987). Interaction of creatine kinase and hexokinase with the mitochondrial membranes, and self-association of creatine kinase: crosslinking studies. *Molecular and Cellular Biochemistry*, 78(2). <https://doi.org/10.1007/bf00229687>
- Franconi, F., Brunelleschi, S., Steardo, L., & Cuomo, V. (2007). Gender differences in drug responses. *Pharmacol Res*, 55(2), 81-95. <https://doi.org/10.1016/j.phrs.2006.11.001>
- Fujii, J., & Ikeda, Y. (2002). Advances in our understanding of peroxiredoxin, a multifunctional, mammalian redox protein. *Redox Report*, 7(3), 123-130. <https://doi.org/10.1179/135100002125000352>
- Gao, J., Wang, H., Liu, Y., Li, Y. Y., Chen, C., Liu, L. M., Wu, Y. M., Li, S., & Yang, C. (2014). Glutamate and GABA imbalance promotes neuronal apoptosis in hippocampus after stress. *Med Sci Monit*, 20, 499-512. <https://doi.org/10.12659/MSM.890589>

- Gao, S., & Hu, J. (2021). Mitochondrial Fusion: The Machineries In and Out. *Trends in Cell Biology*, 31(1), 62-74. <https://doi.org/10.1016/j.tcb.2020.09.008>
- Garcia, I., Jones, E., Ramos, M., Innis-Whitehouse, W., & Gilkerson, R. (2017). The little big genome the organization of mitochondrial DNA. *Frontiers in Bioscience*, 22(4), 710-721. <https://doi.org/10.2741/4511>
- Garoflos, E., Stamatakis, A., Mantelas, A., Philippidis, H., & Stylianopoulou, F. (2005). Cellular mechanisms underlying an effect of "early handling" on pCREB and BDNF in the neonatal rat hippocampus. *Brain Res*, 1052(2), 187-195. <https://doi.org/10.1016/j.brainres.2005.06.032>
- Garoflos, E., Stamatakis, A., Pondiki, S., Apostolou, A., Philippidis, H., & Stylianopoulou, F. (2007). Cellular mechanisms underlying the effect of a single exposure to neonatal handling on neurotrophin-3 in the brain of 1-day-old rats. *Neuroscience*, 148(2), 349-358. <https://doi.org/10.1016/j.neuroscience.2007.06.020>
- Garoflos, E., Stamatakis, A., Rafrogianni, A., Pondiki, S., & Stylianopoulou, F. (2008). Neonatal handling on the first postnatal day leads to increased maternal behavior and fos levels in the brain of the newborn rat. *Dev Psychobiol*, 50(7), 704-713. <https://doi.org/10.1002/dev.20332>
- Gebara, E., Zanoletti, O., Ghosal, S., Grosse, J., Schneider, B. L., Knott, G., Astori, S., & Sandi, C. (2021). Mitofusin-2 in the Nucleus Accumbens Regulates Anxiety and Depression-like Behaviors Through Mitochondrial and Neuronal Actions. *Biological Psychiatry*, 89(11), 1033-1044. <https://doi.org/10.1016/j.biopsych.2020.12.003>
- Ghosal, S., Gebara, E., Ramos-Fernandez, E., Chioino, A., Grosse, J., Guillot de Suduiraut, I., Zanoletti, O., Schneider, B., Zorzano, A., Astori, S., & Sandi, C. (2023). Mitofusin-2 in nucleus accumbens D2-MSNs regulates social dominance and neuronal function. *Cell Rep*, 42(7), 112776. <https://doi.org/10.1016/j.celrep.2023.112776>
- Gluckman, P. D., & Hanson, M. A. (2004). Living with the past: evolution, development, and patterns of disease. *Science*, 305(5691), 1733-1736. <https://doi.org/10.1126/science.1095292>
- Goldstein, J. M., Seidman, L. J., O'Brien, L. M., Horton, N. J., Kennedy, D. N., Makris, N., Caviness, V. S., Jr., Faraone, S. V., & Tsuang, M. T. (2002). Impact of normal sexual dimorphisms on sex differences in structural brain abnormalities in schizophrenia assessed by magnetic resonance imaging. *Arch Gen Psychiatry*, 59(2), 154-164. <https://doi.org/10.1001/archpsyc.59.2.154>
- Gomes, C. M., Donadio, M. V. F., Anselmo-Franci, J., Franci, C. R., Lucion, A. B., & Sanvitto, G. L. (2006). Neonatal handling induces alteration in progesterone secretion after sexual behavior but not in angiotensin II receptor density in the medial amygdala: implications for reproductive success. *Life sciences*, 78(25), 2867-2871. <https://doi.org/10.1016/j.lfs.2005.11.007>
- Gomes, C. M., Rainecki, C., De Paula, P. R., Severino, G. S., Helena, C. V. V., Anselmo-Franci, J. A., Franci, C. R., Sanvitto, G. L., & Lucion, A. B. (2005). Neonatal handling and reproductive function in female rats. *Journal of Endocrinology*, 184(2), 435-445. <https://doi.org/10.1677/joe.1.05907>

- Gong, W., Liao, W., Fang, C., Liu, Y., Xie, H., Yi, F., Huang, R., Wang, L., & Zhou, J. (2021). Analysis of Chronic Mild Stress-Induced Hypothalamic Proteome: Identification of Protein Dysregulations Associated With Vulnerability and Resiliency to Depression or Anxiety. *Front Mol Neurosci*, *14*, 633398. <https://doi.org/10.3389/fnmol.2021.633398>
- Guan, J., Cai, J. J., Ji, G., & Sham, P. C. (2019). Commonality in dysregulated expression of gene sets in cortical brains of individuals with autism, schizophrenia, and bipolar disorder. *Transl Psychiatry*, *9*(1), 152. <https://doi.org/10.1038/s41398-019-0488-4>
- Hanninen, V., & Aro, H. (1996). Sex differences in coping and depression among young adults. *Soc Sci Med*, *43*(10), 1453-1460. [https://doi.org/10.1016/0277-9536\(96\)00045-7](https://doi.org/10.1016/0277-9536(96)00045-7)
- Hodes, G. E., & Epperson, C. N. (2019). Sex Differences in Vulnerability and Resilience to Stress Across the Life Span. *Biological Psychiatry*, *86*(6), 421-432. <https://doi.org/10.1016/j.biopsych.2019.04.028>.
- Hoffmann, A., & Spengler, D. (2018). The Mitochondrion as Potential Interface in Early-Life Stress Brain Programming. *Frontiers in Behavioral Neuroscience*, *12*. <https://doi.org/10.3389/fnbeh.2018.00306>
- Hollis, F., Van Der Kooij, M. A., Zanoletti, O., Lozano, L., Cantó, C., & Sandi, C. (2015). Mitochondrial function in the brain links anxiety with social subordination. *Proceedings of the National Academy of Sciences*, *112*(50), 15486-15491. <https://doi.org/10.1073/pnas.1512653112>
- Hsieh, Y.-C., Guo, C., Yalamanchili, H. K., Abreha, M., Al-Ouran, R., Li, Y., Dammer, E. B., Lah, J. J., Levey, A. I., Bennett, D. A., De Jager, P. L., Seyfried, N. T., Liu, Z., & Shulman, J. M. (2019). Tau-Mediated Disruption of the Spliceosome Triggers Cryptic RNA Splicing and Neurodegeneration in Alzheimer's Disease. *Cell Reports*, *29*(2), 301-316.e310. <https://doi.org/10.1016/j.celrep.2019.08.104>
- Hu, P., Lu, Y., Pan, B.-X., & Zhang, W.-H. (2022). New Insights into the Pivotal Role of the Amygdala in Inflammation-Related Depression and Anxiety Disorder. *International Journal of Molecular Sciences*, *23*(19), 11076. <https://doi.org/10.3390/ijms231911076>
- Hüttemann, M., Pecina, P., Rainbolt, M., Sanderson, T. H., Kagan, V. E., Samavati, L., Doan, J. W., & Lee, I. (2011). The multiple functions of cytochrome c and their regulation in life and death decisions of the mammalian cell: From respiration to apoptosis. *Mitochondrion*, *11*(3), 369-381. <https://doi.org/10.1016/j.mito.2011.01.010>
- Ihenacho, U. K., Meacham, K. A., Harwig, M. C., Widlansky, M. E., & Hill, R. B. (2021). Mitochondrial Fission Protein 1: Emerging Roles in Organellar Form and Function in Health and Disease. *Front Endocrinol (Lausanne)*, *12*, 660095. <https://doi.org/10.3389/fendo.2021.660095>
- Ismail, F. Y., Fatemi, A., & Johnston, M. V. (2017). Cerebral plasticity: Windows of opportunity in the developing brain. *Eur J Paediatr Neurol*, *21*(1), 23-48. <https://doi.org/10.1016/j.ejpn.2016.07.007>
- Jacobson, L. H., & Cryan, J. F. (2010). Genetic approaches to modeling anxiety in animals. *Curr Top Behav Neurosci*, *2*, 161-201. https://doi.org/10.1007/7854_2009_31

- Jiang, M., Wang, L., & Sheng, H. (2024). Mitochondria in depression: The dysfunction of mitochondrial energy metabolism and quality control systems. *CNS Neurosci Ther*, 30(2), e14576. <https://doi.org/10.1111/cns.14576>
- Joel, D. (2011). Male or Female? Brains are Intersex. *Front Integr Neurosci*, 5, 57. <https://doi.org/10.3389/fnint.2011.00057>
- Joel, D., Berman, Z., Tavor, I., Wexler, N., Gaber, O., Stein, Y., Shefi, N., Pool, J., Urchs, S., Margulies, D. S., Liem, F., Hanggi, J., Jancke, L., & Assaf, Y. (2015). Sex beyond the genitalia: The human brain mosaic. *Proc Natl Acad Sci U S A*, 112(50), 15468-15473. <https://doi.org/10.1073/pnas.1509654112>
- Joel, D., & Fausto-Sterling, A. (2016). Beyond sex differences: new approaches for thinking about variation in brain structure and function. *Philosophical Transactions of the Royal Society B: Biological Sciences*, 371(1688), 20150451. <https://doi.org/10.1098/rstb.2015.0451>
- Kageyama, K., Iwasaki, Y., & Daimon, M. (2021). Hypothalamic Regulation of Corticotropin-Releasing Factor under Stress and Stress Resilience. *Int J Mol Sci*, 22(22). <https://doi.org/10.3390/ijms222212242>
- Kageyama, Y., Kasahara, T., Kato, M., Sakai, S., Deguchi, Y., Tani, M., Kuroda, K., Hattori, K., Yoshida, S., Goto, Y., Kinoshita, T., Inoue, K., & Kato, T. (2018). The relationship between circulating mitochondrial DNA and inflammatory cytokines in patients with major depression. *J Affect Disord*, 233, 15-20. <https://doi.org/10.1016/j.jad.2017.06.001>
- Kalin, N. H. (2020). The Critical Relationship Between Anxiety and Depression. *American Journal of Psychiatry*, 177(5), 365-367. <https://doi.org/10.1176/appi.ajp.2020.20030305>
- Kanehisa, M. (2000). KEGG: Kyoto Encyclopedia of Genes and Genomes. *Nucleic Acids Research*, 28(1), 27-30. <https://doi.org/10.1093/nar/28.1.27>
- Kang, I., Chu, C. T., & Kaufman, B. A. (2018). The mitochondrial transcription factor TFAM in neurodegeneration: emerging evidence and mechanisms. *FEBS Letters*, 592(5), 793-811. <https://doi.org/10.1002/1873-3468.12989>
- Katsouli, A., Stamatakis, A., Giompres, P., Kouvelas, E. D., Stylianopoulou, F., & Mitsacos, A. (2014). Sexually dimorphic long-term effects of an early life experience on AMPA receptor subunit expression in rat brain. *Neuroscience*, 257, 49-64. <https://doi.org/10.1016/j.neuroscience.2013.10.073>
- Kenwood, M. M., Kalin, N. H., & Barbas, H. (2022). The prefrontal cortex, pathological anxiety, and anxiety disorders. *Neuropsychopharmacology*, 47(1), 260-275. <https://doi.org/10.1038/s41386-021-01109-z>
- Kessler, R. C., Amminger, G. P., Aguilar-Gaxiola, S., Alonso, J., Lee, S., & St??N, T. B. (2007). Age of onset of mental disorders: a review of recent literature. *Current Opinion in Psychiatry*, 20(4), 359-364. <https://doi.org/10.1097/ycp.0b013e32816ebc8c>
- Killackey, S. A., Philpott, D. J., & Girardin, S. E. (2020). Mitophagy pathways in health and disease. *Journal of Cell Biology*, 219(11). <https://doi.org/10.1083/jcb.202004029>

- Kim, M. Y., Lee, J. W., Kang, H. C., Kim, E., & Lee, D. C. (2011). Leukocyte mitochondrial DNA (mtDNA) content is associated with depression in old women. *Archives of Gerontology and Geriatrics*, *53*(2), 218-221. <https://doi.org/10.1016/j.archger.2010.11.019>
- Kleele, T., Rey, T., Winter, J., Zaganelli, S., Mahecic, D., Perreten Lambert, H., Ruberto, F. P., Nemir, M., Wai, T., Pedrazzini, T., & Manley, S. (2021). Distinct fission signatures predict mitochondrial degradation or biogenesis. *Nature*, *593*(7859), 435-439. <https://doi.org/10.1038/s41586-021-03510-6>
- Krömer, S. A., Keßler, M. S., Milfay, D., Birg, I. N., Bunck, M., Czibere, L., Panhuysen, M., Pütz, B., Deussing, J. M., Holsboer, F., Landgraf, R., & Turck, C. W. (2005). Identification of Glyoxalase-I as a Protein Marker in a Mouse Model of Extremes in Trait Anxiety. *The Journal of Neuroscience*, *25*(17), 4375-4384. <https://doi.org/10.1523/jneurosci.0115-05.2005>
- Kui, H., Su, H., Wang, Q., Liu, C., Li, Y., Tian, Y., Kong, J., Sun, G., & Huang, J. (2022). Serum metabolomics study of anxiety disorder patients based on LC-MS. *Clin Chim Acta*, *533*, 131-143. <https://doi.org/10.1016/j.cca.2022.06.022>
- Lamond, A. I. (1993). The spliceosome. *Bioessays*, *15*(9), 595-603. <https://doi.org/10.1002/bies.950150905>
- Larsson, N.-G., Wang, J., Wilhelmsson, H., Oldfors, A., Rustin, P., Lewandoski, M., Barsh, G. S., & Clayton, D. A. (1998). Mitochondrial transcription factor A is necessary for mtDNA maintenance and embryogenesis in mice. *Nature Genetics*, *18*(3), 231-236. <https://doi.org/10.1038/ng0398-231>
- Le Merre, P., Ahrlund-Richter, S., & Carlen, M. (2021). The mouse prefrontal cortex: Unity in diversity. *Neuron*, *109*(12), 1925-1944. <https://doi.org/10.1016/j.neuron.2021.03.035>
- Lee, S. E., & Park, Y. S. (2021). The Emerging Roles of Antioxidant Enzymes by Dietary Phytochemicals in Vascular Diseases. *Life (Basel)*, *11*(3). <https://doi.org/10.3390/life11030199>
- Lees, J. P., Manlandro, C. M., Picton, L. K., Tan, A. Z., Casares, S., Flanagan, J. M., Fleming, K. G., & Hill, R. B. (2012). A designed point mutant in Fis1 disrupts dimerization and mitochondrial fission. *J Mol Biol*, *423*(2), 143-158. <https://doi.org/10.1016/j.jmb.2012.06.042>
- Leppanen, J., Ng, K. W., Tchanturia, K., & Treasure, J. (2017). Meta-analysis of the effects of intranasal oxytocin on interpretation and expression of emotions. *Neurosci Biobehav Rev*, *78*, 125-144. <https://doi.org/10.1016/j.neubiorev.2017.04.010>
- Levine, S. (1956). A Further Study of Infantile Handling and Adult Avoidance Learning. *Journal of Personality*, *25*(1), 70-80. <https://doi.org/10.1111/j.1467-6494.1956.tb01289.x>
- Levine, S., Chevalier, J. A., & Korchin, S. J. (1956). The effects of early shock and handling on later avoidance learning. *J Pers*, *24*(4), 475-493. <https://doi.org/10.1111/j.1467-6494.1956.tb01283.x>
- Li, D., Wang, Q., Bayat, A., Battig, M. R., Zhou, Y., Bosch, D. G. M., Van Haften, G., Granger, L., Petersen, A. K., Pérez-Jurado, L. A., Aznar-Lain, G., Aneja, A., Hancarova, M., Bendova, S., Schwarz, M., Kremlikova Pourova, R., Sedlacek, Z., Keena, B. A., March, M. E., Hou, C.,

O'Connor, N., Bhoj, E. J., Harr, M. H., Lemire, G., Boycott, K. M., Towne, M., Li, M., Tarnopolsky, M., Brady, L., Parker, M. J., Faghfoury, H., Parsley, L. K., Agolini, E., Dentici, M. L., Novelli, A., Wright, M., Palmquist, R., Lai, K., Scala, M., Striano, P., Iacomino, M., Zara, F., Cooper, A., Maarup, T. J., Byler, M., Lebel, R. R., Balci, T. B., Louie, R., Lyons, M., Douglas, J., Nowak, C., Afenjar, A., Hoyer, J., Keren, B., Maas, S. M., Motazacker, M. M., Martinez-Agosto, J. A., Rabani, A. M., McCormick, E. M., Falk, M. J., Ruggiero, S. M., Helbig, I., Møller, R. S., Tessarollo, L., Tomassoni Ardori, F., Palko, M. E., Hsieh, T.-C., Krawitz, P. M., Ganapathi, M., Gelb, B. D., Jobanputra, V., Wilson, A., Grealley, J., Jacquemont, S., Jizi, K., Bruel, A.-L., Quelin, C., Misra, V. K., Chick, E., Romano, C., Greco, D., Arena, A., Morleo, M., Nigro, V., Seyama, R., Uchiyama, Y., Matsumoto, N., Taira, R., Tashiro, K., Sakai, Y., Yigit, G., Wollnik, B., Wagner, M., Kutsche, B., Hurst, A. C. E., Thompson, M. L., Schmidt, R., Randolph, L., Spillmann, R. C., Shashi, V., Higginbotham, E. J., Cordeiro, D., Carnevale, A., Costain, G., Khan, T., Funalot, B., Tran Mau-Them, F., Fernandez Garcia Moya, L., García-Miñaur, S., Osmond, M., Chad, L., Quercia, N., Carrasco, D., Li, C., Sanchez-Valle, A., Kelley, M., Nizon, M., Jensson, B. O., Sulem, P., Stefansson, K., Gorokhova, S., Busa, T., Rio, M., Hadj Habdallah, H., Lesieur-Sebellin, M., Amiel, J., Pingault, V., Mercier, S., Vincent, M., Philippe, C., Fatus-Fauconnier, C., Friend, K., Halligan, R. K., Biswas, S., Rosser, J., Shoubridge, C., Corbett, M., Barnett, C., Gecz, J., Leppig, K., Slavotinek, A., Marcelis, C., Pfundt, R., De Vries, B. B. A., Van Slegtenhorst, M. A., Brooks, A. S., Cogne, B., Rambaud, T., Tümer, Z., Zackai, E. H., Akizu, N., Song, Y., & Hakonarson, H. (2024). Spliceosome malfunction causes neurodevelopmental disorders with overlapping features. *Journal of Clinical Investigation*, *134*(1). <https://doi.org/10.1172/jci171235>

Liao, W., Liu, Y., Wang, L., Cai, X., Xie, H., Yi, F., Huang, R., Fang, C., Xie, P., & Zhou, J. (2021). Chronic mild stress-induced protein dysregulations correlated with susceptibility and resiliency to depression or anxiety revealed by quantitative proteomics of the rat prefrontal cortex. *Translational Psychiatry*, *11*(1). <https://doi.org/10.1038/s41398-021-01267-0>

Liu, Y., Beyer, A., & Aebersold, R. (2016). On the Dependency of Cellular Protein Levels on mRNA Abundance. *Cell*, *165*(3), 535-550. <https://doi.org/10.1016/j.cell.2016.03.014>

Luchetti, A., Oddi, D., Lampis, V., Centofante, E., Felsani, A., Battaglia, M., & D'Amato, F. R. (2015). Early handling and repeated cross-fostering have opposite effect on mouse emotionality. *Frontiers in Behavioral Neuroscience*, *9*. <https://doi.org/10.3389/fnbeh.2015.00093>

Maassen, J. A., LM, T. H., Van Essen, E., Heine, R. J., Nijpels, G., Jahangir Tafrechi, R. S., Raap, A. K., Janssen, G. M., & Lemkes, H. H. (2004). Mitochondrial diabetes: molecular mechanisms and clinical presentation. *Diabetes*, *53 Suppl 1*, S103-109. <https://doi.org/10.2337/diabetes.53.2007.s103>

Machnicka, M. A., Milanowska, K., Osman Oglou, O., Purta, E., Kurkowska, M., Olchowik, A., Januszewski, W., Kalinowski, S., Dunin-Horkawicz, S., Rother, K. M., Helm, M., Bujnicki, J. M., & Grosjean, H. (2013). MODOMICS: a database of RNA modification pathways--2013

update. *Nucleic Acids Res*, 41(Database issue), D262-267.
<https://doi.org/10.1093/nar/gks1007>

- Madruga, C., Xavier, L. L., Achaval, M., Sanvitto, G. L., & Lucion, A. B. (2006). Early handling, but not maternal separation, decreases emotional responses in two paradigms of fear without changes in mesolimbic dopamine. *Behavioural Brain Research*(166), 241-246.
<https://doi.org/10.1016/j.bbr.2005.08.005>
- Maehashi, S., Arora, K., Fisher, A. L., Schweitzer, D. R., & Akefe, I. O. (2024). Neurolipidomic insights into anxiety disorders: Uncovering lipid dynamics for potential therapeutic advances. *Neurosci Biobehav Rev*, 163, 105741. <https://doi.org/10.1016/j.neubiorev.2024.105741>
- Mairesse, J., Vercoutter-Edouart, A. S., Marrocco, J., Zuena, A. R., Giovine, A., Nicoletti, F., Michalski, J. C., Maccari, S., & Morley-Fletcher, S. (2012). Proteomic characterization in the hippocampus of prenatally stressed rats. *J Proteomics*, 75(6), 1764-1770.
<https://doi.org/10.1016/j.jprot.2011.12.017>
- Mamlouk, G. M., Dorris, D. M., Barrett, L. R., & Meitzen, J. (2020). Sex bias and omission in neuroscience research is influenced by research model and journal, but not reported NIH funding. *Front Neuroendocrinol*, 57, 100835. <https://doi.org/10.1016/j.yfrne.2020.100835>
- Marc, P., Margeot, A., Devaux, F., Blugeon, C., Corral-Debrinski, M., & Jacq, C. (2002). Genome-wide analysis of mRNAs targeted to yeast mitochondria. *EMBO Rep*, 3(2), 159-164.
<https://doi.org/10.1093/embo-reports/kvf025>
- Marković, B., Radonjić, N. V., Jevtić, G., Stojković, T., Velimirović, M., Aksić, M., Poleksić, J., Nikolić, T., Aleksić, D., Radonjić, V., Filipović, B., & Petronijević, N. D. (2017). Long-Term Effects of Maternal Deprivation on Redox Regulation in Rat Brain: Involvement of NADPH Oxidase. *Oxidative Medicine and Cellular Longevity*, 2017, 1-13. <https://doi.org/10.1155/2017/7390516>
- Martins-de-Souza, D., Gattaz, W. F., Schmitt, A., Novello, J. C., Marangoni, S., Turck, C. W., & Dias-Neto, E. (2009). Proteome analysis of schizophrenia patients Wernicke's area reveals an energy metabolism dysregulation. *BMC Psychiatry*, 9, 17. <https://doi.org/10.1186/1471-244X-9-17>
- Martins-de-Souza, D., Guest, P. C., Harris, L. W., Vanattou-Saifoudine, N., Webster, M. J., Rahmoune, H., & Bahn, S. (2012). Identification of proteomic signatures associated with depression and psychotic depression in post-mortem brains from major depression patients. *Transl Psychiatry*, 2(3), e87. <https://doi.org/10.1038/tp.2012.13>
- Martins-de-Souza, D., Guest, P. C., Vanattou-Saifoudine, N., Harris, L. W., & Bahn, S. (2011). Proteomic technologies for biomarker studies in psychiatry: advances and needs. *Int Rev Neurobiol*, 101, 65-94. <https://doi.org/10.1016/B978-0-12-387718-5.00004-3>
- Martins-de-Souza, D., Harris, L. W., Guest, P. C., Turck, C. W., & Bahn, S. (2010). The role of proteomics in depression research. *Eur Arch Psychiatry Clin Neurosci*, 260(6), 499-506.
<https://doi.org/10.1007/s00406-009-0093-2>

- Mastroianni, A. C., Faden, R., & Federman, D. (1994). Women and health research: a report from the Institute of Medicine. *Kennedy Inst Ethics J*, 4(1), 55-62. <https://doi.org/10.1353/ken.0.0121>
- Matsumoto, S., Uchiumi, T., Saito, T., Yagi, M., Takazaki, S., Kanki, T., & Kang, D. (2012). Localization of mRNAs encoding human mitochondrial oxidative phosphorylation proteins. *Mitochondrion*, 12(3), 391-398. <https://doi.org/10.1016/j.mito.2012.02.004>
- Mazurek, S., Boschek, C. B., Hugo, F., & Eigenbrodt, E. (2005). Pyruvate kinase type M2 and its role in tumor growth and spreading. *Semin Cancer Biol*, 15(4), 300-308. <https://doi.org/10.1016/j.semcancer.2005.04.009>
- McCarthy, M. M. (2016). Multifaceted origins of sex differences in the brain. *Philosophical Transactions of the Royal Society B: Biological Sciences*, 371(1688), 20150106. <https://doi.org/10.1098/rstb.2015.0106>
- McCoy, C. R., Rana, S., Stringfellow, S. A., Day, J. J., Wyss, J. M., Clinton, S. M., & Kerman, I. A. (2016). Neonatal maternal separation stress elicits lasting <scp>DNA</scp> methylation changes in the hippocampus of stress-reactive Wistar Kyoto rats. *European Journal of Neuroscience*, 44(10), 2829-2845. <https://doi.org/10.1111/ejn.13404>
- McEwen, B. S., & Morrison, J. H. (2013). The Brain on Stress: Vulnerability and Plasticity of the Prefrontal Cortex over the Life Course. *Neuron*, 79(1), 16-29. <https://doi.org/10.1016/j.neuron.2013.06.028>
- McEwen, B. S., Nasca, C., & Gray, J. D. (2016). Stress Effects on Neuronal Structure: Hippocampus, Amygdala, and Prefrontal Cortex. *Neuropsychopharmacology*, 41(1), 3-23. <https://doi.org/10.1038/npp.2015.171>
- Meaney, M. J., Aitken, D. H., Bodnoff, S. R., Iny, L. J., Tatarewicz, J. E., & Sapolsky, R. M. (1985). Early postnatal handling alters glucocorticoid receptor concentrations in selected brain regions. *Behavioral Neuroscience*, 99(4), 765-770. <https://doi.org/10.1037//0735-7044.99.4.765>.
- Meaney, M. J., Aitken, D. H., Viau, V., Sharma, S., & Sarrieau, A. (1989). Neonatal Handling Alters Adrenocortical Negative Feedback Sensitivity and Hippocampal Type II Glucocorticoid Receptor Binding in the Rat. *Neuroendocrinology*, 50(5), 597-604 <https://doi.org/10.1159/000125287>
- Meaney, M. J., Diorio, J., Francis, D., Weaver, S., Yau, J., Chapman, K., & Seckl, J. R. (2000). Postnatal Handling Increases the Expression of cAMP-Inducible Transcription Factors in the Rat Hippocampus: The Effects of Thyroid Hormones and Serotonin. *The Journal of Neuroscience*, 20(10), 3926-3935. <https://doi.org/10.1523/jneurosci.20-10-03926.2000>
- Meerlo, P., Horvath, K. M., Nagy, G. M., Bohus, B., & Koolhaas, J. M. (1999). The influence of postnatal handling on adult neuroendocrine and behavioural stress reactivity. *Journal of Neuroendocrinology*, 11(12), 925-933. <https://doi.org/10.1046/j.1365-2826.1999.00409.x>.

- Meng, D., Zhang, P., Zhang, L., Wang, H., Ho, C. T., Li, S., Shahidi, F., & Zhao, H. (2017). Detection of cellular redox reactions and antioxidant activity assays. *Journal of Functional Foods*, *37*, 467-579. <https://doi.org/10.1016/j.jff.2017.08.008>
- Moreno-Rius, J. (2018). The cerebellum in fear and anxiety-related disorders. *Prog Neuropsychopharmacol Biol Psychiatry*, *85*, 23-32. <https://doi.org/10.1016/j.pnpbp.2018.04.002>
- Mueller, B. R., & Bale, T. L. (2008). Sex-specific programming of offspring emotionality after stress early in pregnancy. *J Neurosci*, *28*(36), 9055-9065. <https://doi.org/10.1523/JNEUROSCI.1424-08.2008>
- Naon, D., Hernandez-Alvarez, M. I., Shinjo, S., Wieczor, M., Ivanova, S., Martins de Brito, O., Quintana, A., Hidalgo, J., Palacin, M., Aparicio, P., Castellanos, J., Lores, L., Sebastian, D., Fernandez-Veledo, S., Vendrell, J., Joven, J., Orozco, M., Zorzano, A., & Scorrano, L. (2023). Splice variants of mitofusin 2 shape the endoplasmic reticulum and tether it to mitochondria. *Science*, *380*(6651), eadh9351. <https://doi.org/10.1126/science.adh9351>
- Nemeroff, C. B. (2004). Neurobiological consequences of childhood trauma. *J Clin Psychiatry*, *65* Suppl 1, 18-28. <https://www.ncbi.nlm.nih.gov/pubmed/14728093>
- Ngo, H. B., Kaiser, J. T., & Chan, D. C. (2011). The mitochondrial transcription and packaging factor Tfam imposes a U-turn on mitochondrial DNA. *Nat Struct Mol Biol*, *18*(11), 1290-1296. <https://doi.org/10.1038/nsmb.2159>
- Nieborak, A., Lukauskas, S., Capellades, J., Heyn, P., Santos, G. S., Motzler, K., Zeigerer, A., Bester, R., Protzer, U., Schelter, F., Wagner, M., Carell, T., Hruscha, A., Schmid, B., Yanes, O., & Schneider, R. (2023). Depletion of pyruvate kinase (PK) activity causes glycolytic intermediate imbalances and reveals a PK-TXNIP regulatory axis. *Mol Metab*, *74*, 101748. <https://doi.org/10.1016/j.molmet.2023.101748>
- Noschang, C., Krolow, R., Arcego, D. M., Marcolin, M., Ferreira, A. G., da Cunha, A. A., Wyse, A. T. S., & Dalmaz, C. (2020). Early-life stress affects behavioral and neurochemical parameters differently in male and female juvenile Wistar rats. *International Journal of Developmental Neuroscience*, *80*(6), 547-557. <https://doi.org/10.1002/jdn.10050>
- Nunez, J. F., Ferre, P., Garcia, E., Escorihuela, R. M., Fernandez-Teruel, A., & Tobena, A. (1995). Postnatal handling reduces emotionality ratings and accelerates two-way active avoidance in female rats. *Physiol Behav*, *57*(5), 831-835. [https://doi.org/10.1016/0031-9384\(94\)00308-r](https://doi.org/10.1016/0031-9384(94)00308-r)
- Nussbaumer, M., Asara, J. M., Teplytska, L., Murphy, M. P., Logan, A., Turck, C. W., & Filiou, M. D. (2016). Selective Mitochondrial Targeting Exerts Anxiolytic Effects In Vivo. *Neuropsychopharmacology*, *41*(7), 1751-1758. <https://doi.org/10.1038/npp.2015.341>
- Ochi, S., Roy, B., Prall, K., Shelton, R. C., & Dwivedi, Y. (2023). Strong associations of telomere length and mitochondrial copy number with suicidality and abuse history in adolescent depressed individuals. *Mol Psychiatry*, *28*(9), 3920-3929. <https://doi.org/10.1038/s41380-023-02263-0>

- Otera, H., Ishihara, N., & Mihara, K. (2013). New insights into the function and regulation of mitochondrial fission. *Biochim Biophys Acta*, 5, 1256-1268. <https://doi.org/10.1016/j.bbamcr.2013.02.002>
- Padoin, M. J., Cadore, L. P., Gomes, C. M., Barros, H. M. T., & Lucion, A. B. (2001). Long-Lasting Effects of Neonatal Stimulation on the Behavior of Rats. *Behavioral Neuroscience*, 115(6), 1332-1340. <https://doi.org/10.1037/0735-7044.115.6.1332>
- Palanza, P. (2001). Animal models of anxiety and depression: how are females different? *Neurosci Biobehav Rev*, 25(3), 219-233. [https://doi.org/10.1016/s0149-7634\(01\)00010-0](https://doi.org/10.1016/s0149-7634(01)00010-0)
- Palikaras, K., Lionaki, E., & Tavernarakis, N. (2018). Mechanisms of mitophagy in cellular homeostasis, physiology and pathology. *Nat Cell Biol*, 20(9), 1013-1022. <https://doi.org/10.1038/s41556-018-0176-2>
- Palmieri, L., Pardo, B., Lasorsa, F. M., Del Arco, A., Kobayashi, K., Iijima, M., Runswick, M. J., Walker, J. E., Saheki, T., Satrústegui, J., & Palmieri, F. (2001). Citrin and aralar1 are Ca²⁺-stimulated aspartate/glutamate transporters in mitochondria. *The EMBO Journal*, 20(18), 5060-5069. <https://doi.org/10.1093/emboj/20.18.5060>
- Papageorgiou, M. P., & Filiou, M. D. (2024). Mitochondrial dynamics and psychiatric disorders: The missing link. *Neurosci Biobehav Rev*, 165, 105837. <https://doi.org/10.1016/j.neubiorev.2024.105837>
- Papaioannou, A., Dafni, U., Alikaridis, F., Bolaris, S., & Stylianopoulou, F. (2002). Effects of Neonatal Handling on Basal and Stress-Induced Monoamine Levels in the Male and Female Rat Brain. *Neuroscience*, 114, 195-206. [https://doi.org/S0306-4522\(02\)00129-X](https://doi.org/S0306-4522(02)00129-X)
- Parul, Mishra, A., Singh, S., Singh, S., Tiwari, V., Chaturvedi, S., Wahajuddin, M., Palit, G., & Shukla, S. (2021). Chronic unpredictable stress negatively regulates hippocampal neurogenesis and promote anxious depression-like behavior via upregulating apoptosis and inflammatory signals in adult rats. *Brain Res Bull*, 172, 164-179. <https://doi.org/10.1016/j.brainresbull.2021.04.017>
- Pavlidis, P., Kokras, N., & Dalla, C. (2022). Sex Differences in Depression and Anxiety. In (pp. 103-132). Springer International Publishing. https://doi.org/10.1007/7854_2022_375
- Paxinos, G., & Franklin, K. B. (2019). *Paxinos and Franklin's the Mouse Brain in Stereotaxic Coordinates* (5 ed.). Academic Press.
- Pei, L., & Wallace, D. C. (2018). Mitochondrial Etiology of Neuropsychiatric Disorders. *Biological Psychiatry*, 83(9), 722-730. <https://doi.org/10.1016/j.biopsych.2017.11.018>.
- Pereverzev, M. O., Vygodina, T. V., Konstantinov, A. A., & Skulachev, V. P. (2003). Cytochrome c, an ideal antioxidant. *Biochem Soc Trans*, 31(Pt 6), 1312-1315. <https://doi.org/10.1042/bst0311312>
- Perivolidi, V. I., Violitzi, F., Ioannidou, E., Rinotas, V., Stamatakis, G., Samiotaki, M., Panayotou, G., & Douni, E. (2022). Proteomic Identification of the SLC25A46 Interactome in Transgenic Mice

- Expressing SLC25A46-FLAG. *J Proteome Res*, 21(2), 375-394.
<https://doi.org/10.1021/acs.jproteome.1c00728>
- Perkins, A., Nelson, K. J., Parsonage, D., Poole, L. B., & Karplus, P. A. (2015). Peroxiredoxins: guardians against oxidative stress and modulators of peroxide signaling. *Trends Biochem Sci*, 40(8), 435-445. <https://doi.org/10.1016/j.tibs.2015.05.001>
- Pfanner, N., & Geissler, A. (2001). Versatility of the mitochondrial protein import machinery. *Nat Rev Mol Cell Biol*, 2(5), 339-349. <https://doi.org/10.1038/35073006>
- Phasuk, S., Pairojana, T., Suresh, P., Yang, C.-H., Roytrakul, S., Huang, S.-P., Chen, C.-C., Pakaprot, N., Chompoopong, S., Nudmamud-Thanoi, S., & Liu, I. Y. (2021). Enhanced contextual fear memory in peroxiredoxin 6 knockout mice is associated with hyperactivation of MAPK signaling pathway. *Molecular Brain*, 14(1). <https://doi.org/10.1186/s13041-021-00754-1>
- Picard, M. (2021). Blood Mitochondrial DNA Copy Number: What Are We Counting? *Mitochondrion*, 60, 1-11. <https://doi.org/10.1016/j.mito.2021.06.010>
- Picard, M., & McEwen, B. S. (2018). Psychological Stress and Mitochondria: A Systematic Review. *Psychosomatic Medicine*, 80(2), 141-153. <https://doi.org/10.1097/psy.0000000000000545>
- Picca, A., Faitg, J., Auwerx, J., Ferrucci, L., & D'Amico, D. (2023). Mitophagy in human health, ageing and disease. *Nat Metab*, 5(12), 2047-2061. <https://doi.org/10.1038/s42255-023-00930-8>
- Popov, L. D. (2020). Mitochondrial biogenesis: An update. *J Cell Mol Med*, 24(9), 4892-4899. <https://doi.org/10.1111/jcmm.15194>
- Prahabar, A., Zamora, R., Barclay, D., Yin, J., Ramamoorthy, M., Bagheri, A., Johnson, S. A., Badylak, S., Vodovotz, Y., & Jiang, P. (2024). Unraveling the complex relationship between mRNA and protein abundances: a machine learning-based approach for imputing protein levels from RNA-seq data. *NAR Genom Bioinform*, 6(1), lqae019. <https://doi.org/10.1093/nargab/lqae019>
- Pryce, C. R., Bettschen, D., & Feldon, J. (2001). Comparison of the effects of early handling and early deprivation on maternal care in the rat. *Developmental Psychobiology*, 38(4), 239-251. <https://doi.org/10.1002/dev.1018>
- Qin, L., & Xi, S. (2022). The role of Mitochondrial Fission Proteins in Mitochondrial Dynamics in Kidney Disease. *Int J Mol Sci*, 23(23). <https://doi.org/10.3390/ijms232314725>
- Quintana-Cabrera, R., & Scorrano, L. (2023). Determinants and outcomes of mitochondrial dynamics. *Mol Cell*, 83(6), 857-876. <https://doi.org/10.1016/j.molcel.2023.02.012>
- Radhakrishnan, J., Origenes, R., Littlejohn, G., Nikolich, S., Choi, E., Smite, S., Lamoureux, L., Baetiong, A., Shah, M., & Gazmuri, R. J. (2017). Plasma Cytochrome c Detection Using a Highly Sensitive Electrochemiluminescence Enzyme-Linked Immunosorbent Assay. *Biomark Insights*, 12, 1177271917746972. <https://doi.org/10.1177/1177271917746972>
- Raimundo, N. (2014). Mitochondrial pathology: stress signals from the energy factory. *Trends Mol Med*, 20(5), 282-292. <https://doi.org/10.1016/j.molmed.2014.01.005>
- Raineki, C., Lucion, A. B., & Weinberg, J. (2014). Neonatal handling: an overview of the positive and negative effects. *Dev Psychobiol*, 56(8), 1613-1625. <https://doi.org/10.1002/dev.21241>

- Ranganathan, S., & Garg, G. (2009). Secretome: clues into pathogen infection and clinical applications. *Genome Medicine*, 1(11), 113. <https://doi.org/10.1186/gm113>
- Rath, S., Sharma, R., Gupta, R., Ast, T., Chan, C., Durham, T. J., Goodman, R. P., Grabarek, Z., Haas, M. E., Hung, W. H. W., Joshi, P. R., Jourdain, A. A., Kim, S. H., Kotrys, A. V., Lam, S. S., McCoy, J. G., Meisel, J. D., Miranda, M., Panda, A., Patgiri, A., Rogers, R., Sadre, S., Shah, H., Skinner, O. S., To, T.-L., Melissa, Wang, H., Ward, P. S., Wengrod, J., Yuan, C.-C., Calvo, S. E., & Mootha, V. K. (2021). MitoCarta3.0: an updated mitochondrial proteome now with sub-organelle localization and pathway annotations. *Nucleic Acids Research*, 49(D1), D1541-D1547. <https://doi.org/10.1093/nar/gkaa1011>
- Reichert, A. S., & Neupert, W. (2004). Mitochondriomics or what makes us breathe. *Trends Genet*, 20(11), 555-562. <https://doi.org/10.1016/j.tig.2004.08.012>
- Reis, A. R., de Azevedo, M. S., de Souza, M. A., Lutz, M. L., Alves, M. B., Izquierdo, I., Cammarota, M., Silveira, P. P., & Lucion, A. B. (2014). Neonatal handling alters the structure of maternal behavior and affects mother-pup bonding. *Behavioral Brain Research*, 265, 216-228. <https://doi.org/10.1016/j.bbr.2014.02.036>.
- Renz, A., Berdel, W. E., Kreuter, M., Belka, C., Schulze-Osthoff, K., & Los, M. (2001). Rapid extracellular release of cytochrome c is specific for apoptosis and marks cell death in vivo. *Blood*, 98(5), 1542-1548. <https://doi.org/10.1182/blood.v98.5.1542>
- Roger, A. J., Munoz-Gomez, S. A., & Kamikawa, R. (2017). The Origin and Diversification of Mitochondria. *Curr Biol*, 27(21), R1177-R1192. <https://doi.org/10.1016/j.cub.2017.09.015>
- Rosenberg, A. M., Saggar, M., Monzel, A. S., Devine, J., Rogu, P., Limoges, A., Junker, A., Sandi, C., Mosharov, E. V., Dumitriu, D., Anacker, C., & Picard, M. (2023). Brain mitochondrial diversity and network organization predict anxiety-like behavior in male mice. *Nature Communications*, 14(1). <https://doi.org/10.1038/s41467-023-39941-0>
- Ruprecht, J. J., & Kunji, E. R. S. (2020). The SLC25 Mitochondrial Carrier Family: Structure and Mechanism. *Trends Biochem Sci*, 45(3), 244-258. <https://doi.org/10.1016/j.tibs.2019.11.001>
- Ryan, K. M., Doody, E., & McLoughlin, D. M. (2023). Whole blood mitochondrial DNA copy number in depression and response to electroconvulsive therapy. *Prog Neuropsychopharmacol Biol Psychiatry*, 121, 110656. <https://doi.org/10.1016/j.pnpbp.2022.110656>
- Samangouei, P., Crespo-Avilan, G. E., Cabrera-Fuentes, H., Hernandez-Resendiz, S., Ismail, N. I., Katwadi, K. B., Boisvert, W. A., & Hausenloy, D. J. (2018). MiD49 and MiD51: New mediators of mitochondrial fission and novel targets for cardioprotection. *Cond Med*, 1(5), 239-246. <https://www.ncbi.nlm.nih.gov/pubmed/30338314>
- Saper, C. B., & Lowell, B. B. (2014). The hypothalamus. *Curr Biol*, 24(23), R1111-1116. <https://doi.org/10.1016/j.cub.2014.10.023>
- Saviola, F., Pappaianni, E., Monti, A., Grecucci, A., Jovicich, J., & De Pisapia, N. (2020). Trait and state anxiety are mapped differently in the human brain. *Scientific Reports*, 10(1). <https://doi.org/10.1038/s41598-020-68008-z>

- Schlattner, U., Kay, L., & Tokarska-Schlattner, M. (2018). Mitochondrial Proteolipid Complexes of Creatine Kinase. In (pp. 365-408). Springer Singapore. https://doi.org/10.1007/978-981-10-7757-9_13
- Schlattner, U., Tokarska-Schlattner, M., & Wallimann, T. (2006). Mitochondrial creatine kinase in human health and disease. *Biochim Biophys Acta*, 1762(2), 164-180. <https://doi.org/10.1016/j.bbadis.2005.09.004>
- Schröder, H., Moser, N., & Huggenberger, S. (2020). The Mouse Hypothalamus. In (pp. 205-230). Springer International Publishing. https://doi.org/10.1007/978-3-030-19898-5_9
- Scott, J. (2013). An Evolutionary Perspective on Anxiety and Anxiety Disorders. In. InTech. <https://doi.org/10.5772/52902>
- Scotton, E., Colombo, R., Reis, J. C., Possebon, G. M. P., Hizo, G. H., Valiati, F. E., Gea, L. P., Bristot, G., Salvador, M., Silva, T. M., Guerra, A. E., Lopes, T. F., Rosa, A. R., & Kunz, M. (2020). BDNF prevents central oxidative damage in a chronic unpredictable mild stress model: The possible role of PRDX-1 in anhedonic behavior. *Behav Brain Res*, 378, 112245. <https://doi.org/10.1016/j.bbr.2019.112245>
- Sharma, V., Swaminathan, K., & Shukla, R. (2024). The Ribosome Hypothesis: Decoding Mood Disorder Complexity. *International Journal of Molecular Sciences*, 25(5), 2815. <https://doi.org/10.3390/ijms25052815>
- Sheng, J. A., Bales, N. J., Myers, S. A., Bautista, A. I., Roueifar, M., Hale, T. M., & Handa, R. J. (2021). The Hypothalamic-Pituitary-Adrenal Axis: Development, Programming Actions of Hormones, and Maternal-Fetal Interactions. *Frontiers in Behavioral Neuroscience*, 14. <https://doi.org/10.3389/fnbeh.2020.601939>
- Shimogori, T., Lee, D. A., Miranda-Angulo, A., Yang, Y., Wang, H., Jiang, L., Yoshida, A. C., Kataoka, A., Mashiko, H., Avetisyan, M., Qi, L., Qian, J., & Blackshaw, S. (2010). A genomic atlas of mouse hypothalamic development. *Nature Neuroscience*, 13(6), 767-775. <https://doi.org/10.1038/nn.2545>
- Shors, T. J., Chua, C., & Falduto, J. (2001). Sex differences and opposite effects of stress on dendritic spine density in the male versus female hippocampus. *J Neurosci*, 21(16), 6292-6297. <https://doi.org/10.1523/JNEUROSCI.21-16-06292.2001>
- Siddiqui, S. V., Chatterjee, U., Kumar, D., Siddiqui, A., & Goyal, N. (2008). Neuropsychology of prefrontal cortex. *Indian J Psychiatry*, 50(3), 202-208. <https://doi.org/10.4103/0019-5545.43634>
- Sieck, G., & Ramaley, J. A. (1975). Effects of early handling upon puberty: correlations with adrenal stress responsiveness. *Physiology & Behavior*, 15(5), 487-489. [https://doi.org/10.1016/0031-9384\(75\)90219-x](https://doi.org/10.1016/0031-9384(75)90219-x)
- Sies, H., & Jones, D. P. (2020). Reactive oxygen species (ROS) as pleiotropic physiological signalling agents. *Nat Rev Mol Cell Biol*, 21(7), 363-383. <https://doi.org/10.1038/s41580-020-0230-3>

- Singewald, N. (2007). Altered brain activity processing in high-anxiety rodents revealed by challenge paradigms and functional mapping. *Neurosci Biobehav Rev*, 31(1), 18-40. <https://doi.org/10.1016/j.neubiorev.2006.02.003>
- Sjostedt, E., Zhong, W., Fagerberg, L., Karlsson, M., Mitsios, N., Adori, C., Oksvold, P., Edfors, F., Limiszewska, A., Hikmet, F., Huang, J., Du, Y., Lin, L., Dong, Z., Yang, L., Liu, X., Jiang, H., Xu, X., Wang, J., Yang, H., Bolund, L., Mardinoglu, A., Zhang, C., von Feilitzen, K., Lindskog, C., Ponten, F., Luo, Y., Hokfelt, T., Uhlen, M., & Mulder, J. (2020). An atlas of the protein-coding genes in the human, pig, and mouse brain. *Science*, 367(6482). <https://doi.org/10.1126/science.aay5947>
- Smagin, D. A., Kovalenko, I. L., Galyamina, A. G., Bragin, A. O., Orlov, Y. L., & Kudryavtseva, N. N. (2016). Dysfunction in Ribosomal Gene Expression in the Hypothalamus and Hippocampus following Chronic Social Defeat Stress in Male Mice as Revealed by RNA-Seq. *Neural Plasticity*, 2016, 1-6. <https://doi.org/10.1155/2016/3289187>
- Smagin, D. A., Kovalenko, I. L., Galyamina, A. G., Orlov, Y. L., Babenko, V. N., & Kudryavtseva, N. N. (2018). Heterogeneity of Brain Ribosomal Genes Expression Following Positive Fighting Experience in Male Mice as Revealed by RNA-Seq. *Molecular Neurobiology*, 55(1), 390-401. <https://doi.org/10.1007/s12035-016-0327-z>
- Soldin, O. P., & Mattison, D. R. (2009). Sex differences in pharmacokinetics and pharmacodynamics. *Clin Pharmacokinet*, 48(3), 143-157. <https://doi.org/10.2165/00003088-200948030-00001>
- Spicer, Z., Miller, M. L., Andringa, A., Riddle, T. M., Duffy, J. J., Doetschman, T., & Shull, G. E. (2000). Stomachs of mice lacking the gastric H,K-ATPase alpha -subunit have achlorhydria, abnormal parietal cells, and ciliated metaplasia. *J Biol Chem*, 275(28), 21555-21565. <https://doi.org/10.1074/jbc.M001558200>
- Spielberger, C. D., Gorsuch, R., Lushene, R. E., Vagg, P. R., & Gerard, J. (1983). *Manual for the State-Trait Anxiety Inventory*. CA:Consulting Psychologists Press.
- Spinelli, J. B., & Haigis, M. C. (2018). The multifaceted contributions of mitochondria to cellular metabolism. *Nature Cell Biology*, 20(7), 745-754. <https://doi.org/10.1038/s41556-018-0124-1>
- Sprengelli, L. L. (2016). The Protein Biosynthetic Machinery of Mitochondria. *Encyclopedia of Cell Biology*, 1, 545-554. <https://doi.org/10.1016/B978-0-12-394447-4.10066-5>
- Stamatakis, A., Toutountzi, E., Fragioudaki, K., Kouvelas, E. D., Stylianopoulou, F., & Mitsacos, A. (2009). Selective effects of neonatal handling on rat brain N-methyl-d-aspartate receptors. *Neuroscience*, 164(4), 1457-1467. <https://doi.org/10.1016/j.neuroscience.2009.09.032>
- Steffen, J., Vashisht, A. A., Wan, J., Jen, J. C., Claypool, S. M., Wohlschlegel, J. A., & Koehler, C. M. (2017). Rapid degradation of mutant SLC25A46 by the ubiquitin-proteasome system results in MFN1/2-mediated hyperfusion of mitochondria. *Mol Biol Cell*, 28(5), 600-612. <https://doi.org/10.1091/mbc.E16-07-0545>
- Steimer, T. (2002). The biology of fear- and anxiety-related behaviors. *Dialogues in Clinical Neuroscience*, 4(3), 231-249. <https://doi.org/10.31887/dcns.2002.4.3/tsteimer>

- Steimer, T. (2011). Animal models of anxiety disorders in rats and mice: some conceptual issues. *Dialogues in Clinical Neuroscience*, 13(4), 495-506. <https://doi.org/10.31887/dcns.2011.13.4/tsteimer>
- Stelzer, G., Rosen, N., Plaschkes, I., Zimmerman, S., Twik, M., Fishilevich, S., Stein, T. I., Nudel, R., Lieder, I., Mazor, Y., Kaplan, S., Dahary, D., Warshawsky, D., Guan-Golan, Y., Kohn, A., Rappaport, N., Safran, M., & Lancet, D. (2016). The GeneCards Suite: From Gene Data Mining to Disease Genome Sequence Analyses. *Curr Protoc Bioinformatics*, 54, 1 30 31-31 30 33. <https://doi.org/10.1002/cpbi.5>
- Sternberg, W. F., & Ridgway, C. G. (2003). Effects of gestational stress and neonatal handling on pain, analgesia, and stress behavior of adult mice. *Physiology & Behavior*, 78(3), 375-383. [https://doi.org/10.1016/s0031-9384\(03\)00015-5](https://doi.org/10.1016/s0031-9384(03)00015-5)
- Sylvester, C. M., Corbetta, M., Raichle, M. E., Rodebaugh, T. L., Schlaggar, B. L., Sheline, Y. I., Zorumski, C. F., & Lenze, E. J. (2012). Functional network dysfunction in anxiety and anxiety disorders. *Trends in Neurosciences*, 35(9), 527-535. <https://doi.org/10.1016/j.tins.2012.04.012>
- Szego, E. M., Janaky, T., Szabo, Z., Csorba, A., Kompagne, H., Muller, G., Levay, G., Simor, A., Juhasz, G., & Kekesi, K. A. (2010). A mouse model of anxiety molecularly characterized by altered protein networks in the brain proteome. *Eur Neuropsychopharmacol*, 20(2), 96-111. <https://doi.org/10.1016/j.euroneuro.2009.11.003>
- Szklarczyk, D., Kirsch, R., Koutrouli, M., Nastou, K., Mehryary, F., Hachilif, R., Gable, A. L., Fang, T., Nadezhda, Pyysalo, S., Bork, P., Lars, & Christian. (2023). The STRING database in 2023: protein–protein association networks and functional enrichment analyses for any sequenced genome of interest. *Nucleic Acids Research*, 51(D1), D638-D646. <https://doi.org/10.1093/nar/gkac1000>
- Taanman, J.-W. (1999). The mitochondrial genome: structure, transcription, translation and replication [Review]. *Biochimica et Biophysica Acta (BBA) - Bioenergetics*, 1410, 103-123. <https://doi.org/S0005272898001613>
- Tang, M., Huang, H., Li, S., Zhou, M., Liu, Z., Huang, R., Liao, W., Xie, P., & Zhou, J. (2019). Hippocampal proteomic changes of susceptibility and resilience to depression or anxiety in a rat model of chronic mild stress. *Translational Psychiatry*, 9(1). <https://doi.org/10.1038/s41398-019-0605-4>
- Terzenidou, M. E., Segklia, A., Kano, T., Papastefanaki, F., Karakostas, A., Charalambous, M., Ioakeimidis, F., Papadaki, M., Kloukina, I., Chrysanthou-Piterou, M., Samiotaki, M., Panayotou, G., Matsas, R., & Douni, E. (2017). Novel insights into SLC25A46-related pathologies in a genetic mouse model. *PLOS Genetics*, 13(4), e1006656. <https://doi.org/10.1371/journal.pgen.1006656>

- Thomas, P. D., Ebert, D., Muruganujan, A., Mushayahama, T., Albou, L. P., & Mi, H. (2022). PANTHER: Making genome-scale phylogenetics accessible to all. *Protein Science*, 31(1), 8-22. <https://doi.org/10.1002/pro.4218>
- Thomou, C., Nussbaumer, M., Grammenou, E., Komini, C., Vlaikou, A.-M., Papageorgiou, M. P., & Filiou, M. D. (2024). Early Handling Exerts Anxiolytic Effects and Alters Brain Mitochondrial Dynamics in Adult High Anxiety Mice. *Molecular Neurobiology*. <https://doi.org/10.1007/s12035-024-04116-5>
- Tifoun, N., De Las Heras, J. M., Guillaume, A., Bouleau, S., Mignotte, B., & Le Floch, N. (2021). Insights into the Roles of the Sideroflexins/SLC56 Family in Iron Homeostasis and Iron-Sulfur Biogenesis. *Biomedicines*, 9(2). <https://doi.org/10.3390/biomedicines9020103>
- Tilokani, L., Nagashima, S., Paupe, V., & Prudent, J. (2018). Mitochondrial dynamics: overview of molecular mechanisms. *Essays Biochem*, 62(3), 341-360. <https://doi.org/10.1042/EBC20170104>
- Torrell, H., Montana, E., Abasolo, N., Roig, B., Gaviria, A. M., Vilella, E., & Martorell, L. (2013). Mitochondrial DNA (mtDNA) in brain samples from patients with major psychiatric disorders: gene expression profiles, mtDNA content and presence of the mtDNA common deletion. *Am J Med Genet B Neuropsychiatr Genet*, 162B(2), 213-223. <https://doi.org/10.1002/ajmg.b.32134>
- Tyrka, A. R., Parade, S. H., Price, L. H., Kao, H. T., Porton, B., Philip, N. S., Welch, E. S., & Carpenter, L. L. (2016). Alterations of Mitochondrial DNA Copy Number and Telomere Length With Early Adversity and Psychopathology. *Biol Psychiatry*, 79(2), 78-86. <https://doi.org/10.1016/j.biopsych.2014.12.025>
- Uhlen, M., Karlsson, M. J., Hober, A., Svensson, A. S., Scheffel, J., Kotol, D., Zhong, W., Tebani, A., Strandberg, L., Edfors, F., Sjostedt, E., Mulder, J., Mardinoglu, A., Berling, A., Ekblad, S., Dannemeyer, M., Kanje, S., Rockberg, J., Lundqvist, M., Malm, M., Volk, A. L., Nilsson, P., Manberg, A., Dodig-Crnkovic, T., Pin, E., Zwahlen, M., Oksvold, P., von Feilitzen, K., Haussler, R. S., Hong, M. G., Lindskog, C., Ponten, F., Katona, B., Vuu, J., Lindstrom, E., Nielsen, J., Robinson, J., Ayoglu, B., Mahdessian, D., Sullivan, D., Thul, P., Danielsson, F., Stadler, C., Lundberg, E., Bergstrom, G., Gummesson, A., Voldborg, B. G., Tegel, H., Hober, S., Forsstrom, B., Schwenk, J. M., Fagerberg, L., & Sivertsson, A. (2019). The human secretome. *Sci Signal*, 12(609). <https://doi.org/10.1126/scisignal.aaz0274>
- Vagg, P. R., Spielberger, C. D., & O'Hearn Jr, T. P. (1980). Is the state-trait anxiety inventory multidimensional? *Personality and Individual Differences*, 1(3), 207-214. [https://doi.org/10.1016/0191-8869\(80\)90052-5](https://doi.org/10.1016/0191-8869(80)90052-5)
- Vakifahmetoglu-Norberg, H., Ouchida, A. T., & Norberg, E. (2017). The role of mitochondria in metabolism and cell death. *Biochem Biophys Res Commun*, 482(3), 426-431. <https://doi.org/10.1016/j.bbrc.2016.11.088>

- Vallée, M., Mayo, W., Dellu, F., Le Moal, M., Simon, H., & Maccari, S. (1997). Prenatal Stress Induces High Anxiety and Postnatal Handling Induces Low Anxiety in Adult Offspring: Correlation with Stress-Induced Corticosterone Secretion. *The Journal of Neuroscience*, *17*(7), 2626-2636. <https://doi.org/10.1523/jneurosci.17-07-02626.1997>
- Vogel, C., & Marcotte, E. M. (2012). Insights into the regulation of protein abundance from proteomic and transcriptomic analyses. *Nature Reviews Genetics*, *13*(4), 227-232. <https://doi.org/10.1038/nrg3185>
- Wang, X. (2001). The expanding role of mitochondria in apoptosis. *Genes Dev*, *15*(22), 2922-2933. <https://www.ncbi.nlm.nih.gov/pubmed/11711427>
- Wang, X., Sundquist, K., Rastkhani, H., Palmer, K., Memon, A. A., & Sundquist, J. (2017). Association of mitochondrial DNA in peripheral blood with depression, anxiety and stress- and adjustment disorders in primary health care patients. *Eur Neuropsychopharmacol*, *27*(8), 751-758. <https://doi.org/10.1016/j.euroneuro.2017.06.001>
- Wang, Y., Liu, J., Liu, T., An, X., Huang, L., Li, J., Zhang, Y., Xiang, Y., Xiao, L., Yi, W., Qin, J., Liu, L., Wang, C., & Yu, J. (2024). Pyruvate kinase deficiency and PKLR gene mutations: Insights from molecular dynamics simulation analysis. *Heliyon*, *10*(5), e26368. <https://doi.org/10.1016/j.heliyon.2024.e26368>
- Weinberg, J., Krahn, E. A., & Levine, S. (1978). Differential effects of handling on exploration in male and female rats. *Dev Psychobiol*, *11*(3), 251-259. <https://doi.org/10.1002/dev.420110309>
- Weinberg, J., & Levine, S. (1977). Early handling influences on behavioral and physiological responses during active avoidance. *Dev Psychobiol*, *10*(2), 161-169. <https://doi.org/10.1002/dev.420100209>
- Weiner, I., Schnabel, I., Lubow, R. E., & Feldon, J. (1985). The effects of early handling on latent inhibition in male and female rats. *Developmental Psychobiology*, *18*(4), 291-297. <https://doi.org/10.1002/dev.420180402>
- Westermann, B. (2010). Mitochondrial fusion and fission in cell life and death. *Nature Reviews Molecular Cell Biology*, *11*(12), 872-884. <https://doi.org/10.1038/nrm3013>
- Wilkins, M. R., Pasquali, C., Appel, R. D., Ou, K., Golaz, O., Sanchez, J. C., Yan, J. X., Gooley, A. A., Hughes, G., Humphery-Smith, I., Williams, K. L., & Hochstrasser, D. F. (1996). From proteins to proteomes: large scale protein identification by two-dimensional electrophoresis and amino acid analysis. *Biotechnology (N Y)*, *14*(1), 61-65. <https://doi.org/10.1038/nbt0196-61>
- Wilkins, M. R., Sanchez, J. C., Gooley, A. A., Appel, R. D., Humphery-Smith, I., Hochstrasser, D. F., & Williams, K. L. (1996). Progress with proteome projects: why all proteins expressed by a genome should be identified and how to do it. *Biotechnol Genet Eng Rev*, *13*, 19-50. <https://doi.org/10.1080/02648725.1996.10647923>
- Wu, T., Luo, Y., Broster, L. S., Gu, R., & Luo, Y.-J. (2013). The impact of anxiety on social decision-making: Behavioral and electrodermal findings. *Social Neuroscience*, *8*(1), 11-21. <https://doi.org/10.1080/17470919.2012.694372>

- Yamamoto, Y., Ueyama, T., Ito, T., & Tsuruo, Y. (2015). Downregulation of growth hormone 1 gene in the cerebellum and prefrontal cortex of rats with depressive-like behavior. *Physiol Genomics*, 47(5), 170-176. <https://doi.org/10.1152/physiolgenomics.00119.2014>
- Yao, C. H., Wang, R., Wang, Y., Kung, C. P., Weber, J. D., & Patti, G. J. (2019). Mitochondrial fusion supports increased oxidative phosphorylation during cell proliferation. *Elife*, 8. <https://doi.org/10.7554/eLife.41351>
- Yapa, N. M. B., Lisnyak, V., Reljic, B., & Ryan, M. T. (2021). Mitochondrial dynamics in health and disease. *FEBS Lett*, 595(8), 1184-1204. <https://doi.org/10.1002/1873-3468.14077>
- Yates, J. R., Ruse, C. I., & Nakorchevsky, A. (2009). Proteomics by mass spectrometry: approaches, advances, and applications. *Annu Rev Biomed Eng*, 11, 49-79. <https://doi.org/10.1146/annurev-bioeng-061008-124934>
- Yoon, Y., Galloway, C. A., Jhun, B. S., & Yu, T. (2011). Mitochondrial dynamics in diabetes. *Antioxid Redox Signal*, 14(3), 439-457. <https://doi.org/10.1089/ars.2010.3286>
- Youle, R. J., & Van Der Bliek, A. M. (2012). Mitochondrial Fission, Fusion, and Stress. *Science*, 337(6098), 1062-1065. <https://doi.org/10.1126/science.1219855>
- Yu, H., Lee, I., Salomon, A. R., Yu, K., & Hutterman, M. (2009). Mammalian liver cytochrome c is tyrosine-48 phosphorylated in vivo, inhibiting mitochondrial respiration. *Biochim Biophys Acta*, 1777(7-8), 1066-1071. <https://doi.org/10.1016/j.bbabi.2008.04.023>
- Yu, T., Wang, L., Zhang, L., & Deuster, P. A. (2023). Mitochondrial Fission as a Therapeutic Target for Metabolic Diseases: Insights into Antioxidant Strategies. *Antioxidants*, 12(6), 1163. <https://doi.org/10.3390/antiox12061163>
- Zhang, X., Eladawi, M. A., Ryan, W. G., Fan, X., Prevoznik, S., Devale, T., Ramnani, B., Malathi, K., Sibille, E., McCullumsmith, R., Tomoda, T., & Shukla, R. (2023). Ribosomal dysregulation: A conserved pathophysiological mechanism in human depression and mouse chronic stress. *PNAS Nexus*, 2(10). <https://doi.org/10.1093/pnasnexus/pgad299>
- Zhang, Y., Filiou, M. D., Reckow, S., Gormanns, P., Maccarrone, G., Kessler, M. S., Frank, E., Hamsch, B., Holsboer, F., Landgraf, R., & Turck, C. W. (2011). Proteomic and metabolomic profiling of a trait anxiety mouse model implicate affected pathways. *Mol Cell Proteomics*, 10(12), M111 008110. <https://doi.org/10.1074/mcp.M111.008110>
- Zhang, Y., & Xu, H. (2016). Translational regulation of mitochondrial biogenesis. *Biochem Soc Trans*, 44(6), 1717-1724. <https://doi.org/10.1042/BST20160071C>
- Zhong, Q., Xiao, X., Qiu, Y., Xu, Z., Chen, C., Chong, B., Zhao, X., Hai, S., Li, S., An, Z., & Dai, L. (2023). Protein posttranslational modifications in health and diseases: Functions, regulatory mechanisms, and therapeutic implications. *MedComm (2020)*, 4(3), e261. <https://doi.org/10.1002/mco2.261>

7. APPENDIX

P value	*=-LOG(P value)	Fold change	Difference	Genes	Protein name
0.0005478	3.2613438	10.34	3.3703918	Atp4a	Potassium-transporting ATPase alpha chain 1;Potassium-transporting ATPase alpha chain 1;Potassium-transporting ATPase alpha chain 1
0.0000170	4.7693263	4.97	2.3127735	Adgre1	Adhesion G protein-coupled receptor E1
0.0005933	3.2267456	4.85	2.2789154	Yeats2	YEATS domain-containing protein 2
0.0000881	4.0549488	4.80	2.2626969	Aqp2	Aquaporin-2
0.0000032	5.4955476	4.62	2.2075948	Acss3	Acyl-CoA synthetase short-chain family member 3, mitochondrial
0.0002223	3.6529923	3.82	1.9351549	Ckm	Creatine kinase M-type;Creatine kinase M-type
0.0011789	2.9285246	3.48	1.8005784	Rbl2	Retinoblastoma-like protein 2
0.0000897	4.0472278	3.36	1.7471728	Anp32b	Acidic leucine-rich nuclear phosphoprotein 32 family member A;Acidic leucine-rich nuclear phosphoprotein 32 family member B
0.0000143	4.8445594	3.16	1.6582191	Tcn2	Transcobalamin-2
0.0002262	3.6454662	3.03	1.6011963	Pfkfb1	6-phosphofructo-2-kinase/fructose-2,6-bisphosphatase 1
0.0556781	1.2543156	3.00	1.5851435	Rasal3	Ras/Rap GTPase-activating protein SynGAP;RAS protein activator like-3
0.0030019	2.5225985	2.80	1.4829501	Spata18	Mitochondria-eating protein
0.0000200	4.6986280	2.79	1.4810951	Tmem230	Transmembrane protein 230
0.0622209	1.2060638	2.64	1.4020512	Rabac1	Prenylated Rab acceptor protein 1
0.0087995	2.0555419	2.62	1.3869032	Acsl4	Fatty acid CoA ligase Acsl3;Long-chain-fatty-acid--CoA ligase 4
0.0000343	4.4652973	2.56	1.3545277	Copz1	Coatomer subunit zeta-1
0.0034579	2.4611813	2.55	1.3493280	Hint3	Adenosine 5'-monophosphoramidase HINT3
0.0000658	4.1819519	2.45	1.2954910	Actg1	Actin, cytoplasmic 1;Actin, cytoplasmic 1;Actin, cytoplasmic 1;Actin, cytoplasmic 1;Actin, cytoplasmic 1;Actin, cytoplasmic 2;Actin, cytoplasmic 2;Actin, cytoplasmic 2;Actin, cytoplasmic 2
0.0000031	5.5028418	2.40	1.2640049	Olfm2	Noelin-2
0.0000041	5.3905399	2.40	1.2634438	Cpsf2	Cleavage and polyadenylation specificity factor subunit 2
0.0028234	2.5492256	2.32	1.2121876	Mpc2	Mitochondrial pyruvate carrier 2
0.0006688	3.1746944	2.27	1.1840503	Cdk17	Cyclin-dependent kinase 14;Cyclin-dependent kinase 16;Cyclin-dependent kinase 16;Cyclin-dependent kinase 18;Cyclin-dependent kinase 17
0.0017981	2.7451823	2.27	1.1824148	Phf2	Lysine-specific demethylase PHF2
0.0000420	4.3768139	2.21	1.1419874	Lman2l	VIP36-like protein
0.0000014	5.8475558	2.19	1.1301443	Mogs	Mannosyl-oligosaccharide glucosidase
0.0000096	5.0193364	2.18	1.1245117	Trappc13	Trafficking protein particle complex subunit 13
0.0000054	5.2689131	2.17	1.1174624	Smchd1	Structural maintenance of chromosomes flexible hinge domain-containing protein 1
0.0007056	3.1514407	2.15	1.1071213	Gamt	Guanidinoacetate N-methyltransferase
0.0038878	2.4102953	2.14	1.0978130	Anapc1	Anaphase-promoting complex subunit 1
0.0074510	2.1277849	2.14	1.0947463	Traf3ip1	TRAF3-interacting protein 1
0.0000798	4.0979874	2.12	1.0862421	Ythdf2	YTH domain-containing family protein 1;YTH domain-containing family protein 1;YTH domain-containing family protein 2
0.0081072	2.0911316	2.12	1.0860344	Myl6	Myosin light polypeptide 6;Myosin light polypeptide 6
0.0174130	1.7591260	2.11	1.0766192	Dnajc11	DnaJ homolog subfamily C member 11

0.0048133	2.3175605	2.10	1.0720641	Coil	Coilin
0.0026697	2.5735354	2.09	1.0660454	Paox	Peroxisomal N(1)-acetyl-spermine/spermidine oxidase
0.0078068	2.1075274	2.08	1.0554480	B2m	Beta-2-microglobulin
0.0018089	2.7425768	2.07	1.0509508	Ppp2r5b	Serine/threonine-protein phosphatase 2A 56 kDa regulatory subunit gamma isoform;Serine/threonine-protein phosphatase 2A 56 kDa regulatory subunit epsilon isoform;Serine/threonine-protein phosphatase 2A 56 kDa regulatory subunit beta isoform
0.0028461	2.5457497	2.06	1.0425087	Bcl7a	B-cell CLL/lymphoma 7 protein family member A
0.0210769	1.6761939	2.04	1.0302489	Mertk	Tyrosine-protein kinase Mer
0.0040503	2.3925112	2.03	1.0221107	Fbxo42	F-box only protein 42
0.0030792	2.5115585	2.02	1.0133308	Ap3m1	AP-3 complex subunit mu-2;AP-3 complex subunit mu-1
0.0057553	2.2399319	2.01	1.0099938	Gstm4	Glutathione S-transferase Mu 1;Glutathione S-transferase Mu 1;Glutathione S-transferase Mu 1;Glutathione S-transferase Mu 2;Glutathione S-transferase Mu 4
0.0215011	1.6675390	2.00	1.0002861	Map3k19	Mitogen-activated protein kinase kinase kinase 19
0.0001916	3.7175900	1.95	0.9670712	Srek1	Splicing regulatory glutamine/lysine-rich protein 1
0.0208686	1.6805061	1.93	0.9454654	Tnfaip8l3	Tumor necrosis factor alpha-induced protein 8-like protein 3
0.0000538	4.2696055	1.91	0.9343697	Hacd2	Very-long-chain (3R)-3-hydroxyacyl-CoA dehydratase 2
0.0000005	6.3324709	1.90	0.9222262	Loxhd1	Lipoxygenase homology domain-containing protein 1
0.0039282	2.4058037	1.89	0.9216283	Dhodh	Dihydroorotate dehydrogenase (quinone), mitochondrial
0.0057276	2.2420298	1.89	0.9193364	Sgpp1	Sphingosine-1-phosphate phosphatase 1
0.0028062	2.5518784	1.88	0.9129136	Tusc3	Tumor suppressor candidate 3
0.0383078	1.4167124	1.87	0.9043579	Derl1	Derlin-1
0.0000023	5.6468104	1.87	0.9028666	Rrp12	RRP12-like protein
0.0065206	2.1857124	1.87	0.9012103	Fam114a2	Protein FAM114A2
0.0058641	2.2317978	1.85	0.8858857	Cda	Cytidine deaminase
0.0000002	6.6450968	1.85	0.8857530	Nme7	Nucleoside diphosphate kinase 7
0.0006288	3.2014562	1.85	0.8851796	Ndufb11	NADH dehydrogenase [ubiquinone] 1 beta subcomplex subunit 11, mitochondrial
0.0008160	3.0882896	1.84	0.8832777	Tns3	Tensin-1;Tensin-1;Tensin-3
0.0079455	2.0998762	1.84	0.8813873	Slc7a4	Cationic amino acid transporter 4
0.0000880	4.0555775	1.84	0.8794639	Dhrs7	Dehydrogenase/reductase SDR family member 7
0.0001384	3.8589139	1.84	0.8784224	Prpf2	PRA1 family protein 2
0.0014898	2.8268783	1.84	0.8782878	Chadl	Chondroadherin-like protein
0.0000735	4.1338337	1.82	0.8653851	Tial1	Cytotoxic granule associated RNA binding protein TIA1;Nucleolysin TIAR
0.0156078	1.8066582	1.82	0.8618823	Kiaa0319l	Dyslexia-associated protein KIAA0319-like protein
0.0224293	1.6491846	1.82	0.8617864	Hspa12b	Heat shock 70 kDa protein 12A;Heat shock 70 kDa protein 12B
0.0105318	1.9774994	1.82	0.8606243	Cox5a	Cytochrome c oxidase subunit 5A, mitochondrial
0.0037668	2.4240265	1.81	0.8569860	Rab3b	Ras-related protein Rab-8A;Ras-related protein Rab-3C;Ras-related protein Rab-3B
0.0084247	2.0744459	1.81	0.8523189	Impdh1	Inosine-5'-monophosphate dehydrogenase 2;Inosine-5'-monophosphate dehydrogenase 1

0.0050290	2.2985155	1.80	0.8503544	Upp1	Uridine phosphorylase 1
0.0000051	5.2945992	1.80	0.8501685	Csad	Cysteine sulfinic acid decarboxylase
0.0005284	3.2770207	1.80	0.8500376	Fcsk	L-fucose kinase
0.0015191	2.8184240	1.80	0.8488972	Atp5f1d	ATP synthase subunit delta, mitochondrial
0.0008669	3.0620441	1.80	0.8452032	Slc25a5	ADP/ATP translocase 1;ADP/ATP translocase 1;ADP/ATP translocase 2
0.0177690	1.7503379	1.79	0.8431585	Pik3cg	Phosphatidylinositol 4,5-bisphosphate 3-kinase catalytic subunit gamma isoform
0.0418752	1.3780428	1.79	0.8397511	Obox8	Oocyte-specific homeobox 8
0.0248532	1.6046184	1.79	0.8378602	Nat8l	N-acetylaspartate synthetase
0.0044037	2.3561868	1.79	0.8370214	Gabrb1	Gamma-aminobutyric acid receptor subunit beta-1;Gamma-aminobutyric acid receptor subunit beta-1
0.0008312	3.0802754	1.78	0.8312746	Lonrf2	LON peptidase N-terminal domain and ring finger 2
0.0000013	5.8855811	1.77	0.8200632	Syngn1	Synaptogyrin-1
0.0000087	5.0588913	1.75	0.8113226	Ncln	Nicalin
0.0003548	3.4500108	1.75	0.8074697	Rab3a	Ras-related protein Rab-8A;Ras-related protein Rab-8A;Ras-related protein Rab-3C;Ras-related protein Rab-3A
0.0258526	1.5874950	1.75	0.8070824	Srsf11	Serine and arginine-rich-splicing factor 11
0.0035768	2.4465041	1.75	0.8059009	Zswim8	Zinc finger SWIM domain-containing protein 8
0.0055482	2.2558468	1.75	0.8033271	Naa30	N-alpha-acetyltransferase 30
0.0167617	1.7756824	1.74	0.7987820	Ndufb3	NADH dehydrogenase [ubiquinone] 1 beta subcomplex subunit 3
0.0201307	1.6961416	1.73	0.7898963	Mef2d	Myocyte-specific enhancer factor 2D
0.0105140	1.9782320	1.72	0.7847085	Trappc14	Trafficking protein particle complex subunit 14
0.0023508	2.6287848	1.72	0.7829350	Micos10	MICOS complex subunit Mic10
0.0000121	4.9179971	1.71	0.7768086	Slc7a10	Asc-type amino acid transporter 1
0.0004023	3.3954292	1.71	0.7749765	Tmem199	Transmembrane protein 199
0.0037423	2.4268659	1.71	0.7709974	Ntaq1	Protein N-terminal glutamine amidohydrolase
0.0001059	3.9749788	1.70	0.7681373	Tuba4a	Tubulin alpha-4A chain;Tubulin alpha-4A chain;Tubulin alpha-4A chain
0.0000130	4.8863679	1.70	0.7668629	Hid1	Protein HID1
0.0000035	5.4515334	1.70	0.7650821	Strip1	Striatin-interacting protein 1
0.0001572	3.8036695	1.70	0.7640814	Ogn	Mimecan
0.0003291	3.4826212	1.70	0.7639873	Acs1	Long-chain-fatty-acid--CoA ligase 1
0.0106258	1.9736403	1.70	0.7627008	Mpdz	Multiple PDZ domain protein
0.0000307	4.5122932	1.70	0.7621728	Vkorc11	Vitamin K epoxide reductase complex subunit 1-like protein 1
0.0010544	2.9770001	1.69	0.7553336	Ppp2r2d	Serine/threonine-protein phosphatase 2A 55 kDa regulatory subunit B alpha isoform;Serine/threonine-protein phosphatase 2A 55 kDa regulatory subunit B alpha isoform;Serine/threonine-protein phosphatase 2A 55 kDa regulatory subunit B gamma isoform;Serine/threonine-protein phosphatase 2A 55 kDa regulatory subunit B delta isoform
0.0000001	6.8798422	1.69	0.7531828	Mettl26	Methyltransferase-like 26
0.0000954	4.0203048	1.69	0.7528720	Mta3	Metastasis-associated protein MTA3
0.0197353	1.7047564	1.68	0.7500806	Atp13a1	Endoplasmic reticulum transmembrane helix translocase
0.0212068	1.6735251	1.68	0.7491447	Ugt8	2-hydroxyacylsphingosine 1-beta-galactosyltransferase
0.0183915	1.7353835	1.68	0.7453410	Rbck1	RanBP-type and C3HC4-type zinc finger-containing protein 1

0.0159546	1.7971130	1.68	0.7452059	Sugp1	SURP and G-patch domain-containing protein 1
0.0012037	2.9194675	1.67	0.7396156	Dpy191l	Probable C-mannosyltransferase DPY19L1
0.0000518	4.2855284	1.67	0.7380791	Amt	Aminomethyltransferase, mitochondrial
0.0066788	2.1752992	1.67	0.7358523	Slc25a3	Phosphate carrier protein, mitochondrial
0.0240822	1.6183042	1.66	0.7337283	Slc22a17	Solute carrier family 22 member 17
0.0005039	3.2976283	1.66	0.7329241	Tmco1	Calcium load-activated calcium channel
0.0244588	1.6115645	1.66	0.7310637	Ppp1r3f	Protein phosphatase 1 regulatory subunit 3F
0.0072041	2.1424219	1.66	0.7272170	Tmppe	Transmembrane protein with metallophosphoesterase domain
0.0000017	5.7632885	1.65	0.7264916	Mrps11	28S ribosomal protein S11, mitochondrial
0.0000220	4.6570555	1.65	0.7255195	Asns	Asparagine synthetase [glutamine-hydrolyzing]
0.0007605	3.1189058	1.65	0.7202803	Eif3d	Eukaryotic translation initiation factor 3 subunit D
0.0000451	4.3454656	1.64	0.7174068	Pgls	6-phosphogluconolactonase
0.0023131	2.6358016	1.64	0.7165682	Hscb	Iron-sulfur cluster co-chaperone protein HscB
0.0009773	3.0099605	1.64	0.7127797	Kctd4	BTB/POZ domain-containing protein KCTD4
0.0001228	3.9109254	1.64	0.7117698	Tra2b	Transformer-2 protein homolog beta;Transformer-2 protein homolog beta
0.0000105	4.9807590	1.64	0.7103869	Atg9a	Autophagy-related protein 9A
0.0000014	5.8565526	1.63	0.7086792	Gfus	GDP-L-fucose synthase
0.0001551	3.8093591	1.63	0.7080944	Fmn12	Formin-like protein 2;Formin-like protein 2
0.0000015	5.8224695	1.63	0.7074219	Ndufs6	NADH dehydrogenase [ubiquinone] iron-sulfur protein 6, mitochondrial
0.0106127	1.9741753	1.63	0.7054416	Tmem9	Proton-transporting V-type ATPase complex assembly regulator TMEM9;Proton-transporting V-type ATPase complex assembly regulator TMEM9
0.0025931	2.5861880	1.63	0.7040375	Zkscan16	Zinc finger with KRAB and SCAN domains 16
0.0010639	2.9730877	1.63	0.7021265	Fryl	FRY-like transcription coactivator
0.0003791	3.4212030	1.62	0.6943862	Rgs17	Regulator of G-protein signaling 17
0.0000042	5.3803266	1.62	0.6941132	Phkb	Phosphorylase b kinase regulatory subunit beta
0.0000007	6.1514416	1.62	0.6928717	Rpsa	40S ribosomal protein SA
0.0007301	3.1366028	1.62	0.6925470	Bckdk	[3-methyl-2-oxobutanoate dehydrogenase [lipoamide]] kinase, mitochondrial
0.0027808	2.5558259	1.61	0.6873883	Tma7	Translation machinery-associated protein 7
0.0000299	4.5243788	1.61	0.6871697	Elavl3	ELAV-like protein 2;ELAV-like protein 3
0.0228591	1.6409400	1.61	0.6864981	Tmem214	Transmembrane protein 214
0.0297516	1.5264891	1.61	0.6834288	Mtco2	Cytochrome c oxidase subunit 2
0.0000562	4.2502801	1.61	0.6829354	Pum1	Pumilio homolog 1
0.0022894	2.6402696	1.60	0.6823250	Tiam1	Rho guanine nucleotide exchange factor TIAM1
0.0006698	3.1740635	1.60	0.6814183	Ap3m2	AP-3 complex subunit mu-2;AP-3 complex subunit mu-2
0.0032925	2.4824802	1.60	0.6765903	Dpp9	Dipeptidyl peptidase 9
0.0103286	1.9859573	1.59	0.6709128	Aifm1	Apoptosis-inducing factor 1, mitochondrial
0.0001849	3.7329726	1.59	0.6703967	Senp3	Sentrin-specific protease 3
0.0016067	2.7940719	1.59	0.6680483	Rtn4ip1	Reticulon-4-interacting protein 1, mitochondrial
0.0188691	1.7242483	1.59	0.6663823	Dhcr7	7-dehydrocholesterol reductase
0.0127606	1.8941293	1.58	0.6633905	Get3	ATPase GET3
0.0145615	1.8367946	1.58	0.6594392	Pdf	Peptide deformylase, mitochondrial
0.0145319	1.8376786	1.58	0.6583553	Sfxn1	Sideroflexin-1
0.0000161	4.7920460	1.58	0.6579147	Spcs2	Signal peptidase complex subunit 2

0.0000163	4.7883043	1.58	0.6565715	Yme11	ATP-dependent zinc metalloprotease YME1L1
0.0029563	2.5292527	1.57	0.6478395	Ndufb8	NADH dehydrogenase [ubiquinone] 1 beta subcomplex subunit 8, mitochondrial
0.0008919	3.0496904	1.56	0.6455256	Eif2b5	Translation initiation factor eIF-2B subunit epsilon
0.0270023	1.5685993	1.56	0.6403937	Emc4	ER membrane protein complex subunit 4
0.0000223	4.6516642	1.56	0.6388144	Pdk3	[Pyruvate dehydrogenase (acetyl-transferring)] kinase isozyme 1, mitochondrial;[Pyruvate dehydrogenase (acetyl-transferring)] kinase isozyme 3, mitochondrial
0.0070526	2.1516500	1.55	0.6337918	Shq1	Protein SHQ1 homolog
0.0000003	6.4979336	1.55	0.6332661	Lypla2	Acyl-protein thioesterase 2
0.0000053	5.2769657	1.55	0.6302727	Uckl1	Uridine-cytidine kinase-like 1
0.0000744	4.1281646	1.55	0.6288713	Adpgk	ADP-dependent glucokinase
0.0169617	1.7705317	1.55	0.6281553	Shc3	SHC-transforming protein 3
0.0159316	1.7977395	1.54	0.6263784	Hmgn1	Non-histone chromosomal protein HMG-14
0.0007663	3.1156060	1.54	0.6239655	Atp5f1b	ATP synthase subunit beta, mitochondrial
0.0035940	2.4444195	1.54	0.6213805	Tmem43	Transmembrane protein 43
0.0239121	1.6213823	1.54	0.6204292	Prcc	Papillary Renal Cell carcinoma (Translocation-associated)
0.0196694	1.7062087	1.54	0.6197545	Cherp	Calcium homeostasis endoplasmic reticulum protein
0.0182284	1.7392516	1.54	0.6190935	Atl2	Atlastin-2;Atlastin-2
0.0066311	2.1784113	1.53	0.6159156	Tmem245	Transmembrane protein 245
0.0000043	5.3686119	1.53	0.6125162	Nagk	N-acetyl-D-glucosamine kinase
0.0036221	2.4410413	1.53	0.6105501	Dynlrb1	Dynein light chain roadblock-type 1
0.0109081	1.9622521	1.53	0.6102329	Hexa	Beta-hexosaminidase subunit alpha
0.0000040	5.3980724	1.52	0.6081024	Arl6ip1	ADP-ribosylation factor-like protein 6-interacting protein 1
0.0033159	2.4793988	1.52	0.6076275	Nutf2	Nuclear transport factor 2
0.0004096	3.3876421	1.52	0.6068265	Faf1	FAS-associated factor 1
0.0002303	3.6377944	1.52	0.6064108	Mtarc2	Mitochondrial amidoxime reducing component 2
0.0005105	3.2920016	1.52	0.6063579	Dmwd	Dystrophia myotonica WD repeat-containing protein
0.0130047	1.8858987	1.52	0.6051068	Gpaa1	Glycosylphosphatidylinositol anchor attachment 1 protein
0.0002812	3.5509480	1.51	0.5980191	Fam98c	Family with sequence similarity 98, member C
0.0000190	4.7208337	1.51	0.5932072	Hnrnpm	Heterogeneous nuclear ribonucleoprotein M
0.0052621	2.2788370	1.51	0.5929736	Ube2v1	Ubiquitin-conjugating enzyme E2 variant 1;Ubiquitin-conjugating enzyme E2 variant 1
0.0049639	2.3041796	1.51	0.5928725	Kcnc3	Potassium voltage-gated channel subfamily C member 3
0.0000004	6.4156264	1.51	0.5921036	Rpl10a	60S ribosomal protein L10a
0.0100115	1.9994990	1.51	0.5904014	Srsf2	Serine/arginine-rich splicing factor 2
0.0000435	4.3613821	1.50	0.5879368	Sccpdh	Saccharopine dehydrogenase-like oxidoreductase
0.0185564	1.7315058	1.50	0.5854011	Slc25a12	Electrogenic aspartate/glutamate antiporter SLC25A12, mitochondrial;Electrogenic aspartate/glutamate antiporter SLC25A12, mitochondrial
0.0000026	5.5823323	1.50	0.5842461	Abhd4	(Lyso)-N-acylphosphatidylethanolamine lipase
0.0011747	2.9300801	1.50	0.5834935	Ggt7	Glutathione hydrolase 7
0.0093906	2.0273060	1.50	0.5807148	Osbpl8	Oxysterol-binding protein-related protein 8
0.0001091	3.9622131	1.49	0.5800109	Opa3	Optic atrophy 3 protein homolog

0.0000135	4.8681080	1.49	0.5793122	Mmaa	Methylmalonic aciduria type A homolog, mitochondrial
0.0004037	3.3938908	1.49	0.5745615	Wdr45	WD repeat domain phosphoinositide-interacting protein 4
0.0027470	2.5611378	1.48	0.5702142	Slc6a4	Sodium-dependent serotonin transporter
0.0000239	4.6208452	1.48	0.5685886	Cbln1	Cerebellin-1
0.0110723	1.9557630	1.48	0.5668915	Meak7	MTOR-associated protein MEAK7
0.0010888	2.9630372	1.48	0.5636817	Mras	Ras-related protein M-Ras
0.0085097	2.0700834	1.48	0.5607951	Baz1b	Tyrosine-protein kinase BAZ1B
0.0088571	2.0527088	1.47	0.5582702	Slc25a22	Mitochondrial glutamate carrier 1;Mitochondrial glutamate carrier 1
0.0007580	3.1203517	1.47	0.5576370	Dmap1	DNA methyltransferase 1-associated protein 1
0.0055669	2.2543828	1.47	0.5555899	Nipa1	Magnesium transporter NIPA1
0.0052434	2.2803906	1.47	0.5519264	Lmtk3	Serine/threonine-protein kinase LMTK3
0.0001513	3.8201066	1.46	0.5502042	Necab2	N-terminal EF-hand calcium-binding protein 2
0.0005096	3.2927545	1.46	0.5486620	Rps9	40S ribosomal protein S9
0.0000207	4.6845161	1.46	0.5485101	Dgkq	Diacylglycerol kinase theta
0.0003904	3.4085239	1.46	0.5483953	Mrpl9	39S ribosomal protein L9, mitochondrial
0.0002322	3.6340657	1.46	0.5476578	Uqcrc1	Mitochondrial-processing peptidase subunit beta;Cytochrome b-c1 complex subunit 1, mitochondrial
0.0035706	2.4472567	1.46	0.5464658	Trpv2	Transient receptor potential cation channel subfamily V member 2
0.0114668	1.9405562	1.46	0.5454174	Smim8	Small integral membrane protein 8
0.0000004	6.3666456	1.46	0.5446947	Raly1	RNA-binding Raly-like protein;RNA-binding Raly-like protein
0.0094027	2.0267457	1.46	0.5421433	Nup160	Nuclear pore complex protein Nup160
0.0000712	4.1475999	1.46	0.5420122	Pomgnt2	Protein O-linked-mannose beta-1,4-N-acetylglucosaminyltransferase 2
0.0001554	3.8085472	1.45	0.5404080	Ndufv2	NADH dehydrogenase [ubiquinone] flavoprotein 2, mitochondrial
0.0144950	1.8387831	1.45	0.5401417	Ublcp1	Ubiquitin-like domain-containing CTD phosphatase 1
0.0000554	4.2568301	1.45	0.5363282	Camk2d	Calcium/calmodulin-dependent protein kinase type II subunit alpha;Calcium/calmodulin-dependent protein kinase type II subunit alpha;Calcium/calmodulin-dependent protein kinase type II subunit alpha;Calcium/calmodulin-dependent protein kinase type II subunit beta;Calcium/calmodulin-dependent protein kinase type II subunit delta
0.0000007	6.1632884	1.45	0.5362669	Rcc1	Regulator of chromosome condensation
0.0000861	4.0651736	1.45	0.5350388	Aida	Axin interactor, dorsalization-associated protein
0.0000059	5.2291916	1.45	0.5343204	Rab1A	Ras-related protein Rab-8A;Ras-related protein Rab-8A;Ras-related protein Rab-1A;Ras-related protein Rab-1A
0.0000002	6.6573361	1.45	0.5337829	Prune1	Exopolyphosphatase PRUNE1
0.0002086	3.6805869	1.45	0.5315651	Abcf2	ATP-binding cassette sub-family F member 2
0.0102534	1.9891301	1.44	0.5284495	Crhbp	Corticotropin-releasing factor-binding protein
0.0000003	6.5077321	1.44	0.5271759	Pgam5	Serine/threonine-protein phosphatase PGAM5, mitochondrial
0.0011744	2.9301717	1.44	0.5270041	Ppp1r14c	Protein phosphatase 1 regulatory subunit 14C
0.0067594	2.1700913	1.44	0.5252011	Fry	Protein furry homolog
0.0139094	1.8566918	1.44	0.5247396	Atg3	Ubiquitin-like-conjugating enzyme ATG3
0.0004871	3.3123682	1.44	0.5246202	Klhl22	Kelch-like protein 22
0.0001835	3.7363844	1.43	0.5207871	Nipal3	NIPA-like protein 3

0.0000460	4.3367827	1.43	0.5207298	Dap3	28S ribosomal protein S29, mitochondrial
0.0000506	4.2959615	1.43	0.5198799	Wwox	WW domain-containing oxidoreductase
0.0009745	3.0112367	1.43	0.5156907	Bola2	BolA-like protein 2
0.0095601	2.0195359	1.43	0.5147843	Ppp3cb	Serine/threonine-protein phosphatase 2B catalytic subunit beta isoform;Serine/threonine-protein phosphatase 2B catalytic subunit beta isoform;Serine/threonine-protein phosphatase 2B catalytic subunit beta isoform
0.0018631	2.7297732	1.43	0.5127587	Atp6v0d1	V-type proton ATPase subunit d 1
0.0000396	4.4022754	1.43	0.5115347	Rpl11	60S ribosomal protein L11
0.0000121	4.9188583	1.43	0.5110684	Ttc37	Tetratricopeptide repeat domain 37
0.0000557	4.2545316	1.42	0.5107806	Map2k7	Dual specificity mitogen-activated protein kinase kinase 7
0.0000170	4.7697387	1.42	0.5092680	Prpf8	Pre-mRNA-processing-splicing factor 8
0.0031856	2.4968045	1.42	0.5055034	Elavl2	ELAV-like protein 2;ELAV-like protein 2;ELAV-like protein 2
0.0120786	1.9179832	1.42	0.5021586	Tmem263	Transmembrane protein 263
0.0004964	3.3041536	1.41	0.5000014	Rpn1	Dolichyl-diphosphooligosaccharide--protein glycosyltransferase subunit 1
0.0017001	2.7695379	1.41	0.4974628	Copg2	Coatomer subunit gamma-2;Coatomer subunit gamma-2
0.0092663	2.0330945	1.41	0.4968903	Mif	Macrophage migration inhibitory factor
0.0029939	2.5237613	1.41	0.4965450	Ttn	Titin
0.0000876	4.0577197	1.41	0.4919035	Fchsd2	F-BAR and double SH3 domains protein 2
0.0000079	5.1006445	1.41	0.4914382	Mrpl37	39S ribosomal protein L37, mitochondrial
0.0019185	2.7170402	1.40	0.4902186	Stt3b	Dolichyl-diphosphooligosaccharide--protein glycosyltransferase subunit STT3B
0.0142896	1.8449785	1.40	0.4883466	Ilkap	Integrin-linked kinase-associated serine/threonine phosphatase 2C
0.0057747	2.2384675	1.40	0.4863443	Tbl2	Transducin beta-like protein 2
0.0000624	4.2048192	1.40	0.4842206	Mthfd1	Monofunctional C1-tetrahydrofolate synthase, mitochondrial;C-1-tetrahydrofolate synthase, cytoplasmic
0.0107935	1.9668380	1.40	0.4834805	Eloc	Elongin-C
0.0000014	5.8562716	1.40	0.4808308	Eif4a3	Eukaryotic initiation factor 4A-II;Eukaryotic initiation factor 4A-III
0.0000192	4.7158707	1.39	0.4780173	Nsdhl	Sterol-4-alpha-carboxylate 3-dehydrogenase, decarboxylating
0.0007378	3.1320838	1.39	0.4777814	Capn1	Calpain-1 catalytic subunit
0.0000268	4.5722254	1.39	0.4762554	Prps11	ribose-phosphate diphosphokinase
0.0001214	3.9157474	1.39	0.4758425	Elp3	Elongator complex protein 3
0.0000001	7.2869588	1.39	0.4749780	Pten	Phosphatidylinositol 3,4,5-trisphosphate 3-phosphatase and dual-specificity protein phosphatase PTEN
0.0032826	2.4837806	1.39	0.4743814	Tmem126a	Transmembrane protein 126A
0.0041515	2.3817904	1.39	0.4721865	Samm50	Sorting and assembly machinery component 50 homolog
0.0015863	2.7996150	1.39	0.4720735	Pnpt1	Polyribonucleotide nucleotidyltransferase 1, mitochondrial
0.0005809	3.2358803	1.39	0.4719902	Tbc1d23	TBC1 domain family member 23
0.0059972	2.2220508	1.39	0.4718764	P4htm	Transmembrane prolyl 4-hydroxylase
0.0009223	3.0351257	1.39	0.4708142	Gucy1a1	Guanylate cyclase soluble subunit alpha-1
0.0003596	3.4441741	1.39	0.4703372	Ngb	Neuroglobin
0.0002852	3.5447896	1.38	0.4696001	Acaca	Acetyl-CoA carboxylase 1
0.0000324	4.4891190	1.38	0.4694369	Atp5po	ATP synthase subunit O, mitochondrial
0.0060858	2.2156819	1.38	0.4692172	Pdcd6	Programmed cell death protein 6

0.0015065	2.8220319	1.38	0.4664681	Atp5f1a	ATP synthase subunit alpha, mitochondrial
0.0120751	1.9181099	1.38	0.4664597	Uchl1	Ubiquitin carboxyl-terminal hydrolase isozyme L1
0.0115550	1.9372295	1.38	0.4661660	Arl8b	ADP-ribosylation factor-like protein 8A;ADP-ribosylation factor-like protein 8B
0.0024450	2.6117274	1.38	0.4625925	Pnkd	Probable hydrolase PNKD
0.0059493	2.2255324	1.38	0.4594653	Syngn3	Synaptogyrin-3
0.0052496	2.2798749	1.37	0.4589115	Bscl2	Seipin
0.0000645	4.1902014	1.37	0.4553109	Mdp1	Magnesium-dependent phosphatase 1
0.0000004	6.3744892	1.37	0.4542411	Hdac11	Histone deacetylase 11
0.0001169	3.9322674	1.37	0.4517342	Kif16b	Kinesin-like protein KIF16B;Kinesin-like protein KIF16B
0.0000234	4.6310092	1.37	0.4508812	Fbxo22	F-box only protein 22
0.0005443	3.2641528	1.37	0.4508630	Tnpo2	Transportin-1;Transportin-2
0.0000256	4.5924008	1.37	0.4505864	Scyl1	N-terminal kinase-like protein
0.0000786	4.1045862	1.37	0.4505450	Cdipt	CDP-diacylglycerol--inositol 3-phosphatidyltransferase
0.0007121	3.1474676	1.37	0.4505196	Tubgcp2	Gamma-tubulin complex component 2
0.0005158	3.2874914	1.37	0.4503863	Pcyt1a	Choline-phosphate cytidyltransferase A;Choline-phosphate cytidyltransferase A
0.0035319	2.4519959	1.37	0.4502405	Lemd3	Inner nuclear membrane protein Man1
0.0000321	4.4935937	1.36	0.4464050	Spire1	Protein spire homolog 1
0.0027097	2.5670734	1.36	0.4451438	Rab15	Ras-related protein Rab-8A;Ras-related protein Rab-15
0.0001925	3.7156529	1.36	0.4447099	Stam	Signal transducing adapter molecule 1
0.0043476	2.3617468	1.35	0.4381001	Hars2	Histidine--tRNA ligase, cytoplasmic;Histidine--tRNA ligase, mitochondrial
0.0026825	2.5714624	1.35	0.4358215	Credl1	Protein disulfide isomerase Credl1
0.0003858	3.4136491	1.35	0.4357152	Vwa8	von Willebrand factor A domain-containing protein 8
0.0000016	5.7949171	1.35	0.4348873	Cs	Citrate synthase, mitochondrial
0.0020323	2.6920209	1.35	0.4345345	Sema7a	Semaphorin-7A
0.0015425	2.8117652	1.35	0.4343349	Ankrd13d	Ankyrin repeat domain-containing protein 13D
0.0000021	5.6799558	1.35	0.4326178	Usp7	Ubiquitin carboxyl-terminal hydrolase 7
0.0000447	4.3497021	1.35	0.4318794	Mrpl24	39S ribosomal protein L24, mitochondrial
0.0000001	6.8276373	1.35	0.4314644	Vps33a	Vacuolar protein sorting-associated protein 33A
0.0029556	2.5293553	1.35	0.4314023	Abhd17b	Alpha/beta hydrolase domain-containing protein 17B;Alpha/beta hydrolase domain-containing protein 17B
0.0000571	4.2435245	1.35	0.4305041	Ppp2cb	Serine/threonine-protein phosphatase 2A catalytic subunit beta isoform;Serine/threonine-protein phosphatase 2A catalytic subunit beta isoform
0.0032771	2.4845150	1.35	0.4303232	Saraf	Store-operated calcium entry-associated regulatory factor
0.0000000	7.6617747	1.35	0.4302456	Rpl7a	60S ribosomal protein L7a
0.0018645	2.7294390	1.35	0.4297090	Camk2a	Calcium/calmodulin-dependent protein kinase type II subunit alpha;Calcium/calmodulin-dependent protein kinase type II subunit alpha;Calcium/calmodulin-dependent protein kinase type II subunit alpha;Calcium/calmodulin-dependent protein kinase type II subunit alpha
0.0001223	3.9126352	1.35	0.4284292	Atp2b4	Plasma membrane calcium-transporting ATPase 1;Plasma membrane calcium-transporting ATPase 1;Plasma membrane calcium-transporting ATPase 4

0.0000008	6.1032716	1.35	0.4279696	Cdk18	Cyclin-dependent kinase 14;Cyclin-dependent kinase 16;Cyclin-dependent kinase 16;Cyclin-dependent kinase 18;Cyclin-dependent kinase 18
0.0000006	6.2185501	1.35	0.4279318	Rcc2	Protein RCC2
0.0003617	3.4416631	1.34	0.4269150	Ap3s2	AP-3 complex subunit sigma-2
0.0061924	2.2081422	1.34	0.4266677	Emc1	ER membrane protein complex subunit 1
0.0000085	5.0712545	1.34	0.4259618	Grk2	Beta-adrenergic receptor kinase 2;Beta-adrenergic receptor kinase 1
0.0009823	3.0077426	1.34	0.4238772	Stat5b	Signal transducer and activator of transcription 5B
0.0055821	2.2532059	1.34	0.4216966	Armc6	Armadillo repeat-containing protein 6
0.0000002	6.7957695	1.34	0.4213322	Rasal1	RasGAP-activating-like protein 1
0.0000016	5.7907852	1.34	0.4212941	Rbm39	RNA-binding protein 39
0.0002113	3.6751415	1.34	0.4199454	Apmap	Adipocyte plasma membrane-associated protein
0.0003010	3.5214814	1.34	0.4179451	Csk	Tyrosine-protein kinase CSK
0.0031052	2.5079168	1.34	0.4179337	Ergic1	Endoplasmic reticulum-Golgi intermediate compartment protein 1
0.0028245	2.5490617	1.33	0.4159398	Tubgcp3	Gamma-tubulin complex component 3
0.0000007	6.1632277	1.33	0.4157002	Farsb	Phenylalanine--tRNA ligase beta subunit
0.0059547	2.2251383	1.33	0.4145411	Mfn2	Mitofusin-2
0.0000298	4.5264050	1.33	0.4129271	Gsk3b	Glycogen synthase kinase-3 alpha;Glycogen synthase kinase-3 beta
0.0012529	2.9020690	1.33	0.4124091	Psm5	26S proteasome non-ATPase regulatory subunit 5
0.0003297	3.4819299	1.33	0.4123171	Aimp2	Aminoacyl tRNA synthase complex-interacting multifunctional protein 2
0.0003621	3.4411238	1.33	0.4122801	Bri3bp	BRI3-binding protein
0.0000764	4.1166607	1.33	0.4101885	Cars1	Cysteine--tRNA ligase, cytoplasmic
0.0052196	2.2823634	1.33	0.4098989	Me3	NADP-dependent malic enzyme, mitochondrial;NADP-dependent malic enzyme, mitochondrial
0.0000502	4.2994606	1.33	0.4095723	Prdx2	Peroxiredoxin-2
0.0007138	3.1464108	1.33	0.4092914	Emc8	ER membrane protein complex subunit 8
0.0010526	2.9777562	1.33	0.4092302	Smc3	Structural maintenance of chromosomes protein 3
0.0054506	2.2635580	1.33	0.4078788	Kat7	Histone acetyltransferase KAT7
0.0000061	5.2160351	1.32	0.4057418	Rab39b	Ras-related protein Rab-8A;Ras-related protein Rab-39B
0.0000344	4.4639816	1.32	0.4054460	Ap3s1	AP-3 complex subunit sigma-1
0.0010130	2.9943791	1.32	0.4046717	Ppp2r5c	Serine/threonine-protein phosphatase 2A 56 kDa regulatory subunit gamma isoform;Serine/threonine-protein phosphatase 2A 56 kDa regulatory subunit gamma isoform
0.0001099	3.9589002	1.32	0.4038271	Fgd2	FYVE, RhoGEF and PH domain-containing protein 2
0.0000290	4.5380197	1.32	0.4033989	Cdc16	Cell division cycle protein 16 homolog
0.0003502	3.4556942	1.32	0.4023306	Mrpl38	39S ribosomal protein L38, mitochondrial
0.0000001	7.1208988	1.32	0.4019222	Prmt5	Protein arginine N-methyltransferase 5
0.0019671	2.7061731	1.32	0.4015938	Ppp2r1a	Serine/threonine-protein phosphatase 2A 65 kDa regulatory subunit A alpha isoform
0.0000927	4.0330389	1.32	0.4004347	Atp5mpl	ATP synthase subunit ATP5MPL, mitochondrial
0.0050376	2.2977735	1.32	0.3991187	Bnip1	Vesicle transport protein SEC20
0.0000068	5.1650378	1.32	0.3963495	Sntb1	Alpha-1-syntrophin;Beta-1-syntrophin
0.0000000	7.5504724	1.32	0.3959794	Rps11	40S ribosomal protein S11

0.0010401	2.9829296	1.31	0.3900221	Gm21834	Predicted gene, 21834
0.0000198	4.7038217	1.31	0.3896193	Elp4	Elongator complex protein 4
0.0023567	2.6276898	1.31	0.3888516	Cbs	Cystathionine beta-synthase
0.0039877	2.3992737	1.31	0.3884526	Vcam1	Vascular cell adhesion protein 1
0.0017001	2.7695196	1.31	0.3877539	Slc30a1	Proton-coupled zinc antiporter SLC30A1
0.0003445	3.4627885	1.31	0.3873119	Sdr39u1	Epimerase family protein SDR39U1
0.0037947	2.4208218	1.31	0.3868318	Slc27a4	Long-chain fatty acid transport protein 4
0.0000009	6.0367628	1.31	0.3853739	Cenpv	Centromere protein V
0.0001666	3.7783975	1.31	0.3851048	Eef1g	Elongation factor 1-gamma
0.0005147	3.2884648	1.31	0.3842385	Pip4p1	Type 1 phosphatidylinositol 4,5-bisphosphate 4-phosphatase;Type 1 phosphatidylinositol 4,5-bisphosphate 4-phosphatase
0.0000138	4.8612931	1.30	0.3826631	Naxe	NAD(P)H-hydrate epimerase
0.0000177	4.7508802	1.30	0.3805745	Elavl1	ELAV-like protein 1
0.0016524	2.7818777	1.30	0.3802801	Ndufs1	NADH-ubiquinone oxidoreductase 75 kDa subunit, mitochondrial
0.0006632	3.1783283	1.30	0.3799589	Snrnp200	U5 small nuclear ribonucleoprotein 200 kDa helicase
0.0051120	2.2914125	1.30	0.3791231	Msto1	Protein misato homolog 1
0.0000553	4.2573899	1.30	0.3778063	Srsf6	Serine/arginine-rich splicing factor 5;Serine/arginine-rich splicing factor 6;Serine/arginine-rich splicing factor 6
0.0012692	2.8964629	1.30	0.3768078	Ccdc25	Coiled-coil domain-containing protein 25
0.0006192	3.2081436	1.30	0.3756761	Mrps14	28S ribosomal protein S14, mitochondrial
0.0036287	2.4402468	1.30	0.3747746	Rnf114	E3 ubiquitin-protein ligase RNF114
0.0026483	2.5770321	1.30	0.3733015	Fkbp5	Peptidyl-prolyl cis-trans isomerase FKBP5
0.0004095	3.3877025	1.29	0.3713082	Rdh14	Retinol dehydrogenase 14
0.0006964	3.1571714	1.29	0.3705688	Camk2g	Calcium/calmodulin-dependent protein kinase type II subunit alpha;Calcium/calmodulin-dependent protein kinase type II subunit beta;Calcium/calmodulin-dependent protein kinase type II subunit beta;Calcium/calmodulin-dependent protein kinase type II subunit gamma
0.0000346	4.4609170	1.29	0.3691996	Macroh2a1	Core histone macro-H2A.2;Core histone macro-H2A.1
0.0000196	4.7070006	1.29	0.3685321	Qars1	Glutamine--tRNA ligase;Glutamine--tRNA ligase
0.0000931	4.0309692	1.29	0.3666475	Taco1	Translational activator of cytochrome c oxidase 1
0.0002832	3.5479336	1.29	0.3650169	Tst	Thiosulfate sulfurtransferase
0.0000001	7.2568128	1.29	0.3648834	Suclg1	Succinate--CoA ligase [ADP/GDP-forming] subunit alpha, mitochondrial
0.0000083	5.0791992	1.29	0.3633668	Fam120c	Constitutive coactivator of PPAR-gamma-like protein 2
0.0000099	5.0056986	1.28	0.3614809	Gspt1	Eukaryotic peptide chain release factor GTP-binding subunit ERF3B;Eukaryotic peptide chain release factor GTP-binding subunit ERF3A
0.0005709	3.2434451	1.28	0.3609430	Ruvbl1	RuvB-like 1
0.0004609	3.3363855	1.28	0.3606224	Ddx46	Probable ATP-dependent RNA helicase DDX46
0.0001979	3.7035721	1.28	0.3593998	Smc1a	Structural maintenance of chromosomes protein 1A
0.0000325	4.4875051	1.28	0.3583509	Plch2	1-phosphatidylinositol 4,5-bisphosphate phosphodiesterase eta-2
0.0004436	3.3529783	1.28	0.3582111	Svop	Synaptic vesicle 2-related protein
0.0000145	4.8372167	1.28	0.3566384	Lnpk	Endoplasmic reticulum junction formation protein lunapark

0.0003674	3.4348057	1.28	0.3565322	Fxr1	Fragile X messenger ribonucleoprotein 1;RNA-binding protein FXR1;RNA-binding protein FXR1
0.0000507	4.2947061	1.28	0.3559398	Nop56	Nucleolar protein 56
0.0001885	3.7246107	1.28	0.3554427	Ccar2	Cell cycle and apoptosis regulator protein 2
0.0002155	3.6665259	1.28	0.3535634	Rab3gap2	Rab3 GTPase-activating protein non-catalytic subunit
0.0000036	5.4459127	1.28	0.3519086	Rpl18a	60S ribosomal protein L18a
0.0000153	4.8142934	1.28	0.3514071	Dpysl5	Dihydropyrimidinase-related protein 5
0.0000936	4.0284988	1.28	0.3505147	Nampt	Nicotinamide phosphoribosyltransferase
0.0001286	3.8906247	1.27	0.3501708	Gdpd1	Lysophospholipase D GDPD1
0.0002553	3.5929854	1.27	0.3501094	Snta1	Alpha-1-syntrophin;Alpha-1-syntrophin
0.0000046	5.3388604	1.27	0.3481781	Shmt2	Serine hydroxymethyltransferase, mitochondrial
0.0000000	8.5813131	1.27	0.3467313	Rps2	40S ribosomal protein S2
0.0001441	3.8413377	1.27	0.3465716	Thnsl2	Threonine synthase-like 2
0.0000199	4.7006447	1.27	0.3463959	Ag1	Glycogen debranching enzyme
0.0003603	3.4433636	1.27	0.3462331	Hadhb	Trifunctional enzyme subunit beta, mitochondrial
0.0009380	3.0277875	1.27	0.3457197	Clvs2	Clavesin-2;Clavesin-2
0.0000037	5.4305234	1.27	0.3435371	Rps23	40S ribosomal protein S23
0.0003907	3.4081616	1.27	0.3435121	Rab12	Ras-related protein Rab-12
0.0012026	2.9198755	1.27	0.3407137	Cntnap4	Contactin-associated protein-like 4
0.0017280	2.7624672	1.27	0.3406089	Scamp5	Secretory carrier-associated membrane protein 5
0.0001461	3.8354445	1.26	0.3377778	Plxnb1	Plexin-B2;Plexin-B1
0.0006230	3.2054951	1.26	0.3365675	Ipo4	Importin-4
0.0000048	5.3167605	1.26	0.3351358	Cul5	Cullin-5
0.0000409	4.3878366	1.26	0.3346949	Ruvbl2	RuvB-like 2
0.0000000	7.3443215	1.26	0.3343641	Actr10	Actin-related protein 10
0.0000335	4.4744110	1.26	0.3335933	Cox7a2l	Cytochrome c oxidase subunit 7A-related protein, mitochondrial
0.0000678	4.1688625	1.26	0.3308422	Cul1	Cullin-1
0.0017810	2.7493261	1.26	0.3288429	Mapk1	Mast/stem cell growth factor receptor Kit;Mitogen-activated protein kinase 1;Mitogen-activated protein kinase 1;Mitogen-activated protein kinase 1
0.0000011	5.9604188	1.25	0.3251227	Atp6v1d	V-type proton ATPase subunit D
0.0011352	2.9449235	1.25	0.3246018	Tfg	TFG protein
0.0000198	4.7036998	1.25	0.3232146	Hnrnpu	Heterogeneous nuclear ribonucleoprotein U
0.0005789	3.2373702	1.25	0.3231657	Htt	Huntingtin
0.0012532	2.9019716	1.25	0.3226091	Psmg1	Proteasome assembly chaperone 1
0.0009339	3.0296889	1.25	0.3204520	Rpl14	60S ribosomal protein L14
0.0000099	5.0054032	1.25	0.3195635	Ap1g1	AP-1 complex subunit gamma-1
0.0000037	5.4376886	1.25	0.3178740	Ddx17	Probable ATP-dependent RNA helicase DDX17;Probable ATP-dependent RNA helicase DDX17;Probable ATP-dependent RNA helicase DDX17
0.0000087	5.0589290	1.25	0.3175195	Rab18	Ras-related protein Rab-18
0.0002864	3.5430652	1.24	0.3139862	Ccdc71	Coiled-coil domain-containing protein 71
0.0000088	5.0562990	1.24	0.3124458	Igsf8	Immunoglobulin superfamily member 8
0.0000610	4.2144338	1.24	0.3092153	Ndn	Necdin
0.0000002	6.6874991	1.24	0.3066352	Fdxr	NADPH:adrenodoxin oxidoreductase, mitochondrial

0.0000485	4.3139855	1.24	0.3049384	Rpl34	60S ribosomal protein L34
0.0003053	3.5153415	1.23	0.3042264	Atp5f1e	ATP synthase subunit epsilon, mitochondrial
0.0000015	5.8228105	1.23	0.3005257	Rnmt	mRNA cap guanine-N7 methyltransferase
0.0005600	3.2518016	1.23	0.2972156	Decr1	2,4-dienoyl-CoA reductase [(3E)-enoyl-CoA-producing], mitochondrial
0.0000049	5.3132581	1.23	0.2957943	Rab4a	Ras-related protein Rab-4A;Ras-related protein Rab-4A
0.0003789	3.4215089	1.23	0.2953436	Xpo5	Exportin-5
0.0000741	4.1303492	1.23	0.2944147	Adap1	ArfGAP with dual PH domains 1
0.0000000	9.0608241	1.23	0.2942576	Rpl15	60S ribosomal protein L15
0.0000079	5.1020766	1.23	0.2937852	Cct6a	T-complex protein 1 subunit zeta;T-complex protein 1 subunit zeta
0.0000154	4.8131491	1.22	0.2905019	Ehd4	EH domain-containing protein 4;EH domain-containing protein 4;EH domain-containing protein 4
0.0001876	3.7268120	1.22	0.2903005	Inpp4a	Inositol polyphosphate-4-phosphatase type I A
0.0000045	5.3504690	1.22	0.2891829	Pygb	Glycogen phosphorylase, brain form;Glycogen phosphorylase, brain form;Glycogen phosphorylase, brain form
0.0000945	4.0245689	1.22	0.2889816	Dnajc10	DnaJ homolog subfamily C member 10
0.0002880	3.5405397	1.22	0.2875528	Baiap3	BAI1-associated protein 3;BAI1-associated protein 3
0.0001138	3.9436997	1.21	0.2798098	Ndufa13	NADH dehydrogenase [ubiquinone] 1 alpha subcomplex subunit 13
0.0001865	3.7292260	1.21	0.2764458	Fyn	Proto-oncogene tyrosine-protein kinase Src;Tyrosine-protein kinase HCK;Tyrosine-protein kinase Fyn;Tyrosine-protein kinase Fyn
0.0001532	3.8146840	1.21	0.2758725	Bphl	Valacyclovir hydrolase
0.0000416	4.3809120	1.21	0.2720153	Vcpip1	Deubiquitinating protein VCPIP1
0.0000095	5.0215638	1.21	0.2692977	Pck2	Phosphoenolpyruvate carboxykinase [GTP], mitochondrial
0.0000189	4.7228438	1.20	0.2681602	Ptbp2	Polypyrimidine tract-binding protein 2
0.0000110	4.9597817	1.20	0.2666613	Ilk	Integrin-linked protein kinase
0.0000006	6.1984878	1.20	0.2649182	U2af2	Splicing factor U2AF 65 kDa subunit
0.0000011	5.9537465	1.20	0.2583421	Psm11	26S proteasome non-ATPase regulatory subunit 11
0.0000222	4.6545336	1.19	0.2536935	Rpl13a	60S ribosomal protein L13a
0.0000123	4.9092510	1.19	0.2520732	Rpl5	60S ribosomal protein L5
0.0000000	8.7333792	1.18	0.2448646	Eif2s3x	Eukaryotic translation initiation factor 2 subunit 3, X-linked

0.0000002	6.6323169	0.84	-0.2584222	Pex5l	PEX5-related protein
0.0000090	5.0472329	0.83	-0.2674299	Lsm12	Protein LSM12
0.0002162	3.6650936	0.82	-0.2849974	Itgb1	Integrin beta-1
0.0000124	4.9077013	0.81	-0.3030568	Gclm	Glutamate--cysteine ligase regulatory subunit
0.0002321	3.6343160	0.81	-0.3052905	Pdlim5	PDZ and LIM domain protein 5
0.0000046	5.3333030	0.81	-0.3058551	Cops3	COP9 signalosome complex subunit 3
0.0000138	4.8594603	0.80	-0.3153465	Tmod2	Tropomodulin-1;Tropomodulin-1;Tropomodulin-2
0.0000315	4.5017356	0.80	-0.3192720	Rab11fip5	Rab11 family-interacting protein 5
0.0003617	3.4416698	0.80	-0.3232490	Ociad1	OCIA domain-containing protein 1
0.0003027	3.5189964	0.80	-0.3243371	Ctsd	Cathepsin D
0.0002113	3.6750332	0.80	-0.3272958	Gripap1	GRIP1-associated protein 1
0.0000640	4.1940240	0.79	-0.3335380	Myh14	Myosin-11;Myosin-11;Myosin-11;Myosin-10;Myosin-14

0.0007371	3.1324610	0.79	-0.3352685	Eif2b2	Translation initiation factor eIF-2B subunit beta
0.0006199	3.2076997	0.79	-0.3358739	Hdhd3	Haloacid dehalogenase-like hydrolase domain-containing protein 3
0.0000003	6.5394050	0.79	-0.3360471	Pcyt2	Ethanolamine-phosphate cytidyltransferase
0.0002865	3.5428411	0.79	-0.3366890	Clip2	CAP-Gly domain-containing linker protein 1;CAP-Gly domain-containing linker protein 2
0.0006714	3.1730463	0.79	-0.3384579	Gatad2b	Transcriptional repressor p66-beta
0.0003682	3.4338926	0.79	-0.3385034	Anxa4	Annexin A4
0.0000561	4.2514042	0.79	-0.3425389	Mff	Mitochondrial fission factor
0.0004402	3.3563895	0.79	-0.3451660	Peg3	Paternally-expressed gene 3 protein
0.0013530	2.8686917	0.79	-0.3460419	Sh3bgrl	Adapter Sh3bgrl
0.0007633	3.1173319	0.79	-0.3462151	Oxr1	Oxidation resistance protein 1
0.0012643	2.8981462	0.79	-0.3463293	Gfra1	GDNF family receptor alpha-1
0.0004494	3.3473217	0.79	-0.3467115	Cbarp	Voltage-dependent calcium channel beta subunit-associated regulatory protein
0.0006583	3.1815905	0.79	-0.3469980	Ndufa10	NADH dehydrogenase [ubiquinone] 1 alpha subcomplex subunit 10, mitochondrial
0.0000038	5.4240035	0.79	-0.3475490	Stub1	E3 ubiquitin-protein ligase CHIP
0.0023571	2.6276160	0.78	-0.3510045	Pfdn6	Prefoldin subunit 6
0.0029899	2.5243388	0.78	-0.3510587	Vta1	Vacuolar protein sorting-associated protein VTA1 homolog
0.0007055	3.1514735	0.78	-0.3522690	Adal	Adenosine deaminase-like protein
0.0015511	2.8093632	0.78	-0.3525837	Polr2m	DNA-directed RNA polymerase II subunit GRINL1A
0.0003225	3.4915093	0.78	-0.3535279	Szrd1	SUZ domain-containing protein 1
0.0008733	3.0588207	0.78	-0.3539886	Nudc	Nuclear migration protein nudC
0.0001294	3.8882206	0.78	-0.3561764	Hgs	Hepatocyte growth factor-regulated tyrosine kinase substrate
0.0025629	2.5912664	0.78	-0.3569285	Psm8	26S proteasome non-ATPase regulatory subunit 8
0.0022408	2.6495956	0.78	-0.3583350	Cops2	COP9 signalosome complex subunit 2
0.0008297	3.0810825	0.78	-0.3588741	Cep170	Centrosomal protein of 170 kDa;Centrosomal protein of 170 kDa
0.0022333	2.6510476	0.78	-0.3605714	Ak1	Adenylate kinase isoenzyme 1
0.0010016	2.9993257	0.78	-0.3624226	Fxn	Frataxin, mitochondrial
0.0001139	3.9436139	0.78	-0.3632228	Slc9a3r2	Na(+)/H(+) exchange regulatory cofactor NHE-RF2
0.0014167	2.8487298	0.78	-0.3646538	Pcmt1	Protein-L-isoaspartate(D-aspartate) O-methyltransferase
0.0037332	2.4279132	0.78	-0.3649907	Mrps36	Alpha-ketoglutarate dehydrogenase component 4
0.0006543	3.1842522	0.78	-0.3653278	Nmra1	NmrA-like family domain-containing protein 1
0.0012846	2.8912224	0.78	-0.3658550	Cend1	Cell cycle exit and neuronal differentiation protein 1
0.0000165	4.7819739	0.78	-0.3659075	Nde1	Nuclear distribution protein nudE homolog 1;Nuclear distribution protein nudE homolog 1
0.0039132	2.4074638	0.78	-0.3677156	Akap5	A-kinase anchor protein 5
0.0000309	4.5104642	0.77	-0.3690395	Anxa7	Annexin A11;Annexin A7
0.0000131	4.8831607	0.77	-0.3701673	Adgrl1	Adhesion G protein-coupled receptor L1
0.0000311	4.5079213	0.77	-0.3717473	Gfra2	GDNF family receptor alpha-2
0.0003162	3.5000338	0.77	-0.3737636	Rnf214	RING finger protein 214
0.0002398	3.6201200	0.77	-0.3753537	Gltp	Glycolipid transfer protein
0.0020702	2.6839876	0.77	-0.3760764	Fam171a2	Protein FAM171A2

0.0044304	2.3535597	0.77	-0.3778352	Agfg2	Arf-GAP domain and FG repeat-containing protein 2;Arf-GAP domain and FG repeat-containing protein 2
0.0039329	2.4052894	0.77	-0.3787264	Wnk1	Serine/threonine-protein kinase WNK1;Serine/threonine-protein kinase WNK1;Serine/threonine-protein kinase WNK1
0.0011565	2.9368581	0.77	-0.3797717	Slirp	SRA stem-loop-interacting RNA-binding protein, mitochondrial
0.0023360	2.6315247	0.77	-0.3826957	Cacybp	Calcyclin-binding protein
0.0045680	2.3402752	0.77	-0.3846013	Prrc2a	Protein PRRC2C;Protein PRRC2C;Protein PRRC2A
0.0004098	3.3874436	0.77	-0.3854960	Uqcrb	Cytochrome b-c1 complex subunit 7
0.0037908	2.4212655	0.77	-0.3862810	Gigyf2	GRB10-interacting GYF protein 2;GRB10-interacting GYF protein 2
0.0007218	3.1416039	0.76	-0.3865110	Nyap2	Neuronal tyrosine-phosphorylated phosphoinositide-3-kinase adapter 2
0.0006493	3.1875811	0.76	-0.3867743	Ccdc22	Coiled-coil domain-containing protein 22
0.0001080	3.9665170	0.76	-0.3869618	Ndufa8	NADH dehydrogenase [ubiquinone] 1 alpha subcomplex subunit 8
0.0005275	3.2777475	0.76	-0.3898424	Cdkn1b	Cyclin-dependent kinase inhibitor 1B
0.0004135	3.3835336	0.76	-0.3908176	Tnrc6b	Trinucleotide repeat-containing gene 6B protein
0.0019256	2.7154445	0.76	-0.3908873	Sod2	Superoxide dismutase [Mn], mitochondrial
0.0000375	4.4261013	0.76	-0.3913260	Shtn1	Shootin-1
0.0043354	2.3629682	0.76	-0.3918869	Pithd1	PITH domain-containing protein 1
0.0004319	3.3646130	0.76	-0.3931492	Syn3	Synapsin-1;Synapsin-2;Synapsin-3
0.0027381	2.5625465	0.76	-0.3934908	Tnfaip8	Tumor necrosis factor alpha-induced protein 8
0.0000669	4.1743817	0.76	-0.3948261	Gng12	Guanine nucleotide-binding protein G(I)/G(S)/G(O) subunit gamma-12
0.0002427	3.6148966	0.76	-0.3954542	Prr12	Proline-rich protein 12
0.0052468	2.2801051	0.76	-0.3959262	Gga3	ADP-ribosylation factor-binding protein GGA3;ADP-ribosylation factor-binding protein GGA3
0.0052498	2.2798543	0.76	-0.4006988	Ube2i	SUMO-conjugating enzyme UBC9
0.0000091	5.0426534	0.76	-0.4020567	Serpinb1a	Leukocyte elastase inhibitor B;Leukocyte elastase inhibitor A
0.0057896	2.2373550	0.76	-0.4036331	Ppp1r12b	Protein phosphatase 1 regulatory subunit 12B;Protein phosphatase 1 regulatory subunit 12B
0.0001135	3.9451296	0.76	-0.4046941	Bola1	Bola-like protein 1
0.0001145	3.9412190	0.75	-0.4081747	Ndrg1	Protein NDRG1
0.0009455	3.0243539	0.75	-0.4083153	Nptn	Neuroplastin
0.0005281	3.2772815	0.75	-0.4084210	Ahsa1	Activator of 90 kDa heat shock protein ATPase homolog 1
0.0021269	2.6722505	0.75	-0.4101379	Eci2	Enoyl-CoA delta isomerase 2
0.0000269	4.5701513	0.75	-0.4102906	Aldh1a1	Aldehyde dehydrogenase 1A1;Aldehyde dehydrogenase 1A1
0.0002777	3.5563953	0.75	-0.4125418	Gstt3	Glutathione S-transferase theta-2;Glutathione S-transferase theta-3
0.0027363	2.5628395	0.75	-0.4130475	Btf3	Transcription factor BTF3;Transcription factor BTF3
0.0014299	2.8447092	0.75	-0.4139075	Dnajb11	DnaJ homolog subfamily B member 11
0.0000002	6.7000593	0.75	-0.4146998	Ca2	Carbonic anhydrase 2
0.0000050	5.3022049	0.75	-0.4151490	Hook3	Protein Hook homolog 3
0.0000112	4.9518906	0.75	-0.4167053	Habp4	Intracellular hyaluronan-binding protein 4
0.0000073	5.1390535	0.75	-0.4190927	Cdv3	Protein CDV3
0.0006468	3.1891979	0.75	-0.4193600	Cald1	Caldesmon 1

0.0033717	2.4721504	0.75	-0.4231480	Pclo	Protein bassoon;Protein piccolo
0.0062263	2.2057723	0.75	-0.4235850	Nav1	Neuron navigator 1
0.0019280	2.7148949	0.75	-0.4236559	Adgrb1	Adhesion G protein-coupled receptor B1
0.0023092	2.6365449	0.75	-0.4236699	Doc2a	Rabphilin-3A;Double C2-like domain-containing protein alpha
0.0000002	6.6198023	0.74	-0.4263830	Gnpda1	Glucosamine-6-phosphate isomerase 1;Glucosamine-6-phosphate isomerase 1
0.0006940	3.1586125	0.74	-0.4265727	Rgs10	Regulator of G-protein signaling 10
0.0008960	3.0477076	0.74	-0.4269805	Pja1	E3 ubiquitin-protein ligase Praja-1;E3 ubiquitin-protein ligase Praja-1
0.0001225	3.9118758	0.74	-0.4271370	Fkbp1a	Peptidyl-prolyl cis-trans isomerase FKBP1A
0.0000026	5.5872051	0.74	-0.4272498	Manf	Mesencephalic astrocyte-derived neurotrophic factor
0.0000287	4.5423056	0.74	-0.4284844	Golgb1	Golgi autoantigen, golgin subfamily b, macrogolgin 1
0.0053782	2.2693635	0.74	-0.4296401	Sirpa	Tyrosine-protein phosphatase non-receptor type substrate 1
0.0041682	2.3800561	0.74	-0.4296567	Naca	Nascent polypeptide-associated complex subunit alpha, muscle-specific form
0.0029834	2.5252848	0.74	-0.4310466	Dcaf5	DDB1- and CUL4-associated factor 5
0.0076635	2.1155736	0.74	-0.4310729	Apip	Methylthioribulose-1-phosphate dehydratase
0.0082566	2.0831997	0.74	-0.4320310	Ktn1	Kinectin
0.0039011	2.4088135	0.74	-0.4322275	Bud31	Protein BUD31 homolog
0.0002071	3.6838207	0.74	-0.4322429	Arl2	ADP-ribosylation factor-like protein 2
0.0049914	2.3017784	0.74	-0.4331706	Tub	Tubby protein
0.0000928	4.0324798	0.74	-0.4336154	Eea1	Early endosome antigen 1
0.0015902	2.7985439	0.74	-0.4349483	Anln	Anillin
0.0070142	2.1540198	0.74	-0.4354080	Lrrfip2	Leucine-rich repeat flightless-interacting protein 1;Leucine-rich repeat flightless-interacting protein 2
0.0000929	4.0321250	0.74	-0.4361519	Scp2	Sterol carrier protein 2
0.0038425	2.4153854	0.74	-0.4376754	Lamp1	Lysosome-associated membrane glycoprotein 1
0.0000430	4.3670015	0.74	-0.4385780	Lasp1	LIM and SH3 domain protein 1
0.0073764	2.1321529	0.74	-0.4429630	Chmp7	Charged multivesicular body protein 7
0.0018939	2.7226356	0.74	-0.4433198	Limd2	LIM domain-containing protein 2;LIM domain-containing protein 2
0.0000641	4.1933048	0.73	-0.4455900	AW551984	Expressed sequence AW551984
0.0027869	2.5548724	0.73	-0.4464007	Irf2bpl	Interferon regulatory factor 2-binding protein 2;Interferon regulatory factor 2-binding protein 2;Probable E3 ubiquitin-protein ligase IRF2BPL
0.0003906	3.4082811	0.73	-0.4497995	Smarce1	SWI/SNF-related matrix-associated actin-dependent regulator of chromatin subfamily E member 1;SWI/SNF-related matrix-associated actin-dependent regulator of chromatin subfamily E member 1
0.0000739	4.1315722	0.73	-0.4502138	Dda1	DET1- and DDB1-associated protein 1
0.0001518	3.8187809	0.73	-0.4505344	Tsn	Translin
0.0010606	2.9744508	0.73	-0.4527620	Nacad	NAC-alpha domain-containing protein 1
0.0030681	2.5131363	0.73	-0.4530969	Gng5	Guanine nucleotide-binding protein G(I)/G(S)/G(O) subunit gamma-5
0.0000057	5.2455989	0.73	-0.4531746	Arfip1	Arfaptin-1
0.0007251	3.1396037	0.73	-0.4535423	Septin8	Septin-11;Septin-11;Septin-8
0.0003075	3.5121210	0.73	-0.4542350	Spart	Spartin

0.0049440	2.3059239	0.73	-0.4555594	Myh11	Myosin-11;Myosin-11;Myosin-11;Myosin-11;Myosin-11;Myosin-11;Myosin-11;Myosin-11
0.0000000	7.8438796	0.73	-0.4564272	Arfp2	Arfaptin-2
0.0001703	3.7688044	0.73	-0.4579720	Celf4	CUGBP Elav-like family member 6;CUGBP Elav-like family member 4
0.0125805	1.9003034	0.73	-0.4580169	Slc7a6os	Probable RNA polymerase II nuclear localization protein SLC7A6OS
0.0000879	4.0561746	0.73	-0.4580983	Gprasp2	G-protein coupled receptor-associated sorting protein 2
0.0001698	3.7701895	0.73	-0.4599480	Fga	Fibrinogen alpha chain
0.0047839	2.3202182	0.72	-0.4642343	Lym4	LYR motif-containing protein 4
0.0010054	2.9976665	0.72	-0.4673617	Rmdn1	Regulator of microtubule dynamics protein 1 von Willebrand factor A domain-containing protein 5A
0.0051968	2.2842641	0.72	-0.4678174	Vwa5a	Membrane-associated progesterone receptor component 1;Membrane-associated progesterone receptor component 2
0.0082394	2.0841039	0.72	-0.4682446	Pgrmc2	Membrane-associated progesterone receptor component 1;Membrane-associated progesterone receptor component 2
0.0052225	2.2821252	0.72	-0.4685723	Pts	6-pyruvoyl tetrahydrobiopterin synthase
0.0006557	3.1832806	0.72	-0.4703551	Fam171b	Protein FAM171B
0.0000007	6.1821073	0.72	-0.4705664	Gfer	FAD-linked sulfhydryl oxidase ALR
0.0001997	3.6996828	0.72	-0.4715208	Uqcr10	Cytochrome b-c1 complex subunit 9
0.0007810	3.1073645	0.72	-0.4729350	Pgs1	CDP-diacylglycerol--glycerol-3-phosphate 3-phosphatidyltransferase, mitochondrial
0.0000013	5.8812284	0.72	-0.4734210	Cmc4	Cx9C motif-containing protein 4
0.0002841	3.5465479	0.72	-0.4738754	Arpc3	Actin-related protein 2/3 complex subunit 3
0.0061942	2.2080177	0.72	-0.4748492	Stx1a	Syntaxin-1A;Syntaxin-1A
0.0103823	1.9837045	0.72	-0.4752218	Hdgf	Hepatoma-derived growth factor;Hepatoma-derived growth factor
0.0019324	2.7139103	0.72	-0.4754227	St13	Hsc70-interacting protein
0.0118922	1.9247386	0.72	-0.4779410	Pcbp2	Poly(rC)-binding protein 3;Poly(rC)-binding protein 3;Poly(rC)-binding protein 3;Poly(rC)-binding protein 1;Poly(rC)-binding protein 2
0.0092863	2.0321590	0.72	-0.4793852	Gng4	Guanine nucleotide-binding protein G(I)/G(S)/G(O) subunit gamma-4
0.0000002	6.7807589	0.72	-0.4796394	Nup54	Nuclear pore complex protein Nup54
0.0088617	2.0524854	0.72	-0.4801192	Wdr91	WD repeat-containing protein 91
0.0001152	3.9384576	0.72	-0.4826963	Wnk3	Serine/threonine-protein kinase WNK1;Serine/threonine-protein kinase WNK3
0.0089049	2.0503723	0.72	-0.4833665	Cdkn2aip	CDKN2A-interacting protein
0.0007340	3.1343269	0.71	-0.4843663	Pnck	Calcium/calmodulin-dependent protein kinase type 1B
0.0005182	3.2855070	0.71	-0.4860989	Ttc9c	Tetratricopeptide repeat protein 9C
0.0021314	2.6713392	0.71	-0.4868368	Ndufaf2	NADH dehydrogenase [ubiquinone] 1 alpha subcomplex assembly factor 2
0.0031462	2.5022193	0.71	-0.4870589	Itpkb	Kinase
0.0004280	3.3685753	0.71	-0.4872939	Nudt4	Diphosphoinositol polyphosphate phosphohydrolase 2;Diphosphoinositol polyphosphate phosphohydrolase 2
0.0011523	2.9384160	0.71	-0.4873687	Fis1	Mitochondrial fission 1 protein
0.0122638	1.9113742	0.71	-0.4876227	Smim12	Small integral membrane protein 12
0.0002412	3.6176667	0.71	-0.4883518	Penk	Proenkephalin-A
0.0021279	2.6720570	0.71	-0.4891069	Tax1bp1	Tax1-binding protein 1 homolog
0.0097598	2.0105574	0.71	-0.4892973	Bsg	Basigin
0.0055484	2.2558289	0.71	-0.4902640	Atp6v1g2	V-type proton ATPase subunit G 2

0.0000025	5.6100315	0.71	-0.4920375	Cyrib	CYFIP-related Rac1 interactor A;CYFIP-related Rac1 interactor B
0.0011933	2.9232479	0.71	-0.4932646	Arpc5l	Actin-related protein 2/3 complex subunit 5-like protein
0.0157249	1.8034115	0.71	-0.4939266	Dnajb6	DnaJ homolog subfamily B member 6;DnaJ homolog subfamily B member 6
0.0000002	6.6752112	0.71	-0.4946027	Ndufa5	NADH dehydrogenase [ubiquinone] 1 alpha subcomplex subunit 5
0.0039826	2.3998362	0.71	-0.4950006	Atp5mk	ATP synthase membrane subunit K, mitochondrial
0.0001624	3.7894893	0.71	-0.4958632	Actr1a	Alpha-centractin;Alpha-centractin
0.0084850	2.0713471	0.71	-0.4973620	Lymr7	Complex III assembly factor LYRM7
0.0060368	2.2191946	0.71	-0.4992536	Unc119b	Protein unc-119 homolog B
0.0051195	2.2907697	0.71	-0.4993680	Rims2	Regulating synaptic membrane exocytosis protein 1;Regulating synaptic membrane exocytosis protein 2
0.0007437	3.1285940	0.71	-0.4995239	Mrpl12	39S ribosomal protein L12, mitochondrial
0.0074670	2.1268533	0.71	-0.5003991	Phax	Phosphorylated adapter RNA export protein
0.0005147	3.2884747	0.71	-0.5011060	Ca1	Carbonic anhydrase 1
0.0002079	3.6821612	0.71	-0.5012242	Dag1	Dystroglycan 1
0.0097554	2.0107563	0.70	-0.5064306	Isoc1	Isochorismatase domain-containing protein 1
0.0037240	2.4289851	0.70	-0.5077417	Tbca	Tubulin-specific chaperone A
0.0008409	3.0752756	0.70	-0.5089303	Npm1	Nucleophosmin
0.0000189	4.7246702	0.70	-0.5104532	Cmpk1	UMP-CMP kinase
0.0000588	4.2305826	0.70	-0.5130169	Lztf1	Leucine zipper transcription factor-like protein 1
0.0061139	2.2136798	0.70	-0.5170433	Pls1	Plastin-1;Plastin-1
0.0022016	2.6572691	0.70	-0.5177259	Nsg1	Neuronal vesicle trafficking-associated protein 1
0.0095856	2.0183790	0.70	-0.5220167	Cadm3	Cell adhesion molecule 3
0.0012005	2.9206559	0.70	-0.5224872	Tro	Tro protein
0.0102160	1.9907198	0.70	-0.5225500	Cpq	Carboxypeptidase Q
0.0118545	1.9261152	0.69	-0.5263802	Emc10	ER membrane protein complex subunit 10
0.0084055	2.0754356	0.69	-0.5277514	Arhgef1	Rho guanine nucleotide exchange factor 1
0.0000002	6.6078420	0.69	-0.5298933	Clic4	Chloride intracellular channel protein 4
0.0000002	6.7953882	0.69	-0.5345225	Evl	Ena/VASP-like protein;Ena/VASP-like protein
0.0017915	2.7467874	0.69	-0.5394242	Idi1	Isopentenyl-diphosphate Delta-isomerase 1
0.0000000	9.9127342	0.69	-0.5401876	Cyc1	Cytochrome c1, heme protein, mitochondrial
0.0012618	2.8990232	0.69	-0.5426554	Katnal1	Katanin p60 ATPase-containing subunit A-like 1
0.0052216	2.2821949	0.69	-0.5445586	Otud7b	OTU domain-containing protein 7B;OTU domain-containing protein 7B
0.0005104	3.2921229	0.68	-0.5464725	Fgb	Fibrinogen beta chain
0.0012065	2.9184801	0.68	-0.5465240	Pdcd10	Programmed cell death protein 10
0.0023833	2.6228155	0.68	-0.5497771	Cfdp1	Craniofacial development protein 1
0.0000032	5.4983299	0.68	-0.5554568	Actr1b	Alpha-centractin;Beta-centractin
0.0011716	2.9312173	0.68	-0.5570795	Cfap36	Cilia- and flagella-associated protein 36
0.0012430	2.9055378	0.68	-0.5607294	Stoml2	Stomatin-like protein 2, mitochondrial
0.0085592	2.0675675	0.68	-0.5610460	Panx2	Pannexin-2
0.0213536	1.6705299	0.68	-0.5637997	Nme2	Nucleoside diphosphate kinase A;Nucleoside diphosphate kinase B
0.0018153	2.7410453	0.67	-0.5676666	Rab23	Ras-related protein Rab-23
0.0002608	3.5837401	0.67	-0.5677824	Arhgap21	Rho GTPase-activating protein 21

0.0170589	1.7680479	0.67	-0.5691235	Bod11	Biorientation of chromosomes in cell division protein 1-like 1
0.0022074	2.6561261	0.67	-0.5701173	Mtdh	Protein LYRIC
0.0038470	2.4148781	0.67	-0.5737879	Pja2	E3 ubiquitin-protein ligase Praja-1;E3 ubiquitin-protein ligase Praja-2
0.0101431	1.9938307	0.67	-0.5761782	M6pr	Cation-dependent mannose-6-phosphate receptor
0.0207902	1.6821408	0.67	-0.5765247	Fxyd6	FXYP domain-containing ion transport regulator 6
0.0000302	4.5197563	0.67	-0.5794563	Rbm3	RNA-binding protein 3
0.0048905	2.3106486	0.67	-0.5812090	Csrp1	Cysteine and glycine-rich protein 1
0.0033985	2.4687153	0.66	-0.5934230	Mri1	Methylthioribose-1-phosphate isomerase
0.0000505	4.2967744	0.66	-0.5957869	Azi2	5-azacytidine-induced protein 2
0.0000004	6.4097950	0.66	-0.5962246	Prdx6	Peroxiredoxin-6
0.0000477	4.3215341	0.66	-0.6017883	Ndufb7	NADH dehydrogenase [ubiquinone] 1 beta subcomplex subunit 7
0.0005324	3.2737662	0.66	-0.6019848	Myrip	Rab effector MyRIP
0.0007682	3.1145251	0.66	-0.6028418	Aif1	Allograft inflammatory factor 1
0.0235527	1.6279595	0.66	-0.6060586	Scn2b	Sodium channel subunit beta-2
0.0000003	6.4964312	0.66	-0.6092272	Cdc37	Hsp90 co-chaperone Cdc37
0.0065169	2.1859614	0.66	-0.6097065	Surf6	Surfeit locus protein 6
0.0192957	1.7145384	0.66	-0.6101281	Zfyve27	Protrudin
0.0245325	1.6102574	0.65	-0.6114430	Sfr1	Swi5-dependent recombination DNA repair protein 1 homolog
0.0000034	5.4738401	0.65	-0.6125708	Neb	Nebulin
0.0259516	1.5858359	0.65	-0.6153136	Lyar	Cell growth-regulating nucleolar protein
0.0000163	4.7867455	0.65	-0.6183942	Fxyd1	Phospholemman
0.0036901	2.4329638	0.65	-0.6247958	Entpd3	Ectonucleoside triphosphate diphosphohydrolase 3
0.0000579	4.2374599	0.65	-0.6266930	Ywhab	14-3-3 protein sigma;14-3-3 protein sigma;14-3-3 protein gamma;14-3-3 protein gamma;14-3-3 protein zeta/delta;14-3-3 protein theta;14-3-3 protein beta/alpha
0.0035670	2.4476939	0.65	-0.6279309	Edf1	Endothelial differentiation-related factor 1
0.0119157	1.9238788	0.65	-0.6301233	Usp54	Inactive ubiquitin carboxyl-terminal hydrolase 54
0.0000296	4.5284369	0.65	-0.6306305	Commd1	COMM domain-containing protein 1
0.0046203	2.3353306	0.65	-0.6307886	Scpep1	Retinoid-inducible serine carboxypeptidase
0.0089125	2.0499990	0.65	-0.6307932	Armcx4	Armadillo repeat-containing, X-linked 4
0.0001805	3.7436304	0.65	-0.6314560	ApoE	Apolipoprotein E
0.0006687	3.1747373	0.65	-0.6323233	Lsm14a	Protein LSM14 homolog A
0.0006757	3.1702281	0.64	-0.6328164	Minar2	Major intrinsically disordered NOTCH2-binding receptor 1-like homolog
0.0004239	3.3727219	0.64	-0.6366413	Pmm2	Phosphomannomutase 1;Phosphomannomutase 2
0.0084176	2.0748119	0.64	-0.6368376	Znf207	BUB3-interacting and GLEBS motif-containing protein ZNF207
0.0000000	9.2191947	0.64	-0.6368588	Chchd7	Coiled-coil-helix-coiled-coil-helix domain-containing protein 7
0.0038337	2.4163839	0.64	-0.6369622	Tmem9b	Proton-transporting V-type ATPase complex assembly regulator TMEM9;Transmembrane protein 9B
0.0177841	1.7499681	0.64	-0.6373545	Mapk11	Mitogen-activated protein kinase 11
0.0035479	2.4500288	0.64	-0.6385069	Pex14	Peroxisomal membrane protein PEX14
0.0033417	2.4760313	0.64	-0.6387671	Ing4	Inhibitor of growth protein 4
0.0130194	1.8854087	0.64	-0.6400935	Josd2	Josephin-2

0.0181303	1.7415939	0.64	-0.6402568	Pds5a	Sister chromatid cohesion protein PDS5 homolog A
0.0021773	2.6620863	0.64	-0.6403753	Nectin1	Nectin-1
0.0000016	5.7828137	0.64	-0.6407673	Epn1	Epsin-1;Epsin-1
0.0134574	1.8710393	0.64	-0.6461247	Diaph2	Protein diaphanous homolog 2
0.0288963	1.5391582	0.64	-0.6495313	Coa5	Cytochrome c oxidase assembly factor 5
0.0150165	1.8234298	0.64	-0.6505337	Serbp1	Plasminogen activator inhibitor 1 RNA-binding protein
0.0055902	2.2525721	0.64	-0.6511902	Micall2	MICAL-like protein 2
0.0000002	6.7353607	0.64	-0.6512354	S100a16	Protein S100-A16
0.0168870	1.7724469	0.64	-0.6512618	Ybx3	Y-box-binding protein 1;Y-box-binding protein 3
0.0136382	1.8652422	0.64	-0.6530112	Map3k4	Mitogen-activated protein kinase kinase kinase 4
0.0310550	1.5078685	0.63	-0.6604141	Carmil3	Capping protein, Arp2/3 and myosin-I linker protein 3
0.0009928	3.0031289	0.63	-0.6624658	Nelfe	Negative elongation factor E
0.0130479	1.8844608	0.63	-0.6635959	Vstm2a	V-set and transmembrane domain-containing protein 2A
0.0003214	3.4929640	0.63	-0.6651441	Gtf2f2	General transcription factor IIF subunit 2
0.0023752	2.6243019	0.63	-0.6653306	Stx8	Syntaxin-8
0.0000165	4.7813036	0.63	-0.6661246	Tssc4	Protein TSSC4
0.0023504	2.6288670	0.63	-0.6665238	Lrp11	Low-density lipoprotein receptor-related protein 11
0.0086013	2.0654377	0.63	-0.6684083	Bcl2l13	Bcl-2-like protein 13
0.0231802	1.6348825	0.63	-0.6688114	Ncbp2	Nuclear cap-binding protein subunit 2
0.0172008	1.7644510	0.63	-0.6698198	Nanp	N-acylneuraminate-9-phosphatase
0.0104790	1.9796795	0.63	-0.6748326	Mien1	Migration and invasion enhancer 1
0.0212990	1.6716405	0.63	-0.6765783	Itfg1	T-cell immunomodulatory protein
0.0051244	2.2903546	0.63	-0.6777280	Mcc	Mutated in colorectal cancers
0.0005339	3.2725398	0.62	-0.6786436	Stmn4	Stathmin-3;Stathmin;Stathmin-4
0.0000163	4.7886645	0.62	-0.6792823	Crip1	Cysteine-rich protein 1
0.0130513	1.8843476	0.62	-0.6804118	Rtl8b	CAAX box 1 homolog A (Human)
0.0040733	2.3900555	0.62	-0.6805003	Gstp1	Glutathione S-transferase P 1
0.0019828	2.7027246	0.62	-0.6874687	Col6a1	Collagen alpha-1(VI) chain
0.0144168	1.8411319	0.62	-0.6909010	Ube2d1	Ubiquitin-conjugating enzyme E2 D1
0.0000622	4.2063086	0.62	-0.6945529	Adam15	Disintegrin and metalloproteinase domain-containing protein 15
0.0313096	1.5043228	0.62	-0.6952735	Itm2b	Integral membrane protein 2B
0.0000451	4.3457322	0.62	-0.6959261	Stx16	Syntaxin-16
0.0041175	2.3853637	0.62	-0.7003320	Comm5	COMM domain-containing protein 5
0.0227155	1.6436784	0.61	-0.7021244	Abl1	Tyrosine-protein kinase ABL1
0.0000138	4.8611404	0.61	-0.7036502	Arpc5	Actin-related protein 2/3 complex subunit 5 Probable proton-coupled zinc antiporter
0.0191339	1.7181961	0.61	-0.7091503	Slc30a3	SLC30A3
0.0090535	2.0431855	0.61	-0.7097423	Tmem237	Transmembrane protein 237
0.0180285	1.7440402	0.61	-0.7103201	Naa10	N-alpha-acetyltransferase 10
0.0001536	3.8137188	0.61	-0.7129838	Gsdme	Gasdermin-E
0.0066374	2.1780047	0.61	-0.7144145	Unc119	Protein unc-119 homolog A
0.0041561	2.3813186	0.61	-0.7167979	Fez1	Fasciculation and elongation protein zeta-1
0.0002112	3.6753160	0.61	-0.7220730	Pde6d	Retinal rod rhodopsin-sensitive cGMP 3',5'-cyclic phosphodiesterase subunit delta
0.0161549	1.7916959	0.61	-0.7220775	Faim2	Protein lifeguard 2

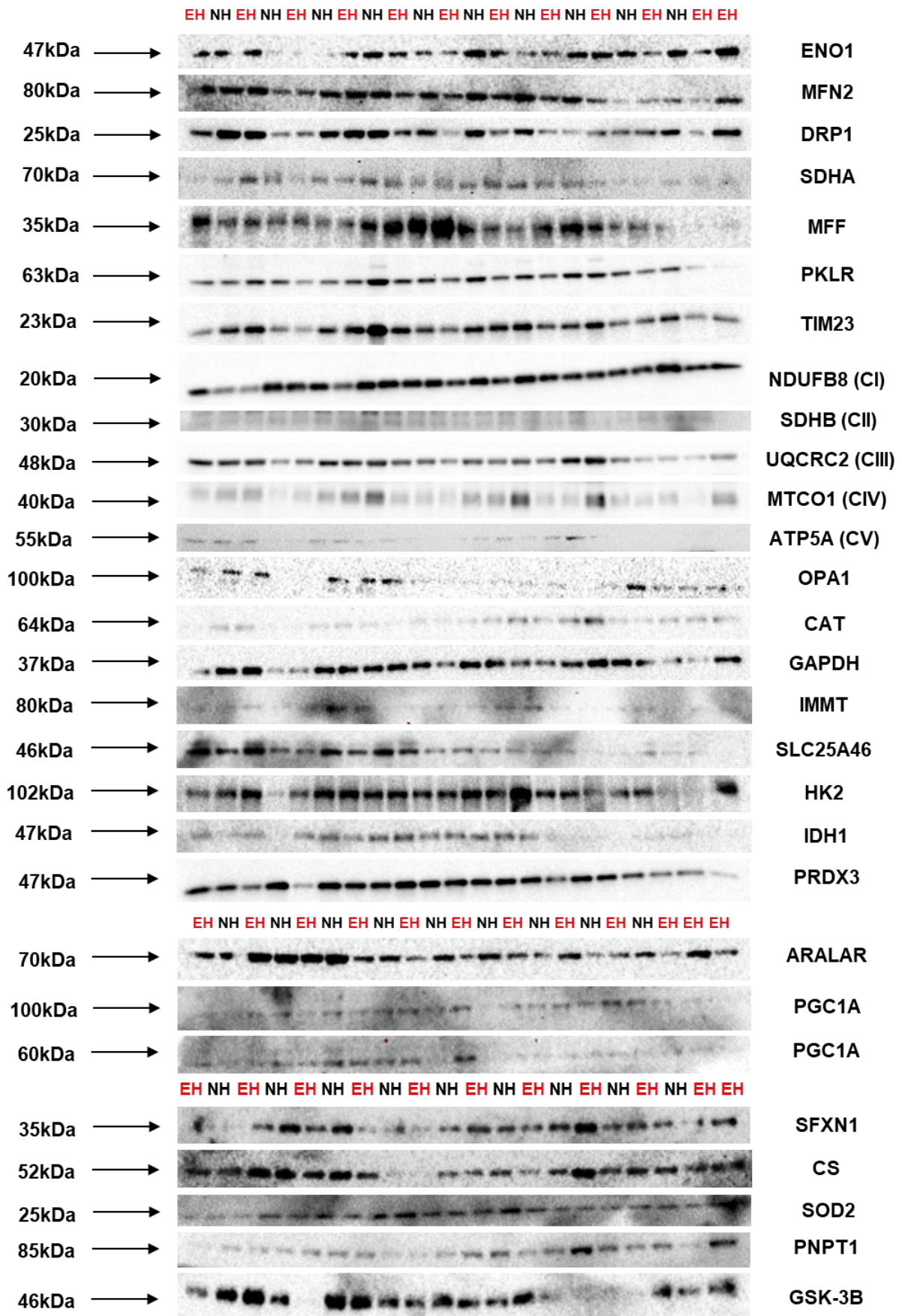
0.0038522	2.4142885	0.61	-0.7236580	Tmed9	Transmembrane emp24 domain-containing protein 4;Transmembrane emp24 domain-containing protein 9
0.0048338	2.3157155	0.61	-0.7243160	Ybx1	Y-box-binding protein 1;Y-box-binding protein 1
0.0000947	4.0234467	0.60	-0.7268667	Psme1	Proteasome activator complex subunit 1
0.0217878	1.6617872	0.60	-0.7296807	Dcxr	L-xylulose reductase
0.0003851	3.4144003	0.60	-0.7380466	Ddrgk1	DDRKG domain-containing protein 1
0.0039628	2.4019945	0.60	-0.7414921	Selenow	Selenoprotein W
0.0208363	1.6811794	0.60	-0.7416319	Arf6	ADP-ribosylation factor 6
0.0297460	1.5265712	0.60	-0.7425137	Cox14	Cytochrome c oxidase assembly protein COX14
0.0107953	1.9667638	0.60	-0.7437608	Gm17455	Predicted gene, 17455
0.0123607	1.9079552	0.60	-0.7457703	Zyg11b	Protein zyg-11 homolog B
0.0000000	7.6438429	0.59	-0.7498221	Lym9	LYR motif-containing protein 9
0.0125677	1.9007427	0.59	-0.7516682	Morn4	MORN repeat-containing protein 4
0.0134569	1.8710544	0.59	-0.7524759	Tmem106b	Transmembrane protein 106B
0.0096145	2.0170715	0.59	-0.7533102	Mlycd	Malonyl-CoA decarboxylase, mitochondrial
0.0228415	1.6412746	0.59	-0.7542646	Mctp1	Multiple C2 and transmembrane domain-containing protein 1
0.0001973	3.7047777	0.59	-0.7553823	Tagln	Transgelin;Transgelin
0.0000850	4.0707747	0.59	-0.7582341	Serpinc1	Antithrombin-III
0.0052091	2.2832361	0.59	-0.7605266	Pltp	Phospholipid transfer protein
0.0022043	2.6567227	0.59	-0.7683693	Zfp512b	Zinc finger protein 512B (Fragment)
0.0340678	1.4676565	0.59	-0.7691149	Gk	Glycerol kinase
0.0387914	1.4112640	0.59	-0.7704332	Srp54	Signal recognition particle 54 kDa protein
0.0160345	1.7949444	0.59	-0.7730901	Atp6v0c	V-type proton ATPase 16 kDa proteolipid subunit c
0.0267152	1.5732413	0.59	-0.7732713	Ppp1r2	Protein phosphatase inhibitor 2
0.0108074	1.9662776	0.58	-0.7779469	Bloc1s2	Biogenesis of lysosome-related organelles complex 1 subunit 2
0.0013886	2.8574272	0.58	-0.7795546	Smim26	Gene model 561, (NCBI)
0.0226965	1.6440403	0.58	-0.7852340	Fmc1	Protein FMC1 homolog
0.0181497	1.7411299	0.58	-0.7870291	Nrip3	Nuclear receptor-interacting protein 3
0.0026892	2.5703797	0.58	-0.7871209	Fam107b	Protein FAM107B
0.0038325	2.4165196	0.58	-0.7898976	Prnp	Major prion protein
0.0000005	6.2753810	0.58	-0.7920908	Fgf1	Fibroblast growth factor 1
0.0026726	2.5730715	0.58	-0.7945325	Nelfa	Negative elongation factor A
0.0004290	3.3675851	0.58	-0.7970150	Cops7b	COP9 signalosome complex subunit 7b
0.0017734	2.7511916	0.58	-0.7972727	Col1a1	Collagen alpha-1(I) chain
0.0071510	2.1456354	0.57	-0.8040081	Cdr2l	Cerebellar degeneration-related protein 2-like
0.0020376	2.6908735	0.57	-0.8061630	Omg	Oligodendrocyte-myelin glycoprotein
0.0001813	3.7416018	0.57	-0.8133236	Tnk2	Activated CDC42 kinase 1
0.0281320	1.5507996	0.57	-0.8200000	Fhip1b	FHF complex subunit HOOK interacting protein 1B
0.0026338	2.5794094	0.57	-0.8222099	Glcci1	Glucocorticoid-induced transcript 1 protein
0.0214897	1.6677696	0.56	-0.8244163	Plce1	1-phosphatidylinositol 4,5-bisphosphate phosphodiesterase epsilon-1
0.0010390	2.9833867	0.56	-0.8281514	Gcc1	GRIP and coiled-coil domain-containing protein 1
0.0039499	2.4034130	0.56	-0.8318796	Slc39a6	Zinc transporter ZIP6
0.0000809	4.0919444	0.56	-0.8494278	Iws1	Protein IWS1 homolog
0.0083061	2.0806022	0.55	-0.8520518	Paf1	RNA polymerase II-associated factor 1 homolog
0.0235526	1.6279607	0.55	-0.8608960	Htatsf1	HIV Tat-specific factor 1 homolog

0.0296362	1.5281779	0.55	-0.8626166	Ube2e3	Ubiquitin-conjugating enzyme E2 E1;Ubiquitin-conjugating enzyme E2 E3
0.0017384	2.7598419	0.55	-0.8708252	Colec12	Collectin-12
0.0004822	3.3167970	0.55	-0.8710375	Cdc42se1	CDC42 small effector protein 1
0.0214355	1.6688673	0.55	-0.8722885	Lsm2	U6 snRNA-associated Sm-like protein LSm2
0.0124410	1.9051446	0.55	-0.8733320	Serpina3k	Serine protease inhibitor A3K
0.0034414	2.4632633	0.54	-0.8813120	Hexim1	Protein HEXIM1
0.0041231	2.3847741	0.54	-0.8880377	Hfm1	Probable ATP-dependent DNA helicase HFM1
0.0138490	1.8585804	0.54	-0.8909819	Selenos	Selenoprotein S
0.0412872	1.3841847	0.54	-0.8918485	S100a9	Protein S100-A9
0.0115859	1.9360705	0.54	-0.8928307	Sdf2l1	Stromal cell-derived factor 2-like protein 1
0.0000039	5.4135653	0.54	-0.8956123	Ptgds	Prostaglandin-H2 D-isomerase
0.0096389	2.0159726	0.54	-0.8958941	Fbxo7	F-box only protein 7
0.0008344	3.0786290	0.53	-0.9183237	Gkap1	G kinase-anchoring protein 1
0.0044625	2.3504204	0.53	-0.9192266	Scaper	S phase cyclin A-associated protein in the ER
0.0024214	2.6159278	0.53	-0.9240184	Zfp941	Zinc finger protein 941
0.0002045	3.6894117	0.52	-0.9327825	Hcrt	Hypocretin neuropeptide precursor
0.0153238	1.8146346	0.52	-0.9406797	Cdh18	Cadherin 18
0.0120659	1.9184392	0.52	-0.9423797	Map4k4	Traf2 and NCK-interacting protein kinase kinase kinase 4;Mitogen-activated protein kinase kinase kinase 4
0.0097519	2.0109101	0.52	-0.9423879	Mepce	BAI1-associated protein 3;7SK snRNA methylphosphate capping enzyme
0.0026871	2.5707093	0.52	-0.9533427	Cep97	Centrosomal protein of 97 kDa
0.0005726	3.2421139	0.51	-0.9592104	Col1a2	Collagen alpha-2(I) chain
0.0001537	3.8134096	0.51	-0.9646822	Pfn3	Profilin-3
0.0063927	2.1943156	0.51	-0.9734443	Hmgn3	High mobility group nucleosome-binding domain-containing protein 3
0.0467723	1.3300111	0.51	-0.9736620	Plekhb1	Pleckstrin homology domain-containing family B member 1
0.0205223	1.6877746	0.51	-0.9830531	Myl12b	Myosin regulatory light chain 12B;Myosin regulatory light chain 12B
0.0007891	3.1028599	0.50	-1.0016426	Gstm2	Glutathione S-transferase Mu 1;Glutathione S-transferase Mu 1;Glutathione S-transferase Mu 2;Glutathione S-transferase Mu 2;Glutathione S-transferase Mu 2
0.0181980	1.7399764	0.50	-1.0030625	Rab33a	Ras-related protein Rab-33B;Ras-related protein Rab-33A
0.0321259	1.4931453	0.50	-1.0136716	Zfand6	AN1-type zinc finger protein 6
0.0006180	3.2090027	0.49	-1.0146002	Ppp1r11	E3 ubiquitin-protein ligase PPP1R11
0.0152996	1.8153196	0.49	-1.0192315	Lamp5	Lysosome-associated membrane glycoprotein 5
0.0000010	5.9902529	0.49	-1.0217229	Capns1	Calpain small subunit 1
0.0430325	1.3662038	0.49	-1.0221025	Cdk5r2	Cyclin-dependent kinase 5 activator 2
0.0000762	4.1180803	0.49	-1.0252595	Vamp1	Vesicle-associated membrane protein 3;Vesicle-associated membrane protein 1
0.0005716	3.2428761	0.49	-1.0259796	Gnpat1	Glucosamine 6-phosphate N-acetyltransferase
0.0006297	3.2008325	0.49	-1.0264206	Tom1l1	TOM1-like protein 1
0.0010293	2.9874456	0.49	-1.0278837	Brd8	Bromodomain-containing protein 8
0.0002211	3.6553461	0.49	-1.0360353	Qrich1	Transcriptional regulator QRICH1
0.0000295	4.5296570	0.49	-1.0367656	Atp6v1g1	V-type proton ATPase subunit G 1
0.0000000	7.3734318	0.48	-1.0671114	Gm50478	Predicted gene, 50478

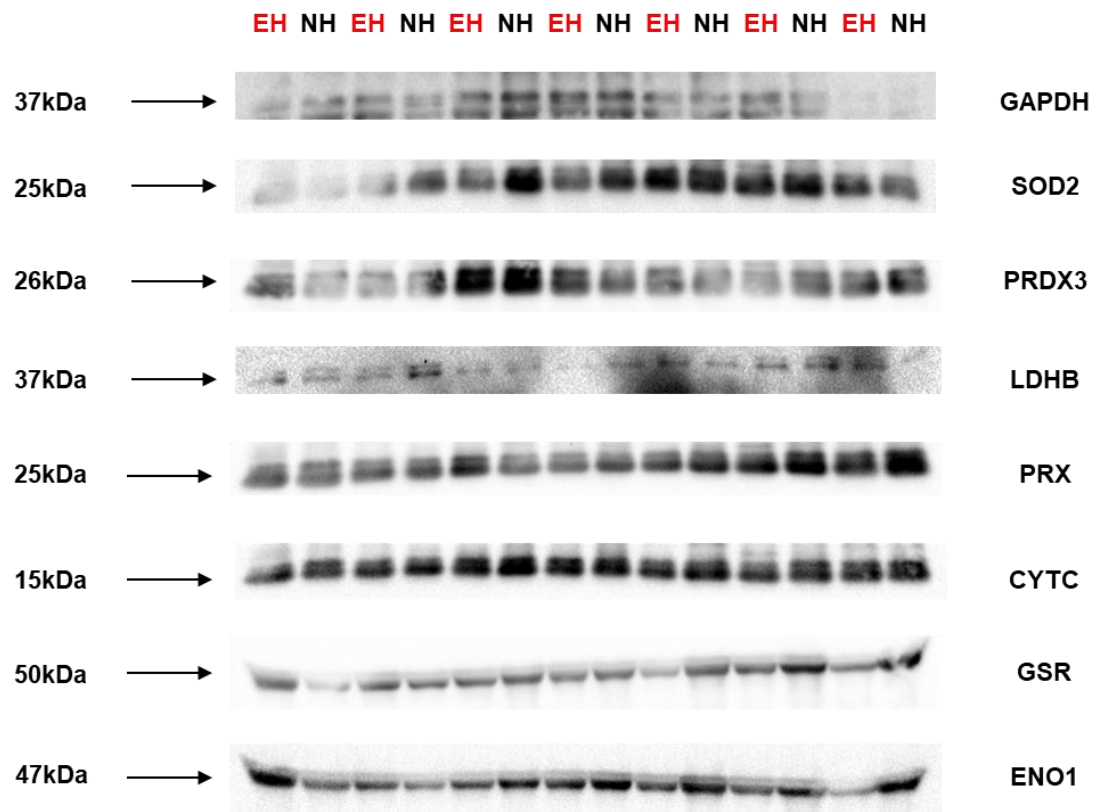
0.0000050	5.2967196	0.47	-1.0802961	Dnajb9	DnaJ homolog subfamily B member 9
0.0040488	2.3926715	0.47	-1.1020932	Cplx1	Complexin-1
0.0029237	2.5340600	0.46	-1.1057598	Nrgn	Neurogranin
0.0070709	2.1505276	0.46	-1.1109954	Hmgn2	Non-histone chromosomal protein HMG-17
0.0001088	3.9632955	0.46	-1.1165517	Mtif2	Translation initiation factor IF-2, mitochondrial
0.0002647	3.5772711	0.46	-1.1179820	Hpcal1	Hippocalcin-like protein 1;Hippocalcin-like protein 1;Hippocalcin-like protein 1
0.0188190	1.7254034	0.46	-1.1191598	Ca4	Carbonic anhydrase 4
0.0001957	3.7084287	0.46	-1.1207476	Acap2	Arf-GAP with coiled-coil, ANK repeat and PH domain-containing protein 2
0.0051640	2.2870141	0.46	-1.1311137	Isy1	Pre-mRNA-splicing factor ISY1 homolog
0.0000007	6.1363109	0.45	-1.1408511	Ncald	Hippocalcin-like protein 1;Neuron-specific calcium-binding protein hippocalin;Neurocalcin-delta
0.0006613	3.1796071	0.45	-1.1417756	Aif1l	Allograft inflammatory factor 1-like
0.0009298	3.0315887	0.45	-1.1446333	Ppp3r1	Calcineurin subunit B type 1
0.0000380	4.4198015	0.45	-1.1673607	Smarcal1	SWI/SNF-related matrix-associated actin-dependent regulator of chromatin subfamily A-like protein 1
0.0005802	3.2364214	0.44	-1.1889345	Lsm14b	Protein LSM14 homolog B
0.0523231	1.2813069	0.44	-1.2004595	Eif5a2	Eukaryotic translation initiation factor 5A-1;Eukaryotic translation initiation factor 5A-2
0.0100740	1.9967992	0.43	-1.2037347	Col4a6	Collagen, type IV, alpha 6
0.0507475	1.2945856	0.43	-1.2109383	Cct6b	T-complex protein 1 subunit zeta;T-complex protein 1 subunit zeta-2
0.0073023	2.1365403	0.43	-1.2279847	Ccdc167	Coiled-coil domain-containing protein 167
0.0000003	6.5800437	0.42	-1.2355497	Bex2	Protein BEX2
0.0000044	5.3535924	0.42	-1.2397921	Cplx2	Complexin-2
0.0059088	2.2285036	0.42	-1.2553027	Prr3	Proline-rich protein 3
0.0007046	3.1520535	0.42	-1.2663103	Cgnl1	Cingulin-like protein 1
0.0054015	2.2674887	0.41	-1.2938237	My19	Myosin regulatory light chain 12B;Myosin regulatory light polypeptide 9
0.0528875	1.2766472	0.41	-1.2950370	Arl10	ADP-ribosylation factor-like protein 10
0.0039958	2.3983926	0.40	-1.3159607	Mgst3	Microsomal glutathione S-transferase 3
0.0021986	2.6578535	0.40	-1.3228076	Echdc2	Enoyl-CoA hydratase domain-containing protein 2, mitochondrial
0.0589004	1.2298820	0.40	-1.3328821	Clec2l	C-type lectin domain family 2 member L
0.0124804	1.9037725	0.37	-1.4221420	Tomm22	Mitochondrial import receptor subunit TOM22 homolog
0.0006232	3.2053574	0.36	-1.4689663	Tceal1	Transcription elongation factor A protein-like 1
0.0000493	4.3070077	0.36	-1.4714463	Ubxn4	UBX domain-containing protein 4
0.0020864	2.6805967	0.36	-1.4779848	Akap1	A-kinase anchor protein 1, mitochondrial
0.0085919	2.0659099	0.35	-1.5027785	Cbfb	Core-binding factor subunit beta
0.0414524	1.3824507	0.35	-1.5179242	Cd81	CD81 antigen
0.0013120	2.8820738	0.35	-1.5227606	Actg2	Actin, cytoplasmic 1;Actin, cytoplasmic 1;Actin, cytoplasmic 2;Actin, cytoplasmic 2;Actin, gamma-enteric smooth muscle
0.0011368	2.9443203	0.35	-1.5337051	Smap	Small acidic protein
0.0001902	3.7208848	0.34	-1.5589840	Kcnp3	Calsenilin
0.0608678	1.2156122	0.33	-1.5879412	Mcm3ap	Germinal-center associated nuclear protein
0.0280731	1.5517099	0.33	-1.6086630	Kmt2a	Histone-lysine N-methyltransferase 2A
0.0024198	2.6162160	0.33	-1.6091043	Chchd10	Coiled-coil-helix-coiled-coil-helix domain-containing 10

0.0020280	2.6929299	0.32	-1.6310331	Gps2	G protein pathway suppressor 2
0.0096515	2.0154052	0.28	-1.8558308	Cox7b	Cytochrome c oxidase subunit 7B, mitochondrial
0.0000228	4.6414202	0.25	-1.9810493	Actb12	Actin, cytoplasmic 1;Actin, cytoplasmic 1;Actin, cytoplasmic 2;Actin, cytoplasmic 2;Beta-actin-like protein 2
0.0021663	2.6642894	0.22	-2.1782933	Fer	Tyrosine-protein kinase Fer

Appendix 1. List of all proteins that were differentially expressed in the hypothalamus of HAB EH compared to HAB NH female mice. Proteins are sorted from largest to smallest fold change values, with red indicating upregulation, and blue downregulation.



Appendix 2. All blot images for proteins for which their expression levels were quantified in the PFC of HAB EH and HAB NH female mice.



Appendix 3. All All blot images for proteins for which their expression levels were quantified in plasma of HAB EH and HAB NH female mice.